Title
Hybrid Fiber Reinforced Concrete Incorporated With Phase Change Material

Author
Chuang, Chia-So

Publication Date
2015

Peer reviewed|Thesis/dissertation

UNIVERSITY OF CALIFORNIA

Los Angeles

Hybrid Fiber Reinforced Concrete Incorporated With Phase Change Material

A dissertation submitted in partial satisfaction of

the requirements for the degree Doctor of Philosophy

in Civil Engineering

By

Chia-So Chuang

2015

ABSTRACT OF THE DISSERTATION

Hybrid Fiber Reinforced Concrete Incorporated

With Phase Change Material

By

Chia-So Chuang

Doctor of Philosophy in Civil Engineering

University of California, Los Angeles, 2015

Professor Jiann-Wen Ju, Chair

To further efforts toward improvement, an innovative and durable High Performance Fiber Reinforced Cementitious Composites (HPFRCC) was developed, using hybrid steel macro-fibers with designed hook-ends, and polyvinyl alcohol micro-fibers for optimal fiber synergistic effects, crack width control, durability, and reduced maintenance and life-cycle costs for bridges. For functional performance improvements, an off-the-shelf phase change material (PCM) was utilized, optimized and incorporated into the HPFRCC as a bridge slab warmer, to improve freeze-thaw cycling durability, to reduce the use of de-icing salts, to provide improved skid resistance, and to improve safety in cold climates and to reduce traffic congestions.

The goal for developing and deploying HPFRCC with controllable functional performance is to utilize new, durable cementitious composites resistant to stringent climate demands compromised of freeze-thaw cycles, de-icing salts, plastic shrinkage and drying shrinkage cracks, chloride and sulfate attacks, corrosion and scaling, and excessive abrasion/wear due to tire chains.

This thesis utilized both numerical modeling and experimental. First, mechanical properties after incorporating PCM were discussed. Subsequently, destructive tests were performed in order to study the effect of adding PCM. In addition, thermal performance after incorporating PCM was also addressed as an important topic. As a result, freeze-thaw testing was performed in order to study PCM performance. Numerical modeling regarding material mechanical properties was proposed and compared with experimental data. Numerical modeling regarding concrete composite thermal performance was also studied. Lastly, concrete interior temperature, mechanical properties and concrete composite residual capacity were discussed.

In chapter 3, several experimental tests were performed in order to study the behavior of hybrid fiber reinforced concrete with PCM and to verify the validity of the theoretical model. Experimental tests can be divided into two categories. One is a destructive test; where concrete composite compressive strength, tensile strength and ductile capacity can be determined. The other category is a freeze-thaw test where concrete composite freeze-thaw resistance can be studied.

In chapter 4, a new crack bridging model accounting for slip-softening interfacial shear stress was proposed for randomly distributed and randomly oriented fibers after PCM were added, based on a micromechanics analysis of single fiber pull-out. The concrete composite

bridging stress versus a crack mouth opening displacement (CMOP) curve and associated fracture energy were theoretically determined. In addition, a constant interfacial shear stress model was also proposed in order to compare this with a slip softening interfacial shear stress model. By applying the proposed model on various concrete composites, including 5% PCM and 7% PCM hybrid fiber reinforced concrete, the present model can well describe the slip-softening behavior during fiber pull-out.

In chapter 5, the new proposed slip-softening model was used to predict the ultimate tensile stress of a single fiber. Maximum fiber debonding stress and fiber pull-out stress was determined based on slip softening interfacial shear stress. By applying the rule of mixture, maximum fiber debonding and pull-out stress, the maximum tensile stress of a concrete composite was able to be predicted when subjected to three point bending test.

In chapter 6, PCM concrete composite interior temperature was modeled and compared with concrete without PCM after being subjected to freeze-thaw cycle. With PCM inside of concrete, interior temperature can be controlled. In preceding chapters, microcracks would be generated inside of the concrete and eventually become larger cracks by going through the freeze-thaw process. The aim of this chapter was to find a temperature gradient inside of concrete using an enthalpy method and specific heat capacity method to solve moving boundary problems. Numerical efficiency from both the enthalpy method and specific heat capacity method were also compared. Two different layouts of how PCM were incorporated into a concrete mix and were discussed in order to determine the efficiency of each design.

In chapter 7, concrete mechanical properties after being subjected to freeze-thaw cycle were modeled. In addition, concrete composite residual capacity after freeze-thaw process was

also determined based on a stress-strain relationship. With PCM inside of concrete, interior temperature can be controlled. However, the relationship between concrete structure mechanical properties, number of freeze-thaw cycles and freeze-thaw temperature differences also needs to be determined.

After a correlation is found between concrete mechanical properties, number of freeze-thaw cycles and temperature difference, the stress-strain relationship can then be determined by using damaged concrete mechanical properties. A Constitutive relationship can be derived based on thermodynamic theory. Elastic damage and plastic damage were both evaluated. Once the stress-strain relationship is obtained, concrete residual life and residual durability can be stimated after going through a freeze-thaw action. Normal concrete was also compared with PCM concrete.

The aim of this chapter was to develop a damage model that account for concrete structure strength, number of freeze-thaw cycles and freeze-thaw temperature differences. Concrete composite residual capacity was also estimated and derived from free energy potential function.

The dissertation of Chia-So Chuang is approved.

Ertugrul Taciroglu

Stanley B. Dong

Jenn-Ming Yang

Jiann-Wen Ju, Committee Chair

University of California, Los Angeles

2015

To my Parents

Fong-Chou Chuang & Hui-Min Yeh;

To my lovely wife

Hsiao-Yin Chen;

To my lovely baby

Hao-Hsi Luca Chuan

TABLE of CONTENTS

Page

LIST of FIGURES

Page

LIST of TABLES

Page

ACKNOWLEDGEMENTS

First of all, I would like to thank my academic advisor, Professor Jiann-Wen Woody Ju, for his constant and continuous encouragement, professional and academic guidance, patience, kindness and unconditional support throughout my graduate studies at UCLA for the past few years. Without his constantly professional advice along with his academic background, it would not be possible to achieve this doctoral degree.

There were several times where I encountered with struggles either in academic field or my personal life. However, Professor Ju's advice always helped me to get through those obstacles. Knowing someone who is accountable and will be there for you all the time is priceless. He is an excellent professor and also a great mentor. I really look up to him and serve him as a role model. With his help for the past few years, I believe that I have become a better person, peer and father. Words cannot describe how much appreciation that I have and I much I feel grateful for having him as my advisor.

I would also like to thank my other committee members including Professor Stanley B. Dong of Civil end Environmental Engineering Department, Professor Ertugrul Taciroglu of Civil end Environmental Engineering Department and Professor Jenn-Ming Yang of Material Science and Engineering Department, for spending their time to evaluate my thesis and giving their valuable opinions and suggestions.

I am also thankful to my office mates and fellow students including Mr. Kuo-Yao Yuan, Mrs Gang-Qin Zhang, Mr. Yu-Kai Wang, Mrs. Yi Wu, Mrs. Ruth Hung, and Mr. Chung-Wen Chuang. Without their assistances and suggestions, I would not be able to achieve my goal either.

Finally, I would like to express my appreciation to my parents, Mr. Fong-Chou Chuang and Mrs. Hui-Min Yeh for their endless support in my entire life. To know that I would have support from my parents whenever I faced obstacles was also my motivation to keep going. My deepest gratitude goes to my wife Mrs. Hsiao-Yin Chen. Her support, encouragement and trust were my biggest strength to support and push me to achieve my dream. I also want to dedicate this thesis to my four month old baby boy, Hao-His Luca Chuang. His presence from four month ago was one of my best moments in my life. Thank you my wife again for taking good care our baby and let me to be able to focus on finishing my Ph.D. thesis. I will not be able to finish this long journey without my wife. Thank you.

VITA

April, 1983	Born, Taichung, Taiwan
June, 2005	Bachelor, Civil Engineering
	National Taiwan University, Taipei, Taiwan
2007-2008	Research Assistant
	Teaching Assistant
	University of Washington, Seattle, Washington
December, 2008	Master of Science
	Department of Civil Engineering
	University of Washington, Seattle, Washington
June, 2010	Master of Science
	Department of Civil and Environmental Engineering
	University of California, Los Angeles

2009-2014	Research Assistant
	Teaching Assistant
	Teaching Associate
	Teaching Fellow
	Department of Civil and Environmental Engineering
	University of California, Los Angeles

Chapter 1 Introduction

1.1 Application of Phase Change Material into Construction Materials

Concrete has been the most commonly used material in the construction industry. Concrete has relatively high compressive strength and can carry a compressive load. However, in real field conditions, concrete is also subjected to tensile stresses due to loading and environmental effects such as temperature change, shrinkage and chemical attacks. Concrete tensile strength is very weak compared to its own compressive strength. In addition, its brittle failure is devastating. As a result, the controls of cracks generated by tensile stresses and enhancing concrete ductile capacity are vital issues worthy of further studies.

Secondly, saving energy has been an increasing concern all around the world. Thermal storage is an important aspect of energy conservation and is mainly attributed to the reasonable use of thermal energy, the effective use of waste heat from waste incineration and from industrial processes. This, there is a growing interest in cogeneration of electricity and heat, and the growing use of solar energy. In a warm or hot climate region, the thermal comfort of a building can be a real problem in the summer. For example, in France, the energy consumption of buildings has increased by 30% during the last 30 years. Housing and tertiary buildings are responsible for the consumption of approximately 46% of all energies because almost every unit turns on their own air condition systems [11]. Therefore, the development of thermal energy

storage systems is essential in order to reduce the use of energy and utilize energy in a more efficient way.

In cold climate regions, the energy saving system is also essential. A concrete composite is porous and water can be stored inside the concrete. When temperature reaches below $0\,°C$, water inside of the concrete will be consolidated into ice and the volume will expand. However, when the temperature rises above $0\,°C$ during the day, ice will melt into water. By going thru this freezing–thawing process day after day, concrete is actually subjected to tensile stresses due to pore pressure. As we all know, concrete is weak in resisting tensile stress and cracks will start to be formulated and propagated. As a result, if concrete interior temperature can be controlled by using thermal storage system and maintained as constant, then cracks formulation can then be delayed and minimized. In addition, chemical attacks can also be prevented, as with the use of de-icing salts.

Phase change material (PCM) has been considered as one of the most efficient thermal energy storage system for buildings. By incorporating PCM into concrete, gypsum board or other wall covering material, PCM can then be part of the building structure and enhance thermal storage capacity and reduce thermal conductivity. The principle of how PCM performs this is unsophisticated. As the temperature rises during the day, PCM transforms in phase from solid to liquid by absorbing the heat. Similarly, when the temperature drops, PCM will transform phase from liquid to solid by releasing the energy. With this energy storage and releasing mechanism of a phase change material, the temperature inside a building system can be better controlled. One of the most important characteristic of PCM is its wide range of melting points. By choosing different PCM melting points, the desired interior temperature can then be reached when adding

PCM into building system. As a result, PCM can be selected and applied either in a hot climate region to maintain building interior temperature and minimize energy consumption or applied in a cold climate region to minimize the formulation of cracks due to pore pressure.

In our application, we propose to collaborate with Caltrans to integrate and implement advanced innovative structural and functional material technologies for casting-place high-performance highway bridge approach/departure slabs. For functional performance improvements, we will design, optimize and incorporate off-the-shelf phase change material (PCM) into the concrete composite as a bridge slab warmer, to improve freeze-thaw cycling durability, to reduce the use of de-icing salts, to provide improved skid resistance, to improve safety in cold climates and to reduce traffic congestions.

As described earlier, the biggest challenge encountered by researchers regarding concrete is its poor tensile strength and low fracture toughness. These undesirable attributes lead to frequent nucleation and propagation of micro-cracks in concrete. When adding PCM, concrete composite strength will decrease significantly because a certain amount of cement and sand will be replaced. One effective method to improve the mechanical behavior of cementitious material is by introducing reinforcing fibers to compensate for the loss of strength from adding PCM.

Fiber reinforcement is considered to be one of the most effective solutions for improving the mechanical behaviors of a cementitious composite. It has been proven that the inclusion of fibers within concrete delays the widening and propagating of cracks after they are formed. Fibers can bridge and prevent separation in concrete. If only considering plain concrete with PCM, the aggregate bridging stress will not be sufficient to resist tensile stress. The fibers hold together the concrete by bridging the gaps between cracks. The incorporation of fibers into a

brittle concrete matrix increases the fracture toughness of the composite by the resultant crack arresting process and by increasing tensile and flexural strength.

Variables that significantly influence the mechanical properties of PCM fiber reinforced concrete composite include fiber diameter, shape, strength, aspect ratio, fiber volume, PCM volume and fiber-matrix interfacial bond strength. There are several types of fiber matrix interactions that lead to energy absorption and increase composite ductile capacity. These include interfacial debonding, slip-softening interfaces, fiber pull-out and inclined angle effect. Although the amount of energy contributed from a single fiber may not be significant, a large amount of fibers bridging over an extended length can contribute enormously to the ductile capacity of the composite. However, there are several composite failure modes that include matrix failure, fiber break and fiber pull-out. Fiber pull-out appears to be the most dominant mechanism of failure. For simplicity, fiber pull-out occurs when the matrix strain ε_m is equal to the fiber strain ε_f and the fiber starts to slip at that instant moment.

$$\varepsilon_m = \varepsilon_f \tag{1.1}$$

For structural improvements, UCLA has developed innovative and durable High Performance Fiber Reinforced Cementitious Composites (HPFRCC), using hybrid steel macro-fibers with designed hook-ends, and polyvinyl alcohol micro-fibers for optimal fiber synergistic effects, crack width control, durability, and reduced maintenance and life-cycle costs for bridges.

The goal for developing and deploying HPFRCC with controllable functional performance is to utilize new, durable cementitious composites resistant to the stringent climate demands of freeze-thaw cycles, de-icing salts, plastic shrinkage and drying shrinkage cracks,

chloride and sulfate attacks, corrosion and scaling, and excessive abrasion/wear due to tire chains. Further, the expected significant enhancement in crack width control and fracture toughness will considerably reduce the rates of ingress of deleterious chloride and sulfate ions, reduce rebar corrosions and concrete deterioration, and reduce maintenance and life-cycle costs. The proposed project will address all eight goals of the DOT/IBRD program and has potential for broad applications for bridge slabs, columns, bent caps, girders, piles, footings, abutments and highway pavements.

The proposed HPFRCC/PCM can potentially mitigate various types of damages from natural disasters. In addition, the proposed integrated approach for this functional HPFRCC with PCM will feature good workability with normal slump values for easy plant mixing, and will reduce maintenance costs by accelerating construction and replacement of damaged/deteriorated bridge approach and departure slabs.

1.2 PCM Properties

There are many phase change materials (PCMs) that have been studied and tested for different practical applications by previous researchers. PCM provides much higher energy stored densities. In addition, heat is stored and released at an almost constant temperature.

A large number of PCMs are available in any desired melting point depending on their application. Basically PCMs can be categorized into organic, inorganic and eutectics. Inorganic PCMS, have a high volumetric latent heat storage capacity, high heat of fusion and high thermal

conductivity. They are also low cost and easy to acquire. Organics PCMS have many advantages, such as the following:

1. Available over a large melting point range.
2. Compatible with conventional construction material.
3. Chemically stable.
4. No segregation.
5. High heat of fusion.
6. Safe and non-reactive.
7. Recyclable.

No single PCM has all of these advantages, however, based on the wide range of melting points and compatibility with concrete material, organic PCM will be used as the energy saving material in our research.

One problem when using PCM is how to incorporate the PCM into a concrete matrix. As mentioned previously, PCM will melt into liquid phase when energy is absorbed. Concrete composite is porous and contain many voids. As a result, the PCM liquid will flow everywhere inside of a concrete composite. As PCM consolidates from liquid to solid phase, the thermal surface area to transfer the heat will be reduced. In addition, the PCM may have a chemical reaction with the concrete material. PCM may easily be broken by fibers in the mixing process because PCM is by itself weak. Therefore, there have been many methods proposed to contain PCM and prevented it from leaking everywhere.

The most popular method is microencapsulation. The basic idea of microencapsulation is implementing PCM into a capsule. Microencapsulation consists of a little container which

embraces the core materiel into a hard shell. Microencapsulating PCM has several important advantages. Microcapsules can handle both liquids and solid material. They tolerate phase changes from solid to liquid or liquid to solid including volume changes in their core and can handle phase change materials as core. Microcapsules may be processed as powder and improve the formulation of phase change materials as many building materials go through a powder state during processing. Microcapsules can be manufactured to handle phase change temperatures between -10 and $80\,°C$. In general, the shell is made of a thin and high molecular weight polymeric film. This thin film has to be compatible with both the PCM and concrete matrix. There are many approaches for microencapsulation technology, including both physical and chemical methods. All the methods have been discussed by other researchers and can be found elsewhere.

Another problem that will be encountered is workability during the mixing process. Microencapsulating PCM can be treated as a powder and is very small in size. It is also hydrophobic because of its own characteristic. In the mixing process, water will be absorbed and the flowability of a concrete mix will be affected. Therefore, adding admixture to increase mixing workability is required. In addition, in order to prevent uneven PCM distribution in the concrete matrix. PCM is dry mixed with sand at the beginning of the mixing process. With this method, PCM is uniformly distributed and can then be guaranteed to mix with other ingredients like cement, aggregate and water. Since there are no current standards regarding mixing PCM concrete composite, trial and error will need to be implemented before in-field mixing and the best mixing formula will then be determined for our own purpose.

The last issue that will need to be solved is strength loss due to PCM. In order to maintain the same volume fraction of the concrete composite when adding PCM, a certain amount of sand and cement will need to be replaced by PCM. As a result, concrete composite strength including compressive strength, tensile strength and flexural strength will be reduced. In order to maintain concrete strength in an acceptable range and maintain PCM with the same energy storing efficiency, it is necessary to incorporate with reinforcing fibers.

Adding fibers can delay and control the formulation of cracks and the concrete composite strength will then be enhanced. In addition, after cracks are formulated, fibers can help concrete to bridge cracks and control the propagation of cracks. As a result, the concrete composite ductile capacity will be increased and fracture energy will also be enhanced.

1.3 Fibers Types and Properties

As briefly discussed before, adding fibers is required to compensate for the loss of strength when incorporating PCM. There are numerous types of fibers that can be chosen dating back a decade leading to the present. These fibers include steel, glass, carbon, polypropylene, polyvinyl alcohol (PVA), nylon, cotton, etc. The most common fibers used in the construction industry and in practice are steel, and polypropylene, polyvinyl alcohol, depending on their application. In our research, we will focus on steel fibers and PVA fibers.

PVA fibers are small, but they have high tensile strength. They can help to reduce the formation of plastic shrinkage cracking in concrete. Therefore, it will be beneficial to use PVA fibers for bridges and to control micro-cracks. Steel fibers are larger in size compared to PVA

fibers and they are more ductile. As a result, steel fibers can be used to bridge larger cracks and increase ductile capacity and fracture toughness.

Table 1.1 shows selected properties such as the specific gravity, modulus of elasticity and tensile strength.

Fiber Types	**Fiber Parameters**		
	E_f (GPa)	Specific Gravity	T_f (MPa)
Steel	210	7.8	1345
PVA	42.8	1.3	1605
Concrete	10-45	3.15	4

Table 1.1 Selected properties of various types of fibers

Steel fibers are available in various sizes and configurations, including round or flat, straight or corrugated with various end conditions such as straight, hooked end, enlarged or twisted. Fiber dimensions vary with different applications. Fiber diameters vary from 0.5 to 2 mm, with length varying from 19 mm to 100 mm. These steel fibers enhance the overall strength, and also greatly increase concrete composite ductile capacity and fracture toughness. First crack strength, flexural strength (modulus of rupture), shear strength, impact strength, fatigue strength, toughness and post-peak energy absorption can all be enhanced. It is noted that for steel fibers in concrete composite the failure mode is dominated by the fiber pull-out.

Efforts have been made to improve the strength of these composites thru different methods, including utilizing different fiber shape to provide mechanical anchorage and modification of fiber surface by means of coating, chemical treatment, etc. Mechanical anchorage has been proven as the most efficient way in practice.

Nycon Corporation has tested different steel fiber configurations and shown that hooked end fibers offer the best performance in anchorage within a concrete matrix. A 1% volume fraction of steel fibers used in concrete composite is considered to be an upper limit in practice. A 2% volume fraction of steel fibers is currently the upper limit for research purposes. When using steel fibers at more than 1%, the workability in the mixing process will become more difficult. In addition, steel fibers with a high volume fraction will tend to have a high fiber concentration and this results in the weakening of the composites instead of toughening. As a result, steel fibers will be used at 1% in our PCM fiber reinforced concrete composite.

PVA fibers are also available in various sizes. In general, PVA fibers are all straight with round ends. As discussed previously, PVA fibers are small compared to steel fibers and it helps a concrete composite to bridge micro-cracks and postpone the formation of larger cracks. As a result, maximum applied tensile strength is increased due to the delay of cracks. PVA fibers are insoluble in water yet are quite hydrophilic. There are many advantages/benefits when using PVA fibers as an additive in concrete composite. They molecularly bond with concrete and can reduce the formation of plastic shrinkage cracking in concrete. It can also provide multi-dimensional reinforcement. It improves the impact, shatter and abrasion resistance of concrete. The most important factor is that they are of low cost.

Polyvinyl alcohol (PVA) fiber emerged during the search for low cost high performance fibers for concrete composite. The hydrophilic nature of PVA fiber imposed a significant challenge in the composite design, as the fibers are apt to rupture instead of being pulled out because of the tendency for the fiber to bond strongly to the concrete matrix. Careful engineering in fiber geometry, fiber/matrix interface and matrix properties is of vital importance to achieve

high ductility. In our research, use of PVA fibers at only 0.1% in the concrete composite and steel fibers can help to bridge macro-cracks in post age. Therefore, we will not do any special treatment for PVA fibers. Regarding the loss of ductile capacity due to the strong bond to the concrete matrix, steel fibers will provide enough ductile capacity and fracture toughness.

As mentioned at the beginning, we will propose a concrete composite with a phase change material (PCM), and PVA fibers and steel fibers are combined with advantages from each different additives. However, with three different additives, the mixing process will then be different compared to conventional plain concrete mixing in order to maintain the same volume fraction. Workability will also be affected. As a result, an adequate amount of water reducer and different method for the mixing process will be presented.

1.4 Mixing Procedure

When adding to a mixture with a phase change material, PVA fibers and steel fibers, some special procedures will have to be taken in the mixing process. In order to integrate PCM into the building material and for it to work efficiently, a uniform distribution has to be guaranteed in the mixing process. To prevent PCMs from having a reaction after adding water and increasing difficulty in mixing, all PCMs will have to be dry mixed with sand before adding cement and water. Doing this will guarantee a uniform distribution.

The necessary technologies have been developed for the integration of the fibers into concrete. A blast machine was developed that is capable of separating the steel fibers as well as injecting them randomly into concrete. From past research, however, there is a known problem

known as fiber balling, which occurs when fibers do not distribute homogeneously and interact as a ball. To overcome this fiber balling drawback, fibers are placed together as a bundle with water soluble glue. Once the fiber bundle is added into a mixer, the steel fibers will disperse uniformly and homogenously distribute within the concrete matrix. There are approximately 40-50 fibers glued together per bundle. The following procedures are the basic rules within the field for fiber reinforced concrete composites:

- Add fibers before adding water
- Fibers can be added together with sand and gravel. This will help the steel fiber bundle to disperse.
- The mixer should have a drum speed of 12-18 rpm while adding fiber at the rate of 130 lbs per minute.
- When all fibers are added, the mixer should be at a mixing speed of 10-12 rpm for at least a minute.
- Since all fibers will absorb water, a water reducer or supercizer is recommended to increase workability during the mixing process.

1.5 Motivation and Scope

The primary goal of the present research is to investigate the behavior of fiber reinforced concrete that incorporates with phase change material (PCM). Mechanical properties need to be discussed when adding PCM, including compressive strength, splitting tension strength and ductile capacity. In addition, the freeze-thaw resistance will be investigated. All mechanical properties after freeze-thaw cycles will be reevaluated. Thermal performance under the action of

freeze-thaw will also be studied. A micromechanical damage model is presented to predict the overall elastic behavior in the composites. A slip-softening interface shear model will be proposed to predict the fibers/matrix interfacial behavior, including fiber debonding and fiber pull-out. The load-crack mouth opening displacement (CMOP) relationship will then be constructed. Fracture energy will be calculated to validate the increased ductile capacity. Experimental tests will need to be conducted to validate the theoretical model. A compressive test, splitting tension test and three point bending test will be done to evaluate PCM fiber reinforced concrete composite mechanical properties. A freeze-thaw test will then be done to investigate frost resistance when adding PCM and reinforcing fibers. Thermal performance will be evaluated under the action of freeze-thaw cycle. Two different material layouts will be compared and two different algorithms will be performed to study concrete interior temperature. A damage model will be presented to study material properties after freeze-thaw test. Concrete residual capacity after a freeze-thaw test will be discussed in terms of the stress-strain relationship. Conclusions will then be made and future work and improvements will be addressed.

Chapter 2 presents a historical review of reinforcing fibers incorporated into concrete matrix and how to use micromechanics to discuss the overall behavior of composite. As is well known, concrete composite is very complicated and has multiple phases. In order to simulate composite behavior, previous researchers had already proposed some useful models in attempts to solve various problems. With increasing requirements around energy consumption, some researchers have started work to find an efficient way to store energy and minimize energy consumption in building. Many studies have shown that using PCM as an energy storage material is an efficient approach and can include PCMs as part of the building structure.

Chapter 3 presents various test methods and procedures. In order to validate the theoretical model, an experimental study has to be made. In order to prepare specimens for various tests, concrete mixing is an important consideration. ASTM only has standard for mixing plain concrete and some suggestions for mixing fiber reinforced concrete. As a result, some adjustments and try and error will have to be made prior to mixing the fiber reinforced concrete. Currently, there are no standards for concrete mixing with phase change material. Therefore, we will present and propose a mixing formula and mixing procedure regarding mixing with PCMs. Four different types of concrete will be made for comparison purpose, including plain concrete, fiber reinforced concrete, 5% PCM fiber reinforced concrete and 7% PCM fiber reinforced concrete. In addition, destructive tests will be performed and results will be compared between each type of concrete. Details on setting up the different destructive tests will also be presented in this chapter. Finally, a freeze-thaw test will be presented to gather data on frost resistance when adding PCM. Some adjustments will be made to our freeze-thaw test in order to suit for the needs of this study. To study and understand the influence of a freeze-thaw test, mass loss measurement and an ultrasonic test will be made for every 40 cycles of the freeze-thaw test. The ultrasonic test is used to measure P-wave speed going through a concrete specimen and then to calculate the corresponding dynamic modulus of elasticity. Destructive tests will be done at the end of freeze-thaw test and the results will be compared with destructive tests done prior to the freeze-thaw test.

In chapter 4, we derive a cracking bridging model based on micromechanical analysis of a single fiber pull-out accounting for linear slip-softening interfacial shear stress for randomly oriented and randomly located discontinuous PCM fiber reinforced concrete composite. Single fiber debonding and single fiber pull-out will be constructed first. Linear slip-softening

interfacial shear stress was proposed after adding PCMs. Since PCM does not have any strength, the shear stress between the concrete matrix and fibers should decrease. The complete concrete composite bridging stress contrasted to the crack opening displacement curve and the related fracture energy will be determined theoretically and compared with experimental results determined from chapter 3. A micromechanical based criterion, which governs the existence of post-debonding (pull-out) of the bridging stress-crack opening displacement curve, was obtained. It was found that the proposed theoretical model can predict the slip-softening behavior very well during fiber pull-out. In addition, the linear slip-softening model can also accurately describe the fracture toughness in terms of fracture energy of the composite. Some researchers have proposed theoretical models by using a constant shear stress model and slip-hardening interfacial shear stress model for prediction. However, these models underestimated when using a constant shear model and overestimated when using a slip-hardening shear model. As a result, our proposed model resolved the deficiencies of the previous proposed models when predicting the fracture energy, which is crucial for material design. A micromechanical-based single fiber pull-out relation and bridging stress-crack opening displacement were constructed theoretically and shown to be quiet accurate in describing the slip-softening interface behavior.

Basic beam theory and rule of mixture are also used to predict the maximum applied force. PVA fibers can bridge micro-cracks and thus maximum tensile strength can then be increased. From the fiber bridging stress derived based on micromechanics and slip-softening interfacial shear stress, we can predict the maximum bridging stress that fibers can provide. Combined with beam theory and rule of mixture, maximum tensile strength and applied force can then be predicted.

In the present study, parameter β was introduced into the interface constitutive relation to take into account the slip-softening effect on interface shear stress. The snubbing coefficient f was also introduced to take fiber angle effect into account. This chapter concludes that parameter β is more sensitive than the snubbing coefficient. Once the frictional shear stress interacted with the linear slip-softening effect, parameter β overcomes the snubbing coefficient effect. We can see the results when changing parameter β and fixing with the snubbing coefficient. The error compared with experimental data will be larger than by changing with the snubbing coefficient.

In chapter 6, PCM concrete composite interior temperature will be modeled and compared with concrete without PCM after being subjected to the freeze-thaw cycle. With PCM inside the concrete, the interior temperature can be controlled. In preceding chapters, microcracks would be generated inside the concrete and eventually become larger cracks after going through a freeze-thaw process. The aim of this chapter is to determine the temperature gradient inside concrete using an enthalpy method and specific heat capacity method to solve moving boundary problems. Numerical efficiency from both the enthalpy method and specific heat capacity method will also be compared.

In chapter 7, concrete mechanical properties after being subjected to the freeze-thaw cycle will be modeled. In addition, concrete composite residual capacity after a freeze-thaw process will also be determined based on a stress-strain relationship. With PCM inside the concrete, interior temperature can be controlled. However, the relationship between concrete structure mechanical properties, number of freeze-thaw cycles and freeze-thaw temperature differences need to be determined.

After the correlation is found between concrete mechanical properties, number of freeze-thaw cycles and freeze-thaw temperature difference, a stress-strain relationship can then be determined by using damaged concrete mechanical properties. A constitutive relationship can be derived based on thermodynamic theory. Elastic damage and plastic damage will both be evaluated. Once the stress-strain relationship is obtained, concrete residual life and residual durability can be estimated after going through a freeze-thaw action. Normal concrete will also be compared with PCM concrete. The aim of this chapter is to develop a damage model that account for concrete structure strength, number of freeze-thaw cycles and freeze-thaw temperature differences. Concrete composite residual capacity will also be estimated and derived from a free energy potential function.

Chapter 8 provides the summary, conclusion and thoughts regarding future work. There will still be necessary research in the future, such as improving the efficiency of the freeze-thaw test. In addition, there are many other interesting topics that can be studied with respect to PCM hybrid fiber reinforced concrete. The correlation between material mechanical properties and phase change phenomenon can be studied by using micromechanics princicple. Details will be described in this chapter.

1.6 References

[1] Ahmed, S. F. U., and Maalej, M. (2009). "Tensile strain hardening behaviour of hybrid steel-polyethylene fibre reinforced cementitious composites." *Construction and Building Materials*, 23(1), 96-106.

[2] Arisoy, B., and Wu, H. C. (2008). "Material characteristics of high performance lightweight concrete reinforced with PVA." *Construction and Building Materials*, 22(4), 635-645.

[3] Bayes-Garcia, L., Ventola, L., Cordobilla, R., Benages, R., Calvet, T., and Cuevas-Diarte, M. A. (2010). "Phase Change Materials (PCM) microcapsules with different shell compositions: Preparation, characterization and thermal stability." *Solar Energy Materials and Solar Cells*, 94(7), 1235-1240.

[4] Bencardino, F., Rizzuti, L., Spadea, G., and Swamy, R. N. (2010). "Experimental evaluation of fiber reinforced concrete fracture properties." *Composites Part B-Engineering*, 41(1), 17-24.

[5] Bentz, D. P., and Turpin, R. (2007). "Potential applications of phase change materials in concrete technology." *Cement & Concrete Composites*, 29(7), 527-532.

[6] Cabeza, L. F., Castellon, C., Nogues, M., Medrano, M., Leppers, R., and Zubillaga, O. (2007). "Use of microencapsulated PCM in concrete walls for energy savings." *Energy and Buildings*, 39(2), 113-119.

[7] Chen, B., and Liu, J. Y. (2005). "Contribution of hybrid fibers on the properties of the high-strength lightweight concrete having good workability." *Cement and Concrete Research*, 35(5), 913-917.

[8] Y. N., You, Z. G., and Jalali, S. (2010). "Hybrid fiber influence on strength and toughness of RC beams." *Composite Structures*, 92(9), 2083-2089.

[9] Hunger, M., Entrop, A. G., Mandilaras, I., Brouwers, H. J. H., and Founti, M. (2009). "The behavior of self-compacting concrete containing micro-encapsulated Phase Change Materials." *Cement & Concrete Composites*, 31(10), 731-743.

[10] Kanda, T., and Li, V. C. (1999). "Effect of fiber strength and fiber-matrix interface on crack bridging in cement composites." *Journal of Engineering Mechanics-Asce*, 125(3), 290-299.

[11] Kuznik, F., David, D., Johannes, K., and Roux, J. J. (2011). "A review on phase change materials integrated in building walls." *Renewable & Sustainable Energy Reviews*, 15(1), 379-391.

[12] Li, V. C., Stang, H., and Krenchel, H. (1993). "Micromechanics of crack bridging in fiber-reinforced concrete." *Materials and Structures*, 26(162), 486-494.

[13] Li, V. C., Wang, S. X., and Wu, C. (2001). "Tensile strain-hardening behavior of polyvinyl alcohol engineered cementitious composite (PVA-ECC)." *Aci Materials Journal*, 98(6), 483-492.

[14] Lin, Z., and Li, V. C. (1997). "Crack bridging in fiber reinforced cementitious composites with slip-hardening interfaces." *Journal of the Mechanics and Physics of Solids*, 45(5), 763-787.

[15] Nelson, P. K., Li, V. C., and Kamada, T. (2002). "Fracture toughness of microfiber reinforced cement composites." *Journal of Materials in Civil Engineering*, 14(5), 384-391.

[16] Passuello, A., Moriconi, G., and Shah, S. P. (2009). "Cracking behavior of concrete with shrinkage reducing admixtures and PVA fibers." *Cement & Concrete Composites*, 31(10), 699-704.

[17] Qian, C. X., and Stroeven, P. (2000). "Fracture properties of concrete reinforced with steel-polypropylene hybrid fibres." *Cement & Concrete Composites*, 22(5), 343-351.

[18] Toutanji, H., Xu, B., Gilbert, J., and Lavin, T. (2010). "Properties of poly(vinyl alcohol) fiber reinforced high-performance organic aggregate cementitious material: Converting brittle to plastic." *Construction and Building Materials*, 24(1), 1-1

Chapter 2 Historical Review

2.1 General and Research Background

Plain concrete applied in construction industry has been developed in the past few decades. However, concrete low tensile strength and brittle damage mode have brought people attention to improve concrete property. Steel bars are commonly incorporated with concrete to sustain tensile strength. In a reinforced concrete structural member, tension is resisted first by concrete and transferred to steel bars after cracks are initiated inside of concrete.

In addition to using concrete in buildings, concrete is used in the massive construction like dams. In this structure, density and compressive strength of concrete are two main characteristics to be considered. In some other areas, there are many concrete structures which do not only require strength and weight, but also require resisting abrasion, fatigue, impact and shearing forces. Conventional concrete is weak when attempting to meet those requirements. The addition of fibers in concrete can improve those properties. Fiber reinforced cement or concrete materials have been developed progressively since the early work by Romualdi and Batson in the 1960s. Over the last 30 years, there has been a dramatic increase in the demand of fiber reinforced concrete. There are many applications in the current industry.

Using steel fibers reinforced concrete on the concrete floor or composite slab such as the bridge deck can improve the crack control. The process of the construction can be reduced in cost and time due to transportation of the regular steel bars as well as the reduction of concrete

volume. The floor thickness can also be reduced compared to the non-reinforced concrete. Industrial concrete floor slab systems are often required to resist intense loading conditions, including point loads from rack legs and impact stresses at contraction joints from moving traffic vehicles. Steel fiber reinforced concrete can increase the ability to sustain intense loading conditions. Concrete floor slabs can fail and cause significant loss and increase of maintenance costs. Steel fibers reinforcement can improve structural ductile capacity and random crack control and load transfer stability at contraction joints. A properly designed fiber reinforced concrete is the most efficient and economical way to maintain the serviceability of concrete floor slab.

Using reinforced fibers into concrete material can be more versatile than conventional steel bars. Fibers are often discontinuous in the concrete composite, which dispersed throughout the matrix and do not go through the specimen in a continuous manner. The contribution of the fibers reinforcement to mechanical behavior is governed by the volume fraction of fibers, fiber's aspect ratio, and by the bond strength between fibers and matrix. Although the mechanical behavior of discontinuous fiber reinforcement has been studied in recent years, most of the researchers mainly focus on the effect of unidirectional aligned short finer composite. Cox [8] is considered to be the first to discuss the elastic behavior of composites containing randomly oriented of short fibers. Cox's results did not account for the matrix phase and the resulting interaction between matrix and fibers. Later, Christensen and Waals [7] proposed a geometric averaging method for determining the effective isotropic elastic properties of randomly oriented short fiber reinforced composites. Their method was based on the stiffness type mechanical properties of aligned and continuous long fiber composites but the end effect of short fibers was neglected.

With increasing understanding of micromechanics, more research and investigators were involved in studying the effective elastic behavior of randomly oriented fiber reinforced composite since 1980s. For example, Takao [31], Benveniste [3] and Ferrari and Johnson [13] presented the effect of randomly oriented fiber on the overall elastic parameters of composites, based on the Mori-Tanaka mean-field theory [26]. It is noted that Ferrari and Marzari also discussed the validity of Mori-Tanaka's theory regarding randomly oriented composites. The effective elasticity of discontinuously reinforced composites with randomly oriented fibers was also investigated by Haddad [14], Chen [6], Sayers [30], Dunn [10], Li [22], and Luo and Stevens [23]. Li [21] also discussed the problem by introducing micromechanics parameters, such as frictional bond strength between matrix and fibers to account for randomly oriented and randomly distributed fibers in the concrete composite.

With increasing studies regarding incorporating fibers into concrete material, adding more types of fiber can be more beneficial by utilizing different characteristics from each fiber. For example, steel fiber can be very ductile and can greatly increase concrete composite ductile capacity and fracture energy. PVA fiber has very strong tensile strength and can improve concrete composite overall maximum tensile strength. The hybridization of different fibers in fiber reinforced concrete composite can be achieved in different ways, such as by combining different lengths, modulus and tensile strengths of fibers.

Chen and Qiao [32] studied the crack growth resistance of hybrid fiber reinforced cement matrix composites. They used PVA fibers and steel fibers in the cement matrix composites. The result showed that PVA fiber can control the growth of micro-cracks and this increase maximum tensile strength. While steel fibers can help to control the beam deflection and increase ductile

capacity. Chen and Liu [5] combined steel fiber and carbon fiber in the light weight concrete and prove that the shrinkage can be reduced, compressive and tensile strength can be enhanced by using hybrid fibers. Ahmed and Maalej [1] studied the flexural responses of hybrid steel-polyethylene cement composites. They also mentioned that large macro fibers bridge the big cracks and provide toughness, while small micro fibers enhance the response prior or just after the cracking. Micro fibers also improve the pull out response of macro fibers, thus produce composites with high strength and toughness.

Ding and You [9] also investigated the influence on RC beams by using steel fiber and plastic fiber into concrete matrix. They concluded that the combination of steel fibers and macro plastic fibers are much more effective in improving the load-bearing capacity as well as the shear toughness than the stirrup with spacing of 150 mm. It means that the conventional transverse ties like stirrups can be partly replaced by fiber cocktail of steel fibers and plastic fibers.

In recent year, improving concrete composite strength and ductile capacity are not the only issue to be discussed. How to store and save energy in construction industry is another topic to be studied. Phase change material (PCM) has been studied by researchers for many years. As people getting to understand and learn PCM properties, some researchers have tried to incorporate PCM into construction material as part of structure.

Bents and Turpin [2] incorporated PCMs into pre-wetted lightweight aggregates (LWA) to increase the energy storage capacity of concrete in residential and commercial construction and also minimize thermal cracking. They also concluded that by using a lower transition temperature PCM, a significant fraction of the freeze-thaw cycles experienced by a bridge deck could potentially be avoided. Meshgin and Xi [25] conducted a systematic study on the effect of

PCMs on various properties of concrete containing PCMs, including mechanical and thermal properties and volumetric stability. Specifically, the compressive strength, flexural strength, drying shrinkage, and thermal behaviors of the PCM-modified concrete are investigated. These material properties are very important to ensure both short and long-term performance of concrete. There are some advantages by using PCMs as addition in the concrete mixture. They found that the PCM can alter the thermal conductivity of the PCM-modified concrete. Specifically, any increase in the amount of PCM in the concrete mixture increases the heat capacity of the PCM-modified concrete, decrease the thermal diffusivity of the concrete, and thus decreases the thermal conductivity. However, there are also some disadvantages when adding PCM in the concrete mixture. They concluded that by adding PCM particles in concrete will decrease the compressive and flexural strength compared to normal plain concrete because certain amount of fine aggregate (sand) and cement have to be replaced. However, the deduction in compressive and flexural strength is acceptable. They also found that the drying shrinkage of the PCM-modified concrete increases due to the low stiffness of the PCM particles that reduce the overall stiffness of the aggregate framework in the concrete.

There are also some field applications and investigations performed by many researchers in recent years. Kuznik and David [18] reviewed the integration of PCMs into building walls. Cabeza and Castellon [4] also use microencapsulated PCMs in concrete walls for energy saving. Their work presented is construction and experimental installation of the two real size concrete cubicles to study the effect of the incorporation of PCMs with melting point of $26°C$. One of the concrete cubicles is normal concrete and the other one contains 5% PCM in weight. The temperature sensors were installed inside of concrete cubicles to record any temperature change. Their results showed that the maximum temperature recorded in normal concrete cubicle was

higher than concrete with PCM by $1\,^{\circ}C$. In addition, the maximum temperature appears in the wall with PCM delays about two hour later than without PCM. As a result, they concluded that concrete cubicle with PCM will have better thermal properties with both energy saving and increased thermal inertia.

Lee [19] have presented the results of large scale tests that compare the thermal storage performance of ordinary concrete blocks with those that have been impregnated with two types of PCMs, BS and commercial paraffin. Two types of blocks were tested and compared, regular block that is made of Portland cement and autoclaved block that consists of Portland cement plus silica. The impregnation was achieved by immersing the heated concrete block in a bath filled with molten PCM until the required amount of PCM was absorbed. The results showed that the concrete blocks are capable of storing the latent and sensible heats of the incorporated PCM as well as the sensible heat of concrete.

Hawes [16] presented the thermal performance of PCM in different types of concrete blocks. The presentation has covered the effects of concrete alkalinity, temperature, immersion time and PCM dilution on PCM absorption during the impregnation process. They examined the mechanisms of absorption and established a means of developing and using absorption constants for PCM in concrete to achieve diffusion of the desired amount of PCM and hence, the required thermal storage capacity. The effects of concrete modification and improved PCM incorporation techniques were shown to have increased thermal storage up to about 300%. Meng Zeng [33] presented the development of a thermally enhanced frame wall that reduces the demand of air-conditioning in residential buildings. Results showed that by incorporating with PCM, the heat flux can be reduced by at least 38%. In building applications, this could reduce the demand of air

conditioning and shifted thermal loads to other time of the day, all while the building interior temperature would remain relatively stable.

There are also a lot of applications with PCM incorporating into building structure, including dry wall, wood-light weight concrete, thermal effective window, etc. They have all shown that they can have better energy saving capacity and reduce the demand of air conditioning. However, they also have disadvantages, including strength reduction and increased dry shrinkage, etc. Results showed that the reduction in strength is acceptable and those applications indeed open a door and provide another opportunity for other researchers are able to incorporated phase change material into building structure and create a better building material. As a result, in our application, with the addition of fibers to enhance concrete composite strength and bridge small cracks and PCM to provide energy saving capacity, we will provide both strength and energy saving outstanding newly developed material in the future material use.

To understand how phase change material will transfer thermal energy and response during freeze-thaw cycle is important and has been studied by other researchers in the recent years.

Hasan and Mujumdar [15] presented the results of a numerical and experimental investigation of one dimensional conduction-controlled cyclic melting and freezing from phase change material. They proposed the energy equations for both solid and liquid layers and use finite-difference method to solve the resulting multiple moving boundary value problem. Due to cyclic temperature changes around the melting point the PCM may contain multiple moving boundaries with separate alternating liquid and solid phases. Jariwala [17] presented an experimental study of the cyclic thermal performances of latent heat storage unit which consisted

of a cylindrical helically coiled copper tube immersed in a cylindrical tank of a commercial paraffin wax. Hot and cold water was filled inside the tube to perform freeze-thaw cycles. Irrespective of the durations of the individual melting and freezing periods, a PSS, which was independent of the initial thermal condition of the PCM was established by the third cycle. He also developed a quasi-steady one dimensional model by assuming conductive heat transfer during the freezing cycle and convective heat transfer during the melting cycle.

Pasupathy and Athanasius [28] presented the experimental investigation and numerical simulation analysis on the thermal performance of a building roof incorporating phase change material for thermal management. They incorporated a PCM panel in between roof top slab and concrete slab to perform thermal storage and used the same governing equation for all three layers to solve the problem.

$$k_m \frac{\partial^2 T_m}{\partial x^2} = \rho_m Cp_m \frac{\partial T_m}{\partial t} \qquad [0 < x < L];\ m = 1,2,3 \tag{2.1}$$

An experiment was also conducted to verify the accuracy of the proposed theoretical model. An experimental set up consisting of two identical test rooms has been constructed to study the effect of having PCM panel on the roof of the building. A water tank is kept at the corner of the PCM room and the cold water from the tank is allowed to pass through the heat exchanger as and when required to perform freeze-thaw cycles.

Darkwa [12] analyzed a laminated phase change concrete duct system numerically for cooling applications in buildings. The concrete duct consists of an inner core of laminated PCM layer and a concrete shell. A one dimensional mathematical model has been proposed. The

differential energy equations for the fluid and PCM may be assumed to be heat transferred to the surface of PCM equals to the heat extracted from the fluid.

Lucia [24] studied the heat transfer and fluid flow processes that occur inside a PCM cavity and found a complex relationship between surface temperature difference and instantaneous melt rate. This complexity is attributed from the moving interface separating two regions of varying thermal properties and some degree of convective heat transfer. Majumdar [27] also developed a heat transfer model for evaluating the performance of phase change material under solid-liquid transformation. Darkwa [11] used numerical model to analyze the encapsulated PCM system for improving heat transfer at the moving boundary layers in PCMs but did found out that the heat transfer was multidimensional. Further studies covering two integrated methods, including randomly mixed PCM and laminated PCM have been conducted and laminated PCM proved to achieve the better performance.

From previous studies and efforts, we can observe that many researchers have discussed the topic regarding inserting different types of fibers into concrete matrix to enhance weak tensile strength. By utilizing different fibers' characteristics, hybrid fiber reinforced concrete composite has been a popular material to be used in the structure design.

Energy storing capacity is another rising topic to be discussed. To incorporate PCM into concrete will be an efficient way to increase energy storing capacity and increasing thermal performance. However, the strength loss of PCM concrete is inevitable. As a result, in this research, we will utilize benefits from both fibers and PCM to develop a new material that can both increase strength and enhance energy saving capacity.

2.2 References

[1] Ahmed, S. F. U., and Mihashi, H. (2007). "A review on durability properties of strain hardening fibre reinforced cementitious composites (SHFRCC)." *Cement & Concrete Composites*, 29(5), 365-376.

[2] Bentz, D. P., and Turpin, R. (2007). "Potential applications of phase change materials in concrete technology." *Cement & Concrete Composites*, 29(7), 527-532.

[3] Benveniste, Y. (1987). "A new approach to the application of Mori-Tanaka theory in composite-materials." *Mechanics of Materials*, 6(2), 147-157.

[4] Cabeza, L. F., Castellon, C., Nogues, M., Medrano, M., Leppers, R., and Zubillaga, O. (2007). "Use of microencapsulated PCM in concrete walls for energy savings." *Energy and Buildings*, 39(2), 113-119.

[5] Chen, B., and Liu, J. Y. (2005). "Contribution of hybrid fibers on the properties of the high-strength lightweight concrete having good workability." *Cement and Concrete Research*, 35(5), 913-917.

[6] Chen, T. Y., Dvorak, G. J., and Benveniste, Y. (1992). "Mori-Tanaka estimates of the overall elastic-moduli of certain composite-materials." *Journal of Applied Mechanics-Transactions of the Asme*, 59(3), 539-546.

[7] Christen.Rm, and Waals, F. M. (1972). "Effective stiffness of randomly oriented fiber composites." *Journal of Composite Materials*, 6(OCT), 518-&.

[8] Cox, H. L. (1952). "The elasticity and strength of paper and other fibrous materials." *British Journal of Applied Physics*, 3(MAR), 72-79.

[9] Ding, Y. N., You, Z. G., and Jalali, S. (2010). "Hybrid fiber influence on strength and toughness of RC beams." *Composite Structures*, 92(9), 2083-2089.

[10] Dunn, M. L., Ledbetter, H., Heyliger, P. R., and Choi, C. S. (1996). "Elastic constants of textured short-fiber composites." Journal of the Mechanics and Physics of Solids, 44(9), 1509-&.

[11] Darkwa K, O'Callaghan PW. "Simulation of phase change drywalls in a passive solar building."*J Appl Therm Eng 2006*; 26(8–9):777–966.

[12] Darkwa K. "Mathematical modelling and simulation of phase change drywall for heating application in a passive solar building. "*Proceedings of the 3rd international energy conversion engineering conference*, August 2005, San Francisco, USA.

[13] Ferrari, M., and Johnson, G. C. (1989). "Effective elasticities of short-fiber composites with arbitrary oriented distribution." *Mechanics of Materials*, 8(1), 67-73.

[14] Haddad, Y. M. (1992). "On the deformation theory of a class of randomly structured composite systems." *Transactions of the ASME. Journal of Energy Resources Technology*, 114(2), 110-116116.

[15] Hasan, M., Mujumdar, A. S., and Weber, M. E. (1991). "Cyclic melting and freezing." *Chemical Engineering Science*, 46(7), 1573-1587.

[16] Hawes, D. W., Banu, D., and Feldman, D. (1990). "Latent-heat storage in concrete .2." *Solar Energy Materials*, 21(1), 61-80.

[17] Jariwala, V. G., Mujumdar, A. S., and Weber, M. E. (1987). "The periodic steady-state for cyclic energy-storage in paraffin wax." *Canadian Journal of Chemical Engineering*, 65(6), 899-906.

[18] Kuznik, F., David, D., Johannes, K., and Roux, J. J. (2011). "A review on phase change materials integrated in building walls." *Renewable & Sustainable Energy Reviews*, 15(1), 379-391.

[19] Lee, T., Hawes, D. W., Banu, D., and Feldman, D. (2000). "Control aspects of latent heat storage and recovery in concrete." *Solar Energy Materials and Solar Cells*, 62(3), 217-237.

[20] Li, V. C., and Stang, H. (1997). "Interface property characterization and strengthening mechanisms in fiber reinforced cement based composites." *Advanced Cement Based Materials*, 6(1), 1-20.

[21] Li, V. C., Stang, H., and Krenchel, H. (1993). "Micromechanics of crack bridging in fiber-reinforced concrete." *Materials and Structures*, 26(162), 486-494.

[22] Lin, Z., and Li, V. C. (1997). "Crack bridging in fiber reinforced cementitious composites with slip-hardening interfaces." *Journal of the Mechanics and Physics of Solids*, 45(5), 763-787.

[23] Luo, J., and Stevens, R. (1996). "Micromechanics of randomly oriented ellipsoidal inclusion composites .1. Stress, strain and thermal expansion." *Journal of Applied Physics*, 79(12), 9047-9056.

[24] Lucia M, Bejan A. "Thermodynamics of energy storage by melting due to conduction or natural convection. "*J Solar Energy Eng 1990*;112:111–6.

[25] Meshgin, P., and Xi, Y. P. (2012). "Effect of Phase-Change Materials on Properties of Concrete." *Aci Materials Journal*, 109(1), 71-80.

[26] Mori, T., and Tanaka, K. (1973). "Average stress in matrix and average elastic energy of materials with misfitting inclusions." *Acta Metallurgica*, 21(5), 571-574.

[27] Majumdar P, Saidbakhsh A. "Heat transfer model for phase change thermalenergy storage. " *Heat Recovery Syst & CHP 1990*; 10(5/6):457–68.

[28] Pasupathy, A., Athanasius, L., Velraj, R., and Seeniraj, R. V. (2008). "Experimental investigation and numerical simulation analysis on the thermal performance of a building roof incorporating phase change material (PCM) for thermal management." *Applied Thermal Engineering*, 28(5-6), 556-565.

[29] Pasupathy, A., Velraj, R., and Seeniraj, R. V. (2008). "Phase change material-based building architecture for thermal management in residential and commercial establishments." *Renewable & Sustainable Energy Reviews*, 12(1), 39-64.

[30] Sayers, C. M. (1992). "Elastic-anusitropy of short-fiber reinforced composites." *International Journal of Solids and Structures*, 29(23), 2933-2944.

[31] Takao, Y., Chou, T. W., and Taya, M. (1982). "Effective longitudinal Young's modulus of misoriented short fiber composites." *Transactions of the ASME. Journal of Applied Mechanics*, 49(3), 536-540540.

[32] Ying, C., and Pizhong, Q. (2011). "Crack Growth Resistance of Hybrid Fiber-Reinforced Cement Matrix Composites." *Journal of Aerospace Engineering*, 24(2), 154-161161.

[33] Zhang, M., Medina, M. A., and King, J. B. (2005). "Development of a thermally enhanced frame wall with phase-change materials for on-peak air conditioning demand reduction and energy savings in residential buildings." *International Journal of Energy Research*,29(9),795-80

Chapter 3 Experimental Study on Fiber Reinforced Concrete Incorporating with Phase Change Material

3.1 Introduction

Low tensile strength and poor ductility of concrete are drawbacks that not only impose difficulty in structural design, but also affect building safety in the near future. Concrete fracture mode tends to be brittle instead of ductile. Therefore, to increase concrete ductile capacity after reaching maximum tensile strength will be predominant. In this regard, by inserting fiber reinforcement in concrete matrix to restrain crack width, crack propagation, enhance matrix tensile strength, fracture toughness and energy absorption capacity.

In addition, concrete damage could be severe when it exposed to freeze-thaw condition in the cold climate region. When freeze-thaw cycles are increased, microcracks and macrocracks would them be formulated inside of concrete matrix because of pore pressure. Pore pressure is caused by ice expansion inside of concrete. As a result, the relatively large thermal mass of concrete can be an advantage, as they store energy during the day and release it at night.

In order to improve concrete tensile strength and ductile capacity, fibers can be inserted into concrete matrix. Fibers serve as “bridges” to transfer stress between cracks and control crack width and crack propagation. Plasticity is also provided for concrete composite to increase fracture resistance. Optimization of mechanical properties of concrete material can be achieved

by combining different types of fibers, such as steel fiber and polyvinyl alcohol fiber (PVA). The benefits of such hybrid fiber concrete composite are listed as follow:

1) In order to improve concrete ultimate strength, for fiber that is stiffer, stronger and relatively smaller in size can bridge micro-cracks and to prevent bigger cracks and thus increase higher tensile strength of composite.
2) In order to increase concrete composite ductile capacity, for fiber that is more flexible, ductile and relatively larger in size can bridge the macro-cracks and thus increases the toughness and ductile behavior in the post cracking stage.

In this chapter, both PVA and steel fibers will be mixed into concrete matrix to achieve the aforementioned benefits of reinforced concrete composite. In general, steel fibers can have the following advantages:

1) It provides high ductility and improves load bearing capacity.
2) It provides cost effective reinforcement solution.
3) It is quick and easy to apply.
4) It can increase concrete composite ductile capacity and fracture energy.

PVA fibers have the following advantages:

1) It provides strong bond strength with concrete.
2) It can reduce the formation of plastic shrinkage cracking in concrete.
3) It can also provide multi-dimensional reinforcement.
4) It improves impact, shatter and abrasion resistance of concrete.
5) Low cost.

In order to improve freeze-thaw resistance, phase change material (PCM) can be incorporated into hybrid fiber reinforced concrete composite. Melting point for PCM can be chosen as $6°C$ and it could be applied in construction to maintain concrete interior temperature as $6°C$. To prevent PCM leaking inside of concrete matrix, PCM is microencapsulated into a shell. However, certain amount of cement and fine aggregates need to be replaced when adding PCM to maintain the correct proportion of hybrid fiber reinforced concrete composite (FRC). As a result, strength of concrete composite will be decreased. Mechanical tests must be done to prove that mechanical properties are still maintained by adding hybrid fibers.

In this chapter, several destructive experiments will be performed to investigate mechanical performance by comparing plain concrete, FRC and hybrid fiber reinforced concrete (FRC) adding PCM, such as composite compressive strength, tensile strength, ductile capacity and freeze-thaw test resistance.

To investigate the freeze-thaw performance when incorporating PCM, freeze-thaw test will be performed up to 340 cycles. The following mass loss measurement and ultrasonic test for determining dynamic young's modulus will also be performed in every 40 cycles. Details will be addressed in the following chapters.

3.2 Literature Review

There have been extensive studies and efforts in order to improve the behavior of concrete or cementitious composite by inserting fibers as reinforcement to increase composite ultimate strength and ductile capacity. Based on the published research results, Chen and Qiao [39] have shown that the concrete performance can be improved by incorporating both steel fibers and PVA fibers. They presented the benefits of fiber reinforced concrete (FRC) composite, such as increasing ultimate tensile strength, crack width control, ductile capacity in post-peak stage and fracture energy. The test data also showed that hybrid fiber reinforced concrete composite had better performance compared to plain concrete or concrete with only one type of fiber.

Wang [38] presented the performance of engineered cementitious composites (ECC) when adding with PVA fibers, such as composite tensile behavior, flexural response, compressive strength, shrinkage behavior and freeze-thaw resistance. They have shown that by incorporating with PVA fibers, composite compressive strength and tensile strength can be improved. In addition, flexural toughness is also increased because of higher ductile capacity. Dry shrinkage can also be controlled and can be neglected. Although the composite presented by Wang and Li only consider one type of fiber, they still proved that all specimens did not have any damage by measuring dynamic modulus after 300 cycles of freeze-thaw test.

Yun and Rokugo [41] investigated the freeze-thaw influence on the flexural properties of hybrid fiber reinforced cementitious composite. They inserted PVA fibers and polyethylene (PE) fibers into cementitious composite. They addressed that the dynamic modulus of elasticity from ultrasonic test after 300 cycles of freeze-thaw test is almost the same than before the test. There

was no significant mass loss were observed after 300 cycles. Only small amount of mass loss was caused by the surface scaling of the specimens. In addition, the modulus of rupture and toughness index did not change considerably and maintain the same ductile capacity.

Bentz and Turpin [16] presented that by utilizing PCM into concrete with a transition temperature of $5\,°C$, the freeze-thaw resistance can be improved by testing a concrete bridge deck or pavement. Meshgin and Xi [25] investigated the effect of PCM on some properties of concrete by an experimental study. They found that by adding PCM into concrete would decrease the compressive and flexural strength since certain amount of cement and sand would be replaced. In addition, the dry shrinkage test results showed that the concrete with PCM incorporated, the dry shrinkage of the composite would increase, which is due to the low stiffness of the PCM particles that reduces the overall stiffness on the entire concrete composite. However, the entire composite performed better thermal behavior because of PCM. It showed that any increase in the amount of PCM in the concrete composite can increase the heat capacity and decrease the thermal conductivity. Therefore, the interior temperature of concrete can be controlled in a constant temperature.

From above studies and literature reviews, we can observe that adding phase change material (PCM) can have both benefits and shortcomings. It can improve concrete thermal performance, but concrete composite mechanical properties will be compensated, such as compressive strength, tensile strength, flexural performance and ductile capacity. Therefore, adding fibers to reinforce the PCM concrete composite to improve mechanical properties and create one of a kind composite will be the primary goal for this study.

In this chapter, the fiber reinforced concrete which includes steel fiber and PVA fiber will be incorporated by adding 5% PCM and 7% PCM. By combining both fibers and PCM, we hope that the composite can have better freeze-thaw resistance without losing significant strength compared to regular plain concrete. In the following sections, mixing preparation and process will be discussed first. Results from destructive tests and freeze-thaw test will also be presented.

3.3 Experimental Preparation and Procedure

3.3.1 Material Preparation

Step 1: Choice of Slump

The slump test is a method for evaluating the flow properties of concrete composite. Mixtures with the stiffest possible consistency which can be easily placed and compacted without segregation should be used. According to ASTM C 995-01, the typical slump is in between 1 inch (25.4mm) to 4 inches (101.6mm).

Step 2: Choice of maximum size of aggregate

For the fixed coarse aggregate volume in concrete composite, well-graded aggregate will produce less empty space than only certain size of aggregate, which in turn, reduces the cement requirement in the concrete mixture. In general, the maximum size of coarse aggregate should be the largest out of those that are economically available and has to be consistent with the dimension of the structure.

Step 3: Estimating of the maxing water content and cement content

According to ACI recommendations, the quantity of mixing water per unit volume of concrete that is required to produce a chosen slump is dependent on the maximum particle size of the aggregate and whether or not the mixture has entrained air. According to ACI, the approximate mixture of water and air content requirements for slumps equal to 3 to 4 inches. The normal maximum size of aggregate is 0.75 of an inch with the air-entrained concrete and the water is suggested to be 305 lbs.

However, additional adjustment will have to be made since fibers are added. In many projects, steel fibers have been added without any changes to the conventional mixture proportions. When large numbers of fiber per unit volume are used, some adjustments may be required to provide better workability of the concrete. As a result, more cement paste is needed in the mixture. In addition, the ratio of fine to coarse aggregate is adjusted upward accordingly. ACI recommends that using 600-1000 lb / yd^3 for the maximum aggregate size is 3/8 in and 500-900 lb / yd^3 for the maximum aggregate size is 3/4 in.

Step 4: Determine water/cement ratio

Because different aggregates and cement types may produce different strength at the same water-cement ratio, it is desirable to develop the relationship between strength and water-cement ratio for the materials to be used. In general, for the compressive strength of the air-entrained concrete at 28 days, according to ASTM C31, the water cement ratio is suggested to be 0.45.

However, the amount of cement will not be sufficient if 0.45 is used as water-cement ratio since two types of fibers will be used in our concrete composite. Therefore, 0.43 as water-cement ratio would be suggested to increase the amount of cement. Water reducer was also used to increase mixing workability.

Step 5: Estimation of the coarse aggregate content

Using the maximum possible volume of coarse aggregate on a dry-rodded basis per unit volume of concrete is economically optimal. Data from a large number of tests have shown that with properly graded materials, the finer the sand and the larger the size of the coarse aggregates are, the higher the volume of coarse aggregate that can be used to produce a concrete mixture of satisfactory workability. According to ASTM C29, the volume of coarse aggregate in a unit volume of concrete can be estimated from its maximum aggregate size and the fineness modulus of the fine aggregate. This volume is converted to the dry weight of the coarse aggregate by multiplying it with the experimentally determined value of the dry-rod unit weight.

Step 5.1: Estimation of the fineness modulus of fine aggregates

The fineness modulus (FM) is computed from the screen analysis data by adding the cumulative percentages of the aggregates retained on each of a specified series of sieves, and dividing the sum by 100. Fineness modulus is defined as the fineness index of an aggregate. The higher the FM is, the coarser the aggregate. Determine FM of the fine aggregate is required to estimate proportions of fine and coarse aggregate according to ASTM C29.

Procedure:

1. Prepare fine aggregates (after they are dried in the over for 24 hours at $110°C$) and measure the weight.
2. Perform screen analysis of the fine aggregates with a series of sieves: No.100, No.50, No.30, No.16, No.8, No.4 and 3/8 in.
3. Record the weight of fine aggregates remain on each sieve.
4. Calculate fineness modules.

The fineness modulus of sands is estimated to be 2.6. According to aggregate per unit weight ASTM C29, for the maximum aggregate size of 0.5 inch with fineness modulus of 2.6, the volume of the dry-rod coarse aggregate per unit volume of concrete is equal to 0.57.

Step 6: Estimation of the fine aggregate content

After completing step 5, all ingredients of the concrete mixtures have been decided except for the fine aggregate. The absolute volume method is used to determine quantity of fine aggregates in which the total volume displaced by the known ingredients (i.e., water, air, cement, and coarse aggregate) is subtracted from the concrete unit volume. This, in turn, is concerted to weight units by multiplying its material density. The associated bulk specific gravity and density of type II cement, fine aggregate and coarse aggregate are listed in table 3.1.

	Type II cement	Fine aggregate	Coarse aggregate
Bulk specific gravity	3.15	2.6	2.7
Bulk density	196	162	168

Table 3. 1 The density of cement, fine aggregate and coarse aggregate

Step 6.1: Adjustments when adding with PCM

When mix PCM fiber reinforced concrete composite, special adjustments has to be made in order to maintain the same concrete unit volume. When adding with PCM, certain amount of fine aggregates and cements will have to be replaced. Since PCM particle is small compared to coarse aggregate, we can treat PCM as cement or sand. For example, if 5% PCM is added into concrete mixture, 5% of cement and sand will have to be replaced.

In order to assure concrete composite strength, how to determine the proportion of cement and sand will be important. There is no standard rule for determining how much amount of sand and concrete need to be replaced. Therefore, trial and error has to be performed. By trying different combination of cement and sand and verify concrete unit weight cannot be lower than a value that is defined by ASTM, the accurate proportion can be decided. In general, for the maximum aggregate size of 0.5 inch, the air entrained concrete unit weight cannot be lower than $3760\,lb/yd^3$.

Step 7: Adjustments for the aggregate moisture

In general, the stock aggregates are either moist or fully dry. Therefore, without moist correction, the actual water-cement ratio of the trial mix will be higher or lower than selected by step 4. The mixture proportions determined from step 1 to step 6 are assumed to be on an SSD (saturated surface dry) basis. As a result, we have to make sure both fine aggregate and coarse aggregate are on an SSD basis.

The fine aggregate that we bought from market is already in SSD basis and there will be no need to do any special treatment. However, all coarse aggregated are stored in the lab for a long time and already are on fully dry state. As a result, the following procedure display how to reach SSD basis for coarse aggregate that will be used in the mixing process:

1. Choose desired coarse aggregates in the concrete mixture.
2. Wash and thoroughly remove dust or other coatings from the surface of particles.
3. Immerse all clean coarse aggregates in water for at least 24 hours before mixing date.
4. Remove all particles from the water and spread them thoroughly in a large absorbent cloth until all visible films of water are removed. (saturated surface dry moisture state)
5. Place the coarse aggregates in a bucket and weight needed amount for mixing.
6. Take coarse aggregates from procedure 5 and mix immediately before the water evaporates.

Step 8: Trail batch adjustments

Due to many assumptions underlying the foregoing theoretical calculations, the mix proportions for the actual materials to be used must be checked and adjusted by means of laboratory trails consisting of small batches.

Finally, the constituents of PCM fiber reinforced concrete are prepared and mixing calculations will be shown in the next.

3.3.2 Mixing Materials

The main components of the concrete mixtures used in this study were cement, sand, coarse aggregate, fly ash and supercizer. In addition, phase change material (PCM), steel fibers and PVA fibers were used to form hybrid fiber reinforced concrete composite. Standard type II Portland cement with specific gravity 3.15 was used. Fine sand with specific gravity of 2.61 and grain size ranging from 105 to 120 μm was used as fine aggregate. Class F fly ash was used in the mixtures to reduce the amount of cement and produce saving in concrete material costs. Three different size of gravel were used as coarse aggregate in the mixtures which included NO. 4 (4.75mm), 3/8 in. (9.5mm) and 1/2 in. (12.7mm). The maximum aggregate size 1/2 in. was chosen based on the economically available and consistent with the dimension of the structure. Adding steel fibers, PVA fibers and PCM will increase difficulty in the mixing process. Therefore, adding water reducer is required to make sure good workability. Superzicer 5 by FRITZ-PAK was used as admixtures.

Steel Fibers

Steel fibers are available with various configurations and sizes, including the round or flat, the straight or corrugated with various end conditions such as straight, hooked end, enlarged or twisted. Efforts have been made to improve the strength of these composites by different methods, including utilizing different fiber shape to provide mechanical anchorage and modification of fiber surface by means of coating or chemical treatment, etc. The mechanical anchorage has been proved to be the most efficient way in practice. It is mentioned that the hooked end fibers offer the best performance in anchorage within concrete matrix. As a result, hooked end steel fibers will be used to increase anchorage.

Steel fibers with a diameter of 0.55mm and length of 35mm were provided by Dramix 65/35 with a tensile strength of 13445 MPa and elastic modulus of 210000 MPa. Figure 3.1 shows steel fibers that will be used in our concrete composite.

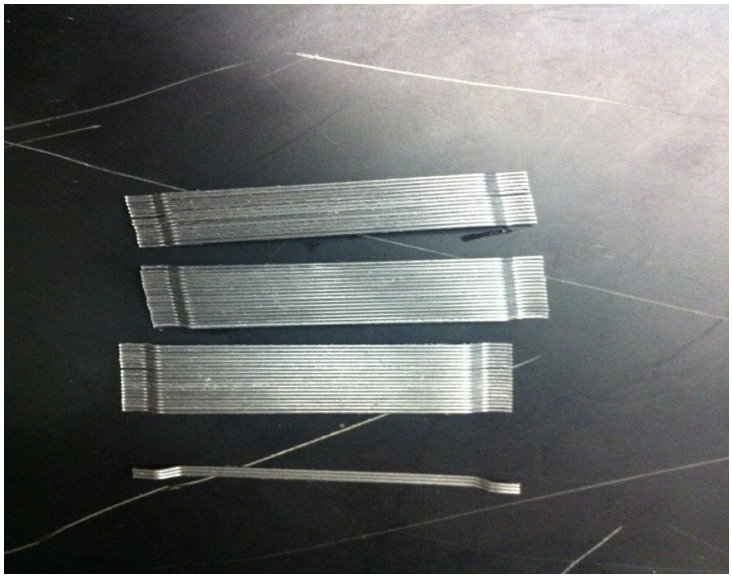

Figure 3.1 Hooked end steel fibers

PVA Fibers

Polyvinyl alcohol (PVA) fiber emerged during a search of low cost high performance fibers for concrete composite. Compared to polypropylene fibers, PVA fibers have stronger tensile strength and composite maximum tensile strength can then be enhanced. However, the hydrophilic nature of PVA fiber imposed great challenge in the composite design, as the fibers are apt to rupture instead of being pulled out because of the tendency for the fiber to bond strongly to concrete matrix. In our research, there are only 0.1% of PVA fibers used in the concrete composit. Therefore, any special treatment will not be made for PVA fibers. For the loss ductile capacity due to its strong bond to concrete matrix, steel fibers will provide enough ductile capacity and fracture toughness.

PVA fibers with a diameter of 39 μm and length of 8mm were added in the mixtures. Figure 3.2 presents the PVA fibers that will be added into our concrete composite. Properties of steel fiber and PVA fiber that are used in this study are listed in table 3.2.

Figure 3.2 PVA fibers

Phase Change Material (PCM)

Phase change material in general can be categorized into organic and inorganic PCMs. From previous researchers, the organic PCM would be the better choice for application in construction because of their better compatibility with concrete material. There are several disadvantages when incorporating PCM into construction material directly.

1) PCM liquid phase will leak everywhere when PCM is melting.
2) PCM will have chemical reaction with construction matrix material and affect the function of building material directly.
3) Decrease the surface area to transfer heat.
4) Easy to break when adding different reinforcing fibers.

By embedding phase change material into a small energy-storing and protecting shell, the thermal capacity can then be enhanced dramatically. This is so called microencapsulated PCM. Figure 3.3 depicts a particle for microencapsulated PCM. The detail of chemical compound and method of how to microencapsulate core material into shell can be found elsewhere.

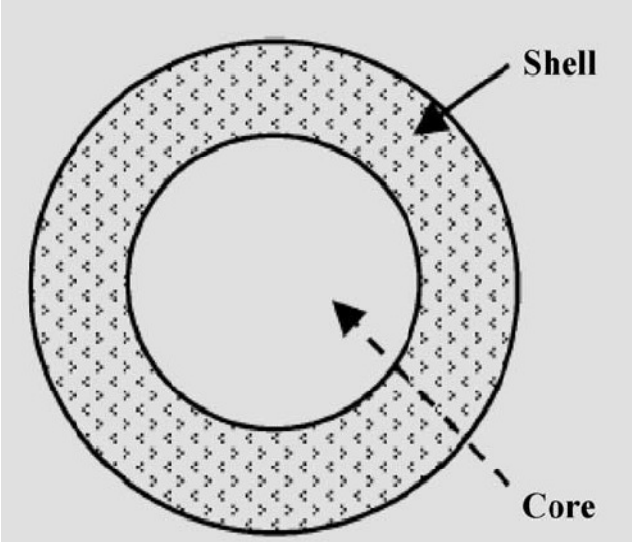

Figure 3.3 Microencapsulated PCM

Phase change material MPCM-6D was manufactured by Microtek Laboratories Inc. The melting point of MPCM-6D is $6\,°C$ $(42.8\,°F)$. The PCM starts to absorb and release energy when temperature reached $6\,°C$ and concrete interior temperature can be controlled in a constant temperature and prevent growth of cracks. PCM was microencapsulated into polymer shell to prevent PCM leaking into concrete matrix.

Fiber Types	Fiber Parameters					
	E_f	L_f	d_f	L_f / d_f	T_f	ρ
	(MPa)	(mm)	(mm)		(MPa)	
Steel	210000	35	0.55	65	1345	490
PVA	42800	8	39	205	1605	81.12

Table 3.2 Fiber material properties

PCM					
	Core	Melting Point	Specific Gravity	Heat of Fusion	Size
MPCM-6D	Paraffin	$6\,°C$	0.6	157-167J/g	17-20 micron

Table 3.3 phase change material properties

3.3.3 Mixing Calculation

The mixing calculation can be computed step by step by following steps in section 3.1. However, following the ASTM standing procedure, the fly ash content is recommend to replace certain amount of cement to reach the goal of environmental friendly and cost reduction. In our concrete composite, 15% of fly ash will be used. The water reducer (supercizer 3) is recommended to be 0.3 to 0.45% of the total cement. Before computing the mixing formula, the characteristics of the material are listed below:

1. Portland cement: Type II
2. Fly ash: Class F coal ash. (15% of the cement mass)
3. Water reducer: Supercizer 3 (FRITZ-PAK Inc.)
4. Maximum size of aggregate: 0.5 in.
5. Slump: 1.5 to 3 in. (For fiber reinforced concrete)
6. Water type: Tap water.
7. Specified 28-day compressive strength: 4000 psi.
8. w/c: 0.43.

Calculation Steps:

1) Determine final mixed concrete volume (8 cylinders and 4 beams) = 0.2327 in^3.
2) Apply safety factor = 0.2327*1.1= 0.256 in^3.
3) Pre-assumed cement content = 900 lbs.
4) Water-cement ratio = 0.43.
5) Mixing water content = 387 lbs.
6) Volume fraction of gravel on dry-rod basis = 0.57*27= 15.39 ft^3

   Weight of gravel = 15.39*100 = 1539 lbs.
7) Applying absolute volume method:

   Volume of water = 387/62.4 = 6.202 ft^3.

   Volume of cement = 900/196 = 4.592 ft^3.

   Volume of gravel = 1539/168 = 9.161 ft^3.

   Volume of air = 27*0.025 = 0.675 ft^3

Total = 20.629 ft^3.

Volume of sand = 27-20.629 = 6.371 ft^3.

Weight of sand = 162*6.371 = 1032.025 lbs.

8) Following the ASTM standard.

9) Table 3.4 shows a breakdown of the coarse aggregates weight for different sizes.

Aggregate size	Weight (lbs)
0.5 in. (55%)	8.0256
3/8 in. (30%)	4.3776
NO. 4 (15%)	2.1888
Total weight	14.592

Table 3.4 The break down for coarse aggregate weight for different sizes

Sample batch for 1% steel fiber and 0.1% PVA fiber volume fraction:

All calculations computed from above is a sample batch for 1% steel fiber and 0.1% PVA fiber with 8 cylinders in size of $4"X\ 8"$ for both compressive test and splitting tension test and 4 rectangular beams in size $4"X\ 4"X14"$ for three point bending test. The volume designed for this batch is 0.256 ft^3. For 1% steel fiber volume fraction is 0.00256 in^3 and the density is 490 lb/ft^3 then the weight is 1.2544 lb. For 0.1% PVA fiber volume fraction is 0.000256 in^3 and the density is 81.12 lb/ft^3 then the weight is 0.021 lb.

The final proportion can be obtained as follows:

Cement = 7.893 lb

Fly ash = 1.28 lb

Sand = 10.314 lb

Gravel = 14.592 lb

Water = 3.804 lb

Water reducer = 0.032 lb

Steel fiber = 1.2544 lb

PVA fiber = 0.021 lb

Total = 37.883 lb

3.3.4 Mixing Procedure

Four different mixture proportions are investigated in this chapter. Each mix has been specified with type of reinforcing fibers, fiber volume fraction and PCM volume fraction as shown in table 3.5. Mixing calculation can be computed step by step from aforementioned absolute volume method. The water/cement ratio was 0.43 for all composite, the fly ash content is recommended to be approximately 15% of the cement mass. The water reducer is 0.35% to ensure good workability.

All of the mixtures were prepared in a standard mixer to produce all specimens. Since PCM particles are small and easy to break during mixing process. Dry mix with sand and PCM first to make sure PCM distribute uniformly. The dry ingredients which include sand, gravel, PCM, PVA fibers and steel fibers were mixed first until a homogeneous mixture was reached. After mixing all dry ingredients, next step would be followed by adding cement and fly ash and dry mix in about 1 minute. This step was followed by adding water and supercizer and only half of them were introduced into the mixer with a mixing time in about 1 minute. In the end, adding the remaining water and supercizer and mix in about three minutes or until all ingredients mixed homogeneously.

Slump test is required to make sure concrete reaches good workability. If the slump is in between 1.5 to 3 in., concrete inside of mixer is ready to pour into mold.

Composite	W/C Ratio	Steel Fiber (%)	PVA Fiber (%)	PCM (%)
00PC	0.43	0	0	0
FRC	0.43	1	0.1	0
5MFRC	0.43	1	0.1	5
7MFRC	0.43	1	0.1	7

Table 3.5 Reinforcing materials proportions

3.3.5 Test Specimens

In each type of concrete, there are 28 cylinders with dimensions $4" X\ 8"$ were cast for different concrete testing. In addition, there are 12 concrete beams in each composite with dimensions $4" X\ 4" X\ 14"$ were also prepared for different testing.

Four cylinders will be used in compressive test to measure 7 days compressive strength and four cylinders will be tested as 28 days compressive strength. Four specimens will be used in splitting tension test to study the concrete tensile strength. There are four beams will be used in three point bending test to study concrete flexural behavior and load-CMOP relationship.

The rest of specimens will be prepared for the freeze-thaw test. There are 16 cylinders in each type of concrete composite will be used for freeze-thaw test and ultrasonic test. Eight beams will be used for freeze-thaw test as well. Details regarding freeze-thaw test and other destructive tests will be discussed in the following section.

All specimens were de-molded after 24 hours from either beam steel mold or plastic cylinder mold. Thereafter, they were cured in the curing tank with lime stone water and temperature was kept in about $23°C$. After reaching 28 days, all specimens will be removed from curing tank and ready for testing.

3.3.6 Compressive Test

In order to see the compressive strength when adding hybrid fibers and PCM, compression tests are conducted. Tests for each type of concrete composite followed ASTM C192/C192M-07. Compressive load is applied on cylinder utilizing hydraulic pressure from MTS machine with displacement control until failure occurred. Four cylinders for each type of concrete will be tested first to get 7 days strength and four cylinders with be testes after 28 days curing to get concrete full strength. Figure 3.4 illustrates the compressive test set-up.

Figure 3.4 Compression test set-up

3.3.7 Splitting Tension Test

Splitting tension test was conducted to study the material's ability to resist a diametric compressive force. This testing is important when the concrete has to meet a minimum strength requirement (ASTM C496/C496M-04e1). The cylindrical material specimen is placed with its axis placed horizontally between the platens of a test machine. A relatively low and uniform force is applied on the test specimen until splitting occurs. Displacement control is also applied in this test. Figure 3.5 shows the splitting tension test set-up.

Figure 3.5 Splitting tension test set-up

3.3.8 Three Point Bending Test

Three point bending test is considered the most important test in studying and analyzing the behavior and ductile capacity of hybrid fibers reinforced concrete composite. Four notched $4"X\ 4"X\ 14"$ beam specimens were tested under three point bending on a free span of 12''. Notch depth is 1" and 0.1" wide. ASTM C1609/C1609M-06 was followed for implementing three point bending test. With pre-formulated notch on beam specimen, it will be easy to observe the formation and propagation of crack. Figure 3.6 shows the testing set-up.

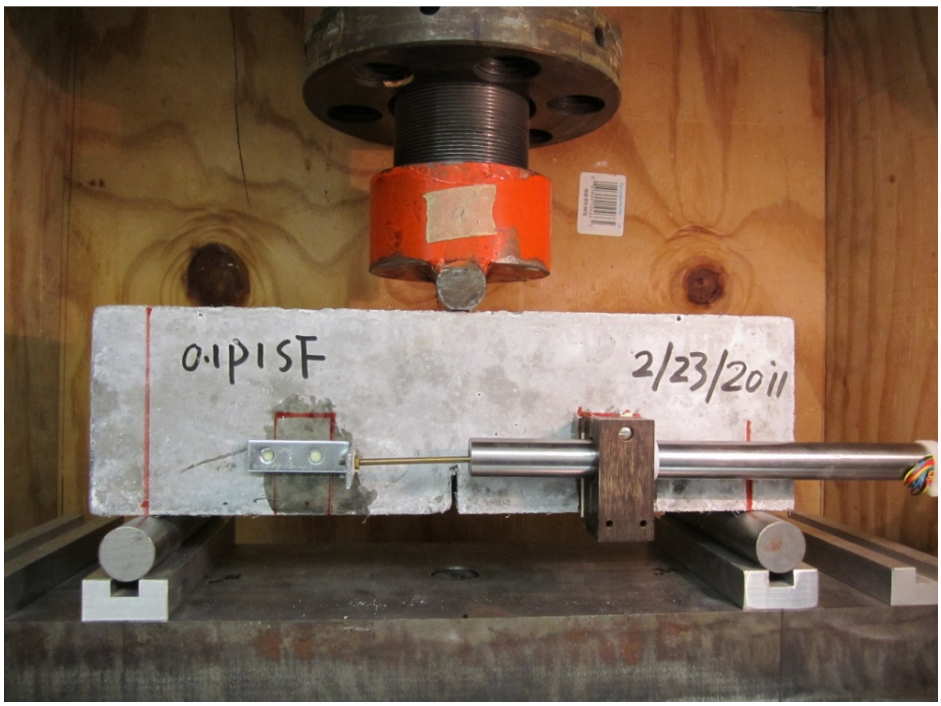

Figure 3.6 Three point bending test set-up

3.3.9 Freeze-Thaw Test

Freeze-thaw test was performed by following "New York State Department of Transportation Materials Bureau, NY 216-73". However, ASTM C666 procedure B was also referenced in this study. Two freezers were prepared for freeze-thaw test. Each cylinder was kept into 6"x12" cylindrical mold and filled with water during the freezing phase. Four beams were put in a plastic container and completely surrounded by air during the freezing phase of the cycle followed by ASTM C666 procedure B. There were 16 concrete cylindrical specimens and 4 beams were kept in one freezer during freezing phase. The other 16 cylinders and 4 beams were put in a tank which completely surrounded by water during the thawing phase.

There are twelve hours for the freezing phase and 12 hours for the thawing phase in one day. In other words, one day represents one cycle of freeze-thaw test. There are four different batches of concrete to be tested. As a result, two freezers will be used at the same time. When one batch of concrete performs freezing phase, the other batch of concrete performs thawing phase. Both freezers can freeze all specimens down to -23$^{\circ}C$. Figure 3.7 shows specimens in the freezing process in the freezer and Figure 3.8 presents specimens in the thawing process in the water tank.

Half of the specimens will be taken out for destructive tests on 100 cycles of freeze-thaw test and see if there is any effect through freeze-thaw test. The rest of specimens will be taken out on 340 cycles. In every 40 cycles, specimens will be tested by ultrasonic test to determine dynamic elastic modules. Mass loss will be measure as well.

Controlled specimens for each type of concrete will be prepared and immerse into water tank until 340 cycles. When concrete specimens submerge in the water and perform freeze-thaw test, concrete strength will actually develop in the early age. In the beginning of freeze-thaw test, the damage inside of concrete is not significant and strength gaining due to water curing would need to be considered. Therefore, controlled specimens have to be prepared and tested and compare the strength of destructive tests in 100 cycles and 340 cycles of freeze-thaw test.

Figure 3.7 Specimens in the freezing process

Figure 3.8 Specimens in the thawing process

3.4 Results and Discussions

3.4.1 Compressive Strength

Test results of compressive strength for each specimen are presented in table 3.6. We can observe that when concrete adding steel fibers and PVA fibers, composite compressive strength is obviously higher than plain concrete. Since PVA fiber would bridge micro-cracks in an early age, the cracks growth would then be controlled. Thereafter, the maximum compressive strength would be increased.

Results also showed that FRC adding with PCM would decrease composite compressive strength. When adding more and more PCM, the amount of strength loss is more and more significant. In the mixing design, replacement method was used when incorporating with PCM. Certain amount of sand and cement were replaced by PCM. As a result, the interfacial shear stress between matrix and fibers would then be decreased because microencapsulated PCM did not provide any stiffness. Composite compressive strength would then be decreased due to weaker fiber bridging stress.

However, the amount of deduction is still acceptable. From table 3.6, we can observe that compressive strength for both 5MFRC and 7MFRC are still higher than 4 ksi of normal concrete.

		Max. load(Kips)			Max. load(Kips)
00PC	Sample 1	67.21	5MFRC	Sample 1	67.62
	Sample 2	62.75		Sample 2	61.53
	Sample 3	70.46		Sample 3	63.7
	Sample 4	70.1		Sample 4	67.86
	Average	67.63		Average	65.18
	STD	3.56		STD	3.09
	C.O.V (%)	5.27		C.O.V (%)	4.74
FRC	Sample 1	95.07	7MFRC	Sample 1	62.94
	Sample 2	83.83		Sample 2	64.44
	Sample 3	87.33		Sample 3	60.27
	Sample 4	93.18		Sample 4	57.07
	Average	89.85		Average	61.18
	STD	5.19		STD	3.24
	C.O.V (%)	5.79		C.O.V (%)	5.29

Table 3.6 Results of compression test

3.4.2 Tensile Strength

In the previous study, concrete has been proved that it is stronger in compression and weaker in tension. As a result, plain concrete would have low tensile strength compared to its compressive strength. When concrete is incorporated with fibers, tensile strength can then be improved by fibers bridging stress. Figure 3.9 showed that plain concrete performed after splitting tension test. Figure 3.10 illustrated concrete adding fibers tested after splitting tension test. We can see that the damage for plain concrete is severe because there are no fibers can provide bridging force.

Results of splitting tension test for each specimen are presented in table 3.7. We can observe that concrete adding with hybrid fibers can provide significant bridging stress and thus increase the tensile strength compared to plain concrete. The increased of tensile strength is about 41%. In addition, tensile strength of composite incorporated with PCM would be reduced because interfacial resistant force between fibers and matrix is weaker. However, tensile strength for both 5% and 7% PCM hybrid fibers reinforced concrete are still higher than plain concrete. As a result, we can conclude that the tensile performance for PCM reinforced concrete is still acceptable even though some tensile strength would need to be sacrificed.

Figure 3.9 Splitting tension test for plain concrete

Figure 3.10 Splitting tension test for concrete with fibers

		Max. load(Kips)			Max. load(Kips)
00PC	Sample 1	26.11	5MFRC	Sample 1	29.95
	Sample 2	25.90		Sample 2	27.14
	Sample 3	19.79		Sample 3	28.28
	Sample 4	23.37		Sample 4	24.7
	Average	23.79		Average	27.52
	STD	2.94		STD	2.2
	C.O.V (%)	12.38		C.O.V (%)	8.01
FRC	Sample 1	49.34	7MFRC	Sample 1	25.66
	Sample 2	39.29		Sample 2	26.16
	Sample 3	33.44		Sample 3	18.21
	Sample 4	39.76		Sample 4	27.64
	Average	40.46		Average	24.42
	STD	4.22		STD	6.55
	C.O.V (%)	17.29		C.O.V (%)	16.13

Table 3.7 Results of splitting tension test

3.4.3 Flexural Performance

As mentioned previously, concrete composite ductile capacity could be considered as the most important property. The typical load versus crack mouth opening displacement (CMOP) would be recorded and the results are shown from Figure 3.11 to Figure 3.14. We can observe that concrete without any reinforcement would have brittle damage mode. After concrete reaches

its own maximum bending stress, the applying load will suddenly drop to zero capacity and concrete will break into half as shown in Figure 3.11. Both hybrid fiber reinforced concrete and hybrid fiber PCM concrete will perform better ductile capacity due to fiber pull-out. From the comparison of the flexural responses of the plain concrete and other fiber reinforced concrete composites, it can be seen that beyond the maximum bending stress, the applying load gradually decreases due to fiber bridging. We can also observe from Figure 3.15 that plain concrete will not perform any ductile behavior after reaching maximum applied force and will break into half. From Figure 3.16, we can see that concrete with fibers can perform extensive ductile behavior ever after the maximum applied force has reached.

Unfortunately, the time was limited to complete the three point bending test and to reach zero capacity. Therefore, a third order nonlinear inverse polynomial was used in order to perform curve fitting from the end of stress-displacement curve to zero capacity.

$$y(x) = a_0 \frac{1}{x^3} + a_1 \frac{1}{x^2} + a_2 \frac{1}{x} + a3 \tag{3.1}$$

By using the curve fitting tool box built in MATLAB, four constants can be obtained.

The ultimate goal is to determine the composite fracture energy from the stress-CMOP relationship. The fracture energy from three point bending test was derived from the area under the stress-CMOP curve. The trapezoidal rule will be used to calculate fracture energy.

Since every experiment was completed with different times, the fracture energy that was calculated cannot reflect the actual behavior. For example, the data of fiber reinforced concrete were stopped when displacement reached about 5 inched and the data of 7% PCM fiber reinforced concrete was stopped when displacement reached about 1.4". Therefore, the fracture energy calculated from the first case was larger in general compared to the fracture energy from

the latter case. As a result, COMD that reached 1.4” in was chosen as a standard point. The fracture energy was calculated by taking the area underneath the stress-COMD relationship when COMD reached 1.4” in for all types of concrete.

Calculated fracture energy from three point bending test for each specimen is presented in table 3.8. We can observe that the fracture energy for plain concrete is low compared to fiber reinforced concrete or fiber reinforced PCM concrete. It proves that ductile capacity for plain concrete is poor and basically no ductile elongation after composite reaches the maximum tensile stress. In addition, the calculated fracture energy shows the similar results as compressive strength and splitting tension test that the fracture energy for FRC is the highest. Fracture energy for 5% and 7% PCM fiber reinforced concrete will not as high as FRC because replacement method was used in the mixing process. However, both 5% and 7% FRC still can perform better ductile behavior than plain concrete. Therefore, we can conclude that the ductile capacity for PCM reinforced concrete is still acceptable even though some fracture energy would need to be sacrificed.

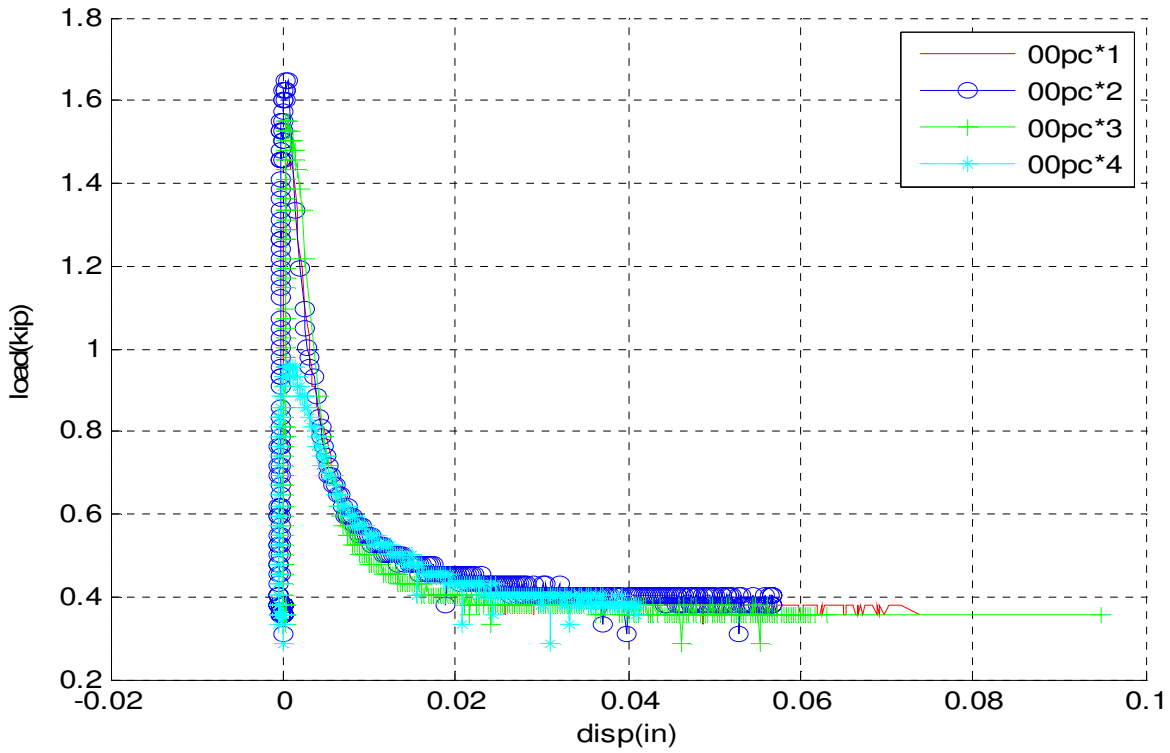

Figure 3.11 00PC load v.s CMOP

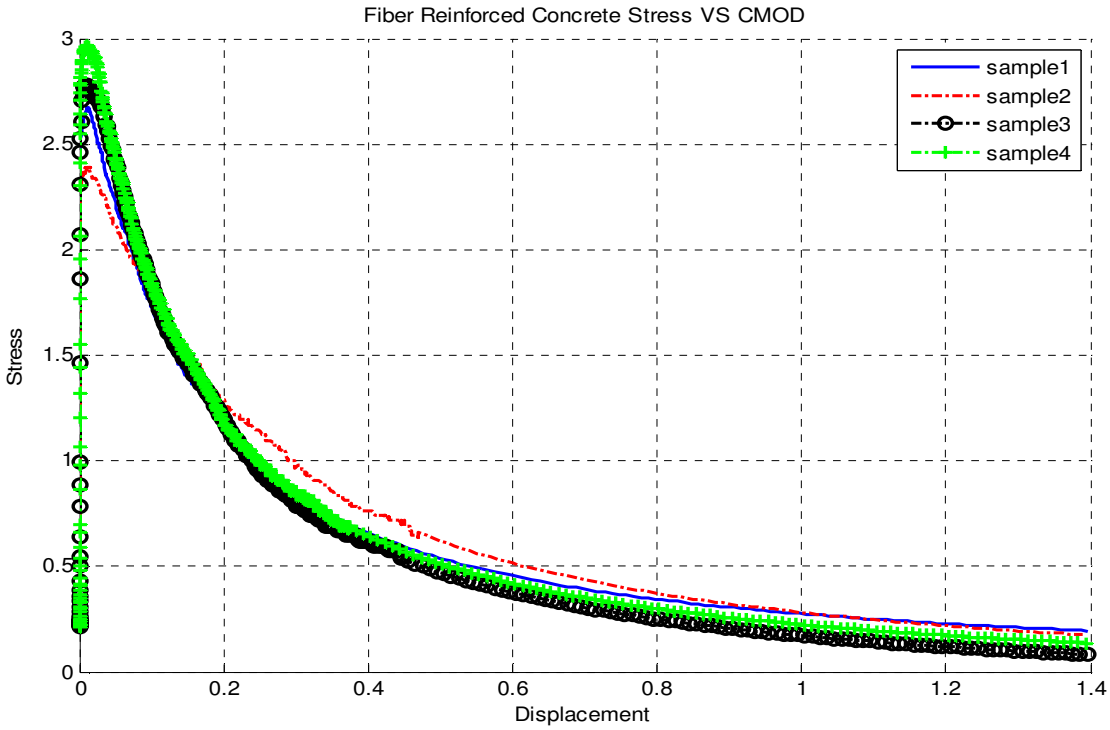

Figure 3.12 FRC load v.s CMOP

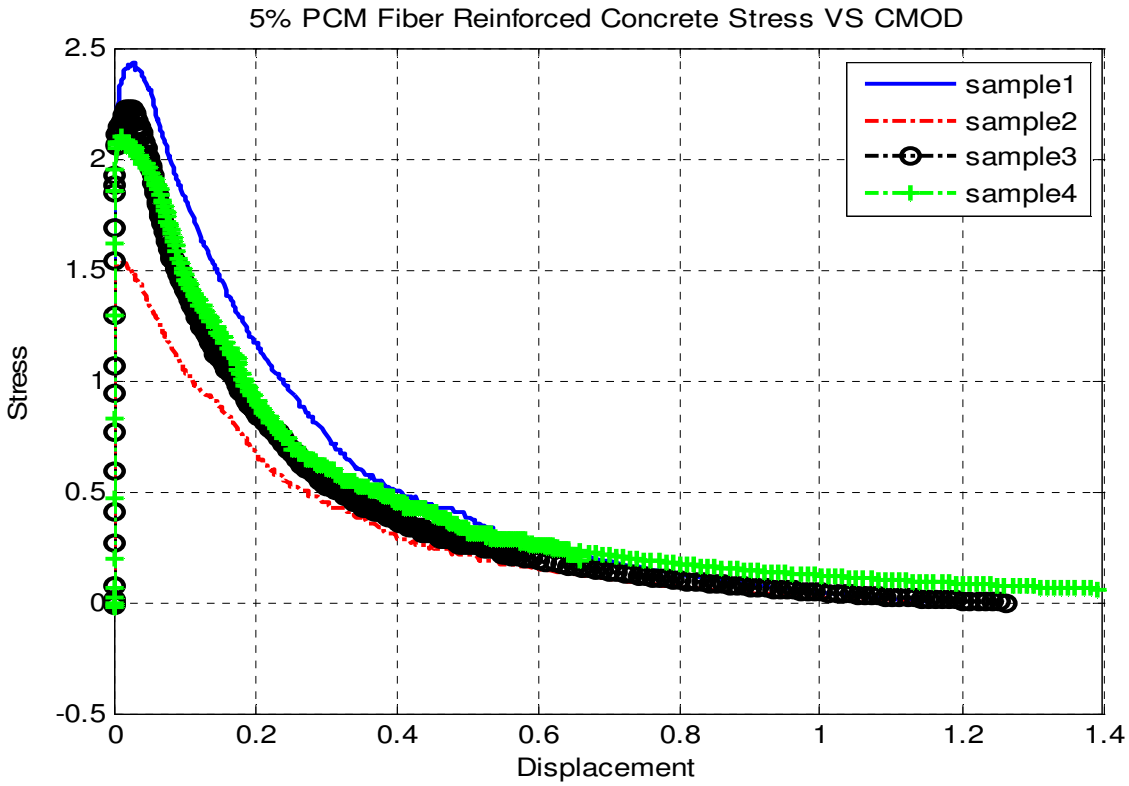

Figure 3.13 5MFRC load v.s CMOP

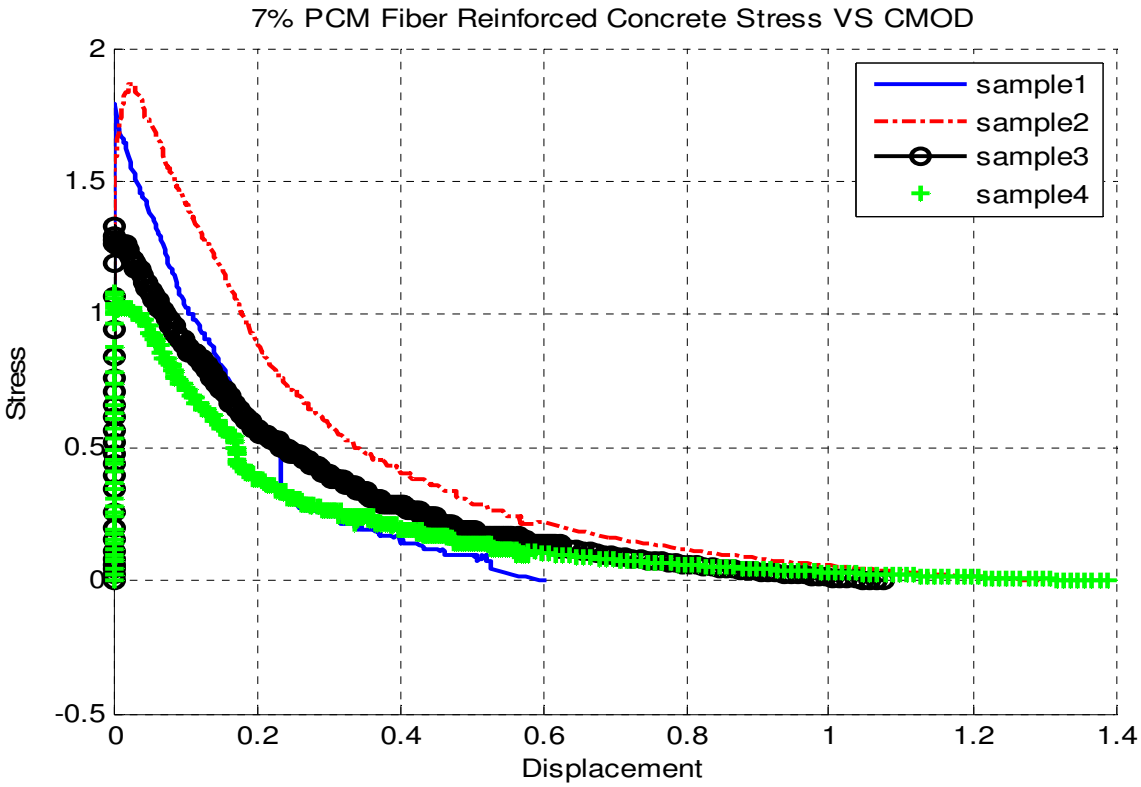

Figure 3.14 7MFRC load v.s CMOP

		Fracture Energy (N.mm)			Fracture Energy (N.mm)
00PC	Sample 1	3891.4	5MFRC	Sample 1	74345
	Sample 2	3263.9		Sample 2	43747
	Sample 3	4581.5		Sample 3	58478
	Sample 4	2364.5		Sample 4	68765
	Average	3525.3		Average	61334
	STD	942.6		STD	13441
	C.O.V (%)	26.7		C.O.V (%)	21.9
FRC	Sample 1	99184	7MFRC	Sample 1	32851
	Sample 2	104690		Sample 2	59087
	Sample 3	90354		Sample 3	37221
	Sample 4	97397		Sample 4	29550
	Average	97908		Average	39677
	STD	5914		STD	13316
	C.O.V (%)	6.04		C.O.V (%)	33.6

Table 3.8 Results of Fracture Energy from Three Point Bending Test

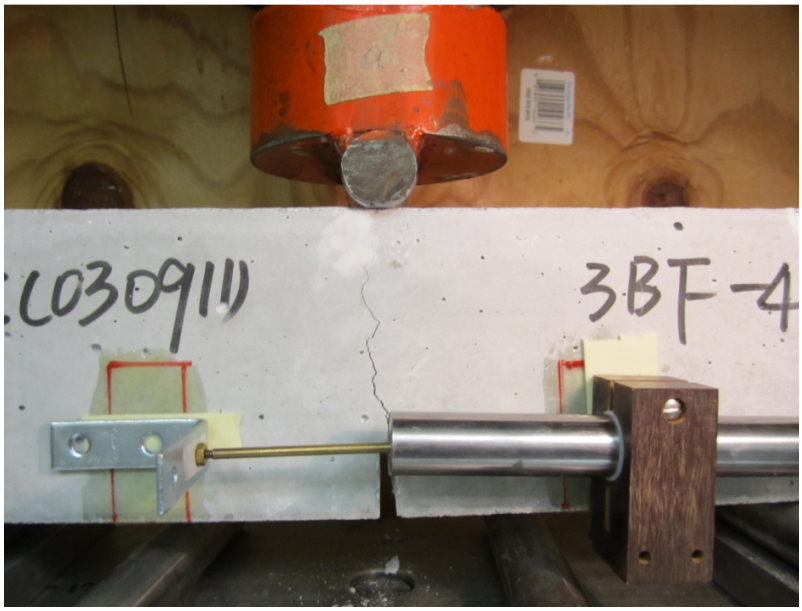

Figure 3.15 Plain concrete after performing three point bending test

Figure 3.16 Concrete with fibers after performing three point bending test

3.4.4 Freeze-Thaw Resistance

In order to evaluate the freeze-thaw resistance of 00PC, FRC, 5MFRC and 7MFRC, two material properties have been measured. The mass of the specimens was measured and recorded in every 40 cycle of freeze-thaw test. The loss of the relative dynamic modulus of elasticity was also measured at various staged of the freeze-thaw cycles. The variation in mass loss and dynamic modulus of elasticity is essentially the same for all type of concrete after 340 cycles of freeze-thaw test. Figure 3.17 shows the set up for ultrasonic test.

The mass loss for all types of concrete basically can be neglected. Some concrete surface scaling phenomenon can be observed in plain concrete. However, with hybrid fibers providing bridging stress and PCM controlling concrete interior temperature, mass measurement is essentially the same after freeze-thaw test. Figure 3.18 to Figure 3.25 depicts the results of mass loss measurement for four different kinds of concrete after 340 cycles of freeze-thaw test. There are eight specimens were measured in each concrete batch and we can observe that there is no significant mass loss in either plain concrete or concrete with fibers and PCM.

Figure 3.26 to Figure 3.29 demonstrates the recorded dynamic modulus with respect to the number of freeze-thaw cycles for different concrete batch. P-wave speed was recorded from ultrasonic test and the variation in the P-wave velocity expressed in terms of the relative dynamic modulus of elasticity, E_d, is defined by the following equation:

$$V^2 = \frac{E_d(1-\nu)}{\rho(1+\nu)(1-2\nu)} \tag{3.2}$$

where E_d is the dynamic elastic Young's modulus, ν is the Poisson's ratio and ρ is the mass density.

The dynamic modulus can then be expressed in terms of P-wave speed, Poisson's ratio and mass density.

$$E_d = \frac{V^2 \rho (1+\nu)(1-2\nu)}{(1-\nu)} \tag{3.3}$$

We can observe that from Figure 3.26 to Figure 3.29, there are no significant changes on dynamic modulus of elasticity and they generally follow the same pattern after 340 cycles of freeze-thaw test. This experimental result and previous studies, such as [41], [33] and [38] show that different kinds of concrete composite with different reinforcing admixture can survive more than 300 cycles of freeze-thaw test without deterioration of the dynamic modulus.

Figure 3.17 Set up for ultrasonic test

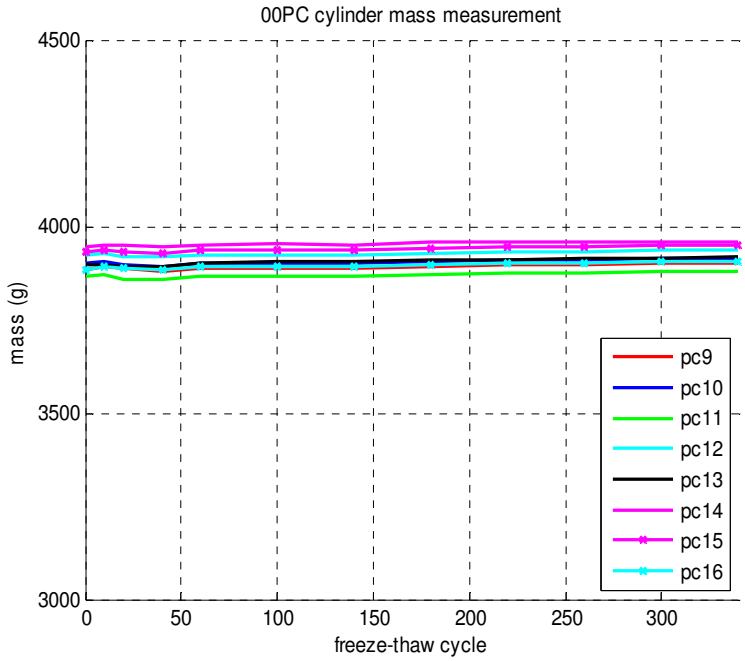

Figure 3.18 Mass measurement of cylinders for plain concrete

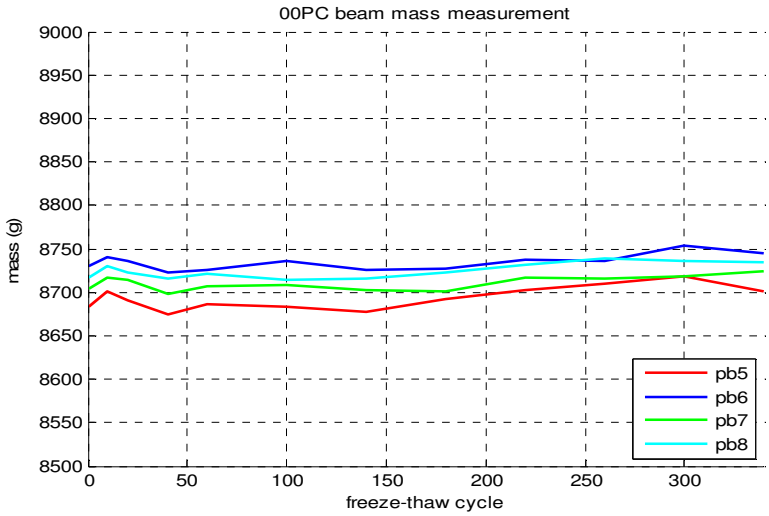

Figure 3.19 Mass measurement of beams for plain concrete

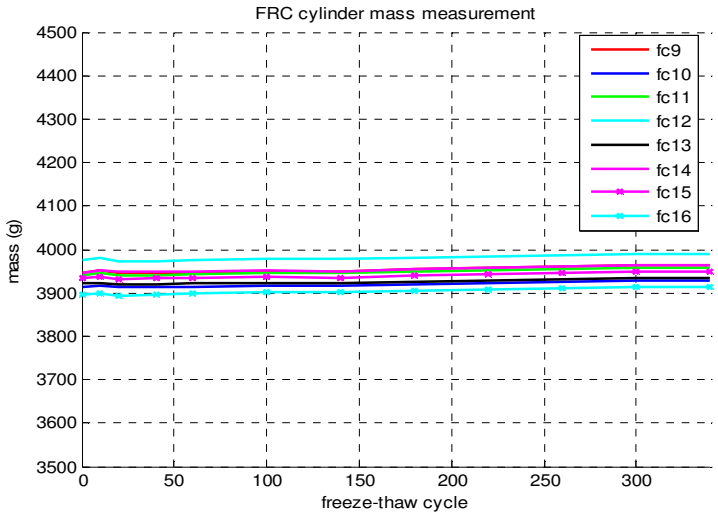

Figure 3.20 Mass measurement of cylinders for fiber reinforced concrete

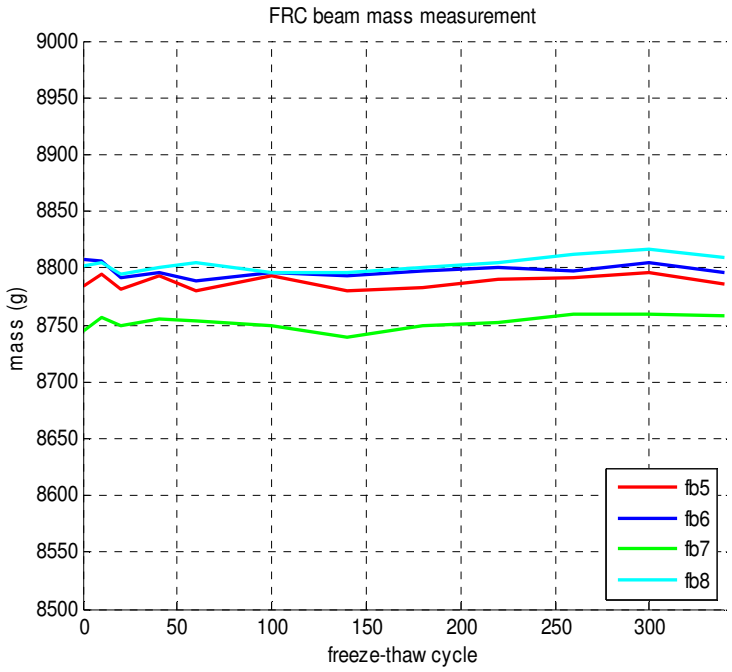

Figure 3.21 Mass measurement of beams for fiber reinforced concrete

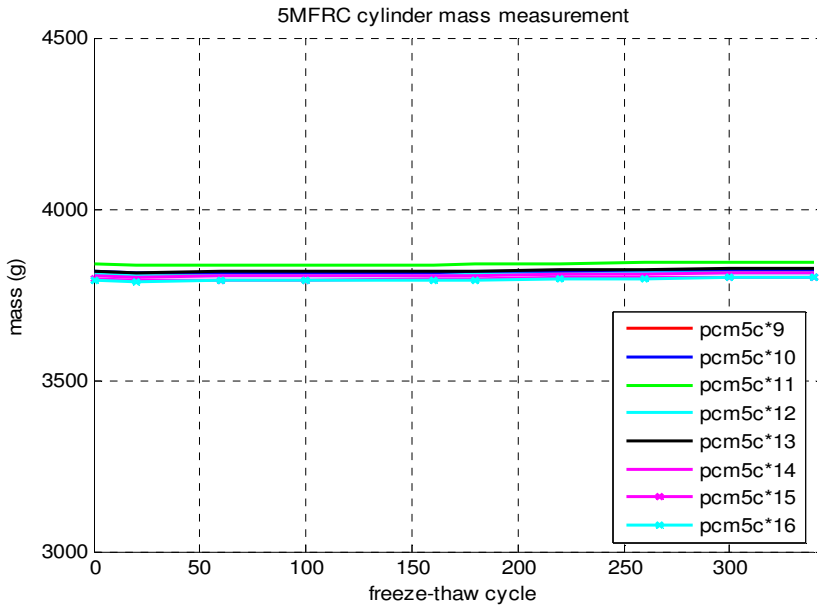

Figure 3.22 Mass measurement of cylinders for 5% PCM fiber reinforced concrete

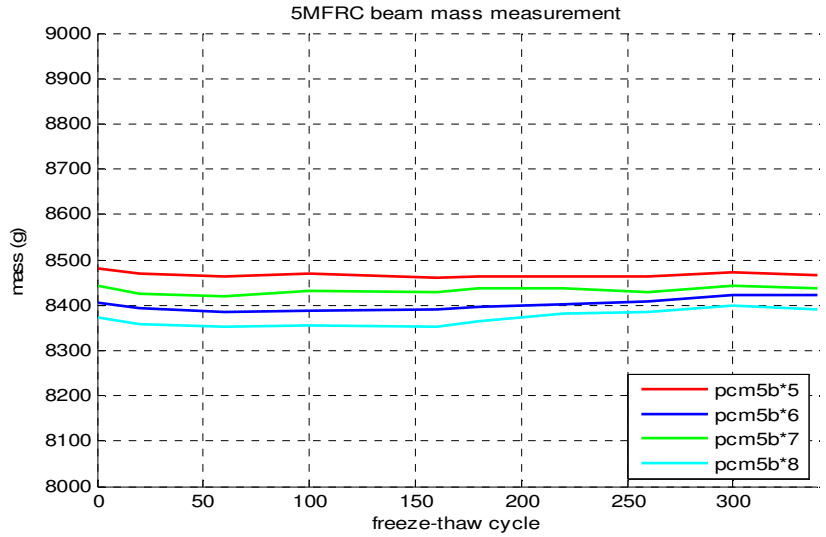

Figure 3.23 Mass measurement of beams for 5% PCM fiber reinforced concrete

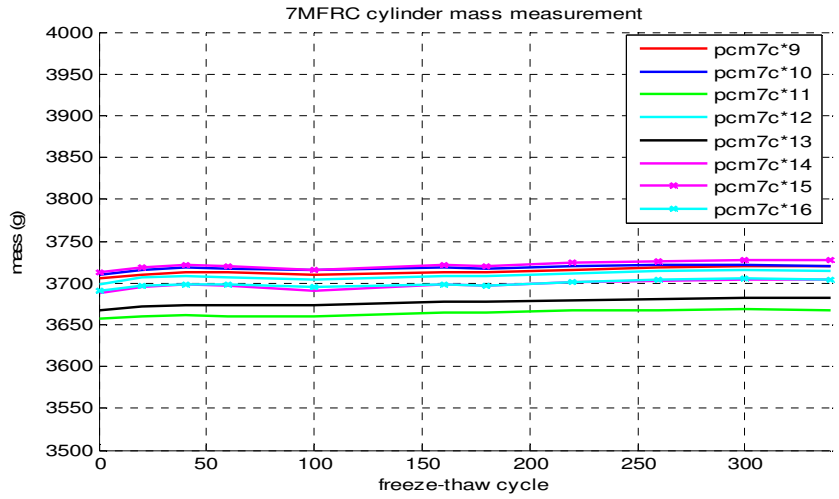

Figure 3.24 Mass measurement of cylinders for 7% PCM fiber reinforced concrete

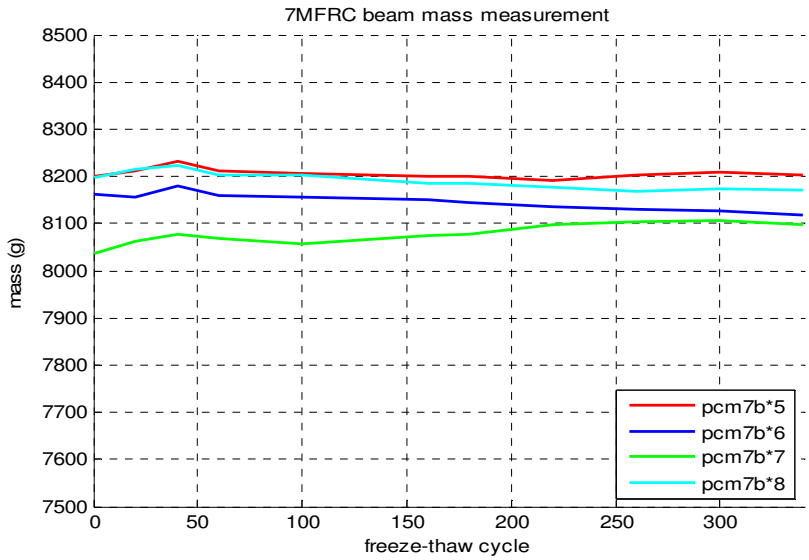

Figure 3.25 Mass measurement of beams for 7% PCM fiber reinforced concrete

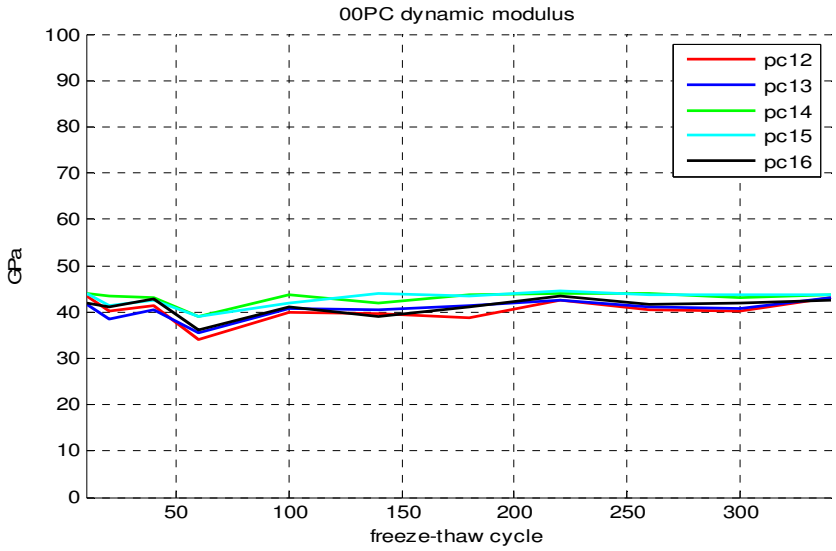

Figure 3.26 Dynamic modulus for plain concrete

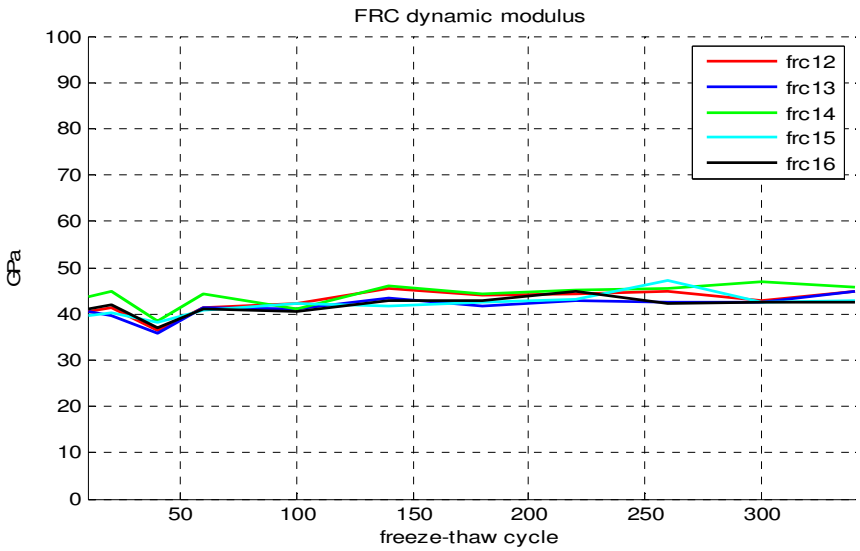

Figure 3.27 Dynamic modulus for fiber reinforced concrete

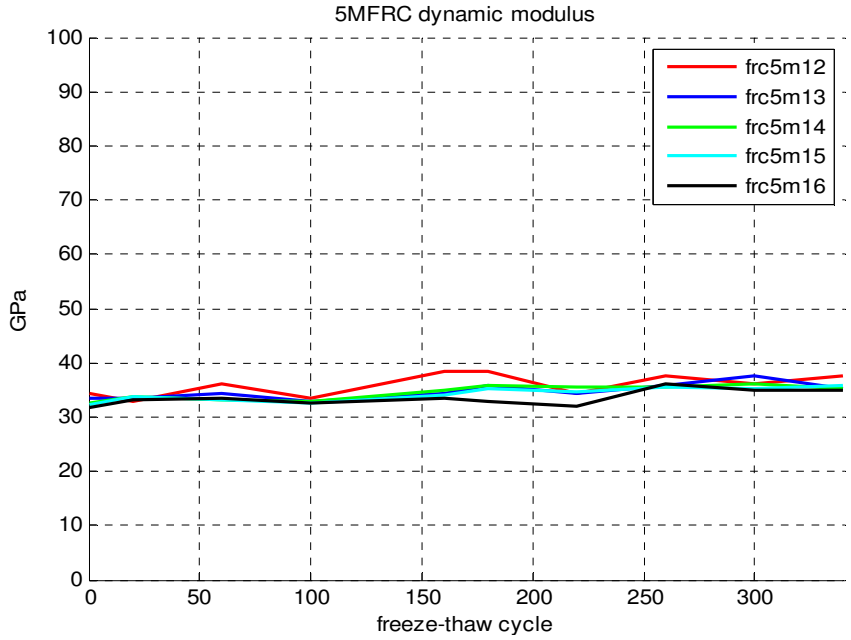

Figure 3.28 Dynamic modulus for 5% PCM fiber reinforced concrete

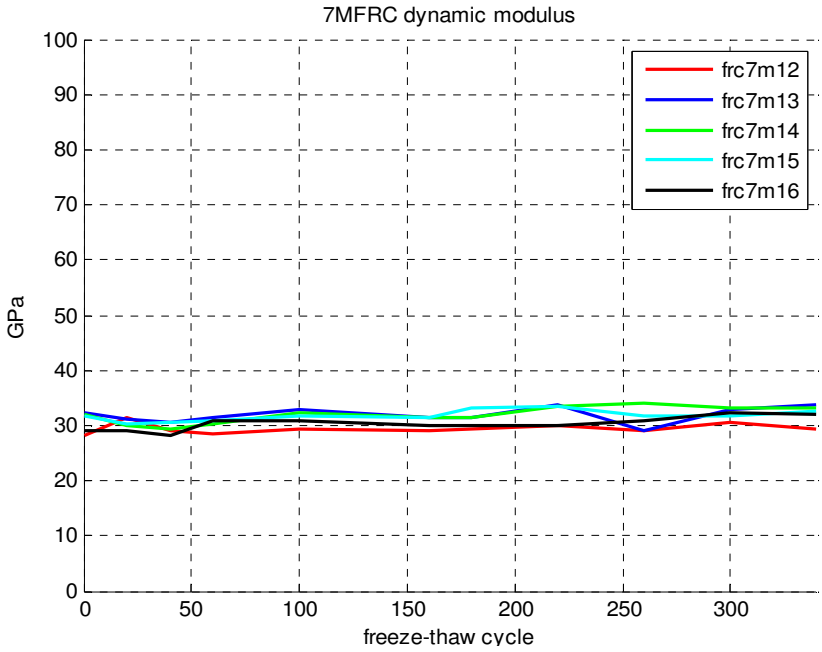

Figure 3.29 Dynamic modulus for 7% PCM fiber reinforced concrete

In 100 cycles of freeze-thaw test, destructive tests are also performed to see if there is any difference regarding concrete strength after performing freeze-thaw test. Half of the specimens are taken out for destructive tests and half of the controlled specimens are also tested as well.

Table 3.9 shows the compressive strength after 100 cycles of freeze-thaw test. It also shows that the comparison between freeze-thaw specimens and controlled specimens.

		Max. load(Kips)			Max. load(Kips)
00PC	Sample 1	82.42	5MFRC	Sample 1	70.77
	Sample 2	83.49		Sample 2	65.49
				Sample 3	66.31
				Sample 4	68.49
	Average	82.96		Average	67.015
	STD	0.76		STD	2.37
	C.O.V (%)	0.91		C.O.V (%)	3.49
	Controlled	78.7		Controlled	79.64
FRC	Sample 1	101.87	7MFRC	Sample 1	61.2
	Sample 2	113.11		Sample 2	67.79
	Sample 3	107.05		Sample 3	71.29
	Sample 4	102.54		Sample 4	67.5
	Average	106.14		Average	66.95
	STD	5.24		STD	4.2
	C.O.V (%)	4.92		C.O.V (%)	6.3
	Controlled	110.24		Controlled	64.86

Table 3.9 Compressive strength after 100 cycles of freeze-thaw test

We can observe that the difference of compressive strength between controlled specimens and freeze-thaw specimens are not too significant. As a result, it can prove that all concrete specimens do not have significant damage after 100 cycles of freeze-thaw test and it is consistent with the results from ultrasonic test and mass loss measurement. From destructive test, it can provide another point of view to observe the influence on concrete specimens after performing freeze-thaw test.

However, we can observe that the difference between 5% PCM fiber reinforced concrete and its corresponding controlled specimen is about 16%. This could be the error since only one controlled specimen was tested. Splitting tension test might be able to provide better comparison. As we know, concrete will gain compressive strength when curing in the water. Therefore, the error will exist between controlled specimens and testing specimens. However, concrete will not be able to gain significant tensile strength when curing in the water.

3.5 Conclusions

Mechanical properties, such as compressive strength, composite splitting tensile strength, composite flexural properties and thermal performance under freeze-thaw test on the of plain concrete, fiber reinforced concrete, 5% and 7% PCM fiber reinforced concrete composite are investigated in this study. Several destructive tests have been done to verify concrete composite strength and flexural capacity. Freeze-thaw test has also been performed to investigate the frost resistance. The results of the investigation are summarized in the following:

1) When adding with PCM, concrete composite compressive strength will reduce since certain amount of sand and cement will be replaced. Results show that the compressive strength for PCM concrete is lower than fiber reinforced concrete without adding PCM and slightly lower than plain concrete. However, they are still stronger than normal concrete which strength is about 4Ksi.
2) For splitting tensile strength, 5% and 7% PCM fiber reinforced concrete perform better strength than plain concrete. The same as compressive strength, adding PCM will reduce the tensile strength of composite. However, adding fibers can provide tensile strength to bridge tensile force and compensate the loss when adding PCM.
3) Flexural capacity of concrete composite can be discussed from load-CMOP relationship and fracture energy calculation. We can observe from load-CMOP curve that concrete composite with fibers and PCM perform extensive ductile behavior after reaching the maximum applied load. However, plain concrete would not perform any ductile behavior after reaching maximum load and the load-COMP curve suddenly drop to zero. Therefore, the brittle damage mode when reaching maximum applied force can be prevented for PCM fiber reinforced concrete composite. Fracture energy can then be calculated from load-COMP curve. The results show that fracture energy for both 5% and 7% PCM fiber reinforced concrete are still larger compared to plain concrete. Therefore, the flexural capacity for concrete composite adding phase change material can be guaranteed.
4) Freeze-thaw resistance can also be validated from two criterions, the relative dynamic modulus of elasticity and mass loss measurement. The value of the relative elastic dynamic modulus obtained from ultrasonic test after 340 freeze-thaw cycles does not have significant change for all different kinds of concrete composite. In addition, mass

loss is also recorded in every 40 cycles of freeze-thaw test and up to 340 cycles. It is observed that the mass loss follows the same pattern and do not have any significant mass loss. Some concrete surface scaling phenomena did observe during the freeze-thaw test due to lack of fiber bridging. However, in general, after 340 cycles of freeze-thaw test, concrete can still keep good freeze-thaw resistance.

5) Destructive tests after performing freeze-thaw test are also investigated. The results show that there are not significant changes for compressive strength, splitting tensile strength.

From results of various tests, we have learned that concrete composite would become weaker when adding phase change material. With adding more and more PCM, more and more cement and sand have to be replaced to keep the mixing formula correct and concrete strength would then be reduced. Therefore, adding fibers can not only increase concrete composite strength and compensate the loss of cement and sand, but also increase the composite ductile capacity.

Based on the manufacture, phase change material can have different melting point. As a result, we can apply PCM into concrete and control concrete interior temperature by choosing different melting point. In the cold climate region, lower melting point PCM can be applied into concrete composite and to minimize cracks after everyday freeze-thaw cycles. 5% and 7% PCM have been adopted into our fiber reinforced concrete composite. The results show that concrete composite with PCM can still perform enough strength and ductile capacity. The most important thing is that they are still superior when endure freeze-thaw cycles after 340 days. Adding PCM more than 7% will not be recommended because more cement and sand will have to be replaced. In that case, the loss of strength will be significant and will be lower than plain concrete.

3.6 References

[1] ACI Committee 544, ACI 544. IR-82, "State-of-the-art report on fiber reinforced concrete", Concr. Int. (1982) 9-30.

[2] ACI Committee 363 (1984), "State-of-the-art report on high-strength concrete", ACI Journal, Proceedings V.81, No. 4, pp.363-411.

[3] ACI Committee 210R-87 (1987), "Erosion of concrete in hydraulic structures", ACI Materials Journal, Vol.84, No. 4, pp.136-157.

[4] ACI Committee 544 (1988), "Measurement of properties of fiber reinforced concrete", ACI Materials Journal, V.85, No. 6, pp.583-589.

[5] ACI Committee 544 (1988), "Design considerations for steel fiber reinforced concrete", ACI Materials Journal, V.85, No. 6, pp.563-580

[6] ACI Committee 544 (1993), "Guide for specifying, mixing, placing, and finishing steel fiber reinforced concrete", ACI Materials Journal, V.90, No. 6, pp.94-101

[7] ACI Committee 211 (1991), "Standard practice for selecting proportions for normal, heavyweight, and mass concrete", ACI Materials Journal, pp.1-91

[8] ASTM C 1018 , "Standard test methods for flexural toughness and first crack strength fiber reinforced concrete", ASTM, V4.02, No. 6, pp.637-644

[9] ASTM, "Standard specification for steel fibers for fiber reinforced concrete", ASTM 820-96, ASTM, Philadelphia, (1996), 3pp

[10] ASTM E399-08 , "Standard test method for linear-elastic plane-strain fracture toughness of metallic materials", pp.491-509

[11] ASTM C666/C666M-03 (2008), "Standard test method for resistance of concrete to rapid freezing and thawing", pp.349-354

[12] Arisoy, B., and Wu, H. C. (2008). "Material characteristics of high performance lightweight concrete reinforced with PVA." *Construction and Building Materials*, 22(4), 635-645.

[13] Banthia, N., and Sappakittipakorn, M. (2007). "Toughness enhancement in steel fiber reinforced concrete through fiber hybridization." *Cement and Concrete Research*, 37(9), 1366-1372.

[14] Bayes-Garcia, L., Ventola, L., Cordobilla, R., Benages, R., Calvet, T., and Cuevas-Diarte, M. A. (2010). "Phase Change Materials (PCM) microcapsules with different shell compositions: Preparation, characterization and thermal stability." *Solar Energy Materials and Solar Cells*, 94(7), 1235-1240.

[15] Bencardino, F., Rizzuti, L., Spadea, G., and Swamy, R. N. (2010). "Experimental evaluation of fiber reinforced concrete fracture properties." *Composites Part B-Engineering*, 41(1), 17-24.

[16] Bentz, D. P., and Turpin, R. (2007). "Potential applications of phase change materials in concrete technology." *Cement & Concrete Composites*, 29(7), 527-532.

[17] Cabeza, L. F., Castellon, C., Nogues, M., Medrano, M., Leppers, R., and Zubillaga, O. (2007). "Use of microencapsulated PCM in concrete walls for energy savings." *Energy and Buildings*, 39(2), 113-119.

[18] Chen, B., and Liu, J. Y. (2005). "Contribution of hybrid fibers on the properties of the high-strength lightweight concrete having good workability." *Cement and Concrete Research*, 35(5), 913-917.

[19] Ding, Y. N., You, Z. G., and Jalali, S. (2010). "Hybrid fiber influence on strength and toughness of RC beams." *Composite Structures*, 92(9), 2083-2089.

[20] Hunger, M., Entrop, A. G., Mandilaras, I., Brouwers, H. J. H., and Founti, M. (2009). "The behavior of self-compacting concrete containing micro-encapsulated Phase Change Materials." *Cement & Concrete Composites*, 31(10), 731-743.

[21] Kuznik, F., David, D., Johannes, K., and Roux, J. J. (2011). "A review on phase change materials integrated in building walls." *Renewable & Sustainable Energy Reviews*, 15(1), 379-391.

[22] Li, V. C. (2002). "Large volume, high-performance applications of fibers in civil engineering." *Journal of Applied Polymer Science*, 83(3), 660-686.

[23] Li, V. C., Lin, Z., and Matsumoto, T. (1998). "Influence of fiber bridging on structural size-effect." *International Journal of Solids and Structures*, 35(31-32), 4223-4238.

[24]] Li, V. C., and Stang, H. (1997). "Interface property characterization and strengthening mechanisms in fiber reinforced cement based composites." *Advanced Cement Based Materials*, 6(1), 1-20.

[25] Meshgin, P., and Xi, Y. P. (2012). "Effect of Phase-Change Materials on Properties of Concrete." *Aci Materials Journal*, 109(1), 71-80.

[26] Nelson, P. K., Li, V. C., and Kamada, T. (2002). "Fracture toughness of microfiber reinforced cement composites." *Journal of Materials in Civil Engineering*, 14(5), 384-391.

[27] NYSDOT Materials Bureau 502-3P (1986), "Test method for slow freezing and thawing", NY 216-74, pp.1-4.

[28] Passuello, A., Moriconi, G., and Shah, S. P. (2009). "Cracking behavior of concrete with shrinkage reducing admixtures and PVA fibers." *Cement & Concrete Composites*, 31(10), 699-704.

[29] Pasupathy, A., Athanasius, L., Velraj, R., and Seeniraj, R. V. (2008). "Experimental investigation and numerical simulation analysis on the thermal performance of a building roof incorporating phase change material (PCM) for thermal management." *Applied Thermal Engineering*, 28(5-6), 556-565.

[30] Pasupathy, A., Velraj, R., and Seeniraj, R. V. (2008). "Phase change material-based building architecture for thermal management in residential and commercial establishments." *Renewable & Sustainable Energy Reviews*, 12(1), 39-64.

[31] Qian, C. X., and Stroeven, P. (2000). "Fracture properties of concrete reinforced with steel-polypropylene hybrid fibres." *Cement & Concrete Composites*, 22(5), 343-351.

[32] Redon, C., Li, V. C., Wu, C., Hoshiro, H., Saito, T., and Ogawa, A. (2001). "Measuring and modifying interface properties of PVA fibers in ECC matrix." *Journal of Materials in Civil Engineering*, 13(6), 399-406.

[33] Sahmaran, M., Lachemi, M., and Li, V. C. (2009). "Assessing the durability of engineered cementitious composites under freezing and thawing cycles." *Journal of ASTM International*, 6(7), JAI102406 (102413 pp.)-JAI102406 (102413 pp.)JAI102406 (102413 pp.).

[34] Schossig, P., Henning, H. M., Gschwander, S., and Haussmann, T. (2005). "Micro-encapsulated phase-change materials integrated into construction materials." *Solar Energy Materials and Solar Cells*, 89(2-3), 297-306.

[35] Shao, Y. X., Li, Z. J., and Shah, S. P. (1993). "Matrix cracking and interface debonding in fiber-reinforced cement-matrix composites." *Advanced Cement Based Materials*, 1(2), 55-66.

[36] Toutanji, H., Xu, B., Gilbert, J., and Lavin, T. (2010). "Properties of poly(vinyl alcohol) fiber reinforced high-performance organic aggregate cementitious material: Converting brittle to plastic." *Construction and Building Materials*, 24(1), 1-10.

[37] Tyagi, V. V., Kaushik, S. C., Tyagi, S. K., and Akiyama, T. (2011). "Development of phase change materials based microencapsulated technology for buildings: A review." *Renewable & Sustainable Energy Reviews*, 15(2), 1373-1391.

[38] Wang, S., " Micromechanics based matrix design for engineered cementitious composites", Ph.D. thesis, University of Michigan, 2005.

[39] Ying, C., and Pizhong, Q. (2011). "Crack Growth Resistance of Hybrid Fiber-Reinforced Cement Matrix Composites." *Journal of Aerospace Engineering*, 24(2), 154-161161.

[40] Yun, H. D., Kim, S. W., Lee, Y. O., and Rokugo, K. (2011). "Tensile behavior of synthetic fiber-reinforced strain-hardening cement-based composite (SHCC) after freezing and thawing exposure." *Cold Regions Science and Technology*, 67(1-2), 49-57.

[41] Yun, H. D., and Rokugo, K. (2012). "Freeze-thaw influence on the flexural properties of ductile fiber-reinforced cementitious composites (DFRCCs) for durable infrastructures." *Cold Regions Science and Technology*, 78, 82-88.

[42] Zhang, J., and Li, V. C. (2004). "Simulation of crack propagation in fiber-reinforced concrete by fracture mechanics." *Cement and Concrete Research*, 34(2), 333-339.

[43] Zhang, M., Medina, M. A., and King, J. B. (2005). "Development of a thermally enhanced frame wall with phase-change materials for on-peak air conditioning demand reduction and energy savings in residential buildings." *International Journal of Energy Research*,29(9),795-809.

Chapter 4 Crack Bridging and Ductile Behavior in Fiber Reinforced Concrete with Phase Change Material

4.1 Introduction

From previous study, adding fibers to a cementitious composite can significantly increase ductile capacity and fracture toughness. Additionally, energy storing capacity is also increased. In cold region where concrete undergoes a freeze-thaw process everyday, micro cracks can occur inside of the concrete matrix. Therefore, adding fibers can control crack width by the mechanism of fiber bridging. In addition, concrete temperature can be controlled by adding phase change material (PCM) that absorbs and releases thermal energy.

In the mixing process, a replacement method was used when mixing fiber reinforced concrete with PCM. As a result, a certain amount of sand and cement were replaced by PCM. As expected, the compressive strength, tensile strength and fracture toughness decreased. Thus, it is important to find a balance between effective thermal control and concrete strength. Understanding concrete ductile behavior when adding PCM is the most important topic addressed in this chapter.

Over the past years, micromechanics models for fiber reinforced cementitious composites have evolved gradually. A constant shear model was proposed by Li [23] to develop a crack bridging model. This model can be used to predict fiber debonding and fiber pull-out behavior. However, there were several discrepancies observed with the constant shear model, especially

for fiber matrix systems with a strong slip hardening interface. In some cases, the constant shear model underestimated fracture toughness compared with experimental data. Some researchers showed that interfacial shear stress depends on the slippage distance between fiber and matrix. Wang [37] suggested that to have increasing interfacial shear stress with slippage distance was necessary for nylon and polypropylene fibers in order to match the experimental result. For randomly distributed and randomly oriented discontinuous fiber reinforced cementitious composites, Li [25] developed a crack bridging model based on the linear slip hardening model. In this model, the interfacial shear stress between the matrix and fiber is linear along with slippage distance. Therefore, fracture toughness is also increased when increasing slippage distance.

Phase change materials can be made of a polymer material and does not provide any additional strength and stiffness between fiber and matrix. Therefore, lower interfacial shear stress should be expected when increasing slippage distance. Some researchers have shown that the fiber can perform sliding with slip hardening, constant friction or a slip softening effect, characterized by the coefficient β. As a result, the β value could be positive, zero or negative.

In general, slip softening interface shear stress can be attributed from PCM properties and deduction of fine aggregates. In fact, slip softening behavior can occur in the fiber pull-out process.

The temperature inside fiber reinforced concrete with phase change material can be controlled effectively after a performing freeze-thaw test of a few hundred cycles. However, the deduction of concrete strength and ductile behavior including fracture toughness should also be taken into account. As a result, this chapter focuses on determining fiber bridging behavior of

discontinuous fiber/concrete matrix systems after adding phase change material. A simple interface constitutive relationship is presented to address slip softening behavior. Aggregate bridging behavior will also be discussed and fracture energy due to contribution from aggregate bridging will then be calculated. Theoretical models for single fiber debonding and pull-out load will be constructed first based on the linear slip softening model. Slip softening interface shear stress is derived based on the linear interface constitutive relationship. A crack bridging model will then be constructed that accounts for random fiber orientation and fiber snubbing effect. Fracture energy will be evaluated based on the crack bridging model. In addition, adding PVA fibers will also increase the maximum tensile stress because PVA fibers can bridge micro-cracks and control the growth of micro-cracks. As a result, a theoretical model will also be proposed to simulate the maximum applied force.

The validity of the crack bridging model will be evaluated based on fracture energy. Fracture energy will be compared with experimental data that includes 1% steel fiber, 0.1% PVA fiber and 5% PCM or 7% PCM reinforced concrete to illustrate the effects of slip softening interface behavior. Conclusions will be addressed at the end of this chapter.

4.2 Modeling of Fiber Pull-out in PCM Fiber Concrete Composite

4.2.1 Poisson's Effect

When a fiber is pulled out from the concrete matrix by an applied load, a triaxial stress state exists at the fiber-matrix interface due to the radial contraction of the fiber. This effect of radial fiber radial contraction is so called Poisson's effect and was discussed by Kelly and

Zweben, Pinchm, Baggott and Gandhi [4]. They have shown that for certain types of fibers (i.e.polypropylene), the pull-out process will involve unstable debonding. In addition, the experimental results from Baggott and Gandhi [4] show that a slight misalignment in the specimen and the asperities of the fiber surface could offset Poisson's effect. However, an unstable load drop was not observed in the fiber pill-out process for polypropylene fibers during experiments by Wang [37]. As a result, Baggott and Gandh concluded that Poisson's effect can be neglected in the fiber pull-out process and a one-dimensional model is sufficient to describe the fiber pull-out behavior.

4.2.2 Elastic Bond and Frictional Bond Effect

Debonding occurs when the maximum shear stress reaches the elastic bond strength (τ_s). The shear stress in the debonded region can then be determined by the frictional bond strength (τ_i). Gopatatnum and Shah [11] showed that both elastic bond strength (τ_s) and frictional bond strength (τ_i) are important parameters to characterize the debonding process before fiber pull-out as well as for determining the conditions for unstable debonding. Li, Wang and Backer [37] showed that the effect of the elastic bond strength on the overall pull-out process is not always significant. During the debonding process, the shear stress intensity in the elastically bonded region decays approximately exponentially with the distance from the debonding point, with the maximum stress reaching the elastic bond strength (τ_s). For low modulus fibers or even high modulus fibers with high aspect ratios, the elastic stress field has relatively little effect on the overall pull-out process except at the very early age of fiber debonding. Li [23] provided a

calculation example for load-displacement curve for both $\tau_s = 2\tau_i$ and $\tau_s = 0$ are compared with cases where $E_f / E_m = 10$, but with different fiber lengths. They have shown that there is no significant effect of elastic bond strength on the pull-out load-displacement relationship with different embedded lengths. They also showed that for a lower E_f / E_m ratio or a higher fiber aspect ratio, the elastic bond strength effect is even less. After complete debonding, the elastic bond strength has no consequential effect. As a result, in most cases, the pull-out analysis can be simplified by neglecting the elastic stress field.

Frictional bond strength τ_i is a function of slippage distance (S) between the fibers and the concrete matrix during the fiber pull-out process. The effect of the variation of frictional bond strength with slippage distance was discussed by Wang and Li [37]. With the addition of different fibers and different matrix characteristics, frictional bond strength τ_i can be increased, remain constant or decreased with increasing slippage distance. Li [25] has shown that by using a constant shear model between fiber and matrix can describe the fiber pull-out process. In this chapter, the theoretical model will take into consideration the linear slip-softening interfacial shear stress in order to describe the fiber pull-out process more accurately.

4.2.3 Comparing Strength-Based and Fracture-Based Debond Modes

To study and understand fiber debonding behavior is important because it affects the fiber reinforced concrete composite. A proposed theoretical model needs to be consistent with a realistic description of the debonding behavior of fibers. There are two different approaches that have been developed to describe the fiber debonding problem: strength-based and fracture-based approaches. In a strength-based approach, fiber debonding takes place once the limit of interfacial bond strength is reached. In a fracture-based approach, the debonded interfacial zone is regarded as a tunnel crack that grows in length once the limit for interfacial toughness is exceeded at the crack tip. Since fiber debonding and interfacial bond properties play an important role in micromechanical models of fiber reinforced concrete composite, it is necessary to establish the appropriate debonding mode for a given material system.

Two parameters are usually used to describe the interfacial bond properties of fiber reinforced concrete composite due to the characteristics of fiber debonding and pull-out process. For the strength-based approach, interfacial bond strength and frictional stress are adopted. For the fracture-based approach, an interfacial critical release rate and frictional stress are used.

To determine whether interfacial debondiing is governed by the bond strength of the critical energy release rate of the fiber-matrix interface, Li and Chan [20] did a fiber pull-out experiment using steel fibers with various diameters. They interpreted bond properties, including effective bond strength and frictional stress, using a theoretical model of the fiber pull-out. Based on the experimental results, they found that interfacial frictional stress was independent of fiber

diameter, and dominated interfacial debonding. This result proved that the debonding mode of a fiber reinforced concrete system is strength-based. In addition, frictional stress is found to be a dominant bond property and a single parameter is sufficient to describe interfacial debonding in a composite model.

Li and Chan [20] also found that the debond mode is not necessarily related to the location of the interfacial debonding, whether it is at the fiber-cement interface or at the interfacial zone. In order to predict the pull-out response of fiber reinforced concrete composite, it is necessary to determine the debonding mode for the particular material system supporting the methodology proposed for this research.

4.2.4 Model Assumptions

In order to derive the following theoretical model, some assumptions will have to be made.

1. The matrix crack is planar.
2. The matrix deformation is negligible during fiber pull-out.
3. The fibers are randomly oriented and randomly distributed.
4. The fibers are straight between the hooks.
5. The fibers have cylindrical geometry for both straight and hook-end elements.
6. The fibers behave linear elasticity.
7. No fibers rupture during the debonding and pull-out process.
8. No Poisson's ratio effect during pull-out.

9. Debond mode control is strength-based, rather than fracture based.
10. The fiber-matrix bond is frictional and the elastic bond strength is neglected.
11. A snubbing coefficient f is introduced to account for fiber angle effect.

4.3 Aggregate Bridging

Contribution from aggregate bridging action should also be considered as part of fracture energy in the entire fiber bridging process. Because concrete is made of multi-phases material, it is difficult to determine the physical parameter based on the complicated micro-structure. Since a good theoretical model is lacking, an empirical model should be adopted as proposed by previous researcher, such as Stang [30]. Aggregated bridging stress is expressed as a function of the crack opening w:

$$\sigma_a = \frac{\sigma_m^u}{1+(w/w_0)^p} \tag{4.1}$$

Where σ_m^u is the maximum bridging stress due to aggregate action when w=0. P is a material parameter that describes the shape of the softening process with an increasing crack opening. ρ has been determined to be close to unity for most concrete. w_0 is 0.015mm. σ_m^u = 3.4 MPa for normal strength concrete and σ_m^u =5.0 MPa for high strength concrete. For fiber reinforced concrete with phase change material, a lower σ_m^u will be used in this chapter.

4.4 Interface Constitutive Relationship

To understand the slip softening behavior between fibers and matrix, a model need to be proposed to correlate slippage distance S and resistant shear stress τ. A convenient polynomial form was proposed by previous researcher, such as Li and Stang [21].

$$\tau(s) = \tau_0 + a_1 s + a_2 s^2 \tag{4.2}$$

Normally, effects from both fiber and PCM are coupled. Therefore, both strain hardening and strain softening effect will both need to be included. However, in this chapter, we assumed strain softening effect dominate since PCM weaken the interface between concrete matrix and fiber. For simplicity, a simple two parameters linear model is proposed, which describes the relation between slippage distance and resistant shear stress.

$$\tau = \tau_0 (1 - \beta \frac{S}{d_f}) \tag{4.3}$$

where τ_0 is the frictional sliding shear stress at the tip of the debonding zone when $s = 0$, β is a dimensionless strain softening parameter and d_f is the fiber diameter. It should be noted that both τ_0 and β need to be determined experimentally from a single fiber pull-out test. Li [25] showed that frictional sliding shear stress τ_0 at the tip of the debonding zone is approximately 2-4 MPA for steel fibers and β is between 0.01-0.04; both are for a slip hardening interface case. Some researchers, such as Redon and Li [29] also showed that τ_0 for PVA fiber is between 2.7-5.9 MPA and β is between 0.4-2.5.

It is important to note that equation (4.3) is the basic frame work for deriving subsequent theoretical modeling, such as single fiber debonding and pull-out load, debonding and pull-out stress and fracture energy contributed from fiber debonding and a pull-out process. Equation (4.3) might require additional higher order terms to more accurate describe interface shear stress. However, with a small slippage distance, equation (4.3) is sufficient to describe the fiber interface behavior without a loss of accuracy.

4.5 Single Fiber Debonding and Pullout Analysis

The main objective of this section is to study and provide a numerical evaluation of the fibers debonding and the pull-out process embedded within a concrete matrix with phase change material.

Consider a single fiber loaded with a force P at one end, resisted by a slip interfacial shear stress τ along entire length L and embedded in a cement matrix. Fibers debonding are activated due to load P. Debonding length l is increased along with load P until it reaches its maximum value L. Fiber pull-out will be assumed after fibers completely debond without any fiber rupture. The effect of Poisson's ratio and elastic bond between the fiber and matrix are neglected.

Following the research of Marshel and Bao and Song [5], a cylindrical model is proposed to derive slippage distance S. The model's compatibility condition states that when in the bonded zone, the axial strain for fiber ε_f and for matrix ε_m will be the same.

$$\varepsilon_f = \varepsilon_m \tag{4.4}$$

Neglecting Poisson's effect,

$$\frac{\sigma_f}{E_f} = \frac{\sigma_m}{E_m} \tag{4.5}$$

Where σ_f and σ_m refers to the stress in the fiber and the matrix, respectively.

The balance of axial forces within the matrix and the fibers gives

$$\sigma_m = \frac{\pi d_f l \bar{\tau}}{A_m} \tag{4.6}$$

And

$$\sigma_f = \frac{P - \pi d_f l \bar{\tau}}{A_f} \tag{4.7}$$

where A_f and A_m are the cross section area of the fiber and matrix, respectively. l is the debonded zone length and $\bar{\tau}$ is the average interfacial shear stress.

$$\bar{\tau} = \frac{1}{l}\int_0^l \tau(z)dz \tag{4.8}$$

We then set

$$\sigma_m = \sigma_f \tag{4.9}$$

From equation (4.4) to (4.9), the axial force can be expressed as:

$$P = \pi d_f l \overline{\tau}(1+\eta) \tag{4.10}$$

The slip interfacial distance can be defined as the relative displacement between the fiber and the matrix, and can be expressed as:

$$S(z) = u_f(z) - u_m(z) \tag{4.11}$$

Hence

$$\frac{dS}{dz} = \varepsilon_f(z) - \varepsilon_m(z) \tag{4.12}$$

It is important to note that the local equilibrium requires the following condition:

$$\frac{d\sigma_f(z)}{dz} = \frac{d}{dz}\left(\frac{P - \pi d_f l \overline{\tau}}{A_f}\right) \tag{4.13}$$

Which is further calculated as:

$$\frac{d\sigma_f(z)}{dz} = \frac{4}{d_f}\tau(S) \tag{4.14}$$

And

$$\frac{d\sigma_m(z)}{dz} = -\frac{\pi d_f}{A_m}\tau(S) \tag{4.15}$$

By differentiating equation (4.12) and combining (4.14) and(4.15), the following governing equation for slippage distance S is as follows:

$$\frac{d^2 s}{dz^2} = \frac{4(1+\eta)}{E_f d_f}\tau(s) \tag{4.16}$$

$$\tau = \tau_0(1-\beta\frac{S}{d_f}) \tag{4.17}$$

$$\eta = \frac{V_f E_f}{V_m E_m} \tag{4.18}$$

where E_f and E_m are Young's modulus for fiber and matrix respectively. V_f and V_m are the volume fractions for fiber and matrix respectively.

Slippage distance S can be solved from equations (4.16), (4.17) and (4.18).

$$S(z) = \frac{d_f}{\beta}\left[1-\cos\left(\frac{\omega z}{d_f}\right)\right] \tag{4.19}$$

$$\tau(z) = \tau_0 \cos\left(\frac{\omega z}{d_f}\right) \tag{4.20}$$

$$\omega = \sqrt{\frac{4(1+\eta)\beta\tau_0}{E_f}} \tag{4.21}$$

From equations(4.19), (4.20) and(4.21), load P for the fiber debonding stage can be derived as follows:

$$P = \frac{\pi d_f^2 \tau_0 (1+\eta)}{\omega}\sqrt{1-\left(1-\frac{\beta\delta}{2d_f}\right)^2} \qquad for\ 0 \le \delta \le \delta_0 \tag{4.22}$$

$$\delta_0 = \frac{2d_f}{\beta}\left[1-\cos\left(\frac{\omega z}{d_f}\right)\right] \tag{4.23}$$

δ_0 represents the displacement when the debonding process is completed along the entire embedded fiber segment.

In the fiber pull-out stage, the fiber-matrix slip distance can be approximated as:

$$S(z) = \frac{d_f}{\beta}\left[1 - \cos\left(\frac{\omega z}{d_f}\right)\right] + (\delta - \delta_0) \tag{4.24}$$

And

$$\tau = \tau_0(1 - \beta\frac{S}{d_f}) \tag{4.25}$$

The following is then calculated:

$$\tau(z) = [\tau_0 \cos\left(\frac{\omega z}{d_f}\right) + \frac{\beta}{d_f}(\delta - \delta_0)] \tag{4.26}$$

Load P for the fiber pull-out stage can be derived as:

$$P = \frac{\pi d_f^2 \tau_0 (1+\eta)}{\omega}\left[\sin\left(\frac{\omega L}{d_f}\right) - \sin\left(\frac{\omega(\delta - \delta_0)}{d_f}\right)\right] + \pi\tau_0\beta(1+\eta)(\delta_0 - \delta)(L - \delta + \delta_0) \tag{4.27}$$

$for\ \delta_0 \le \delta \le L$

Equations (4.22) and (4.27) are derived based on load P applied in the same direction as the fiber embedded length. For randomly distributed and randomly oriented discontinuous fiber reinforced concrete with phase change material, the angle effect should also be taken into account. In other words, load P is increased with angle ϕ of inclination of fiber to the loading axis. This snubbing effect can then be incorporated into load P as follows:

$$P(\delta;\phi) = P(\delta)e^{f\phi} \tag{4.28}$$

where f is a snubbing coefficient.

4.6 Crack Bridging stress-Displacement Relationship

Equations (4.22) and (4.27) are single fiber debonding and pull-out load. To account for contributions of all fibers within a composite, Li [23] suggested that the composite stress-displacement relationship can be analyzed by integrating the contributions of each single fiber that crosses the matrix crack plane.

$$\sigma_B(\delta) = \frac{4V_f}{\pi d_f^2}\int_{\phi=0}^{\pi/2}\int_{z=0}^{(L_f/2)\cos\phi} P(\delta)e^{f\phi}p(\phi)p(z)dzd\phi \tag{4.29}$$

where $p(\phi)$ and $p(z)$ are probability density functions that account for orientation angle and the centroidal distance of the fibers from the crack plane , respectively.

The number of fibers bridging across a given matrix plane clearly depends on the distribution of z and ϕ. Stating that there is a three-dimensional random orientation of fibers in the concrete matrix is equivalent to saying that a fiber end has an equal likelihood of being located at any point on a hemisphere. The probability density function $p(\phi)$ of the inclining angle ϕ is:

$$p(\phi) = \sin\phi \tag{4.30}$$

For a uniform random distribution, the probability density function $p(z)$ of the centroidal distance z is simply:

$$p(z) = 2 / L_f \tag{4.31}$$

Equation (4.29) can be normalized by σ_0 and re-expressed in the form:

$$\tilde{\sigma}_B = \frac{\sigma_B(\delta)}{\sigma_1} = \frac{8}{\pi\tau_0(\frac{L_f}{d_f})d_f^2}\int_{\phi=0}^{\pi/2}\int_{z'=0}^{\cos\phi} P(\delta)e^{f\phi}\sin\phi dz'd\phi \tag{4.32}$$

$$\sigma_1 = \frac{1}{2}\tau_0 V_f(\frac{L_f}{d_f}) \tag{4.33}$$

Insert equations (4.22) and (4.27) into (4.32) can lead to fiber bridging stress for both fiber debonding and fiber pull-out. In most of cases, the contribution from fiber debonding is small compared to a fiber pull-out process. In the latter context, the experimental result shows that fracture energy contributed from the fiber debonding stage is negligible compared to the fiber pull-out stage. Therefore, the bridging stress due to fiber debonding will not be derived here and only fiber pull-out bridging stress will be addressed. Again, post peak bridging stress can be calculated by putting equation (4.27) into equation (4.32) and the result can be found after tedious derivation:

$$\begin{aligned}\tilde{\sigma}_B = &\{(1+\eta)[8d_f^2(4-5\cos(k)+\cos(2k))]+\\ &2d_f\beta L_f[3-5\tilde{\delta}+2\cos(k)(-1+2\tilde{\delta})]\\ &+\beta^2(-1+\tilde{\delta})\tilde{\delta}L_f^2\}/\beta L_f d_f\end{aligned} \tag{4.34}$$

where

$$k = \frac{wL_f}{2d_f} \tag{4.35}$$

By multiplying σ_1 and some simplifications, the post peak bridging stress can then be expressed as follows:

$$\sigma_B = gV_f(1+\eta)\tau_0 L_f(\tilde{\delta}-1)(\beta\tilde{\delta}L_f - 2d_f) \tag{4.36}$$

Parameter g is defined as a snubbing factor and it is a function of f and can be expressed as:

$$g \equiv \frac{2}{4+f^2}(1+e^{\pi f/2}) \tag{4.37}$$

σ_B can then be normalized again by σ_0 and can be calculated as:

$$\frac{\sigma_B}{\sigma_0} = \frac{(-1+\tilde{\delta})(-2d_f + \beta L_f\tilde{\delta})}{d_f} \tag{4.38}$$

where

$$\sigma_0 = \frac{1}{2}g(1+\eta)\tau_0 V_f(\frac{L_f}{d_f}) \tag{4.39}$$

Equation (4.38) represents the post peak fiber bridging stress of a concrete matrix with phase change material. It will be used to calculate fracture energy and compared with experimental results in the next chapter.

4.7 Fracture Energy

There are two different kinds of fiber that are used in a PCM concrete composite. One is steel fiber and the other is PVA fiber. The volume fractions are 1% and 0.1% respectively. In the following context, fracture energy that is contributed from the PVA fiber and steel fiber will be discussed separately.

4.7.1 Fracture Energy due to PVA Fiber

The fracture energy of PVA fiber is contributed from two parts, fiber debonding and fiber pull-out. In the fiber debonding stage, slip hardening or softening behavior is not obvious since slippage distance is small up to the full debonding point. In addition, only a small amount of PVA was used in the PCM reinforced concrete composite. As a result, the bridging stress-displacement relationship is derived based on the constant friction shear model. Li [1991] demonstrated use of a constant shear model to formulate single fiber pull-out load, fiber bridging stress and fracture energy.

Fracture energy from PVA fiber debonding can be expressed as:

$$\begin{aligned} G_{r\_PVA} &= \int_0^{L_f/2} \sigma_B(\delta) d\delta \\ &= \frac{5}{24} g \tau V_f d_f \left(\frac{L_f}{d_f} \right)^2 \tilde{\delta}^* \end{aligned} \tag{4.40}$$

where

$$\tilde{\delta}^* \equiv \left(\frac{\tau}{E_f} \right) \left(\frac{L_f}{d_f} \right) \tag{4.41}$$

By using the constant shear model, the fiber pull-out energy can also be derived based on the post-peak stress-displacement relationship.

Fracture energy due to PVA fiber-pull out can be addressed as follow:

$$G_{c\_PVA} = \frac{1}{12} g \tau_0 V_f d_f \left(\frac{L_f}{d_f} \right)^2 \tag{4.42}$$

Therefore, the total fracture energy contributed from a PVA fiber can be expressed as:

$$G_{total\_PVA} = G_{r\_PVA} + G_{c\_PVA} \tag{4.43}$$

4.7.2 Fracture Energy due to Steel Fiber

Fiber strain hardening or softening effect was not considered in the fiber debonding stage since the fiber slip is small enough before reaching the full debonding point. Therefore, the constant shear model for fiber debonding was used. The fiber debonding fracture energy for steel fiber shared the same numerical model but with different material parameters.

$$\begin{aligned} G_{r\_steel} &= \int_0^{L_f/2} \sigma_B(\delta) d\delta \\ &= \frac{5}{24} g \tau V_f d_f \left(\frac{L_f}{d_f} \right)^2 \tilde{\delta}^* \end{aligned} \tag{4.44}$$

Fracture energy due to steel fiber pull-out is derived from crack bridging stress found in chapter 4.6. Fracture energy can then be found by applying equation (4.38) and integrating the stress displacement relationship.

$$G_{c\_steel} = \int_0^{L_f/2} \tilde{\sigma}_B(\delta) d\delta = \frac{L_f}{2} - \frac{\beta L_f^2}{12 d_f} \tag{4.45}$$

Multiplying equation (4.45) by (4.39), steel fiber pull-out energy can be expressed as follow:

$$G_{c\_steel} = \frac{1}{24} g \tau_0 V_f (1+\eta) d_f \left(\frac{L_f}{d_f}\right)^2 \left[6 - \frac{\beta L_f}{d_f}\right] \tag{4.46}$$

As a result, the total fracture energy contributed from steel fiber can be found by adding eq.(4.44) and (4.46):

$$G_{total\_steel} = G_{r\_steel} + G_{c\_steel} \tag{4.47}$$

4.7.3 Fracture Energy Due To Aggregate Bridging Action

In chapter 4.3, aggregate bridging action was discussed and an aggregate bridging stress displacement relationship was also proposed. Therefore, fracture energy can then be found by integrating equation(4.1).

From section 4.7.1, 4.7.2 and 4.7.3, fracture energy can be derived by adding a contribution from the aggregate bridging action, PVA fiber and steel fiber.

$$G_{total} = G_{aggregate} + G_{total\_steel} + G_{total\_PVA} \tag{4.48}$$

4.8 Constant Interfacial Shear Stress Model

In the previous section, we proposed a linear strain softening interfacial shear stress model between a fiber and concrete matrix because PCM is added into concrete and interfacial shear stress is assumed to decrease when increasing slippage distance. We then can calculate the corresponding fiber debonding stress, pull-out stress and fracture energy. In this section, we will propose a constant shear stress interface model and calculate corresponding debonding, pull-out stress and fracture energy to compare with the results from a slip softening model.

A slip softening shear stress model can be expressed as in equation (4.3). A constant shear stress model can be expressed as following.

$$\tau(\mathrm{s})=\tau_0 \tag{4.49}$$

Consider a single fiber loaded with a force P at one end, resisted by a constant shear stress τ along entire length L and embedded in a cement matrix. Fibers debonding are activated due to load P. Debonding length l is increased along with load P until it reaches its maximum value L. Fibers pull-out will be assumed after fibers completely debond without any fibers rupture. The effect of Poisson's ratio and elastic bond between the fiber and matrix are neglected. By ignoring the elastic bond, the length of the slip-activated zone where τ acts on the fiber can be calculated based on a simple force equilibrium.

When an elastic fiber is embedded into a concrete matrix and is pulled by an axial force P at its end, Li [23] suggested that the slippage distance $s(\mathrm{x})$, axial strain $\varepsilon(\mathrm{x})$ and axial force $F(\mathrm{x})$ at any point x along the length of the fiber can be governed by the following equations.

$$s(\mathrm{x}) = s(0) + \int_0^x \varepsilon(\mathrm{x}')dx' \tag{4.50}$$

$$\varepsilon(\mathrm{x}) = \frac{4}{\pi d_f^2 E_f} F(\mathrm{x}) \tag{4.51}$$

$$F(\mathrm{x}) = \int_0^x \pi\tau d_f [1 + \varepsilon(\mathrm{x}')]\mathrm{dx}' \tag{4.52}$$

From equations (4.50), (4.51) and (4.52), we will be able to derive the corresponding peak load.

$$P_{peak} = \frac{1}{4}\pi d_f^2 E_f \left[\exp\left(\frac{4\tau l}{d_f E_f} \right) - 1 \right] \tag{4.53}$$

The peak displacement of the loaded end at peak load is expressed in the following.

$$\delta_{peak} = \frac{d_f E_f}{4\tau} \left[\exp\left(\frac{4\tau l}{d_f E_f} \right) - 1 \right] - l \tag{4.54}$$

From equation (4.53) and (4.54), we can derive a corresponding $P - \delta$ relationship.

The $P - \delta$ relationship can be expressed in two stages.

$$P(\delta) = \pi \sqrt{\frac{E_f d_f^3 \tau \delta}{2}} \qquad for \qquad \delta \le \delta_0 \tag{4.55}$$

$$P(\delta) = \pi\tau l d_f \left[1 - \frac{\delta - \delta_0}{l} \right] \qquad for \qquad l \ge \delta \ge \delta_0 \tag{4.56}$$

Equation (4.55) and (4.56) represent single fiber debonding and pull-out load. For the whole concrete composite, the overall debonding and pull-out stress can be predicted by integrating the contributions of those individual fibers.

$$\sigma_B(\delta) = \frac{4V_f}{\pi d_f^2} \int_{\phi=0}^{\pi/2} \int_{z=0}^{(L_f/2)\cos\phi} P(\delta) p(\phi) p(z) dz d\phi \tag{4.57}$$

where $p(\phi)$ and $p(z)$ are both a probability density function that account for orientation angle of fiber and fiber distribution.

By using equation (4.57) and integrating equation (4.55) and (4.56), we will be able to find fiber debonding and pull-out stress.

$$\tilde{\sigma}_B(\tilde{\delta}) = g\left[2\left(\frac{\tilde{\delta}}{\tilde{\delta}^*}\right)^{\frac{1}{2}} - \frac{\tilde{\delta}}{\tilde{\delta}^*}\right] \qquad for \qquad 0 \le \tilde{\delta} \le \tilde{\delta}^* \tag{4.58}$$

where g is a snubbing coefficient and is defined in the previous section.

$$\tilde{\sigma}_B = \frac{\sigma_B}{\sigma_0} \tag{4.59}$$

$$\sigma_0 = \frac{1}{2}\tau V_f \left(\frac{L_f}{d_f}\right) \tag{4.60}$$

$$\tilde{\delta} = \frac{\delta}{\left(\frac{L_f}{2}\right)} \tag{4.61}$$

with

$$\tilde{\delta}^* \equiv \left(\frac{\tau}{E_f}\right)\left(\frac{L_f}{d_f}\right) \tag{4.62}$$

Equation (4.58) is used to compute the pre-peak stress and $\sigma_B - \delta$ curve. For $\delta^* << 1$, the maximum bridging stress can be approximated to $g\sigma_0$. By using a similar method, post-peak stress can also be computed and is expressed in the following equation.

$$\tilde{\sigma}_B(\tilde{\delta}) = g\left[\left(1-\tilde{\delta}^*\right)^2 + \frac{2}{3}\tilde{\delta}^*\left(1-\tilde{\delta}^3\right)\right] \qquad for \qquad \tilde{\delta} > \tilde{\delta}^* \tag{4.63}$$

If $\delta^* << 1$, the second term may be neglected without loss of much accuracy and the post-peak stress-displacement relationship can be stated as:

$$\tilde{\sigma}_B(\tilde{\delta}) = g\left(1-\tilde{\delta}^*\right)^2 \qquad for \qquad \tilde{\delta} > \tilde{\delta}^* \tag{4.64}$$

Equation (4.58) and (4.64) can be used to describe the stress-displacement relationship in pre-peak and post-peak, respectively.

As mentioned in the previous section, fracture energy is another important property to be computed. We will be able to study ductility of the concrete composite. The fracture energy for randomly oriented and randomly distributed fiber reinforced concrete composite can be estimated by summing the contribution from the damage mechanism. The energy absorption mechanisms in fiber reinforced concrete composite are aggregate bridging, fiber bridging, fiber debonding and fiber pull-out. It should be emphasized that fiber pull-out plays an important role because it governs the behavior of fiber reinforced concrete after the concrete matrix failure or cracking.

The contributions from both fiber debonding and fiber pull-out mechanisms depends on fiber fraction, fiber embedded length and fiber aspect ratio.

The fracture energy contributed from fiber debonding and fiber pull-out are essentially the area underneath the stress-displacement curve $\sigma(\delta)$. This can be computed by integrating a stress-displacement equation. Fracture energy contributed from fiber pull-out can be computed as in the following:

$$G_c = \int_0^{L_f/2} \tilde{\sigma}_B(\tilde{\delta}) d\tilde{\delta} \tag{4.65}$$

where

$$\tilde{\sigma}_B(\tilde{\delta}) = g\left(1-\tilde{\delta}^*\right)^2 \tag{4.66}$$

By plugging equation (4.66) into (4.65), the fracture due to fiber pull-out is as in the following.

$$G_c = \frac{1}{12} g \tau_0 V_f d_f \left(\frac{L_f}{d_f} \right)^2 \tag{4.67}$$

By plugging equation (4.58) into (4.65), the fracture due to fiber debonding is as in the following.

$$G_c = \frac{5}{24} g \tau V_f d_f \left(\frac{L_f}{d_f} \right)^2 \tilde{\delta}^* \tag{4.68}$$

By combining fracture energy from fiber debonding and fiber pull-out, we will be able to estimate the overall fracture energy of a fiber reinforced concrete composite derived from a constant interfacial shear stress model. It should be noted again that the contribution from fiber pull-out is more significant than fiber debonding.

In the following section, we will compare fracture energy calculated from both use of slip softening interfacial shear stress model and a constant shear stress interfacial model.

4.9 Experimental Setup for Determining Stress-Crack Width Relationship

In order to validate theoretical model accuracy derived from the above chapter, an experimental setup for determining stress-crack width relationship must be made. Deformation controlled three point bending tests were conducted on notched beams with a length of 14 in., width of 4 in. and height of 4 in. Notch width is about 0.1 in. and notch height is 1 in. in every specimen. There were four types of concrete tested which included plain concrete, fiber reinforced concrete without PCM, fiber reinforced concrete with 5% PCM and fiber reinforced concrete with 7% PCM. Each type of concrete had four specimens. There were a total of 16 specimens tested with the three point bending test. Every specimen were mixed and cured for 28 days.

Crack width was measured by using LVDT mounted on the surface of a beam. LVDT was mounted 3.5 in. from the center of the beam. A steel rod was put on the top of the beam and load applied from a MTS machine. There were two steel rods were put 1 in. from the end of the beam to lift the specimen. Both applied force and then crack width was recorded through an electronic signal. A calibration factor had to be applied in order to obtain real data for the crack width and applied force.

Figure 4.1 Set-up for the three point bending test of FRC

Figure 4.2 Fiber bridging and fiber pull-out

The experiment set-up is shown in Figure 4.1. Technical details on conducting a three point bending test can be found elsewhere.

The raw data consisted of time, position and load in volts recording from an extensometer. Data were recorded by the testing machine and transferred to a computer. The crack opening and real applied force were obtained by applying a calibration factor of 0.2 and 23.8684 to obtain the correct units.

The stress-crack width relationship was then determined for the four types of concrete. Details of recipes, mixing procedures, preparations and curing can be found elsewhere and are not addressed in this chapter. Fracture energy can then be determined by calculating the area under the stress-crack width relationship.

4.10 Comparison between Theoretical Model Prediction and Experimental Data

4.10.1 Parameters Used for Theoretical Model

The material properties and interfacial parameters required in the theoretical model consists of the constant interfacial bond strength τ_0, slip softening parameter β and snubbing coefficient f that will be discussed in the following context.

As indicated by the aggregate bridging section, parameters $\rho=1$ and $w_0=0.015$mm were obtained from experimental study. The ultimate aggregate bridging stress σ_m^u is equal to 3.4MPa for normal strength concrete and 5.0MPa for the high strength concrete. The same normal strength concrete matrix has been used in plain concrete and the same high strength concrete matrix has been used in the fiber reinforced concrete. As mentioned before, certain amount of cement and sand was replaced by PCM. As a result, the concrete aggregate bridging stress will also decrease. Ultimate aggregate bridging stress σ_m^u is equal to 3.0MPa and will be used in all the PCM fiber reinforced concrete samples.

Table 4.1 and table 4.2 lists all material and interfacial parameters that we used in the theoretical model.

Fiber Types	Fiber Parameters					
	E_f	L_f	d_f	L_f / d_f	T_f	V_f
	(MPa)	(mm)	(mm)		(MPa)	
Steel	210000	35	0.55	65	1345	1%
PVA	42800	8	39	205	1605	0.1%

Table 4.1 Fiber material parameters as model input

	Interfacial Parameters					
	Steel fiber			PVA		
Concrete Types	τ_0	β	f	τ_0	β	f
FRC	3.5	0.02	0.5	4	1.5	0.5
5% PCM+FRC	2	0.05	0.4	3	2	0.4
7% PCM+FRC	1.5	0.06	0.4	2	3	0.4

Table 4.2 Fiber interfacial parameters as model input

Slip dependent bond strength τ_0 has been measured by previous researchers and showed quite large variations from single fiber pull-out tests. In general, τ_0 is in the range of 2 MPa to 4 MPa for steel fiber. For fiber reinforced concrete (FRC), τ_0 was adopted as its value equals to 3.5 MPa. A certain amount of sand and cement was replaced by PCM and PCM was made of a slippery wax material. As a result, we expect that the frictional force between fibers and matrix would actually decrease and τ_0 equals to 2 MPa and 1.5MPa for 5% PCM FRC and 7% PCM FRC, respectively. Since only 0.1% PVA was used in the concrete composite and PVA helps control early age micro-cracks, fracture energy contributed from PVA was small compared to steel fiber. However, τ_0 is assumed to be 3 MPa and 2 MPa for 5% PCM FRC and 7% PCM FRC, respectively.

β, a softening parameter, is expected to be increased when increasing PCM because of a lower frictional bond force between fibers and the concrete matrix. Therefore, β equals to 0.02 and 4 for both steel fiber and PVA fiber were adopted with FRC for the theoretical model. β equals 0.05 and 0.06 for steel fiber with 5% PCM FRC and 7% PCM FRC, respectively. β equals 2 and 3 for PVA fiber with 5% PCM FRC and 7% PCM FRC, respectively.

A snubbing effect coefficient f for steel fibers in a concrete matrix was proposed by Li [23]. They referred to the maximum post-peak stress of a test by Visalvanich and Naaman [34] where f varies somewhere between 0 to 1. An average value of 0.5 was used for FRC and 0.4 was adopted for both 5% PCM FRC and 7% PCM FRC. The same snubbing coefficient was used for all PVA fibers since the fracture energy contribution from PVA is neglected compared to steel fiber.

4.10.2 Model Results Compared with Experimental Data

Figure 4.3 to Figure 4.6 show the stress-crack mouth opening displacement relationship from three point bending tests for all types of concrete, consisting of plain concrete, fiber reinforced concrete (FRC), 5% PCM+FRC and 7% PCM+FRC.

Unfortunately, the time was limited to complete the three point bending test and reach zero capacity. Therefore, a third order nonlinear inverse polynomial was used in order to perform curve fitting from the end of stress-displacement curve to zero capacity.

$$y(x) = a_0 \frac{1}{x^3} + a_1 \frac{1}{x^2} + a_2 \frac{1}{x} + a3 \tag{4.69}$$

By using the curve fitting tool box built in Matlab, four constants can be obtained.

The fiber pull-out model is based on the relationship of bridging stress versus CMOP, where the CMOP is dependent on fiber length. As a result, extended curve fitting in the experimental data is necessary to make sure that all fibers have been pulled-out and that the pull-out embedment length reaches the maximum. The ultimate goal is to compare the composite fracture energy from the theoretical model with the experimental data. The fracture energy from three point bending test was derived from the area under the stress-CMOP relationship. The trapezoidal rule will be used to calculate fracture energy. After the area under the stress-CMOP relationship is calculated, crack surface area has to be multiplied to be consistent with the units from the theoretical model. The crack surface area was 4” by 3”.

Since every experiment was completed with different times, the fracture energy that was calculated cannot reflect the actual behavior. For example, the data from fiber reinforced were

completed when displacement reached about 5 inches and the data from 7% PCM reinforced concretes was stopped when displacement reached about 1.4 in. Therefore, the fracture energy calculated from the first case was larger in general compared from the fracture energy from the latter case. As a result, COMD that reached 1.4 was chosen as a standard point to stop. The fracture energy was calculated by taking the area underneath the stress-COMD relationship when COMD reached 1.4 in for all types of concrete.

From Figure 4.4, we can observe that plain concrete will lose its ductile capacity after reaching the maximum applied load. This proves that plain concrete is weak in tensile strength. For other fiber reinforced concrete composites, we can observe that the load-COMP relationship performs in a descending trend after a specimen reaching its own maximum strength.

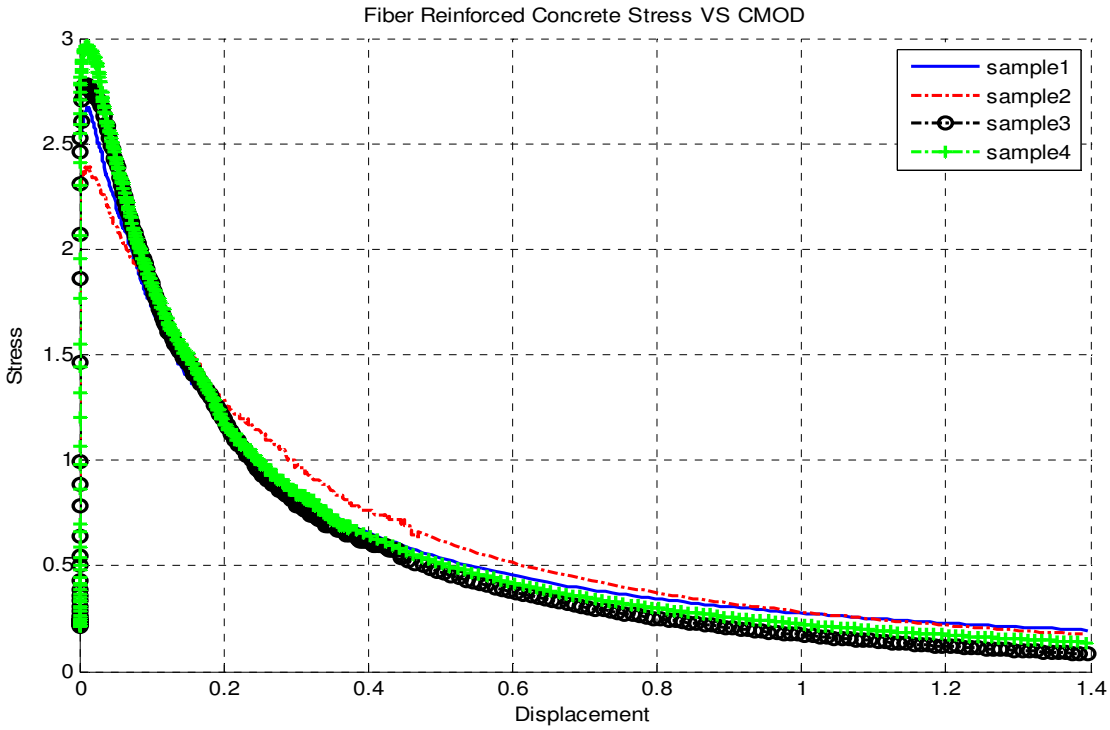

Figure 4.3 FRC stress-COMD relationship

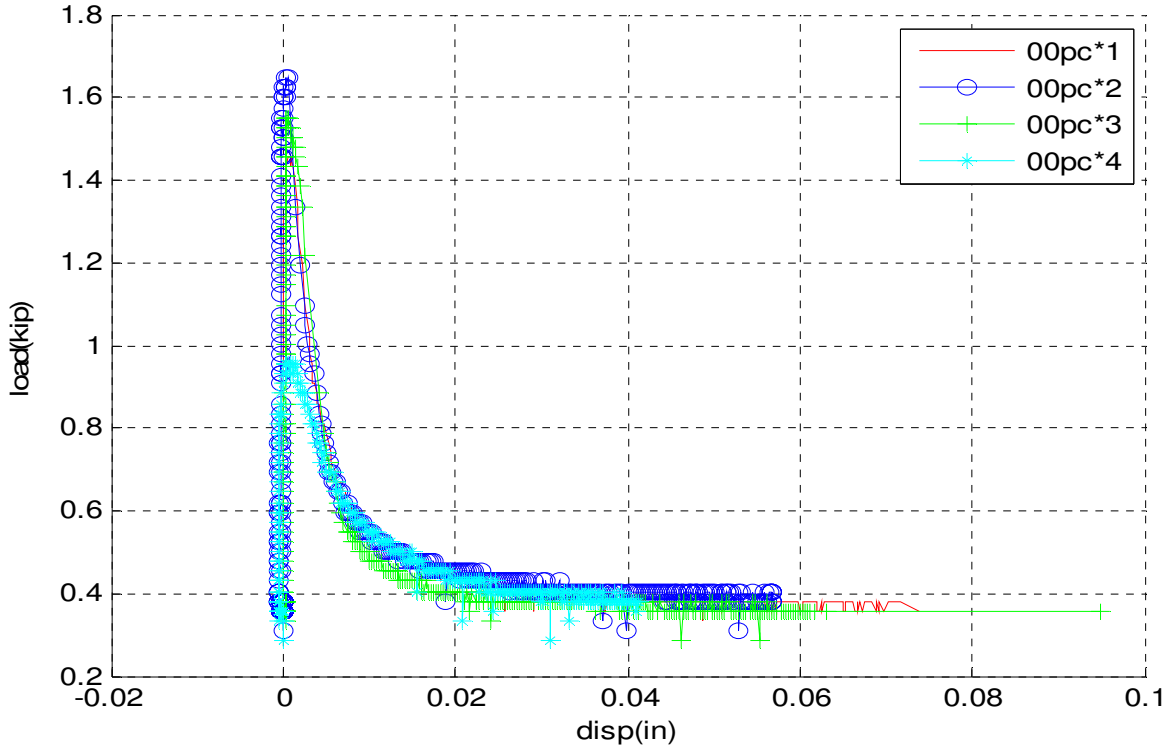

Figure 4.4 Plain concrete stress-COMD relationship

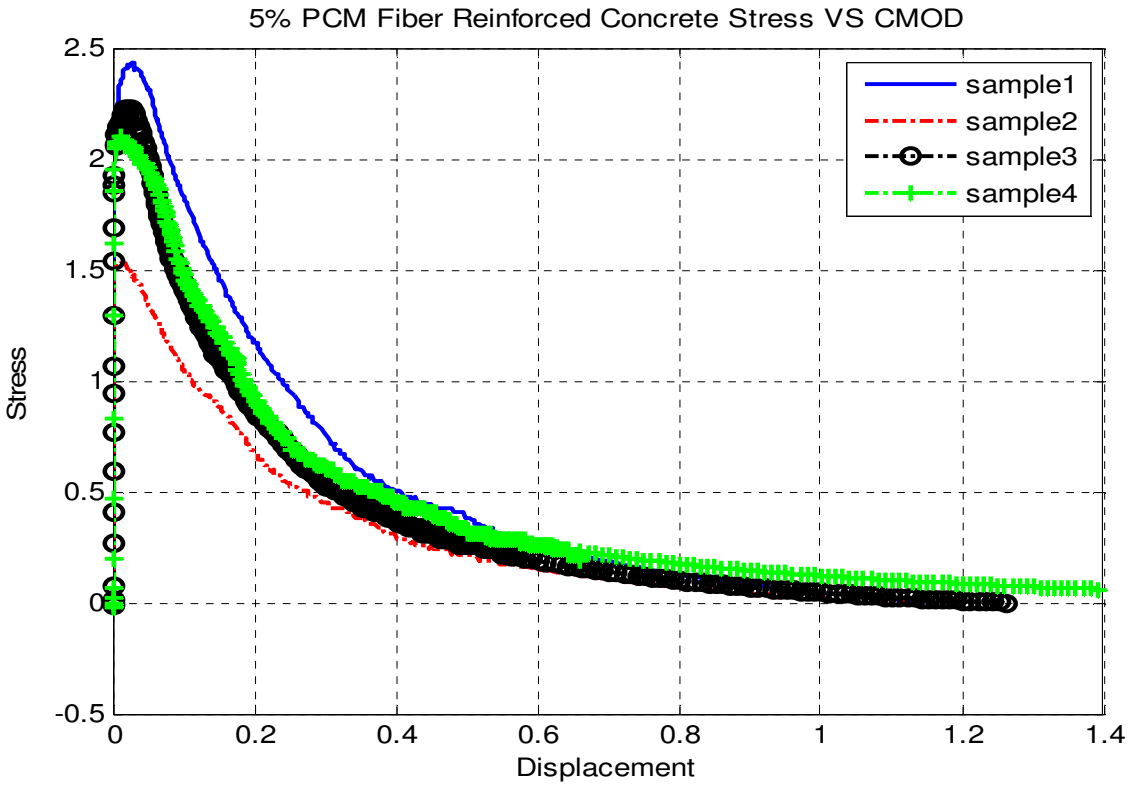

Figure 4.5 FRC+5% PCM stress-COMD relationship

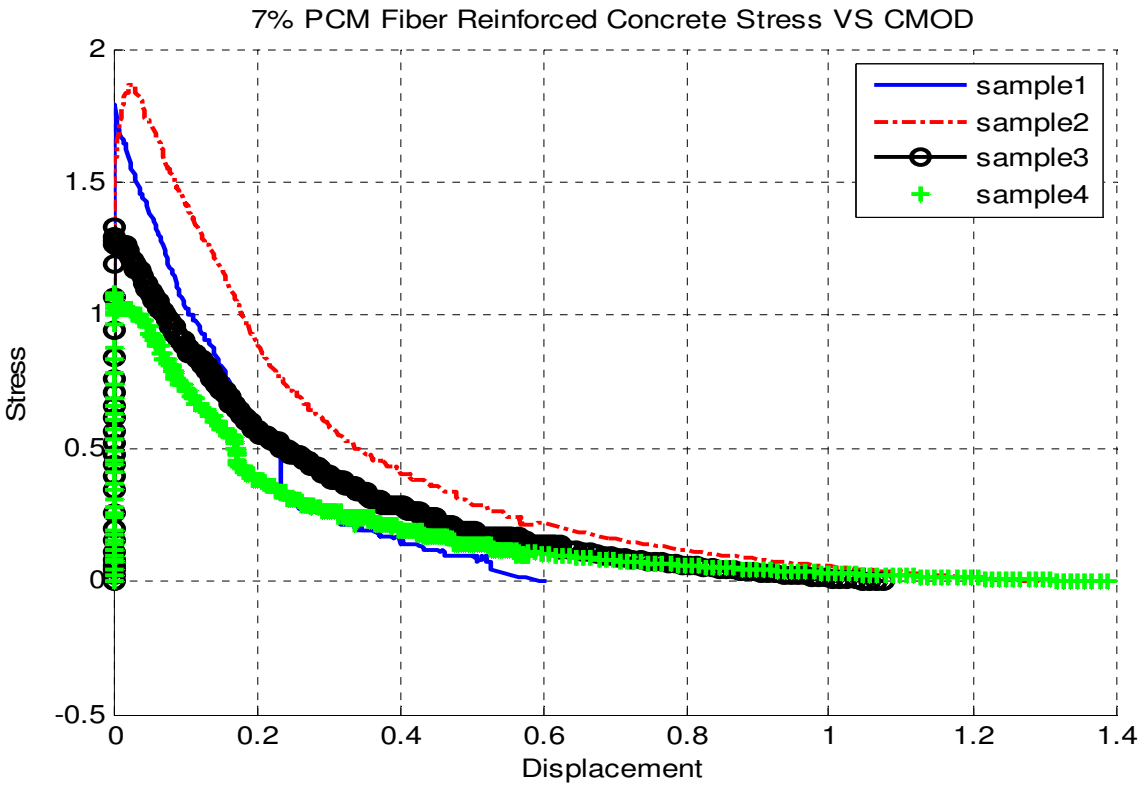

Figure 4.6 FRC+7% PCM stress-COMD relationship

As discussed in chapters 4.7 and 4.8, fracture energy can be computed by adding equations (4.43), (4.47) and (4.48).

Table 4.3 to table 4.5 display the computed fracture energy compared with fracture energy estimated from the theoretical model with a varying snubbing coefficient f for all types of concrete. We also calculated the fracture energy with a varying slip-softening parameter β for all types of concrete and depicted this in table 4.6 to table 4.8.

Since contribution from the PVA fiber debonding stage is small compared to pull-out due to the small volume fraction, fracture energy from the debonding stage is negligible. In addition, contribution from steel fiber debonding can also be neglected because the energy is too small compared to steel fiber pull-out. As s result, table 4.3 to table 4.8 only accounts for the fracture energy contributed from an aggregate bridging action, PVA fiber pull-out and steel fiber pull-out. However, energy contributed from an aggregate bridging action and PVA fiber pull-out are still small compared to steel fiber pull-out. This proves again that PVA fibers only control early age micro-cracks and does not contribute much to later ductile behavior. However, steel fibers would contribute the most fracture energy and greatly increase overall ductile capacity.

Fiber Concrete:

Snubbing Coefficient f	Fracture Energy-aggregate bridging (N.mm)	Fracture Energy-PVA Pullout (N.mm)	Fracture Energy-Steel Pullout (N.mm)	Total Fracture Energy (N.mm)	Total Fracture Energy-constant model (N.mm)	Fracture Energy Experiment (Avg) (N.mm)	Error (%)
0	3492.8	2055.3	62420	67968.1	50716.5	97908.00	30.58
0.2	3492.8	2410.5	73208	79111.3	59481.7	97908.00	19.20
0.4	3492.8	2840.3	86262	92595.1	70088.5	97908.00	5.43
0.5	3492.8	3088.5	93800	100381.3	76213.4	97908.00	2.53
0.55	3492.8	3222	97855	104569.8	79507.9	97908.00	6.80

Table 4.3 Fracture energy for FRC with varying f

5% PCM Concrete:

Snubbing Coefficient f	Fracture Energy-aggregate bridging (N.mm)	Fracture Energy-PVA Pullout (N.mm)	Fracture Energy-Steel Pullout (N.mm)	Total Fracture Energy (N.mm)	Total Fracture Energy-constant model (N.mm)	Fracture Energy Experiment (Avg) (N.mm)	Error (%)
0	2445	1949.2	43362	47756.2	50716.5	61334.00	22.14
0.2	2445	2286.1	50856	55587.1	59481.7	61334.00	9.37
0.3	2445	2480.1	55172	60097.1	70088.5	61334.00	2.02
0.4	2445	2693.7	59924	65062.7	76213.4	61334.00	6.08
0.5	2445	2929.1	65161	70535.1	79507.9	61334.00	15.00

Table 4.4 Fracture energy for FRC+5% PCM with varying f

7% PCM concrete

Snubbing Coefficient f	Fracture Energy-aggregate bridging (N.mm)	Fracture Energy-PVA Pullout (N.mm)	Fracture Energy-Steel Pullout (N.mm)	Total Fracture Energy (N.mm)	Total Fracture Energy-constant model (N.mm)	Fracture Energy Experiment (Avg) (N.mm)	Error (%)
0	2095.7	1843.2	25178	29116.9	50716.5	39677.00	26.62
0.2	2095.7	2161.8	29529	33786.5	59481.7	39677.00	14.85
0.3	2095.7	2345.2	32035	36475.9	64529.8	39677.00	8.07
0.4	2095.7	2547.2	34795	39437.9	70088.2	39677.00	0.60
0.5	2095.7	2769.8	37835	42700.5	76213.4	39677.00	7.6

Table 4.5 Fracture energy for FRC+7% PCM with varying f

Fiber Concrete:

Hardening Coefficient β	Fracture Energy-aggregate bridging (N.mm)	Fracture Energy-PVA Pullout (N.mm)	Fracture Energy-Steel Pullout (N.mm)	Total Fracture Energy (N.mm)	Total Fracture Energy-constant model (N.mm)	Fracture Energy Experiment (Avg) (N.mm)	Error (%)
0.02	3492.8	2840.3	97855	104188.1	50716.5	97908.00	6.41
0.03	3492.8	2840.3	104570	110903.1	59481.7	97908.00	13.27
0.04	3492.8	2840.3	111290	117623.1	70088.5	97908.00	20.14
0.05	3492.8	2840.3	118000	124333.1	76213.4	97908.00	26.97
0.06	3492.8	2840.3	124720	131053.1	79507.9	97908.00	33.85

Table 4.6 Fracture energy for FRC with varying softening coefficient

5% PCM Concrete:

Hardening Coefficient β	Fracture Energy-aggregate bridging (N.mm)	Fracture Energy-PVA Pullout (N.mm)	Fracture Energy-Steel Pullout (N.mm)	Total Fracture Energy (N.mm)	Total Fracture Energy-constant model (N.mm)	Fracture Energy Experiment (Avg) (N.mm)	Error (%)
0.04	2445	2840.3	73455	78740.3	50716.5	61334.00	28.38
0.05	2445	2840.3	59924	65209.3	59481.7	61334.00	6.32
0.06	2445	2840.3	46393	51678.3	70088.5	61334.00	15.74
0.07	2445	2840.3	32862	38147.3	76213.4	61334.00	37.80
0.08	2445	2840.3	19330	24615.3	79507.9	61334.00	59.87

Table 4.7 Fracture energy for FRC+5% PCM with varying softening coefficient

7% PCM Concrete:

Hardening Coefficient β	Fracture Energy-aggregate bridging (N.mm)	Fracture Energy-PVA Pullout (N.mm)	Fracture Energy-Steel Pullout (N.mm)	Total Fracture Energy (N.mm)	Total Fracture Energy-constant model (N.mm)	Fracture Energy Experiment (Avg) (N.mm)	Error (%)
0.04	2095.7	2840.3	55092	60028	50716.5	39677.00	51.29
0.05	2095.7	2840.3	44943	49879	59481.7	39677.00	25.71
0.06	2095.7	2840.3	34795	39731	70088.5	39677.00	0.14
0.07	2095.7	2840.3	24646	29582	76213.4	39677.00	25.44
0.08	2095.7	2840.3	14498	19434	79507.9	39677.00	51.02

Table 4.8 Fracture energy for FRC+7% PCM with varying softening coefficient

Plain Concrete	Fracture Energy (N.mm)
Specimen 1	3891.4
Specimen 2	3263.9
Specimen 3	4581.5
Specimen 4	2364.5
Average	3525.5

Table 4.9 Fracture energy for plain concrete

4.11 Discussion

We can expect that total fracture energy is decreased when adding phase change material since there is a weaker aggregate bridging action and slip-softening effect between fibers and the concrete matrix. We can observe that FRC had the highest fracture energy and FRC+7% PCM had the lowest fracture energy. Both τ_0 and β account for the effect of aggregate bridging action and slip-softening. τ_0 is decreased and β is increased when adding PCM.

From table 4.3, we can observe that fracture energy computed from the theoretical slip hardening model for FRC has a good agreement with the experimental data. When snubbing coefficient f reaches 0.5, error between the experimental data and theoretical model is only 2.5%. We can also observe that fracture energy computed from a constant interfacial shear stress model is underestimated compared to experimental data. When increasing the snubbing coefficient, fracture energy does increase because the fiber is harder to pullout. However, the constant shear stress model does not account for the increasing shear stress when fibers are pulled out. As a result, fracture energy is lower than the experimental data and cannot represent the real behavior.

Both table 4.4 and table 4.5 show excellent predictions when using a theoretical slip-softening model to estimate experimental data of PCM fiber reinforced concrete. For FRC + 5% PCM, error can be observed at only 2.01% and 6.07% when the snubbing coefficient f are 0.3 and 0.4, respectively. For FRC + 7% PCM, error can be observed at only 0.6% when the snubbing coefficient f is 0.04.

The snubbing coefficient used for 5% and 7% PCM concrete was slightly lower than fiber reinforced concrete without PCM. As we mentioned previously for randomly distributed fiber reinforced concrete, the nonaligned fibers will have an angle effect on the pull-out process. This angle effect can be incorporated by using snubbing coefficient f . Therefore, the fracture energy increases along with the angle ϕ to the loading axis. It is observed that with a higher snubbing coefficient f , more fracture energy can be obtained because it needs more energy to pull-out inclination fibers. The snubbing coefficient is supposed to be lower when adding PCM because of a weaker interface between fibers and the concrete matrix. As a result, fibers inclination would not be as high as FRC.

We can observe that for 5% PCM concrete the fracture energy computed from the constant shear stress model initially is lower than the experimental data and eventually higher when increasing the snubbing coefficient. Compared to fracture energy computed from a slip softening shear stress model, the fracture energy calculated from a constant shear stress model is much higher because it does not account for a slip softening effect. As a result, a constant shear stress model will produce an overestimated result and will not be as accurate as a slip softening model. The same observation is seen for 7% PCM concrete, as the fracture energy computed by using constant interfacial shear stress model was much higher than the experimental data. When PCM volume fraction is increased, the slip softening parameter is also increased due to a weaker fiber-matrix interface. If interfacial shear stress remains constant during the fiber pull-out process, the result is expected to be overestimated.

We can also calculate fracture energy with a different softening parameter β when the snubbing coefficient f is fixed. From table 4.6 to table 4.8, we can observe that error will be

more significant when β is increased. We can conclude that changing parameter β is more sensitive compared to modifying the snubbing coefficient because it directly affects the interfacial shear stress in between the fiber and matrix. As a result, corresponding fiber pull-out stress and fracture energy will be affected directly. Once the frictional shear stress interacted with the linear slip-softening effect, parameter β overcomes the snubbing coefficient effect. We can see the results of that when changing parameter β and fixing with the snubbing coefficient, where the error compared with the experimental data will be larger than changing with the snubbing coefficient. Fracture energy computed by using a constant shear stress model will be overestimated because shear stress remains constant and will not decrease when there is an increase in PCM volume fraction. This proves again that fracture energy computed using a slip softening shear stress model will be more accurate than using a constant shear stress model.

Fracture energy for plain concrete specimens is also calculated and results can be found in table 4.9. We can observe that fracture energy for plain concrete is small compared to fiber reinforced concrete or PCM fiber reinforced concrete and this proves that plain concrete without any reinforcing fibers does not perform with good ductile capacity.

In summary, a slip softening interfacial shear stress model can account for both a snubbing effect and slip softening effect when PCM is added. A snubbing coefficient can be used to reflect fibers that are randomly oriented and a slip softening parameter can be used to represent a weaker fiber-matrix interface when PCM is added. A constant shear stress model does not account for these effects. Instead, it basically assumes interfacial shear stress is constant between a fiber and concrete matrix during the pull-out process, regardless of whether there is any PCM added. Therefore, fracture energy computed by using a constant shear stress model will

be either underestimated for fiber reinforced concrete or overestimated for PCM concrete. Utilizing a slip softening shear stress model will lead to more accurate results.

4.12 References

[1] Ahmed, S. F. U., and Maalej, M. (2009). "Tensile strain hardening behaviour of hybrid steel-polyethylene fibre reinforced cementitious composites." *Construction and Building Materials*, 23(1), 96-106.

[2] Ahmed, S. F. U., and Mihashi, H. (2007). "A review on durability properties of strain hardening fibre reinforced cementitious composites (SHFRCC)." *Cement & Concrete Composites*, 29(5), 365-376.

[3] Arisoy, B., and Wu, H. C. (2008). "Material characteristics of high performance lightweight concrete reinforced with PVA." *Construction and Building Materials*, 22(4), 635-645.

[4] Baggott, R., and Gandhi, D. (1981). "Multiple cracking in aligned polypropylene fiber reinforced cement composites." *Journal of Materials Science*, 16(1), 65-74.

[5] Bao, G. and Song, Y. (1993), "Cracking bridging models for fiber composites with degraded interfaces", J. Mech. Phys. Solids 41, 1425-1444.

[6] Banthia, N., and Sappakittipakorn, M. (2007). "Toughness enhancement in steel fiber reinforced concrete through fiber hybridization." *Cement and Concrete Research*, 37(9), 1366-1372.

[7] Bencardino, F., Rizzuti, L., Spadea, G., and Swamy, R. N. (2010). "Experimental evaluation of fiber reinforced concrete fracture properties." *Composites Part B-Engineering*, 41(1), 17-24.

[8] Chen, B., and Liu, J. Y. (2005). "Contribution of hybrid fibers on the properties of the high-strength lightweight concrete having good workability." *Cement and Concrete Research*, 35(5), 913-917.

[9] Deng, Z. C. (2005). "The fracture and fatigue performance in flexure of carbon fiber reinforced concrete." *Cement & Concrete Composites*, 27(1), 131-140.

[10] Ding, Y. N., You, Z. G., and Jalali, S. (2010). "Hybrid fiber influence on strength and toughness of RC beams." *Composite Structures*, 92(9), 2083-2089.

[11] Gopalaratnam, V. S., and Shah, S. P. (1985). "Softening response of plain concrete in direct tension." *Journal of the American Concrete Institute*, 82(3), 310-323.

[12] Kakemi, M., and Hannant, D. J. (1995). "Mathematical-model for tensile behavior of hybrid continuous fiber cement composites." *Composites*, 26(9), 637-643.

[13] Kanda, T., and Li, V. C. (1999). "Effect of fiber strength and fiber-matrix interface on crack bridging in cement composites." *Journal of Engineering Mechanics-Asce*, 125(3), 290-299.

[14] Kullaa, J. (1994). "Constitutive modeling of fiber-reinforced concrete under uniaxial tensile loading." *Composites*, 25(10), 935-944.

[15] Laranjeira, F., Molins, C., and Aguado, A. (2010). "Predicting the pullout response of inclined hooked steel fibers." *Cement and Concrete Research*, 40(10), 1471-1487.

[16] Leung, C. K. Y., and Li, V. C. (1991). "New strength-based model for the deboning of discontinuous fibers in an elastic matrix." *Journal of Materials Science*, 26(22), 5996-6010.

[17] Li, V. C. (2002). "Large volume, high-performance applications of fibers in civil engineering." *Journal of Applied Polymer Science*, 83(3), 660-686.

[18] Li, V. C., Lin, Z., and Matsumoto, T. (1998). "Influence of fiber bridging on structural size-effect." *International Journal of Solids and Structures*, 35(31-32), 4223-4238.

[19] Li, V. C., and Stang, H. (1997). "Interface property characterization and strengthening mechanisms in fiber reinforced cement based composites." *Advanced Cement Based Materials*, 6(1), 1-20.

[20] Li, V. C., and Chan, Y. W. (1994). "Determination of interfacial debond mode for fiber-reinforced cementitious composites." Journal of Engineering Mechanics-Asce, 120(4), 707-719.

[21] Li, V. C., Stang, H., and Krenchel, H. (1993). "Micromechanics of crack bridging in fiber-reinforced concrete." *Materials and Structures*, 26(162), 486-494.

[22] Li, V. C., Wang, S. X., and Wu, C. (2001). "Tensile strain-hardening behavior of polyvinyl alcohol engineered cementitious composite (PVA-ECC)." *Aci Materials Journal*, 98(6), 483-492.

[23] Li, V. C., Wang, Y. J., and Backer, S. (1991). "A micromechanical model of tension-softening and bridging toughening of short random fiber reinforced brittle matrix composites." *Journal of the Mechanics and Physics of Solids*, 39(5), 607-625.

[24] Li, V. C., Wang, Y., and Backer, S. (1990). "Effect of inclining angle, bundling and surface-treatment on synthetic-fiber pull-out from a cement matrix." *Composites*, 21(2), 132-140.

[25] Lin, Z., and Li, V. C. (1997). "Crack bridging in fiber reinforced cementitious composites with slip-hardening interfaces." *Journal of the Mechanics and Physics of Solids*, 45(5), 763-787.

[26] Nelson, P. K., Li, V. C., and Kamada, T. (2002). "Fracture toughness of microfiber reinforced cement composites." *Journal of Materials in Civil Engineering*, 14(5), 384-391.

[27] Passuello, A., Moriconi, G., and Shah, S. P. (2009). "Cracking behavior of concrete with shrinkage reducing admixtures and PVA fibers." *Cement & Concrete Composites*, 31(10), 699-704.

[28] Qian, C. X., and Stroeven, P. (2000). "Fracture properties of concrete reinforced with steel-polypropylene hybrid fibres." *Cement & Concrete Composites*, 22(5), 343-351.

[29] Redon, C., Li, V. C., Wu, C., Hoshiro, H., Saito, T., and Ogawa, A. (2001). "Measuring and modifying interface properties of PVA fibers in ECC matrix." *Journal of Materials in Civil Engineering*, 13(6), 399-406.

[30] Stang, H., "Evaluation of properties of cementitious materials in high performance fiber reinforced cement composites", *Profeedings of International RILEM/ACI Workshop*, edited by H.W. Reinhardt and A.E. Naaman (Spon, 1992) pp. 388-406.

[31] Sayers, C. M. (1992). "ELASTIC-ANISOTROPY OF SHORT-FIBER REINFORCED COMPOSITES." *International Journal of Solids and Structures*, 29(23), 2933-2944.

[32] Shao, Y. X., Li, Z. J., and Shah, S. P. (1993). "Matrix cracking and interface debonding in fiber-reinforced cement-matrix composites." *Advanced Cement Based Materials*, 1(2), 55-66.

[33] Toutanji, H., Xu, B., Gilbert, J., and Lavin, T. (2010). "Properties of poly(vinyl alcohol) fiber reinforced high-performance organic aggregate cementitious material: Converting brittle to plastic." *Construction and Building Materials*, 24(1), 1-10.

[34] Visalvanich, K. and Naaman, A.E. (1982). "Fracture modeling of fiber reinforced cementitious composites", Programming Report for NSF Grant ENG. 77-23534, Department of Material Engineering, University of Illinois at Chicago Circle.

[35] Wang, Y. J., Li, V. C., and Backer, S. (1990). "Experimental-determination of tensile behavior of fiber reinforced concrete." *Aci Materials Journal*, 87(5), 461-468.

[36] Wang, Y. J., Li, V. C., and Backer, S. (1991). "Tensile failure mechanics in synthetic fiber-reinforced mortar." *Journal of Materials Science*, 26(24), 6565-6575.

[37] Wang, Y. J., Li, V. C., and Backer, S. (1988). "Modeling of fiber pull-out from a cement matrix." *Int. J. Cement Compos*, Lightweight Concrete 10(3), 143-149.

[38] Yang, E. H., Wang, S., Yang, Y., and Li, V. C. (2008). "Fiber-bridging constitutive law of engineered cementitious composites." *Journal of Advanced Concrete Technology*, 6(1), 181-193.

[39] Ying, C., and Pizhong, Q. (2011). "Crack Growth Resistance of Hybrid Fiber-Reinforced Cement Matrix Composites." *Journal of Aerospace Engineering*, 24(2), 154-161161.

[40] Zhang, J., and Li, V. C. (2004). "Simulation of crack propagation in fiber-reinforced concrete by fracture mechanics." *Cement and Concrete Research*, 34(2), 333-339.

[41] Zhang, J., Stang, H., and Li, V. C. (2001). "Crack bridging model for fibre reinforced concrete under fatigue tension." *International Journal of Fatigue*, 23(8),655-6

Chapter 5 Tensile Strength Prediction of Concrete Composite

5.1 Introduction

In our hybrid fiber PCM reinforced concrete composite, both PVA and steel fibers play an important role. In chapter 4, we proved that adding steel fiber can increase fiber bridging stress and pull-out stress and thus increase composite ductile capacity. We can observe from experimental results that the concrete composite can perform very good ductile behavior after maximum tensile strength has reached and fracture energy has been increased by a significant amount.

However, PVA fibers do not play an important role on improving composite ductile capacity. PVA fibers are stiffer, stronger and relatively smaller in size and bridges micro-cracks to prevent bigger cracks and thus early age tensile strength can be improved. In hybrid fiber concrete composite, PVA fibers control micro-cracks and thus increase composite tensile strength. Steel fibers control macro-cracks and thus improve composite ductile capacity. Because adding PCM in concrete composite would decrease aggregate bridging stress, both PVA and steel fibers would compensate the loss of strength and ductility.

Numerical modelings of fiber bridging stress and composite fracture energy have been discussed in the previous chapter. In this chapter, the maximum tensile strength will be modeled

by using fiber bridging stress and rule of mixture. Comparison between model results and experimental data will be made.

5.2 Rule of Mixture

Before reaching maximum tensile strength, fibers and concrete matrix behave elastically because of low strain. Composite elastic modules E is determined by a modulus balance which weights the PVA fiber modulus, E_{fa}, steel fiber modulus, E_{fs}, and matrix modulus, E_m, by their corresponding volume fractions V_{fa}, V_{fs} and V_m, respectively.

$$E = E_{fa}V_{fa} + E_{fs}V_{fs} + E_mV_m \tag{5.1}$$

Equation (5.1) is the well known rule of mixture (ROM) for the tensile modulus of a composite material and is applicable when the fibers are both continuous and well aligned with stress applied in the same direction of the fibers. Sun Z [18]. In the linear elastic state, the matrix and the fibers develop the same strain and equation (5.1) can be reformulated as follows:

$$\sigma = \sigma_{fa}V_{fa} + \sigma_{fs}V_{fs} + \sigma_mV_m \tag{5.2}$$

$$V_m = 1 - V_{fa} - V_{fs} \tag{5.3}$$

Equation (5.2) can then be written as:

$$\sigma = \sigma_{fa}V_{fa} + \sigma_{fs}V_{fs} + \sigma_m(1 - V_{fa} - V_{fs}) \tag{5.4}$$

5.3 Ultimate Tensile Strength of Fibers

In chapter 4, the bridging stress of fiber reinforced concrete composite with PCM has been shown that it is a function of fiber material property, the interface between the matrix and

the fiber, and the concrete matrix characteristics. To account for contributions of all fibers within composite, the composite stress-displacement relationship can be analyzed by integrating the contributions of each single fiber that cross the matrix crack plane.

$$\sigma_B(\delta) = \frac{4V_f}{\pi d_f^2} \int_{\phi=0}^{\pi/2} \int_{z=0}^{(L_f/2)\cos\phi} P(\delta) e^{f\phi} p(\phi) p(z) dz d\phi \tag{5.5}$$

where $p(\phi)$ and $p(z)$ are probability density functions account for orientation angle and the centroidal distance of the fibers from the crack plane , respectively.

The number of fibers bridging across a given matrix plane clearly depends on the distribution of z and ϕ. Stating that there is a three-dimensional random orientation of fibers in the concrete matrix is equivalent to that a fiber end has an equal likelihood of being located at any point on a hemisphere. The probability density function $p(\phi)$ of the inclining angle ϕ is:

$$p(\phi) = \sin\phi \tag{5.6}$$

For a uniform random distribution, the probability density function $p(z)$ of the centroidal distance z is simply:

$$p(z) = 2 / L_f \tag{5.7}$$

Eq. (4.29) can be normalized by σ_0 and re-expressed in the form:

$$\tilde{\sigma}_B = \frac{\sigma_B(\delta)}{\sigma_1} = \frac{8}{\pi\tau_0 (\frac{L_f}{d_f}) d_f^2} \int_{\phi=0}^{\pi/2} \int_{z'=0}^{\cos\phi} P(\delta) e^{f\phi} \sin\phi dz' d\phi \tag{5.8}$$

$$\sigma_1 = \frac{1}{2} \tau_0 V_f (\frac{L_f}{d_f}) \tag{5.9}$$

The post peak bridging stress has derived in chapter 4 and result can be shown in the following:

$$\tilde{\sigma}_B = \{(1+\eta)[8d_f^2(4-5\cos(k)+\cos(2k))]+ \\ 2d_f\beta L_f[3-5\tilde{\delta}+2\cos(k)(-1+2\tilde{\delta})] \\ +\beta^2(-1+\tilde{\delta})\tilde{\delta}L_f^2\}/\beta L_f d_f \tag{5.10}$$

where

$$k = \frac{wL_f}{2d_f} \tag{5.11}$$

By multiplying σ_1 and some simplifications, the post peak bridging stress can then be expressed as follow:

$$\sigma_B = gV_f(1+\eta)\tau_0 L_f(\tilde{\delta}-1)(\beta\tilde{\delta}L_f - 2d_f) \tag{5.12}$$

Parameter g is defined as snubbing factor and it is function of f and can be expressed as:

$$g \equiv \frac{2}{4+f^2}(1+e^{\pi f/2}) \tag{5.13}$$

σ_B can then be normalized again by σ_0 and can be calculated as:

$$\frac{\sigma_B}{\sigma_0} = \frac{(-1+\tilde{\delta})(-2d_f+\beta L_f\tilde{\delta})}{d_f} \tag{5.14}$$

where

$$\sigma_0 = \frac{1}{2}g(1+\eta)\tau_0 V_f(\frac{L_f}{d_f}) \tag{5.15}$$

The ultimate tensile strength can then be found from equation (5.14). By setting equation (5.14) equals to zero, we can find that when $\tilde{\delta} = 1/2 + \frac{d_f}{L_f \beta}$, the ultimate tensile strength can be expressed as follows:

$$\sigma_t = \frac{1}{2} g(1+n)\tau_0 V_f (\frac{L_f}{d_f})(1 - \frac{d_f}{L_f \beta} - \frac{L_f \beta}{4 d_f}) \tag{5.16}$$

$$\eta = \frac{V_f E_f}{V_m E_m} \tag{5.17}$$

Where g is defined as snubbing factor, β is slip softening coefficient, τ_0 is the fiber/matrix frictional bond strength, V_f is fiber volume fraction, L_f and d_f are length of fiber and diameter of the fiber, respectively.

For the regular hybrid fiber reinforced concrete without adding any PCM, the ultimate tensile strength has been shown by Li [11] by using linear slip hardening model.

$$\sigma_t = \frac{1}{2} g(1+n)\tau_0 V_f (\frac{L_f}{d_f}) \tag{5.18}$$

All parameters that will be used in the theoretical model can be found from Table 3.2 and Table 4.2 in the previous chapter.

5.4 Maximum Applied Force at Mid Span

The tensile stress of the composite at mid-span in the single edge notched beam is given by equation (5.4). Assuming fiber pull-out dominates the failure mode. Equation (5.4) can then be rewritten by using equation (5.16) and then be expressed as:

$$\sigma = \frac{1}{2} g(1+n_1)\tau_{0a} V_{fa} (\frac{L_{fa}}{d_{fa}})(1 - \frac{d_{fa}}{L_{fa}\beta_a} - \frac{L_{fa}\beta_a}{4d_{fa}}) + \frac{1}{2} g(1+n_2)\tau_{0s} V_{fs} (\frac{L_{fs}}{d_{fs}})(1 - \frac{d_{fs}}{L_{fs}\beta_s} - \frac{L_{fs}\beta_s}{4d_{fs}}) + \sigma_m (1 - V_{fa} - V_{fs}) \quad (5.19)$$

In equation (5.19), σ is the tensile stress of the composite which can be calculated based on the beam theory.

In beam theory, the maximum tensile strength can be expressed as:

$$\sigma = \frac{MC}{I} \quad (5.20)$$

where C is the distance from the neutral axis to the extreme tensile fiber.

$$C = \frac{W-a}{2} \quad (5.21)$$

Where W is the beam thickness and a is the initial notch length.

As a result, equation (5.20) can then be rewritten as:

$$\sigma = \frac{MC}{I} = \frac{M(\frac{W-a}{2})}{I} = \frac{PS(W-a)}{8I} \quad (5.22)$$

where P is the force applied at mid-span, S is the length of free span, W is the height of the beam and I is the moment of inertia parallel to the axis about which the moment is applied. The maximum tensile stress that concrete matrix can provide is equal to:

$$\sigma_m = \frac{P_0 S(W-a)}{8I} \quad (5.23)$$

where P_0 is the failure load of the specimen without any fiber.

By combining equations (5.22), (5.23) and (5.19) yields:

$$\frac{PS(W-a)}{8I}=\frac{P_0S(W-a)}{8I}(1-V_{fa}-V_{fs})+$$
$$\frac{1}{2}g(1+n_1)\tau_{0a}V_{fa}(\frac{L_{fa}}{d_{fa}})(1-\frac{d_{fa}}{L_{fa}\beta_a}-\frac{L_{fa}\beta_a}{4d_{fa}})+ \quad (5.24)$$
$$\frac{1}{2}g(1+n_2)\tau_{0s}V_{fs}(\frac{L_{fs}}{d_{fs}})(1-\frac{d_{fs}}{L_{fs}\beta_s}-\frac{L_{fs}\beta_s}{4d_{fs}})+$$

Therefore, the maximum applied force at mid-span can then be solved.

$$P=\frac{8I}{(W-a)S}[\frac{P_0S(W-a)}{8I}(1-V_{fa}-V_{fs})+$$
$$\frac{1}{2}g(1+n_1)\tau_{0a}V_{fa}(\frac{L_{fa}}{d_{fa}})(1-\frac{d_{fa}}{L_{fa}\beta_a}-\frac{L_{fa}\beta_a}{4d_{fa}})+ \quad (5.25)$$
$$\frac{1}{2}g(1+n_2)\tau_{0s}V_{fs}(\frac{L_{fs}}{d_{fs}})(1-\frac{d_{fs}}{L_{fs}\beta_s}-\frac{L_{fs}\beta_s}{4d_{fs}})+]$$

The moment of inertia I can be expressed as:

$$I=\frac{1}{12}B(W-a)^3 \quad (5.26)$$

By using equation (5.25), the maximum applied force at mid-span can then be calculated and compared with experimental data.

5.5 Model Results Compared with Experimental Data

By implementing the modeling input parameters from Table 3.1 and Table 4.2 into equation (5.25), the maximum applied force at mid-span can be calculated. In chapter 4, applied force V.S. COMP relationship has been shown from Figure 4.3 to Figure 4.6. The maximum applied force at mid-span can be found from experimental data and can then be compared with theoretical model.

Max. Applied Force(Kips)	FRC	5MFRC	7MFRC
Specimen 1	2.6733	2.4346	1.7901
Specimen 2	2.3868	1.5276	1.8617
Specimen 3	2.7767	2.2277	1.3287
Specimen 4	2.9676	2.1004	1.082
Avg	2.7011	2.072575	1.515625
STD	0.24	0.39	0.37
C.O.V (%)	8.97	18.75	24.6
Model results	2.236	1.9837	1.5354

Table 5.1 Maximum applied force at mid-span compared with experimental data

Table 5.1 depicts the experimental results compared with theoretical model calculated based on the equation (5.25).

5.6 Discussion

We can observe from table 5.1 that the theoretical model underestimates the maximum applied force for both fiber reinforced concrete and 5% PCM fiber reinforced concrete. For 7% PCM fiber reinforced concrete, equation (5.25) can predict the result well.

In section 5.4, all theoretical models were derived based on fiber bridging stress and rule of mixture. H. Toutanji and B. Xu [16] mentioned that rule of mixture is applicable when the fibers are both continuous and well aligned with applied tensile stress. In other words, applied

tensile stress and fiber are in the same direction. Since our concrete composite consists of fine aggregate, coarse aggregate, PVA fibers, steel fibers and PCM, all fibers are randomly oriented and distributed. In the mixing process, the uniform and homogeneous distribution cannot be guaranteed. Randomly oriented and distributed fibers reinforced composite indeed can increase composite ultimate tensile strength and ductile capacity because larger force would be needed to overcome fiber bridging stress. As a result, the underestimated result can then be expected by using rule of mixture.

We can observe that the mathematical model can predict better result for the 7% PCM fiber reinforced concrete. When adding more and more PCM, the interfacial resistant stress between fibers and matrix will become weaker and weaker. Therefore, all fibers would have bigger chance to align in the same direction during the mixing process. In that case, equation (5.25) can then be used to predict maximum applied force with better accuracy.

PVA fibers could control micro-cracks and cracks growth in the pre-peak stage and thus increase concrete composite tensile strength. However, only small amount of PVA fibers were used in our hybrid fiber reinforced concrete composite. Therefore, in order to provide enough tensile strength to match experimental data, we can conclude that all steel fibers also contribute not only in the post-peak stage, but also help PVA fibers to bridge the early age micro-cracks.

5.7 Conclusion

Slip hardening interfacial shear stress has been commonly observed between synthetic fibers and cement matrix in the present application. However, slip softening interface behavior

should also be investigated when different interface condition is presented. Adding energy conserving material into construction material to improve energy conservation ability has been a highly demanding application. However, certain sand and cement have to be replaced when PCM needs to be incorporated. Therefore, cement based fiber reinforced concrete would have different strength and ductile behavior. In our fiber reinforced concrete composite, adding wax shell micro-encapsulate phase change material will be one of the case that frictional interface stress becomes weaker. As a result, a different slip softening interface theoretical model has to be proposed to simulate crack bridging stress-displacement relationship and fracture energy. A micromechanics based single fiber pull-put relation is constructed first. Furthermore, a new crack bridging law is developed for randomly distributed and randomly oriented fiber reinforced concrete adding PCM with slip softening interfaces. Based on the proposed crack bridging model, the following conclusions can then be addressed.

1) For fiber reinforced concrete without adding PCM, slip hardening interfacial shear stress can significantly increase the composite ductile capacity and fracture energy due to fiber pull-out process while increase in composite tensile strength. For material system satisfying some special condition, adding PCM, slip softening interfacial shear stress can be observed. As mentioned before, the composite ductile capacity and fracture energy will decrease compared to fiber reinforced concrete due to decreasing interface shear stress. However, the whole ductile capacity and fracture energy still perform better than plain concrete. In addition, temperature inside of composite can be controlled in a constant value and damage can be reduced from freeze-thaw test.
2) The proposed micromechanical model provides a useful tool for design purpose and proves that it can be matched well with experimental data.

3) Slip softening parameter β plays an important role on performing ductile behavior of FRC+PCM composite. When adding more and more PCM, β would also increase and that represents the weaker interface shear stress.

In order to prove adding PVA fibers can increase ultimate tensile strength of hybrid fiber reinforced concrete composite, the theoretical model has also been proposed based on the rule of mixture.

The maximum tensile stress that fibers can provide is based on the fiber bridging stress derived in chapter 5.3. Ultimate tensile stress that concrete matrix can provide is based on the beam theory. Based on the proposed theoretical model, the following conclusions can then be addressed.

1) Results predicted from theoretical model are underestimated for both fiber reinforced concrete and 5% PCM fiber reinforced concrete. By using rule of mixture, all fibers are assumed to be well aligned with stress applied in the same direction of the fibers. However, all fibers cannot be guaranteed all aligned uniformly in the mixing process. Therefore, the ultimate tensile strength and ductile capacity would then be increase in the actual experiment due to fibers randomly distributed and randomly oriented. Result from 7% PCM fiber reinforced concrete seems to be more accurate because weaker interfacial resistant stress between fibers and matrix.
2) The same observation as in chapter 4, when adding more and more PCM, the interface slip-softening behavior between concrete matrix and fibers would be more significant. The constant interfacial shear stress τ_0 for both PVA fibers and steel fibers would decrease when adding more PCM. In addition, the slip softening parameter β would also

increase when adding more PCM. Therefore, the ultimate tensile strength would decrease when increasing the amount of PCM.

3) From comparison of theoretical model and experimental data, we can observe that the ultimate tensile strength is not only contributed from PVA fibers. The amount of PVA fibers that we used in fiber reinforced concrete composite was only 0.1%. After we calculated the contribution from PVA fibers, the ultimate tensile strength which included concrete matrix and PVA fibers was still lower than experimental data. As a result, we can conclude that steel fibers also contributed to composite maximum tensile strength. In the pre-peak stage, both PVA fibers and steel fibers can bridge micro-cracks and control cracks growth and increase composite ultimate tensile strength. In the post-peak stage, only steel fibers can increase composite ductile capacity.

Based on the above consideration and observation, we believe that the slip-softening interface behavior is the dominant mechanism when adding phase change material into fiber reinforced concrete composite. It has been already proven that the presented model is accurate when predicting crack bridging stress-COMP relationship and fracture energy.

The slip softening behavior, composite ductile capacity and fracture energy will be discussed in the future when concrete composite performing freeze-thaw test.

5.8 References

[1] ASTM E399-08 , "Standard test method for linear-elastic plane-strain fracture toughness of metallic materials", pp.491-509

[2] Ahmed, S. F. U., and Maalej, M. (2009). "Tensile strain hardening behaviour of hybrid steel-polyethylene fibre reinforced cementitious composites." Construction and Building Materials, 23(1), 96-106.

[3] Ahmed, S. F. U., and Mihashi, H. (2007). "A review on durability properties of strain hardening fibre reinforced cementitious composites (SHFRCC)." Cement & Concrete Composites, 29(5), 365-376.

[4] Anderson TL. Fracture Mechanics. Taylor and Francis Group, 2005. p. 288-9.

[5] Bencardino, F., Rizzuti, L., Spadea, G., and Swamy, R. N. (2010). "Experimental evaluation of fiber reinforced concrete fracture properties." Composites Part B-Engineering, 41(1), 17-24.

[6] Facca, A. G., Kortschot, M. T., and Yan, N. (2007). "Predicting the tensile strength of natural fibre reinforced thermoplastics." Composites Science and Technology, 67(11-12), 2454-2466.

[7] Kakemi, M., and Hannant, D. J. (1995). " Mathematical-model for tensile behavior of hybrid continuous fiber cement composites." Composites, 26(9), 637-643.

[8] Kanda, T., and Li, V. C. (1999). "Effect of fiber strength and fiber-matrix interface on crack bridging in cement composites." Journal of Engineering Mechanics-Asce, 125(3), 290-299.

[9] Li, V. C. (2002). "Large volume, high-performance applications of fibers in civil engineering." Journal of Applied Polymer Science, 83(3), 660-686.

[10] Li, V. C., Stang, H., and Krenchel, H. (1993). "Micromechanics of crack bridging in fiber-reinforced concrete." Materials and Structures, 26(162), 486-494.

[11] Li, V. C., Wang, S. X., and Wu, C. (2001). "Tensile strain-hardening behavior of polyvinyl alcohol engineered cementitious composite (PVA-ECC)." Aci Materials Journal, 98(6), 483-492.

[12] Lin, Z., and Li, V. C. (1997). "Crack bridging in fiber reinforced cementitious composites with slip-hardening interfaces." Journal of the Mechanics and Physics of Solids, 45(5), 763-787.

[13] Madsen, B., Hoffmeyer, P., and Lilholt, H. (2007). "Hemp yarn reinforced composites - II. Tensile properties." Composites Part a-Applied Science and Manufacturing, 38(10), 2204-2215.

[14] Mouhmid, B., Imad, A., Benseddiq, N., Benmedakhene, S., and Maazouz, A. (2006). "A study of the mechanical behaviour of a glass fibre reinforced polyamide 6,6: Experimental investigation." Polymer Testing, 25(4), 544-552.

[15] Qian, C. X., and Stroeven, P. (2000). "Fracture properties of concrete reinforced with steel-polypropylene hybrid fibres." Cement & Concrete Composites, 22(5), 343-351.

[16] Toutanji, H., Xu, B., Gilbert, J., and Lavin, T. (2010). "Properties of poly(vinyl alcohol) fiber reinforced high-performance organic aggregate cementitious material: Converting brittle to plastic." Construction and Building Materials, 24(1), 1-10.

[17] Ying, C., and Pizhong, Q. (2011). "Crack Growth Resistance of Hybrid Fiber-Reinforced Cement Matrix Composites." Journal of Aerospace Engineering, 24(2), 154-161161.

[18] Zhihui, S., Garboczi, E. J., and Shah, S. P. (2007). "Modeling the elastic properties of concrete composites: Experiment, differential effective medium theory, and numerical simulation."Cement and Concrete Composites,29(1),22-3838

Chapter 6 Numerical Modeling for Thermal Performance of Phase Change Material Incorporated into Hybrid Fiber Reinforced Concrete in a Cold Climate Region

6.1 Introduction

Passive energy storage systems have been applied extensively in hot regions to address the need to reduce energy consumption [1] [7] [14] [17]. It is known that during the summer or in a hot climate region, temperature can become very high and be uncomfortable for people inside a building. Incorporating a passive energy storage system into building can help to store the energy during the day, and then release the energy at night. As a result, interior temperature can be better controlled and air conditioning energy consumption minimized. There is increasing interest around the world in developing energy storage system.

Over the past few years, incorporating phase change material (PCM) into a building has been studied as a potential technology to improve energy storage and minimize energy consumption [5], [8], [11], [26]. Using phase change material (PCM) as passive energy storage system has many benefits, such as its very high heat storage density and low heat conductivity. During the phase change process, PCM can store most of the energy and has very little temperature variation [26]. During the day PCM can absorb excessive energy and phase change from solid to liquid. After the temperature drops during the night, the PCM would release the

energy and phase change from liquid to solid. By going through this phase change process over and over, the temperature can then be controlled.

PCM can also be applied in cold climate region. In a cold climate region, the temperature drops down to below $0°C$ and water inside of concrete or asphalt pavement will solidify into ice. The ice then melts into water during the day due to radiation from sun light or due to higher temperatures. By going through this freeze and thaw process inside of concrete, microcracks can be generated and eventually macrocracks are formed and propagated. Further damage may then be caused due to various cracks.

As mentioned previously, PCM has very high heat storage ability compared to other materials and low thermal conductivity. Therefore, by choosing an appropriate melting temperature for a PCM and incorporating PCM into hybrid fiber reinforced concrete, the interior temperature of concrete is assumed to be controlled and the formation of cracks can then be delayed or minimized.

How thermal energy transfer inside of concrete after adding PCM is an important issue. Studying heat transfer and the interior temperature gradient of concrete can help us to understand the functions of PCM. The heat transfer problem in PCM hybrid fiber reinforced concrete is a transient, nonlinear problem with a moving solid-liquid interface, generally referred to as a moving boundary problem [9]. Because of the difficulties in tracking down the solid-liquid interface due to the phase change process, analytical solutions for phase change problems can only be found in some extremely limited conditions. As a result, some approximated analytical solutions for phase change problems with different boundary conditions have been proposed. These include the quasi-stationary approximation, perturbation methods, the Megerlin method

and heat balance integral method. All of these methods assume that the melting temperature and solidification temperature is constant. However, certain materials such as paraffin can have a wide temperature range where solidification or melting occurs. As a result, these approximated approximated solutions cannot be applied and numerical methods have to be used to simulate and develop an accurate solution regarding heat transfer for phase change problems.

Numerical methods for phase change heat transfer problem are usually solved by using finite difference or finite element methods. During the phase change process, some special treatments needed to be made with finite difference or finite element methods. There are many approaches that can be applied to deal with a phase change zone and the most common methods are a specific heat capacity method and the enthalpy method. These methods can both deal with a PCM that has a single phase change temperature or has a wide phase change temperature range.

Vollar and Cross [22] solved a one dimensional moving boundary problem by using a conventional enthalpy method and obtained accurate results. They then extended the problem into two dimensions and applied a modified enthalpy method. A relatively accuracy of 0.1% was obtained in a comparison between numerical results from other researchers and results from their proposed model [23], [24].

The specific heat capacity method is another approach to solve the moving boundary problem. The phase change process can be represented by using temperature dependent specific heat. Bonacina [1973] solved a one-dimensional moving boundary problem by using a finite difference method in which the phase change was expressed as a large heat capacity over a small temperature range. The results had 3% accuracy compared to an analytical solution. Lamberg and Lehtiniemi [15] applied PCM to telecommunication electronics that were both portable and

large scale and helped to control and dissipate energy. They also proposed a numerical model to validate the function of PCM. The enthalpy method and specific heat capacity method were both used to model a heat conduction problem. The finite difference method was used when the above two methods were applied. When specific heat capacity method was performed, two different phase change ranges were proposed. The results showed that both methods do well in predicting the function of PCM. Farid and Wang [8] tried to improve an existing underfloor heating system by using an encapsulated phase change material with melting temperature of about $28\,°C$. A specific heat capacity method was adapted to model the heat conduction problem. Heat capacity was replaced by a linear function with a larger number to address the phase change phenomenon.

In this chapter, phase change materials are incorporated into hybrid fiber reinforce concrete as a bridge deck in a cold climate region. With PCMs inside of the concrete, the interior temperature can be controlled. As described earlier, by going through a freeze-thaw process, microcracks are generated inside the concrete and eventually become larger cracks. The aim of this chapter is to find a temperature gradient inside of concrete by using an enthalpy method and a specific heat capacity method to solve the moving boundary problems. From the temperature gradient, we can observe that whether the interior temperature of the concrete is controlled by adding PCM. We also need to compare numerical results from both the enthalpy method and specific heat capacity method. In addition, we can also prove that by incorporating PCM into concrete, the interior temperature can be controlled.

6.2 Materials

Phase change material MPCM-6D was manufactured by Microtek Laboratories Inc. The melting point of MPCM-6D is 6 $°C$ (42.8 $°F$). The PCM starts to absorb and release energy when the temperature reaches 6 $°C$ and this allow the interior temperature of concrete to be controlled at a constant temperature and prevent the growth of cracks. PCM was microencapsulated into a polymer shell to prevent PCM from melting inside the concrete.

Table 6.1 shows the thermal properties of the MPCM 6D used in our study. In addition, the thermal properties of concrete are shown in table 6.2.

Materials	**Density (Kg/m3)**	**Specific heat capacity-liquid (J/(Kg K)**	**Specific heat capacity-solid (J/(Kg K)**	**Heat of fusion (KJ/Kg)**	**Enthalpy Phase transition (KJ/mol)**
PCM (MPCM-6D)	900	1870	2208	2287	44.267

Table 6.1 Thermal properties of PCM

Materials	**Density (Kg/m3)**	**Specific heat capacity (J/(Kg K)**	**Heat of fusion (KJ/Kg)**	**Thermal conductivity (W/(m K))**	**Thickness (m)**
Concrete	2200	880		1.28	

Table 6.2 Thermal properties of concrete

Figure 6.1 depicts a general heat conduction model of a PCM concrete composite. The length of this model is 100m, with a width of 10m and a height of 1m for modeling purposes. There are two cases were considered. The first case uses a thin PCM layer on the top of the concrete layer. The second case uniformly mixes PCM inside of the concrete. Two different cases are then compared in the following chapter.

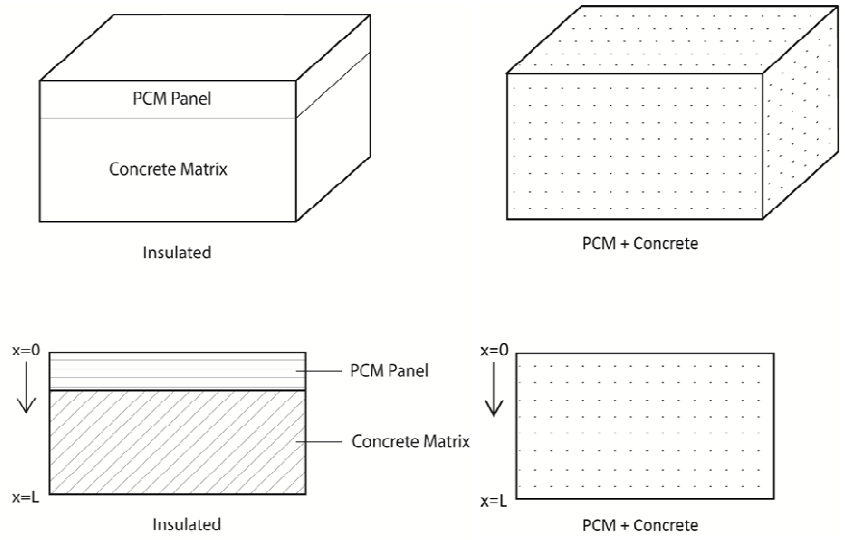

Figure 6.1 1-D heat conduction model of PCM concrete

6.3 Numerical Algorithm

6.3.1 One-dimensional Moving Boundary Problem

The heat transfer problem can be very complicated and involves heat conduction, heat convection and radiation. In our study, we will focus on heat transfer within a PCM concrete composite. Therefore, only heat conduction will be considered. Sometimes heat convection will be considered during a melting or thawing process. However, we will only account for heat conduction on both the freezing and thawing process.

Ju and Zhang [12] proposed a thermomechanical model for airfield concrete pavement under transient high temperature loading. They used a 1-D heat conduction model to first find the temperature gradient inside of concrete pavement when it was subjected to high temperature and proposed a subsequent damage model. They then use the same heat conduction equation to find a temperature gradient and propose an axisymmetric thermomechanical constitutive and damage model for airfield concrete pavement under transient high temperatures.

The basic one dimensional heat conduction problem can be expressed as the following heat conduction governing equations:

$$\rho C_s \frac{\partial T}{\partial t} = \nabla(k\nabla T) = \frac{\partial}{\partial x}(k\frac{\partial T}{\partial x}) \tag{6.1}$$

$$\rho C_l \frac{\partial T}{\partial t} = \nabla(k\nabla T) = \frac{\partial}{\partial x}(k\frac{\partial T}{\partial x}) \tag{6.2}$$

Equation (6.1) represents the solid-state heat conduction equation and equation (6.2) represents the liquid state heat conduction equation. Using finite difference or a finite element method can easily solve the above governing equations. However, during the phase change process, solid/liquid interface $X(t)$ will need to be tracked down accurately.

Accurately tracing the phase change boundary renders a large proportion of numerical schemes and difficult to implement. As a result, the enthalpy method and specific heat capacity method will be used to describe the phase change phenomenon without finding the location of the solid/liquid interface.

6.3.2 Enthalpy Method

As the track phase change interface is difficult to implement, one solution is to reformulate the governing equation in terms of enthalpy. Enthalpy is the sum of sensible heat and latent heat. In this case, the governing equation can be expressed as the following:

$$\rho \frac{\partial H}{\partial t} = \nabla (k \nabla T) = \frac{\partial}{\partial x} (k \frac{\partial T}{\partial x}) \tag{6.3}$$

We can observe that the temperature on the left hand side of equation (6.3) has been replaced by enthalpy. The advantages of this replacement are:

1. There are no conditions that need to be satisfied at the phase change interface.
2. There is no need to track the location of the solid/liquid interface.
3. It is easier to implement by using a numerical model.

The finite differences method will be used to solve the above governing equation. Explicit and implicit are two numerical schemes in the finite difference method. When using a implicit finite difference scheme, the solution is unconditionally stable and there are no restrictions regarding the size of the time step. However, two unknowns are involved at the current time step, which are enthalpy and temperature. Therefore, a certain iteration process such as Newton's method will need to be used in order to solve a finite difference equation.

The explicit finite difference method is easier to implement since it only needs to solve one unknown at the current time. From the previous time step, the enthalpy and temperature are known variables and they can be used to solve for enthalpy at the current time step. After enthalpy at the current time has been solved, we can utilize the enthalpy and temperature relationship to calculate temperature at the current time step.

Equation (6.3) can be discretized by using an explicit finite difference method. In other words, a central space and forward time algorithm will be adopted.

$$\rho \frac{H_i^{j+1} - H_i^j}{\Delta t} = k \frac{T_{i-1}^j - 2T_i^j + T_{i+1}^j}{\Delta x^2} \tag{6.4}$$

$$H_i^{j+1} = H_i^j + \frac{K\Delta t}{\rho \Delta x^2}[(T_{i-1}^j) - 2(T_i^j) + (T_{i+1}^j)] \tag{6.5}$$

Equation (6.5) is an explicit finite difference expression for the enthalpy method and it has to satisfy the following stability condition.

$$\Delta t \le \frac{1}{2} \frac{\rho C \Delta x^2}{K} \tag{6.6}$$

By using the enthalpy/temperature relationship, we can covert enthalpy into temperature.

$$H(T) = \begin{cases} C_P T & T < T_s \\ C_P T + \dfrac{T - T_S}{T_l - T_S} & T_S \le T \le T_l \\ C_P T + L & T > T_l \end{cases} \tag{6.7}$$

Equation (6.7) can be used to describe the phase change that takes place over a temperature range rather than at a single value. For some pure materials, phase change occurs at a single value and its enthalpy/temperature relationship can be expressed as:

$$H(T) = \begin{cases} C_P T & T < T_m \\ C_P T + L & T > T_m \end{cases} \tag{6.8}$$

During the phase change process, if the solid/liquid interface is located at discretized point i, then the temperature will be equal to melting temperature and enthalpy equal to the following equation.

$$\begin{cases} T = T_m \\ H = CT_m + L/2 \end{cases} \tag{6.9}$$

However, the temperature during phase change will be accurate if we apply equation (6.7) or (6.8) directly. The phase change interface will not always be at a discretized point in every element. In other words, the phase change interface at some of the points may already have passed a discretized point or has not reached it. Figure 6.2 shows the solid/ liquid interface during a freeze-thaw action. It is clear that the solid/ liquid interface would not necessary fall into the middle of the element.

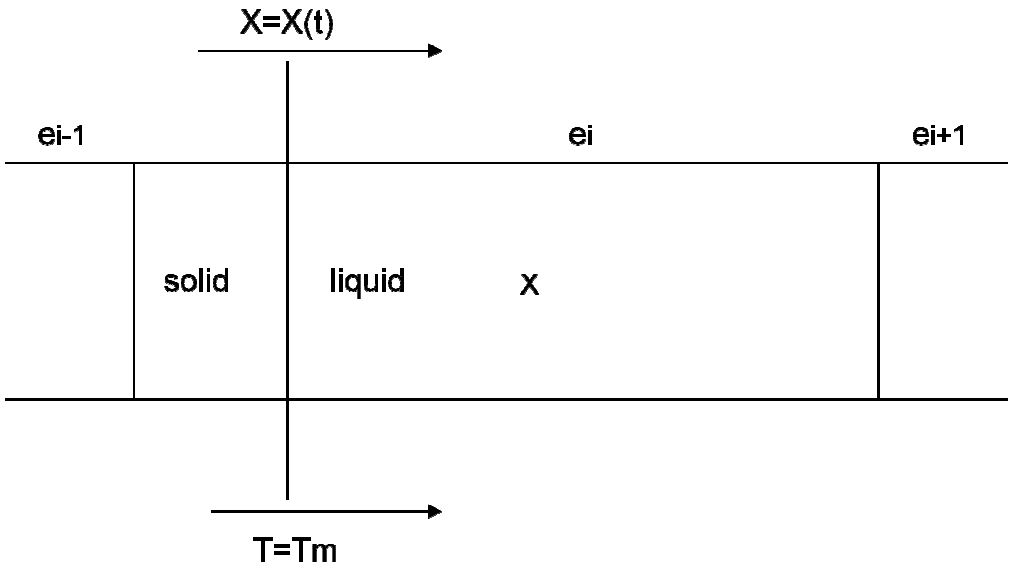

Figure 6.2 Solid/ liquid interface moving in one element

As a result, we utilize known temperatures and enthalpies from a previous point and the point where the solid/liquid interface lies to estimate the temperature at a current point by using linear interpolation.

$$X = \frac{(L/2 + CT_m - H_i^{j-1})}{H_i^j - H_i^{j-1}} \tag{6.10}$$

$$T_i^j = \frac{(T_m - T_i^{j-1})}{X} + T_i^{j-1} \tag{6.11}$$

Equation (6.10) and (6.11) explain linear interpolation during the phase change process. Temperature can be estimated by using a previous known enthalpy and temperature.

6.3.3 Specific Heat Capacity Method

The specific heat capacity method is another method that is frequently used to solve a phase change problem. Similar to the enthalpy method, a solid/liquid interface does not need to be traced. However, heat capacity will be assumed by a specific function to represent the freezing and thawing process.

The relationship between specific heat capacity and the phase change process has been studied by previous researchers. Lamberg [15] mentioned that the effective heat capacity of a material is directly proportional to latent heat storage during the phase change and heat capacity in the liquid and solid phase.

$$C_{eff} = \frac{L}{T_2 - T_1} + C_p \tag{6.12}$$

where T_2 is the melting or solidification temperature when phase change begins and T_1 represents the temperature where melting or the solidification process has completely finished.

In some other studies, Farid and Kong [8] expressed heat capacity during phase change process with a very large number. That assumption indicates that PCM can absorb or release a large amount of energy during the phase change process.

Similar to the enthalpy method, the finite difference method will be used to solve the heat conduction governing equation. Since only one variable will be involved when using the specific heat capacity method, the implicit method will also be easier to implement and does not introduce an iteration process. In the specific heat capacity method, an implicit finite difference algorithm will be implemented since it is unconditionally stable. As a result, time step size will not be considered.

The governing equation when applied to the specific heat capacity method can be expressed as:

$$\rho C_{eff} \frac{\partial T}{\partial t} = \nabla(k \nabla T) = \frac{\partial}{\partial x}(k \frac{\partial T}{\partial x}) \tag{6.13}$$

We can observe that heat capacity on the left hand side of equation has been replaced by effective or specific heat capacity C_{eff}. The governing equation can be discretized by using an implicit finite difference algorithm.

$$\rho C_{eff} \frac{T_i^{n+1} - T_i^n}{\Delta t} = k \frac{T_{i-1}^{n+1} - 2T_i^{n+1} + T_{i+1}^{n+1}}{\Delta x^2} \tag{6.14}$$

Equation (6.14) can be arranged with the following:

$$-\beta R T_{i-1}^{j+1} + (C_i^{j+1} + 2\beta R) T_i^{j+1} - \beta R T_{i+1}^{j+1} = C_i^{j+1} T_i^j \tag{6.15}$$

$$\beta = K / \rho \tag{6.16}$$

$$R = \frac{\Delta t}{\Delta x^2} \tag{6.17}$$

Equation (6.15) can further be simplified as:

$$a T_{i-1}^{j+1} + b T_i^{j+1} + c T_{i+1}^{j+1} = Q \tag{6.18}$$

$$a = c = -\beta R \tag{6.19}$$

$$b = C_i^{j+1} + 2\beta R \tag{6.20}$$

$$Q = C_i^{j+1} T_i^j \tag{6.21}$$

Equation (6.18) cannot be solved directly because it involves a series of nonlinear equations. Therefore, we can use a tri-diagonal matrix algorithm (TDMA) to solve this systematically. Equation (6.18) can be represented as the following matrix form:

$$\begin{pmatrix} b_1 & c_1 & 0 & 0 & 0 & 0 \\ a_2 & b_2 & c_2 & 0 & 0 & 0 \\ 0 & a_3 & b_3 & c_3 & 0 & 0 \\ 0 & 0 & \ddots & \ddots & \ddots & 0 \\ 0 & 0 & 0 & a_{n-1} & b_{n-1} & c_{n-1} \\ 0 & 0 & 0 & 0 & a_n & b_n \end{pmatrix} \begin{pmatrix} h_1 \\ h_2 \\ \vdots \\ \vdots \\ h_{n-1} \\ h_n \end{pmatrix} = \begin{pmatrix} Q_1 \\ Q_2 \\ \vdots \\ \vdots \\ Q_{n-1} \\ Q_n \end{pmatrix} \tag{6.22}$$

From finding the lower and upper tri-diagonal matrix of equation (6.22) and combining this with the initial condition and boundary conditions, the temperature at the current point at a specific time can then be estimated.

Since the phase change material has a range of phase change temperature, specific heat capacity will need to be estimated during the phase change process. In our numerical model, phase change temperature is set to be from $6\,°C$ to $10\,°C$ during the melting process. In addition, the phase change temperature is set to be from $8\,°C$ to $2\,°C$ during a solidification process. The above assumptions are made to match the experimental result.

Specific heat capacity is assumed to be a large number in order to properly represent phase change behavior. In our simulated model, effective heat capacity is estimated as the following:

$$\begin{cases} C_{eff} = 1870 & T_i^j \le 6°C \\ C_{eff} = 2039 + 16700 * (T_i^j - 6) & 6°C \le T_i^j < 8°C \\ C_{eff} = 2039 + 16700 * (10 - T_i^j) & 8°C < T_i^j \le 10°C \\ C_{eff} = 2208 & T_i^j > 10°C \end{cases} \tag{6.23}$$

$$\begin{cases} C_{eff} = 1870 & T_i^j < 2°C \\ C_{eff} = 2039 + 16700 * (T_i^j - 2) & 2°C \le T_i^j < 8°C \\ C_{eff} = 2208 & T_i^j > 8°C \end{cases} \tag{6.24}$$

Equation (6.23) represents the specific heat capacity during the melting process and equation (6.24) expresses the effective heat capacity during the solidification process. By applying specific heat capacity into the heat conduction governing equation and using the above finite difference algorithm, temperature can then be solved.

Boundary conditions and initial conditions also need to be defined in order to solve the heat conduction governing equation.

$$T(x,0) = T_i \tag{6.25}$$

$$T(0,t) = T_s \tag{6.26}$$

$$T(L,t) = T_m \tag{6.27}$$

6.4 Numerical Results and Discussions

6.4.1 Numerical Modeling for PCM and Concrete Layer

As mentioned in the previous section, there are two types of PCM concrete composite. Comparisons regarding temperature gradient will be made later. Here, we will model the interior temperature and discuss the thermal efficiency between a PCM layer and concrete layer.

Figure 6.3 compares the temperature gradient between a PCM layer and concrete layer by using the specific heat capacity method.

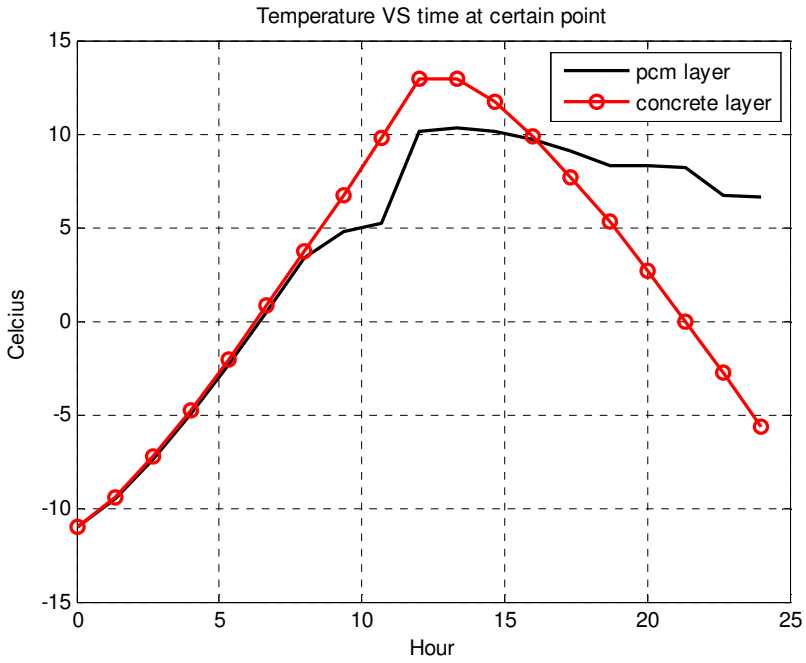

Figure 6.3 Temperature gradient in both PCM layer and concrete layer at x=10 cm

These results show a heating process for 12 hours and 12 hours for a solidification process. We can observe that during the phase change temperature range, temperature is not as high as in the concrete layer because PCMs absorb more energy by utilizing phase change than concrete. One of the important benefits when using PCM is that the temperature in the solidification process is about $6\,°C$ after 12hours. As mentioned previously, PCM can be applied in a cold climate region and our goal is to prevent solidification from water inside of the concrete when the temperature drops. As a result, we can observe that energy absorbed by PCM during the day was released at night when the temperature becomes lower and it can maintain the concrete interior temperature. We can also observe that the temperature in the concrete layer drops very quickly in the solidification process and it is below $0\,°C$. The difference can be seen

between concrete and the PCM layer and proves that PCM indeed can provide better thermal performance than concrete.

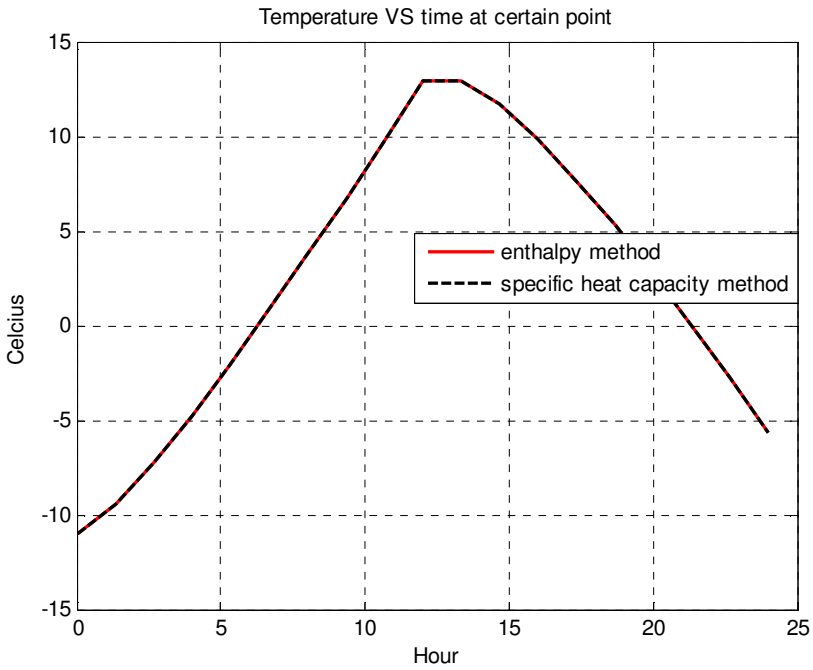

Figure 6.4 Temperature distributions in concrete layer with two numerical models

Figure 6.4 compares the temperature gradient of a concrete layer when using both an enthalpy method and a specific heat capacity method. The results of the temperature gradient reflects 12 hours for the heating process and solidification for another 12 hours. We can observe that using either method yields the same result. Since there is no phase change phenomenon in the concrete layer, there are no additional assumptions that need to be made for all of the heating and solidification process.

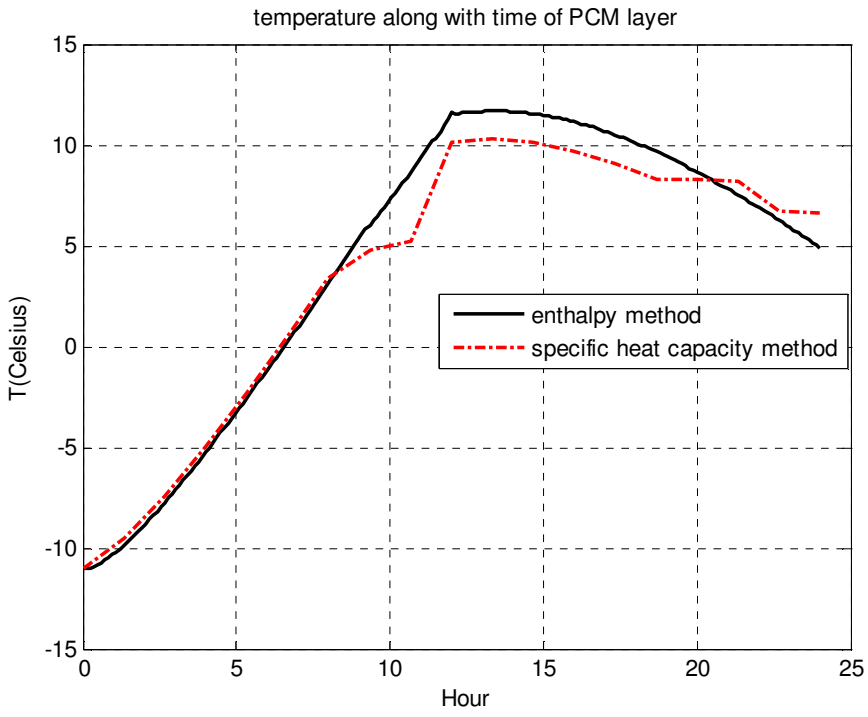

Figure 6. 5 Temperature distributions in PCM layer with two numerical models

Figure 6.5 displays the temperature gradient in the PCM layer when using both an enthalpy method and specific heat capacity method. We can observe that both curves do not match exactly due to different approaches when the phase change process occurs. When using the enthalpy method, we utilized enthalpy and the temperature mentioned from the previous section to do a linear interpolation. Details were addressed in equation (6.10) and (6.11). When specific heat capacity is used, we assumed that the heat capacity is large enough to represent the phase change process. From equation (6.23) and (6.24), we can observe that the phase change process has been addressed during both the melting and solidification process. Modeling using a specific heat capacity method is easier to implement. However, the temperature gradient curve would not be as smooth as that by using the enthalpy method. Therefore, for the following

analysis, the enthalpy method will be utilized to model the temperature gradient inside of concrete.

6.4.2 Modeling of PCM Layer Laminated with Concrete

Figure 6.1 depicts the one dimensional heat transfer model. The length of this model is 100m, the width is 10m and height is 1m for modeling purpose. There are two types of model, one type includes a PCM layer on top of the concrete layer, and the other type has PCMs uniformly distributed into the concrete matrix. We already compared thermal performance between a PCM layer and concrete layer separately. In this section, we look at performance when the PCM layer is assembled on top of the concrete layer.

Figure 6.6 shows the temperature gradient comparisons of a PCM layer concrete composite and only the concrete itself when the location is set to be 0.5m. The model was simulated by using an enthalpy method. The total thickness of the concrete plus PCM was 1 m and the thickness of the PCM layer is set to be 0.07 m. We can observe that when the melting process is complete, the temperature of PCM layer concrete composite is still higher than the temperature in only the concrete layer. In addition, the temperature is still higher than $0°C$ compared to the concrete layer only.

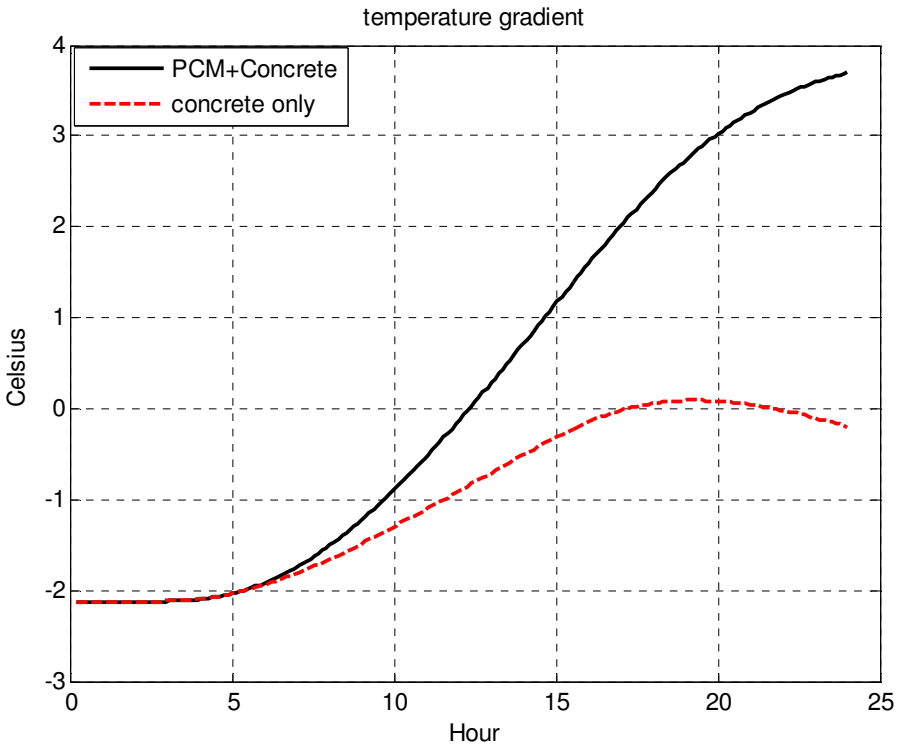

Figure 6.6 Temperature gradient comparison when x = 0.07m

6.4.3 Thickness Effect of PCM Layer

The thickness of the PCM panel can have a great influence on the thermal performance of the PCM concrete composite.

Figure 6.6 depicts the temperature gradient when the thickness of the PCM panel is 0.07m and 7% of total volume fraction. In addition to the thickness of 0.07m, we also proposed another PCM layer with a thickness of 0.05m and 5% of total volume fraction.

Figure 6.7 demonstrates the temperature when the thickness of the PCM layer was set as 0.05 m. We can observe that the temperature gradient is lower when we compare with Figure 6.6 because less PCM can be used to absorb and release energy. Therefore, we can assume that adding more and more PCM on the top of concrete can greatly enhance the thermal performance of a concrete composite.

However, the thickness cannot be increased further just to suit thermal performance because the strength of the concrete composite will be compromised. We can see from previous experiments that adding more and more PCM will significantly decrease concrete compressive strength, tensile strength and bending capacity. As discussed at the beginning, the PCM concrete composite will be used as bridge deck. As a result, strength capacity is also important because it will need to carry loads every day. In addition, the high cost of PCM would not meet budget considerations.

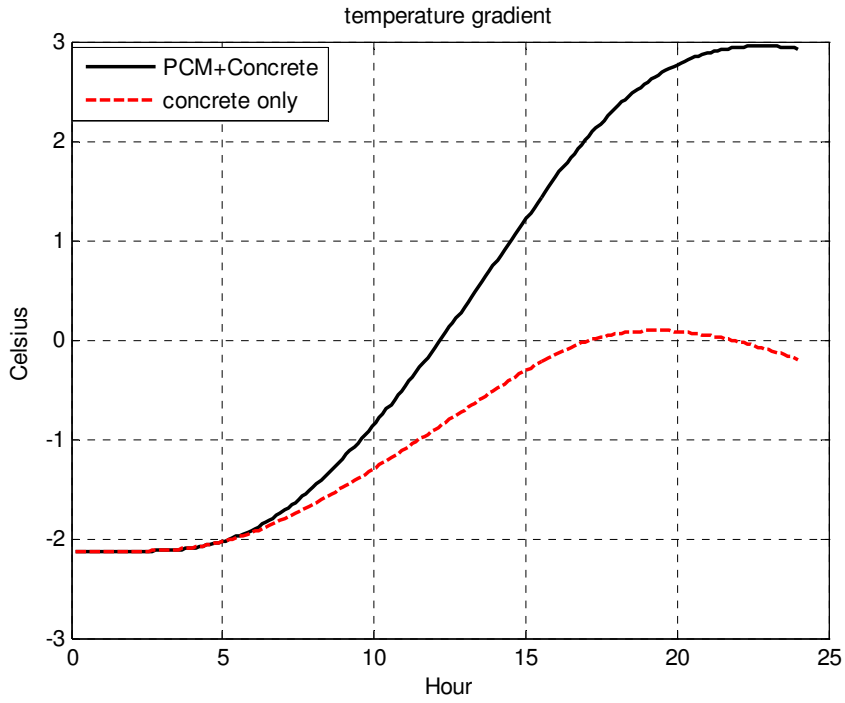

Figure 6.7 Temperature gradient comparison when thickness of PCM layer = 0.05m

6.4.4 Modeling of PCM Uniformly Distributed into Concrete Matrix

As discussed in section 6.4.2, the concrete interior temperature gradient of a PCM layer adding on top of a concrete layer has been modeled. In addition, the second case where PCMs are uniformly distributed into the concrete matrix will be discussed in this section. Figure 6.1 also shows that PCMs that are uniformly distributed into a concrete matrix with the same dimension as described in section 6.4.2. In this section, we will compare results from section 6.4.2.

In general, adding a PCM layer on top of concrete will provide better performance than mixing PCMs uniformly distributed into concrete. When PCMs are mixed and uniformly distributed into concrete, many PCMs might not be efficient used as for thermal performance purpose. For example, some PCMs on the lower part of the concrete composite will not be able to absorb heat from the surface. In contrast, using a PCM layer at the top of concrete will guarantee that all of the PCM is used to absorb and release energy without wasting any material.

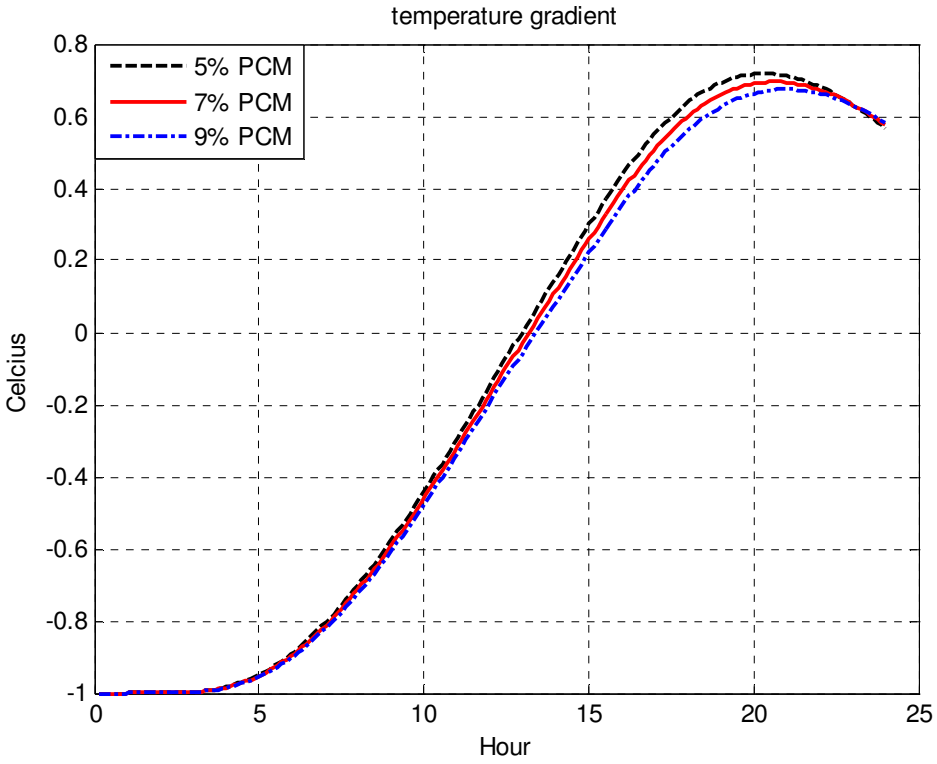

Figure 6.8 Temperature gradient comparison with different PCM ratio at x = 0.5 m

Figure 6.8 shows the temperature gradient with a different PCM ratio at x=0.5m. The volume fraction of PCM that we used was 5%, 7% and 9% in this numerical model. In general, adding more and more PCM will improve thermal performance of the PCM concrete composite.

We can observe that the temperature gradient of 9% PCM concrete composite is lower than 5% PCM added into concrete during the melting process. In addition, the temperature of 9% PCM concrete composite is higher than other two models at the end of the solidification process. In other words, adding more PCM can help concrete composite to absorb and release more energy during phase change. We can also observe that the temperature gradients are all higher than $0\,°C$ at the end of the solidification process.

Table 6.3 depicts temperature at the end of solidification process with different PCM ratio. We can see the temperature of 9% PCM concrete composite is higher than 7% and 5% PCM concrete composite. Thus, adding more PCM can increase thermal performance and is consistent with the results from section 6.4.2. However, we cannot infinitely increase PCM because it will compromise the strength of the concrete composite. In addition, more PCMs will not be able to perform since they will be uniformlyly mixed into concrete.

PCM %	5%	7%	9%
Temperature at 0.5m ($°C$)	0.5661	0.5753	0.5815

Table 6.3 Temperature at x=0.5m with different PCM ratios

Figure 6.9 shows a temperature comparison between laminated PCM concrete and uniformly distributed PCM concrete. We can observe that the temperature during the melting process of 5% PCM mixed uniformly distributed in concrete is higher than laminated PCM concrete. In addition, the temperature of 5% PCM mixed uniformly distributed concrete is lower

than laminated PCM concrete during the solidification process. In other words, thermal performance in the uniformly distributed PCM concrete is less efficient than the laminated PCM concrete system.

The reasons for this have already been explained at the beginning of this section. Most of the energy is absorbed and released from the surface of concrete. As a result, if a PCM layer is added on top of concrete, the PCM will be able to absorb and release most of the energy. However, when PCMs are uniformly mixed into a concrete matrix, some PCM might locate at the lower part of the concrete. Therefore, it will not able to absorb the energy very efficiently. In other words, some of the PCM will be wasted.

However, uniformly distributed PCM concrete is easier to mix since we only need to add PCM during the concrete mixing process. Because the PCM that we used is in the form of a dry powder, it will be difficult to form a PCM layer without any special treatment. We can see from Figure 6.9 that both types of PCM concrete can reach a temperature above $0\,°C$ at the end of the solidification process. As a result, both types of concrete model are acceptable for use.

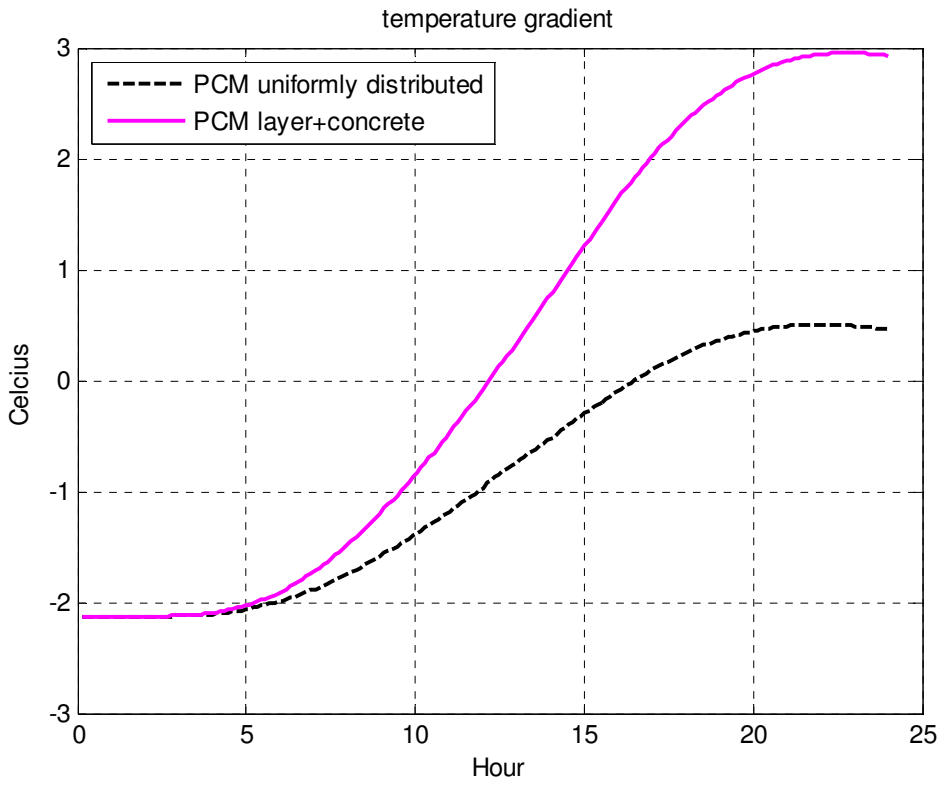

Figure 6.9 Temperature gradient of PCM layer concrete compared to unoformly distributed PCM

6.5 Conclusion

In this chapter, PCM incorporated into a building material was adopted and the thermal performance of PCM concrete was investigated. Three different PCM concrete models were presented. At first, PCM layer and concrete layer are compared with two different numerical methods. Secondly, laminated PCM concrete was modeled to examine thermal performance. Last but not the least, we also modeled uniformly distributed PCM concrete to measure its thermal performance and compare this with laminated PCM concrete. Conclusions include the following:

- An enthalpy method and specific heat capacity method were used to model both a PCM layer and concrete layer. During the phase change process, some special treatments have been made to describe the phase change. When the enthalpy method is used, linear interpolation is applied to model enthalpy and temperature during the phase change based on known enthalpy and temperature from a previous point and the point where the phase change interface is in the middle of an element. When a specific heat capacity method is used, heat capacity is assumed to be a large number to represent the phase change process. Results form both methods showed they could both produce reasonable results. Errors do exist between the two methods because different assumptions were made to represent the phase change process. In addition, we also prove that using a PCM layer achieves better thermal performance than using a concrete layer from both numerical methods.

- In the field application, a PCM layer as the only material without any treatment cannot be used to carry load since the strength capacity would not be satisfied. A PCM layer was added on top of a concrete layer to avoid wasting PCM and to improve thermal performance in a more efficient way. In addition, it can utilize the strength of concrete to sustain loads. If PCMs are uniformly mixed into concrete matrix, some PCM will not be used to absorb and release energy to improve thermal performance. This happens because some PCMs may locate at the bottom of a concrete matrix, making it difficult to absorb the energy from sunlight through the concrete surface. As a result, by incorporating a PCM layer on the top of concrete to absorb and release energy during phase change might be the most efficient approach. Numerical results proved that laminated PCM concrete can improve thermal performance compared to normal concrete. In addition, we also looked at the effect from different thicknesses in the PCM layer. Obviously, increasing the thickness of the PCM

layer can help a PCM concrete composite to improve thermal performance. However, the thickness of a PCM layer cannot continuously built up because it will compromise the strength of the concrete composite. Thermal performance is important in our application, but to maintain essential strength is also important to carry load.

- In order to compare the efficiency of laminated PCM concrete, uniformly distributed PCM concrete was also studied in this chapter. It is easier to mix PCM uniformly into concrete during the mixing process. We only need to mix PCM with sand and then mix it with other fine and coarse aggregates. This could be done easily before construction or even done in the field. Similar to laminated PCM concrete, adding more and more PCM can help concrete composite to increase its thermal performance. Therefore, we used 5%, 7% and 9% as various PCM volume fractions to investigate the effect of increasing phase change material. The results showed that adding more PCM indeed could increase the thermal performance of concrete composite, though it is not very significant. From previous experimental results, the strength capacity of 9% PCM concrete was greatly reduced. As a result, PCM volume fraction cannot be further increased. In addition, thermal performance might not be as good as laminated PCM concrete because some PCM will not be able to absorb energy from the surface. We also showed temperature comparison between laminated PCM concrete and uniformly distributed PCM concrete. The results showed that both laminated PCM concrete and uniformly distributed PCM concrete can reach the required temperature after finishing the melting process. Overall, However, laminated PCM concrete has better thermal performance than uniformly distributed PCM concrete.

In a forthcoming chapter, we will consider a coupled effect between thermal performance of PCM concrete composite and fracture mechanics. In this chapter, we focus on using different numerical algorithms to solve a 1-D heat conduction problem and investigate thermal performance with different PCM concrete models. It will also be important to study fracture behavior when considering thermal effect. When there is no PCM added into the concrete matrix, cracks will develop and propagate at a faster rate by going through the freeze and thaw process everyday. However, after PCM is added, the rates of crack development and propagation should become slower because temperature can be maintained at a higher level. As a result, it is necessary to study the relationship between fracture mechanism and thermal performance of PCM concrete composite.

First, we will study mechanical property degradation after going through a freeze-thaw cycle. As mentioned previously, the freeze-thaw process can induce cracks formation and propagation. As a result, mechanical properties, such as elastic modulus, Poisson's ratio, ultimate stress and ultimate strain are expected to be affected. In the next chapter, the relationship between mechanical properties and a freeze-thaw cycle are discussed.

Secondly, stress strain relationship coupled with thermal effect will be investigated. We are also interested in understanding concrete residual capacity after going through a freeze-thaw action. After certain freeze-thaw cycles, the concrete structure might not be entirely damaged and still can perform as needed. As a result, it is important to know the concrete residual capacity and remaining strength after performing certain freeze-thaw cycles. In order to evaluate concrete residual capacity, we will develop a concrete stress-strain relationship after freeze-thaw cycle. By evaluating mechanical property degradation and combining this with free energy potential

and thermodynamics basics, a stress-strain relationship will be proposed. The stress strain relationship is important for studying the strength and durability of a material in the field of structural mechanics. Since the thermal performance of PCM concrete composite will be improved after adding PCM, it will also affect the stress and strain relationship. As a result, it is important to study the effect of adding PCM on the stress strain relationship.

Lastly, we will develop a damage model to predict crack development and propagation. Fracture mechanics is an important topic in the field of concrete since it can define the fracture criteria of a concrete composite. The energy method will be used to define the criteria for crack formulation. We will also combine with thermal effect to find stress intensity factor k_{IC} and use this as a fracture criteria. For designing purposes, if fracture toughness of concrete composite is larger than a stress intensity factor, then cracks will start to formulate and propagate. Finally, commercial software such as ABAQUS and COMSOL can be used to verify the numerical modeling

6.6 References

[1] Athienitis, A. K., Liu, C., Hawes, D., Banu, D., and Feldman, D. (1997). "Investigation of the thermal performance of a passive solar test-room with wall latent heat storage." *Building and Environment*, 32(5), 405-410.

[2] Bell, G. E. (1982). "On the performance of the enthalpy method." *International Journal of Heat and Mass Transfer*, 25(4), 587-589

[3] Crowley, A. B. (1978). "Numerical-solution of Stefan problems." International Journal of Heat and Mass Transfer, 21(2), 215-219.

[4] Darkwa, J. (2009). "Mathematical evaluation of a buried phase change concrete cooling system for buildings." Applied Energy, 86(5), 706-711.

[5] Darkwa, K., and O'Callaghan, P. W. (2006). "Simulation of phase change drywalls in a passive solar building." Applied Thermal Engineering, 26(8-9), 853-858.

[6] Date, A. W. (1992). "Novel strongly implicit enthalpy formulation for multidimensional Stefan-problems." Numerical Heat Transfer Part B-Fundamentals, 21(2), 231-251.

[7] Dutil, Y., Rousse, D., Lassue, S., Zalewski, L., Joulin, A., Virgone, J., Kuznik, F., Johannes, K., Dumas, J. P., Bedecarrats, J. P., Castell, A., and Cabeza, L. F. (2014). "Modeling phase change materials behavior in building applications: Comments on material characterization and model validation." Renewable Energy, 61, 132-135.

[8] Farid, M., and Kong, W. J. (2001). "Underfloor heating with latent heat storage." Proceedings of the Institution of Mechanical Engineers Part a-Journal of Power and Energy, 215(A5), 601-609.

[9] Hasan, M., Mujumdar, A. S., and Weber, M. E. (1991). "CYCLIC MELTING AND FREEZING." Chemical Engineering Science, 46(7), 1573-1587.

[10] Izquierdo-Barrientos, M. A., Belmonte, J. F., Rodriguez-Sanchez, D., Molina, A. E., and Almendros-Ibanez, J. A. (2012). "A numerical study of external building walls containing phase change materials (PCM)." Applied Thermal Engineering, 47, 73-85.

[11] Joulin, A., Younsi, Z., Zalewski, L., Rousse, D. R., and Lassue, S. (2009). "A numerical study of the melting of phase change material heated from a vertical wall of a rectangular enclosure." International Journal of Computational Fluid Dynamics, 23(7), 553-566.

[12] Ju, J. W., and Zhang, Y. (1996). "Thermo-micromechanical damage modeling of airfield concrete pavement." Engineering Mechanics: Proceedings of the 11th Conference, Vols 1 and 2, 727-730.

[13] Ju, J. W., and Zhang, Y. (1998). "Axisymmetric thermomechanical constitutive and damage modeling for airfield concrete pavement under transient high temperature." Mechanics of Materials, 29(3-4), 307-323.

[14] Kuznik, F., and Virgone, J. (2009). "Experimental investigation of wallboard containing phase change material: Data for validation of numerical modeling." Energy and Buildings, 41(5), 561-570.

[15] Lamberg, P., Lehtiniemi, R., and Henell, A. M. (2004). "Numerical and experimental investigation of melting and freezing processes in phase change material storage." International Journal of Thermal Sciences, 43(3), 277-287.

[16] Liu, M., Saman, W., and Bruno, F. (2011). "Validation of a mathematical model for encapsulated phase change material flat slabs for cooling applications." Applied Thermal Engineering, 31(14-15), 2340-2347.

[17] Mirzaei, P. A., and Haghighat, F. (2012). "Modeling of phase change materials for applications in whole building simulation." Renewable & Sustainable Energy Reviews, 16(7), 5355-5362.

[18] Muhieddine, M., Canot, É., and March, R. "Various approaches for solving problems in heat conduction with phase change."

[19] Pasupathy, A., Athanasius, L., Velraj, R., and Seeniraj, R. V. (2008). "Experimental investigation and numerical simulation analysis on the thermal performance of a building roof incorporating phase change material (PCM) for thermal management." Applied Thermal Engineering, 28(5-6), 556-565.

[20] Pasupathy, A., Velraj, R., and Seeniraj, R. V. (2008). "Phase change material-based building architecture for thermal management in residential and commercial establishments." Renewable & Sustainable Energy Reviews, 12(1), 39-64.

[21] Sadasivam, S., Zhang, D. H., Fung, A. S., Almeida, F., and Ashrae (2011). "An Iterative Enthalpy Method to Overcome the Limitations in ESP-r's PCM Solution Algorithm." Ashrae Transactions 2011, Vol 117, Pt 2, 117, 100-107.

[22] Voller, V., and Cross, M. (1981). "Accurate solutions of moving boundary-problems using the enthalpy method." International Journal of Heat and Mass Transfer, 24(3), 545-556.

[23] Voller, V. R. (1985). "Implicit finite-difference solutions of the enthalpy formulation of Stefan-problems." Ima Journal of Numerical Analysis, 5(2), 201-214.

[24] Voller, V. R. (1990). "Fast Implicit finite-difference method for the analysis of phase-change problems." Numerical Heat Transfer Part B-Fundamentals, 17(2), 155-169.

[25] Xing, J., and Xiaosong, Z. (2011). "Thermal analysis of a double layer phase change material floor." Applied Thermal Engineering, 31(10), 1576-1581.

[26] Xu, B., and Li, Z. (2013). "Paraffin/diatomite composite phase change material incorporated cement-based composite for thermal energy storage." Applied Energy, 105, 229-237.

[27] Yinping, Z., Xu, X., Kunping, L., Hongfa, D., and Rui, Y. (2005). "Modeling and simulation on the thermal performance of shape-stabilized phase change material floor used in passive solar buildings." Energy and Buildings, 37(10), 1084-1091.

[28] Zhang, M., Medina, M. A., and King, J. B. (2005). "Development of a thermally enhanced frame wall with phase-change materials for on-peak air conditioning demand reduction and energy savings in residential buildings." International Journal of Energy Research, 29(9), 795-809.

[29] Zukowski, M. (2007). "Mathematical modeling and numerical simulation of a short term thermal energy storage system using phase change material for heating applications." Energy Conversion and Management, 48(1), 155-16

Chapter 7 Mathematical Modeling of Mechanical Properties of PCM Concrete and Residual Capacity under Action of Freeze Thaw

7.1 Introduction

Passive energy storage systems have been applied extensively in hot climate regions to address the need to reduce energy consumption [27]. It is known that PCM can be applied either in a warm climate region or cold climate region. These systems can serves different purposes depending on different climate conditions. In a cold climate region, temperatures drop to below 0 $°C$ and water inside the concrete can solidify into ice. Ice may then melt into water during the day when temperatures rise. By going through this freeze-thaw process, the pore pressure inside concrete increases and eventually surpasses material mechanical resistance. Microcracks are then generated. By incorporating a passive energy storage system into the structure, it is possible to storage energy during the day and release the energy at night. As a result, concrete interior temperature can then be maintained and the formation of microcracks can also be minimized or delayed. In a warm climate region, a passive energy system generally follows the same energy saving process, although for a different purpose. For example, systems can help maintain building interior temperature and provide more comfortable temperatures for occupants. As such, there is increasing interest around the world in developing energy storage systems.

Over the past few years, incorporating phase change material (PCM) into a building has been studied by many researchers as a potential technology for improving energy storage and minimizing energy consumption. Researchers such as Xu and Li [27] applied PCM for maintaining interior temperature in a warm climate region [5], [6], [15]. Using phase change material (PCM) as passive energy storage system has many benefits, such as its very high heat storage density and low heat conductivity. During the phase change process, PCM can store most of the energy and has very little temperature variation [27]. During the day PCM can absorb excessive energy and phase change from solid to liquid. After the temperature drops during the night, PCM releases the energy and phase changes from liquid to solid. By going through this phase change process over and over, the temperature can be controlled.

Recently, researchers have found that applying PCM in a cold climate region is also beneficial. As mentioned at the beginning, temperature drops down to below $0\,°C$ and water inside of concrete or asphalt pavement can solidify into ice. Ice then melt into water during the day due to radiation from sun-light. Going through this freeze and thaw process inside of concrete, microcracks are generated and eventually macrocracks are formed and propagate. Further damage may be caused due to various cracks.

Vollar and Cross [23] solved a one dimensional moving boundary problem by using a conventional enthalpy method that lead to accurate results [24] [25]. They were able to calculate a temperature gradient inside of concrete and observe the temperature variation under freeze-thaw action. They then extended the problem into two dimensions and applied modified an enthalpy method. A relatively accuracy of 0.1% was obtained in the comparison between numerical results from other researchers and result from their proposed model.

Zuber and Marchand [30] proposed a numerical model to predict the behavior of saturated cement composites subjected to a freezing process. The model was derived based on thermal dynamics and needs to be solve numerically. It yields the pore pressure generated in the liquid and solid phases by mass transfer and crystal growth. However, the relationship between concrete structure strength and the freeze-thaw cycle is still unknown after pore pressure can be calculated. If pore pressure exceeds material strength, microcracks will be generated. Understanading how pore pressure will change under a freeze-thaw cycle and eventually how it can exceed material strength is still a challenge.

Ueda and Hasan [22] attempted to develop models for stress-strain relationships in tension and compression of concrete damaged by freezing and thawing cycles. A freeze-thaw test was performed to observe freeze-thaw damage. Mechanical properties, such as compressive stress, tensile stress and dynamic Young's modulus were also measured. They introduced a fracture parameter to represent the degradation of stiffness. Clearly, it is a function of number of freeze-thaw cycles. A fracture parameter can be determined from experimental data. However, the model of stress-strain relationship after a freeze-thaw process has not been discussed.

Song and Ji [20] tried to estimate concrete structure residual life after suffering freeze-thaw cyclic damage. The damage to a concrete structure subjected to a freeze-thaw action may be approximately regarded as the damage due to a sequential cyclic action with various positive-negative peak temperature differences. Since the temperature difference is not always a constant, the reliability of damaged concrete needs to be analyzed. The failure of concrete can be described by three parameters in the Weibull distribution model. Combining experimental data and Weibull distribution model will allow estimation about the residual life of a concrete structure that has gone thru after number of freeze-thaw cycles.

All the discussion above regarding concrete structure residual life after a freeze-thaw action, the temperature gradient inside of concrete or how the concrete interior structure can change are based on micromechanics and thermodynamics theories. Researchers have also mentioned the stress-strain relationship with a specific freeze-thaw cycle. However, there have been no discussions regarding how concrete structure strength would evolve under the action of a freeze-thaw cycle.

Wei, Wu and Zhao [26] proposed a damage model to study the frost durability of concrete. Their model is able to describe the deterioration of concrete during the complete freeze-thaw process. They introduced a damage parameter to describe damage under a freeze-thaw process and it is function of freeze-thaw cycles and other material properties. Liu and Wang [17] also proposed a damage model based on the concept of a damage parameter. They suggested that the failure process of concrete goes through a freeze-thaw process is similar to concrete subjected to mechanical actions, such as compressive loading, as suggested by some researchers. The characteristic failure point when concrete is subjected to loading can be observed. Thus, they used the concept of multiple characteristic failure points to describe the damage parameter under the action of a freeze-thaw. After a damage parameter is found, it will be possible to predict material mechanical properties.

Zhu, Li and Liu [29] did a freeze-thaw experiment to study mechanical properties. They measured mechanical properties, such as dynamic Young's modulus, elastic modulus and compressive stress at 0, 100, 200, 300 freeze-thaw cycles. They also proposed two numerical models to estimate elastic modulus and compressive stress. They were all a function of the freeze-thaw cycle and fit experimental data well. However, most of the constants from the

numerical models use data fitting to come to their determination. As a result, these numerical models may not be able to estimate another set of experimental data accurately.

In this chapter, phase change materials are incorporated into hybrid fiber reinforced concrete as bridge deck in a cold climate region. With PCMs inside of concrete, interior temperature can be controlled. However, the relationship between concrete structure mechanical properties, freeze-thaw cycle, and freeze-thaw temperature will need to be determined. The aim of this paper is to develop a damage model that account for concrete structure strength, freezing-thawing cycle, and freeze-thaw temperature differences. Different sets of data will be presented and comparison made using our damage model. We can thus also then prove that the damage degradation of PCM concrete is indeed slower than concrete without PCM after going through freeze-thaw cycle.

After the relationship is found regarding concrete mechanical properties, freezing-thawing cycle and temperature difference, we can determine the stress-strain relationship by using damaged concrete mechanical properties. A constitutive relationship can be derived by using thermodynamics theory. Elastic damage and plastic damage will both be evaluated. Once a stress-strain relationship can be obtained, we will be able to estimate concrete residual life and residual durability after going through a freeze-thaw action. Normal concrete will also be compared with PCM concrete. The damage degradation of PCM concrete is indeed slower than concrete without PCM after going through freeze-thaw cycle.

7.2 Pore Pressure of PCM Cell

7.2.1 Mass Transfer Equation

Concrete strength degradation or the damage process when subjected to a by freeze-thaw process is complicated when using mathematical models for prediction. The freeze-thaw damage mechanism can be basically divided into two parts. First, it can be analyzed from micromechanics point of view. A microcrack is generated due to pressure inside of a pore when the water phase changes from liquid to solid. Because of volume expansion, pressure will be applied on the surface of concrete. When concrete goes through freeze-thaw cycles, similar to a fatigue mechanism, concrete nominal strength will decrease. If pressure inside of a pore surpasses concrete nominal strength, a microcrack will then be generated. However, from a structural point of view, the whole structure will not be directly affected due to microcracks directly. Therefore, we will study concrete at a macro scale and construct a relationship between concrete strength degradation and freeze-thaw cycles to help engineers set design criteria.

To calculate pore pressure inside of concrete at a micro scale, we will briefly discuss several considerations. We will start with the mass balance equations [30]. When liquid inside of a pore begins to freeze into solid, mass balance needs to be followed.

$$\frac{n}{\rho_l}\frac{d\rho_l}{dt}+\frac{n}{S_l}\frac{dS_l}{dt}+\frac{dn}{dt}+\frac{1}{S_l}divj_l+\frac{j_l}{S_l\rho_l}grad\,\rho_l=\frac{-1}{S_l\rho_l}\frac{1}{V}\frac{dm_{l\to i}}{dt} \tag{7.1}$$

$$j_l=-\frac{D}{\eta_l}grad\,\rho_l \tag{7.2}$$

Equation (7.1) is the mass balance equation with a phase change phenomena of fluids in a porous medium, where S is the fraction of the pore volume filled with phase j, n represents the total porosity of the porous materiel and j stands for the heat flux.

The mass balance equation with respect to the ice and solid phase that forms the porous skeleton can also be developed.

$$\frac{(1-n)}{\rho_s}\frac{d\rho_s}{dt}-\frac{dn}{dt}+(1-n)divu=0 \tag{7.3}$$

Where u is solid skeleton velocity.

For ice, the mass balance equation corresponding to the phase change is similar to equation (7.1) and can be expressed as:

$$\frac{n}{\rho_i}\frac{d\rho_i}{dt}+\frac{n}{S_i}\frac{dS_i}{dt}+\frac{dn}{dt}=\frac{-1}{S_i\rho_i}\frac{1}{V}\frac{dm_{l\to i}}{dt} \tag{7.4}$$

Where $R_{p_{eq}}(t)$ stands for critical radius of curvature of liquid/solid interface.

Pressure exerted on the pore walls also need to be determined.

$$p^* = p_l+\frac{1}{n}\int_{R_{p_{eq}}(t)}^{\infty}\chi(r,t)\frac{d\varphi}{dr}dr \tag{7.5}$$

$$\chi(r,t)=\frac{\gamma_{li}(t)}{r-\delta(t)} \tag{7.6}$$

Where p^* is the averaged pressure exerted by the ice crystals and the liquid phase on the pore walls.

At this point, the mass balance equation and pressure exerted on the pore walls have been proposed. We will also need to develop the constitutive relations. Basically, the density is a function of temperature and pressure inside of pore. For the liquid phase this can be expressed as:

$$\frac{1}{\rho_l}\frac{d\rho_l}{dt} = \frac{1}{K_l}\dot{p}_l - \alpha_l \dot{T} \tag{7.7}$$

Similarly, equation (7.7) can also be used to represent ice.

$$\frac{1}{\rho_i}\frac{d\rho_i}{dt} = \frac{1}{K_i}\dot{p}_i - \alpha_i \dot{T} \tag{7.8}$$

For the solid phase, which is formed in the solid skeleton; the density is a function of temperature, pore pressure and effective stress.

$$\frac{1}{\rho_s}\frac{d\rho_s}{dt} = \left(\frac{b-n}{1-n}\right)\frac{\dot{p}^*}{K_s} - \left(\frac{b-n}{1-n}\right)\alpha_s \dot{T} - \left(\frac{1-b}{1-n}\right) divu \tag{7.9}$$

7.2.2 Pore Pressure of PCM Cell

Based on the above mass balanced equations, pore pressure and constitutive equations, the following system of equations can be developed to solve the problem.

$$\beta \dot{p}_l = div\left(\frac{D}{\eta_l} gradp_l\right) + S \tag{7.10}$$

$$div\sigma = 0 \tag{7.11}$$

$$\beta = \frac{nS_l}{K_l} + \frac{nS_i}{K_i} + \frac{b-n}{K_s} \tag{7.12}$$

$$S = \left(1 - \frac{\rho_i}{\rho_l}\right)\Phi(t) + \bar{\alpha}\dot{T} - \frac{b-n}{K_s}\dot{X} - \frac{nS_i}{K_i}\dot{\kappa} - bdivu + \frac{D}{\eta_l \rho_l} gradp_l grad\,\rho_l \tag{7.13}$$

$$\bar{\alpha} = nS_l\alpha_l + nS_i\alpha_i + (b-n)\alpha_s \tag{7.14}$$

From equation (7.10) to equation (7.14), a system of equations can be used to study the behavior of a saturated porous solid subjected to freezing temperature. However, there are three unknowns, which are temperature, pore pressure and fluid velocity that are involved in these nonlinear equations. As a result, it is relatively complex to solve directly.

After we can solve the system of equations, we will be able to study how a microcrack is initiated based on pore pressure. If pore pressure exceeds concrete matrix nominal strength, a microcrack will be generated. However, a microcrack does not cause damage to the entire structure. To understand how a freeze-thaw process would cause damage to an entire structure is more important.

Most people use dynamic Young's modulus to study freeze-thaw damage. However, we are more interested in strength loss rather than a dynamic Young's modulus. To date, there are no direct theories to describe the relation between freeze-thaw cycles and concrete strength degradation by using a mathematical model. Some researchers such as Wei and Zhao [26] did freeze-thaw test and use a statistical model to fit experimental data [2] [29]. Therefore, an empirical formula can then be presented. Some researchers used damage theory to study behavior when concrete is subjected to a freezing process and used statistical methods to account for the effect from the freeze-thaw process. As a result, a half analytical model can be expressed.

In our work, damage theory will be used to study how a structure is damaged and then takes into account a freeze-thaw process.

7.3 Damage Model Going through Freeze-Thaw Cycles

7.3.1 Damage Degradation Evolution Function

As we mentioned in the previous section, freeze-thaw damage is usually studied by the loss of a dynamic Young's modulus. However, the loss of dynamic Young's modulus cannot directly be related to the strength loss of a concrete structure. Stress variation could be very complex when concrete goes thru a under freeze-thaw condition and is directed related to the strength of the entire structure. As such, it is important to study how concrete damage would evolve along with freeze-thaw cycles.

We introduce a new parameter D which is called material damage grade variable. It can be used to define how damage evolves and can be expressed as:

$$D = 1 - \frac{\delta^{'}(t)}{\delta(t_0)} \tag{7.15}$$

Where $\delta^{'}(t)$ is a material damage parameter and $\delta(t_0)$ is undamaged material parameter at initial state. Both $\delta^{'}(t)$ and $\delta(t_0)$ could be any material parameter, such as stress, strain or dynamic Young's modulus.

Scalar damage variables were widely used for isotropic or one-dimensional damage model. Higher order tensorial damage variables were often used for anisotropic damage models [7][8][9][10]. However, Ju [9] pointed out that scalar damage which implies that the Poisson's ratio always remained constant is actually a special case of isotropic damage and the most general form of the fourth-order isotropic damage tensor can be decomposed into two parts: volumetric and deviatoric parts. As a result, the fourth rank damage tensor can be defined as in the following.

$$\boldsymbol{D} = \boldsymbol{d}_v \underset{\sim}{1} \otimes \underset{\sim}{1} + \boldsymbol{d}_d \boldsymbol{I}_{dev} \tag{7.16}$$

where $\boldsymbol{d}_v$ denotes volumetric damage parameter , $\boldsymbol{d}_d$ represents deviatoric damage parameter and $\boldsymbol{I}_{dev}$ denotes identity deviatoric tensor.

Damaged Cauchy stress can also be described by using a fourth rank damage tensor.

After damage tensor is defined by using two damage parameters, bulk modulus, shear modulus, Young's modulus and Poisson's ratio can then be determined. Damages Cauchy stress can be calculated by using equation(7.17).

$$\bar{\boldsymbol{\sigma}}_{ij} = \boldsymbol{\sigma}_{kl} : (\mathrm{I}_{ijkl} - \mathrm{D}_{ijkl}) \tag{7.17}$$

In addition, damaged Young's modulus can also be determined by introducing damage tensor.

$$\bar{\boldsymbol{E}}_{ijkl} = \boldsymbol{E}_{ijmn} \left(\boldsymbol{I}_{mnkl} - \boldsymbol{D}_{mnkl} \right) \tag{7.18}$$

Based on equation(7.16), (7.17) and(7.18), mechanical properties degradation can then be determined.

As we mentioned earlier, pore pressure after freezing process can be determined by solving a complex system of equations. However, there is currently no direct theory that can model the relation between freeze-thaw cycles and pore pressure. From the above, we can observe that if we can find the damage evolution function to represent damage tensor, Cauchy stress and other material parameters after performing freeze-thaw cycles can then be determined.

Damage evolution functions regarding freeze-thaw damage can also be decomposed into volumetric and deviatoric parts. However, there is no direct theoretical background or data can well describe volumetric damage and deviatoric damage induced by freeze-thaw cycles. Therefore, in my thesis, one damage parameter damage evolution function will be proposed and the following assumptions will be made.

$$d_v = d_d \tag{7.19}$$

$$\begin{cases} \overline{E} \neq E_0 \\ \overline{K} \neq K_0 \\ \overline{G} \neq G_0 \\ \overline{\upsilon} = \upsilon_0 \end{cases} \tag{7.20}$$

Where $\overline{E}$ denotes damaged Young's modulus, $\overline{K}$ denotes damaged bulk modulus, $\overline{G}$ denotes damaged shear modulus and $\overline{\upsilon}$ denotes damages Poisson's ratio.

Equation (7.19) and (7.20) are basic assumptions to define one parameter damage model. Damage after number of freeze-thaw cycles generally can be considered as temperature cyclic fatigue problem and it is a function of freeze-thaw cycle, freeze-thaw temperature difference and dynamic Young's modulus. As a result, the following damage evolution function is proposed.

$$d = 1 - \exp(-a \times b \times N) \tag{7.21}$$

N is the number of freeze-thaw cycles, a is a function of dynamic Young's modulus, both a and b are material constants and can be determined from various experiments.

$$a = \frac{c(\xi + 1)\sigma_{\max}^{\xi}}{E^{\xi}} \tag{7.22}$$

$$b = \frac{1}{\xi + 1} \tag{7.23}$$

Where c and ξ are both material constants.

If we only consider isotropic scalar damage, damage tensor can be simplified into a damage parameter.

$$\sigma = \sigma \times (1 - d) \tag{7.24}$$

Equations (7.21) and (7.24) can then be used to describe material strength degradation with respect to the number of freeze-thaw cycles. Various parameters in equations (7.22) and (7.23) can be determined by performing various tests. However, it will not be practical to perform all tests. Most of the freeze-thaw tests are evaluated by measuring dynamic Young's modulus. As a result, the data of dynamic Young's modulus can then be used to find parameters a, b and ξ.

7.3.2 Damage Degradation Parameter Based on Freeze-Thaw Cycles and Freeze-Thaw Temperature Difference

From equation (7.21), the damage parameter is a function of the freeze-thaw cycle. However, temperature difference is another important factor that can affect concrete damage behavior.

Chapter 6 looked at the temperature gradient in normal concrete and concrete with PCM. The results showed that the temperature gradient did not vary significantly with PCM added inside of concrete. However, temperature would change along with the freeze-thaw process if there was no PCM added inside of the concrete. Since concrete interior temperature can be maintained when PCM is added, microcracks would not be generated or can be delayed. For normal plain concrete, it would be subjected to the freeze-thaw process and the interior temperature would vary dramatically. Therefore, more microcracks would be initiated due to the pore pressure inside of the concrete. Microcrcks will eventually become macrocracks and affect the strength of the entire structure.

However, there is no direct evidence that can prove that temperature difference due to the freeze-thaw process affect the strength of a concrete structure. As a result, a temperature difference variable should be incorporated into our damage degradation parameter. The damage degradation parameter will be a function of freeze-thaw cycle, freeze-thaw temperature difference and material constants.

The freeze-thaw temperature in our application varies from -11+/-2 $°C$ to 23+/-2 $°C$. Damage evolution function can be modified as the following:

$$d = 1 - \exp(-a \times b \times N \times \Delta T) \tag{7.25}$$

where ΔT represents the freeze-thaw temperature difference.

Corresponding damaged Cauchy stress and damaged Young's modulus can then be updated.

$$\bar{\boldsymbol{\sigma}} = \boldsymbol{\sigma} \times (1 - \boldsymbol{d}) \tag{7.26}$$

$$\bar{\boldsymbol{E}} = \boldsymbol{E} \times (1 - \boldsymbol{d}) \tag{7.27}$$

When temperature difference is considered in the damage model, we can describe how a phase change materiel would affect a concrete structure's mechanical properties. If the phase change temperature difference fluctuates greatly, we can assume that there is no PCM added inside of the concrete because the temperature gradient is not controlled. This is based on our previous paper. However, if the phase change temperature difference does not change significantly, we should be able to assume that PCM is included in the concrete. In order to compare with our one parameter damage model, experimental data and empirical model will be used to compare. [29]

Table 7.1 shows a comparison with the compressive strength of normal concrete. We will use a damage degradation model with and without freeze-thaw temperature difference to compare with the experimental data.

Table 7.1 also depicts the error between experimental data and the numerical model. Error is increased when the freeze-thaw cycle increases. The freeze thaw temperature difference will be included in the next model.

Figure 7.1 shows a comparison of the compressive stress between the experimental data and damage model. In this case, the freeze-thaw temperature difference is not included.

	0 cycle	100 cycle	200 cycle	300 cycle
Test(average) (Mpa)	28.82	22.46	17.12	12.71
Model (Mpa)	28.82	21.35	15.82	11.71
error	/	4.9%	7.6%	8%

Table 7.1 Test data compared with model without considering freeze-thaw temperature

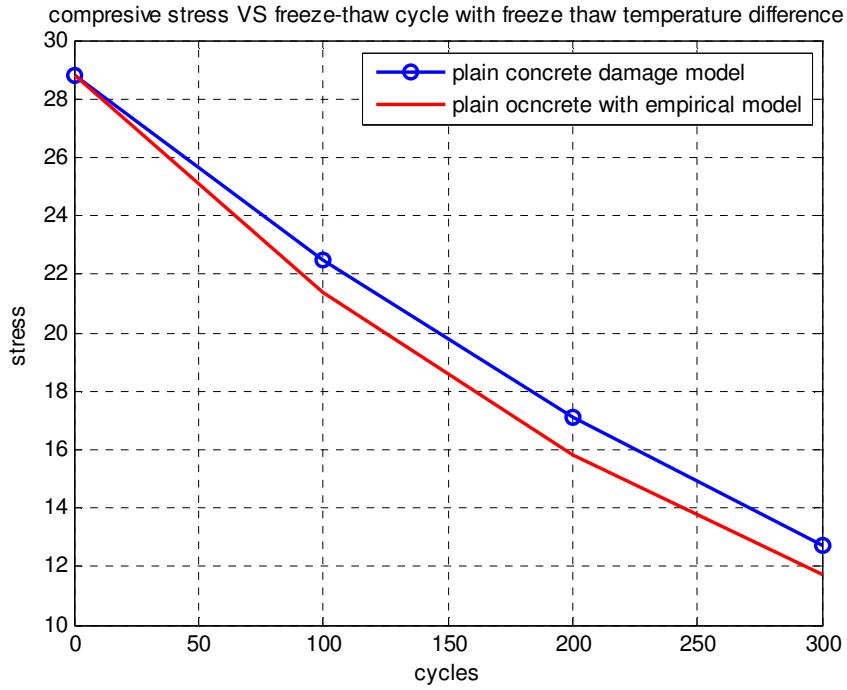

Figure 7.1 Compressive stress with freeze-thaw cycle for plain concrete

	0 cycle	100 cycle	200 cycle	300 cycle
Model(w/o PCM)	22.28	17.4	13.3	9.91
Model(PCM)	22.28	21.41	20.56	19.72
Difference	/	4.01	7.26	9.81

Table 7.2 5% PCM concrete considering freeze thaw temperature

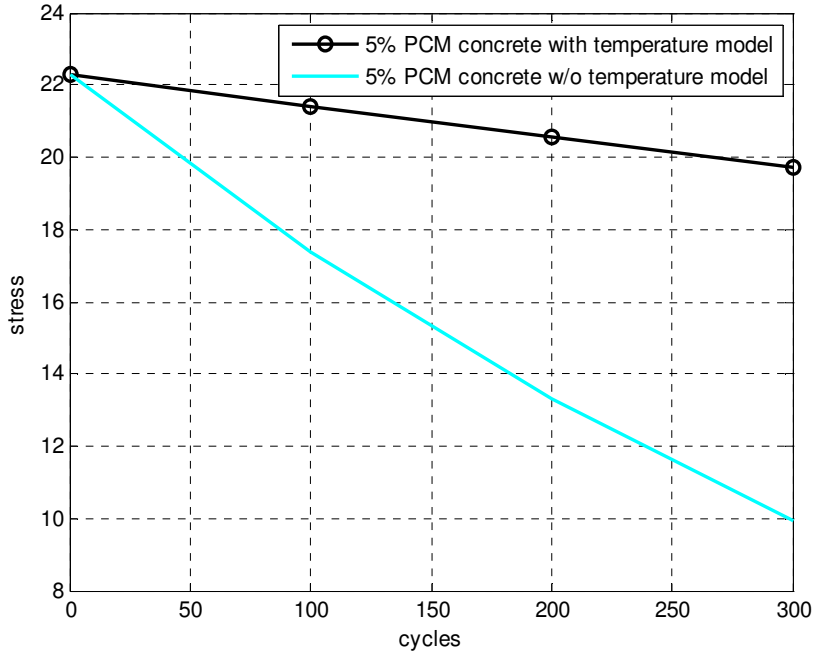

Figure 7.2 Compressive stress with freeze-thaw cycle considering temperature difference with 5% PCM concrete

Figure 7.2 shows a comparison between the damage model with and without considering a freeze-thaw temperature difference. We can observe that the compressive strength will decrease when the freeze-thaw cycle increases in both models. However, the model without considering a freeze-thaw temperature difference experiences much more stress degradation. The black color represents the model considering freeze-thaw temperature differences and the blue color represents a model without a temperature effect.

Table 7.2 depicts the difference between a damage model without considering PCM and a model when considering a temperature difference effect. Compared with table 7.1, much improvement regarding compressive stress can then be observed.

Figure 7.3 depicts a comparison between plain concrete and 5% PCM concrete. We can observe that the compressive strength of plain concrete decreases about 58% after 300 cycles of freeze-thaw. However, for 5% PCM concrete, the compressive strength only decreases 11% after 300 cycles of freeze-thaw. Before applying any freeze-thaw action, the compressive strength of 5% PCM concrete is a little bit lower than plain concrete. After performing a freeze-thaw test, we can clearly observe that thermal performance and mechanical performance are indeed better when adding PCM.

In addition, we can also observe that the theoretical model can predict well compared to the empirical model after a number of freeze-thaw cycles.

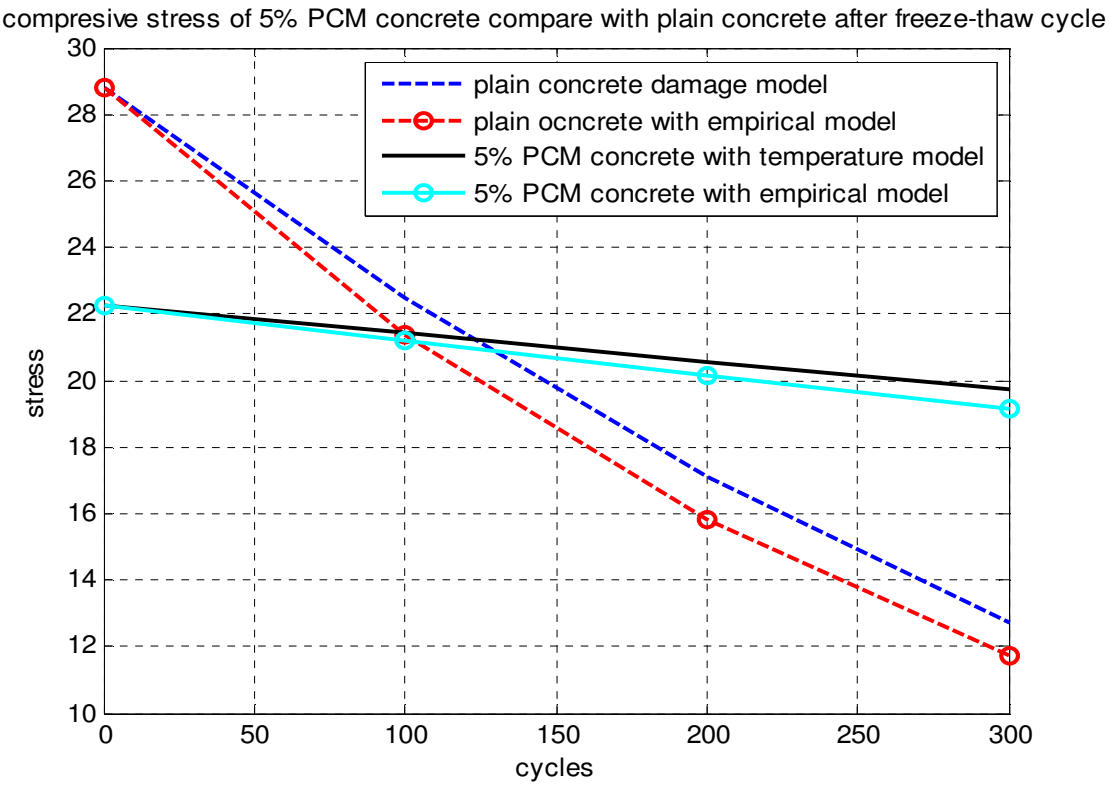

Figure 7.3 Compressive stress with freeze-thaw cycle considering temperature difference with 5% PCM concrete

Results from the above showed that adding PCM help concrete to maintain strength. When the freeze-thaw temperature difference is $34\,°C$, concrete interior temperature will also change from -11 $°C$ to 23 $°C$. Strength degradation is more obvious compared to when the temperature difference is $0\,°C$ from Figure 7.2. In other words, concrete going through a freeze-thaw cycle would indeed damage concrete and strength would then be decreased. From chapter 3,

test showed that dynamic Young's modulus and mass loss of PCM concrete would not change significantly after 300 freeze-thaw cycles. As a result, we can imagine that compressive strength will not change significantly either because the damage degradation parameter will remain the same.

7.4 Constitutive Relationship after Freeze-Thaw Cycle

At present, research on concrete behavior under the action of freeze-thaw primarily focused on the degradation of concrete mechanical properties, such as weight loss, relative dynamic elastic modulus, compressive strength and elastic modulus. There is come research looking at the stress-strain relationship based on the testing of concrete undergoing repeated cycles of freeze-thaw, such as Song and Ji [20], Wei and Wu [26] and Zhu and Li [29] However, their models were based on experimental data and could not be applied widely. As a result, a theoretical freeze-thaw constitutive model would be beneficial to study the stress-strain relationship of concrete under the action of freeze-thaw cycles.

From previous chapters, the concrete interior temperature gradient can be modeled by using two different algorithms based on a heat conduction model. Concrete interior temperature can be controlled when adding PCM and can be observed from a numerical model. Three different concrete layouts are proposed and laminated PCM layer on top of concrete was proved as the most efficient model. Mechanical properties, such as compressive strength degradation and loss of elastic modulus along with freeze-thaw cycle have been discussed. Concrete with and

without PCM were also compared. The strength degradation rate of PCM concrete was shown to be slower compared to normal concrete after going through a freeze-thaw action.

The other important property of concrete after going through freeze-thaw action is concrete residual life. As studied previously, concrete strength will eventually decrease with or without PCM adding into concrete under freeze-thaw action. After a certain number of freeze-thaw cycles and before concrete is completely damaged, concrete will lose a partial amount of its own durability and can still perform. A constitutive relationship could be a useful index to estimate residual durability. As a result, it would be beneficial to study the remaining strength or residual durability in concrete that goes thru after freeze-thaw action.

Some researchers have used the probability density function, such as the Weibull distribution density function to model the stress-strain relationship [20]. Here, we will start with an energy potential function to do modeling. In addition, we will examine both elastic damage and plastic damage to compare both damage modes.

7.4.1 The Additive Stress Split

Within the strain space framework proposed by Ju and Simo [7] [8] [9], plastic flow is introduced by means of an additive split of the stress tensor into initial and inelastic parts.

$$\bar{\sigma} = \frac{\partial^0 \psi^0(\varepsilon)}{\partial \varepsilon} - \bar{\sigma}^p \tag{7.28}$$

where $\bar{\sigma}$ is the effective stress, $\psi^0(\varepsilon)$ is the initial elastic stores energy function of the undamaged material, ε is the total strain, and $\bar{\sigma}^p$ denotes the effective plastic relaxation stress. For linear elasticity, we write:

$$\psi^0(\varepsilon) = \frac{1}{2}\varepsilon : C^0 : \varepsilon \tag{7.29}$$

where C^0 represents elastic modulus tensor. Eqn.(7.28) can be rewritten as the following:

$$\bar{\sigma} = C^0 : \varepsilon - \bar{\sigma}^p \tag{7.30}$$

7.4.2 Principle of Thermodynamics

In order to derive the damaged constitutive relationship regarding elastic and plastic damage, a free potential energy function is proposed as following:

$$\psi(\varepsilon, \sigma^p, q, d) \equiv (1-d)\psi^0(\varepsilon) - \varepsilon : \sigma^p + \Xi(q, \sigma^p) \tag{7.31}$$

where σ^p denotes a plastic relaxation stress tensor, q is a suitable set of internal (plastic) variables. Further, d defines the increment damage variable [7] [8] [9] [10] [11]. This scalar variable ranges from 0 to 1 in numerical values. Moreover, $\psi^0(\varepsilon)$ is the initial elastic stores energy function of the undamaged material as described previously, $\Xi(q, \sigma^p)$ is the plastic potential function.

We will focus on purely mechanical theory, the Clausius-Duhem (reduced dissipation) inequality takes the form for any admissible process:

$$-\dot{\psi} + \sigma : \dot{\varepsilon} \geq 0 \tag{7.32}$$

By taking time derivative of equation (7.31), plugging into equation (7.32) and making use of standard arguments (the Gurtin-Coleman argument) along with an additional assumption that damage and plastic unloading is an elastic process, we can obtain the stress-strain constitutive relationship:

$$\sigma = \frac{\partial \psi(\varepsilon)}{\partial \varepsilon} = (1-d)\frac{\partial \psi^0(\varepsilon)}{\partial \varepsilon} - \sigma^p = (1-d)\bar{\sigma} \tag{7.33}$$

and the dissipative inequalities:

$$-\frac{\partial \Xi}{\partial q} \bullet \dot{q} - \left(\frac{\partial \Xi}{\partial \sigma^p} - \varepsilon \right) : \dot{\sigma}^p \geq 0 \tag{7.34}$$

$$\psi^0(\varepsilon)\dot{d} - \frac{\partial \Xi}{\partial q} \bullet \dot{q} - \left(\frac{\partial \Xi}{\partial \sigma^p} - \varepsilon \right) : \dot{\sigma}^p \geq 0 \tag{7.35}$$

It follows from equation (7.33) that within the present strain space formulation, the stress tensor is split into an elastic damage part and plastic relaxation part. From equations(7.34) and (7.35), we can observe that dissipative energy by plasticity itself is positive, and the sum of damage and plasticity effect is also positive. Another important observation from equation(7.33),(7.34) and (7.35) is the present framework is capable of accommodating a general elastic and general plastic response.

The potential function $\Xi(q, \sigma^p)$ is linked to plastic dissipation. Its role is that inequality (7.35) is satisfied for an arbitrary purpose. Note that we have assumed that $\Xi(q, \sigma^p)$ is independent of d . From equation (7.31), it then follows that:

$$-Y = \frac{\partial \psi(\varepsilon, \sigma^p, q, d)}{\partial d} = \psi^0(\varepsilon) \tag{7.36}$$

Here, from equation (7.36), we can observe that thermodynamic force Y is the initial elastic strain energy $\psi^0(\varepsilon)$ that conjugates to the damage variable.

7.4.3 Characterization of Elastic Strain Energy Based Isotropic Damage Evolution

We characterized the progressive degradation of mechanical properties of concrete due to damage by means of a simple isotropic damage mechanism. We describe the notion of an equivalent compressive strain ξ^+ as the undamaged energy norm of the compressive strain tensor. Compute this equivalent strain tensor involves the principle direction of a total strain tensor. This definition is at variance with that employed by Lemaitre [16] as the J2-norm of the strain tensor.

$$\xi^+ = \sqrt{\psi^0(\varepsilon^+)} = \sqrt{\frac{1}{2}\varepsilon^+ : C^0 : \varepsilon^+} \tag{7.37}$$

where $\varepsilon^+ \equiv P^+ : \varepsilon$. ε denotes the total strain tensor and the fourth rank tensor P^+ denotes the mode I positive projection tensor with components and it is a function of transformation tensor in the principle direction.

$$P^+_{ijkl}(\varepsilon) = \frac{1}{2}(Q^+_{ik}Q^+_{jl} + Q^+_{il}Q^+_{jk}) \tag{7.38}$$

where $Q^+ \equiv \sum_{i=1}^{2} \hat{H}(\varepsilon_i) p_i \otimes p_i$; $\varepsilon = \sum_{i=1}^{2} \varepsilon_i p_i \otimes p_i$. Here ε_i is the ith principal strain, p_i is the ith corresponding unit vector in principal direction and $\hat{H}(\varepsilon_i)$ is a smoothed Heaviside function.

We now can define the state of damage in concrete by means of a damage criterion $\phi^d(\xi_t^+, g_t) \le 0$, formulated in strain space, with the following functional form:

$$\phi^d(\xi_t^+, g_t) \equiv \xi_t^+ - g_t \le 0 \tag{7.39}$$

where the subscript t denotes to a value at current time and g^+ is the damage threshold at the current time. Let g_0 denotes the initial damage threshold before any loading is applied; we then have $g_t \ge g_0$. The criterion (7.39) states that damage in a solid is initiated if the energy norm of the strain tensor ξ_t^+ exceeds the initial damage threshold g_0. For the isotropic damage case, we can define the damage evolution variable d and the damage threshold g_t respectively by using rate equations:

$$\dot{d}_t = \dot{\mu} H(\xi_t^+, d_t) \tag{7.40}$$

$$\dot{g} = \dot{\mu} \tag{7.41}$$

where $\dot{\mu} \ge 0$ is a damage consistency parameter that defines the damage loading/unloading condition according to Kuhn-Tucker conditions:

$$\dot{\mu} \ge 0, \qquad \phi^d(\xi_t^+, g_t) \le 0, \qquad \dot{\mu}\phi^d(\xi_t^+, g_t) = 0 \tag{7.42}$$

Kuhn-Tucker conditions are commonly used as damage criteria for design problems. If $\phi^d(\xi_t^+, g_t) \le 0$, the damage criterion is not satisfied and by the last condition of (7.42), $\dot{\mu} = 0$. Therefore, equation (7.40) implies that $\dot{d}_t = 0$ and there is no further damage taking places. If, on the other hand, $\dot{\mu} > 0$ which means that further damage is induced, then conditions (7.42)

implies that $\phi^d(\xi_t^+, g_t) = 0$. In other words, the energy norm induced by strain is equal to the damage threshold at the current time.

$$\xi_t^+ = g_t \tag{7.43}$$

In addition, the value of $\dot{\mu}$ can also be determined by the damage consistency condition.

$$\dot{\mu} = \xi_t^+ \tag{7.44}$$

where g_t can be defined by using the following equation:

$$g_t = \max(g_0, \xi_t^+) \tag{7.45}$$

If $H(\xi_t^+, d_t)$ in equation (7.40) is independent of the damage degradation parameter, the above formulation may be rephrased as follows. $H(\xi_t^+, d_t)$ can be defined as $H(\xi_t^+) \equiv \partial G(\xi_t^+) / \partial \xi_t^+$ and we shall assume that $G(\bullet)$ is a monotonic function. An equivalent damage criterion is given by $\bar{\phi}^d(\xi_t^+, g_t) \equiv G(\xi_t^+) - G(g_t) \le 0$. The flow rule and Kuhn-Tucker condition then become:

$$\dot{d}_t = \dot{\mu} \frac{\partial \bar{\phi}^d(\xi_t^+, g_t)}{\partial \xi_t^+}, \qquad \dot{g} = \dot{\mu} \tag{7.46}$$

$$\dot{\mu} \ge 0, \qquad \bar{\phi}^d(\xi_t^+, g_t) \le 0, \qquad \dot{\mu}\bar{\phi}^d(\xi_t^+, g_t) = 0 \tag{7.47}$$

Since we will focus on an effective stress space, the characterization of the plastic response should be formulated in the effective stress space in terms of effective stress $\bar{\sigma}$ and $\bar{\sigma}^p$. In this regards, the homogenized Cauchy stress tensor σ should be replaced by the effective stress tensor $\bar{\sigma}$ in the yield function, so that the elastic damage domain is characterized by $f(\bar{\sigma}, q) \le 0$. Here, q can be defined as internal plastic variable. With the assumption of an

associative flow rule, rate-independent plastic response is defined in the strain space by the following constitutive equations.

$$\dot{\bar{\sigma}}^{p} = \dot{\lambda}\frac{\partial f}{\partial \varepsilon}\left(\frac{\partial \psi^{0}(\varepsilon)}{\partial \varepsilon} - \bar{\sigma}^{p}, q\right) \qquad (\textit{associative flow rule}) \tag{7.48}$$

$$\dot{q} = \dot{\lambda} h\left(\frac{\partial \psi^{0}(\varepsilon)}{\partial \varepsilon} - \bar{\sigma}^{p}, q\right) \qquad (\textit{plastic hardening low}) \tag{7.49}$$

$$f\left(\frac{\partial \psi^{0}(\varepsilon)}{\partial \varepsilon} - \bar{\sigma}^{p}, q\right) \le 0 \qquad (\textit{plastic hardening low}) \tag{7.50}$$

where $\dot{\bar{\sigma}}^{p}$ denoted the plastic relaxation effective stress rate tensor, $\dot{\lambda}$ represents plastic consistency parameter and h signifies the hardening law. Equations (7.48), (7.49) and (7.50) express the characterization of plasticity in the strain space. Loading and unloading conditions can be expressed with the compact form:

$$\dot{\lambda} \ge 0, \quad f\left(\frac{\partial \psi^{0}(\varepsilon)}{\partial \varepsilon} - \bar{\sigma}^{p}, q\right) \le 0, \quad \dot{\lambda} f\left(\frac{\partial \psi^{0}(\varepsilon)}{\partial \varepsilon} - \bar{\sigma}^{p}, q\right) = 0 \tag{7.51}$$

7.4.4 Computational Algorithm

Section 7.2 already developed a damage evolution parameter and initial elastic strain energy from free energy potential function based on the effective stress concept. We also introduced Kuhn-Tucker conditions as damage criterion to consider plasticity damage. In this section, we will focus on the details of the computational algorithm in order to utilize the

proposed damage model. More precisely, attention is focused on the following local elastoplastic damage constitutive equations:

The basic framework can be summarized as the following chart:

$$
\begin{aligned}
&\dot{\varepsilon} = \nabla^s \dot{u}(t) \\
&\begin{cases} \dot{d}_t = \dot{\mu} H(\xi_t^+, d_t) \\ \dot{g} = \dot{\mu} \\ \dot{\mu} \geq 0, \qquad \phi^d(\xi_t^+, g_t) \leq 0, \qquad \dot{\mu}\phi^d(\xi_t^+, g_t) = 0 \end{cases} \\
&\dot{\bar{\sigma}} = \frac{d}{dt}\left[\frac{\partial \psi^0(\varepsilon)}{\partial \varepsilon}\right] - \dot{\bar{\sigma}}^p \\
&\begin{cases} \dot{\bar{\sigma}}^p = \dot{\lambda}\dfrac{\partial f}{\partial \varepsilon}\left(\dfrac{\partial \psi^0(\varepsilon)}{\partial \varepsilon} - \bar{\sigma}^p, q\right) & (\textit{associative flow rule}) \\ \dot{q} = \dot{\lambda} h\left(\dfrac{\partial \psi^0(\varepsilon)}{\partial \varepsilon} - \bar{\sigma}^p, q\right) & (\textit{plastic hardening low}) \\ f\left(\dfrac{\partial \psi^0(\varepsilon)}{\partial \varepsilon} - \bar{\sigma}^p, q\right) \leq 0 & (\textit{plastic hardening low}) \end{cases}
\end{aligned}
\tag{7.52}
$$

In equation (7.52), the problem can simply imply updating basic variables numerically $\{\sigma, d, \bar{\sigma}^p, q\}$ in a manner consistent with the constitutive model. It is necessary to realize that the history of strains ε is assumed to be given in this numerical process.

Equation (7.52) can to be solved systematically and incrementally over a sequence of given time steps. In this case, it can be referred as given strain. Therefore, initial conditions will need to be defined.

$$
\{\sigma, d, \bar{\sigma}^p, q\}|_{t=t_0} = \{\sigma_0, d_0, \bar{\sigma}_0^p, q_0\} \tag{7.53}
$$

The damage evolution problem can be decomposed into an elastic-damage part and plasticity damage part.

$$
\begin{aligned}
&\textit{Elastic damage part}\\
&\dot{\varepsilon} = \nabla^s \dot{u}(t)\\
&\dot{d}_t = \begin{cases} H(\xi^+)\dot{\xi}^+ & \textit{iff} \quad \phi_t^d = \dot{\phi}_t^d = 0 \\ 0 & \textit{otherwise} \end{cases}\\
&\dot{g} = \left\{ \begin{cases} \dot{\xi}^+ & \textit{iff} \quad \phi_t^d = \dot{\phi}_t^d = 0 \\ 0 & \textit{otherwise} \end{cases} \right\}\\
&\dot{\bar{\sigma}} = \frac{d}{dt}\left[\frac{\partial \psi^0(\varepsilon)}{\partial \varepsilon} \right]\\
&\begin{cases} \dot{\bar{\sigma}}^p = 0 \\ \dot{q} = 0 \end{cases}
\end{aligned}
\tag{7.54}
$$

$$
\begin{aligned}
&\textit{Platicity part}\\
&\dot{\varepsilon} = 0\\
&\dot{d}_t = 0\\
&\dot{g} = 0\\
&\dot{\bar{\sigma}} = -\dot{\bar{\sigma}}^p\\
&\begin{cases} \dot{\bar{\sigma}}^p = \dot{\lambda}\dfrac{\partial f}{\partial \varepsilon}\left(\dfrac{\partial \psi^0(\varepsilon)}{\partial \varepsilon} - \bar{\sigma}^p, q \right) & (\textit{associative flow rule}) \\ \dot{q} = \dot{\lambda} h\left(\dfrac{\partial \psi^0(\varepsilon)}{\partial \varepsilon} - \bar{\sigma}^p, q \right) & (\textit{plastic hardening low}) \\ f\left(\dfrac{\partial \psi^0(\varepsilon)}{\partial \varepsilon} - \bar{\sigma}^p, q \right) \le 0 & (\textit{plastic hardening low}) \end{cases}
\end{aligned}
\tag{7.55}
$$

Equations (7.54) and (7.55) can be added up and should be consistent with the result from equation (7.52). Two algorithms will be used to solve two problems. The first algorithm will be

used to solve an elastic damage problem and the second algorithm will be used to solve plasticity problem.

7.4.5 Elastic-Damage Predictor

In order to solve an elastic-damage problem as mentioned in equation (7.54), the following algorithm will be listed step by step:

Step 1: Update strain: the incremental strain is given and the strain tensor is updated as:

$$\varepsilon_{n+1} = \varepsilon_n + \Delta\varepsilon \tag{7.56}$$

Step 2: In order to calculate Q^+**,** we need to find the eigenvalue and eigenvector p_i which gives the unit vector in the principal direction from total strain ε_{n+1} at each time step.

Step 3: Compute the positive forth rank projection tensor P^+_{n+1}. The fourth rank projection tensor is based on the total strain given from step 1.

$$P^+_{ijkl}(\varepsilon_{n+1}) = \frac{1}{2}(Q^+_{ik}Q^+_{jl} + Q^+_{il}Q^+_{jk}) \tag{7.57}$$

where $Q^+ \equiv \sum_{i=1}^{2} \hat{H}(\varepsilon_i) p_i \otimes p_i$; $\varepsilon = \sum_{i=1}^{2} \varepsilon_i p_i \otimes p_i$. Here ε_i is the ith principal strain, p_i is the ith corresponding unit vector in principal direction and $\hat{H}(\varepsilon_i)$ is a smoothed Heaviside function.

Step 4: Apply fourth rank projection tensor P^+_{ijkl} and find only positive strain tensor ε^+ at each time step.

Step 5: Compute the initial (undamaged) strain energy norm ξ^+.

$$\xi_{n+1}^{+} = \sqrt{\psi^{0}(\varepsilon_{n+1}^{+})} = \sqrt{\frac{1}{2}\varepsilon_{n+1}^{+} : C^{0} : \varepsilon_{n+1}^{+}} \tag{7.58}$$

where $\varepsilon^{+} = P^{+} : \varepsilon$

Step 6: Compute the scalar damage threshold d_{n+1} based on ξ_{n+1}^{+}.

If ξ_{n+1}^{+} at the current time step is lower than the initial damage threshold, no further damage is generated and $\Delta d_{n+1} = 0$. However, if ξ_{n+1}^{+} at the current time step is greater than the initial damage threshold, further damage will be generated and the scalar damage parameter will need to be computed. Scalar damage evolution parameter d_{n+1} can be calculated by using one of the following nonlinear damage evolutional functions.

Damage threshold during unloading will remain the same as the damage threshold at the end of the loading process.

$$d_{n+1}(\xi_{n+1}^{+}) = \frac{k_c\left[\xi_{n+1}^{+} - k_i\right]}{\xi_{n+1}^{+}\left[k_c - k_i\right]} \tag{7.59}$$

where k_c and k_i are both material constants

$$d_{n+1}(\xi_{n+1}^{+}) = 1 - \frac{A(1-B)}{\xi_{n+1}^{+}} - B\exp\left[A - \xi_{n+1}^{+}\right] \tag{7.60}$$

where A and B are both material constants

Step 7: Check incremental scalar damage evolutional parameter.

Compute Δd_{n+1}.

If $\Delta d_{n+1} \le 0$, there is no further damage will be generated and we set $\Delta d_{n+1} = 0$. (7.61)

If $\Delta d_{n+1} > 0$, further damage will be generated and continue all previous and the following steps.

Step 8: Compute fourth rank incremental damage predictor tensor based on the Δd_{n+1} from the previous step.

$$\Delta \boldsymbol{D}_{n+1} = \Delta d_{n+1} \boldsymbol{I} \tag{7.62}$$

$$\boldsymbol{D}_{n+1} = \boldsymbol{D}_{n} + \Delta \boldsymbol{D}_{n+1} \tag{7.63}$$

Step 9: Compute current elastic homogenized stress based on the previous computed damage evolution parameter.

$$\sigma = (1-d)\bar{\sigma} \tag{7.64}$$

7.4.6 The Effective Plastic Return Mapping Corrector

The previous section demonstrated the elastic damage predictor algorithm. However, concrete can also experience plasticity damage in most cases. Therefore, it is also important to construct an algorithm that takes plasticity into account.

Step 10: Check for yielding condition.

Kuhn-Tucker conditions will be used to check for yielding. The counterpart of Kuhn-Tucker conditions is implemented in terms of the elastic-damage trial stress. Initially, elastic damage trial stress is set to be equal to elastic homogenized stress.

$$f(\sigma_{n+1}^{trial}, q_{n+1}^{trial}) \begin{cases} \leq 0 & elastic-damage \rightarrow predictor\, a\lg orithm \\ > 0 & plastic-damage \rightarrow return\, mapping \end{cases} \tag{7.65}$$

In the case of plastic loading, clearly the trial homogenized stress would not be the solution of the current problem. As a result, the predictor stresses and internal variables are "returned back" to the yield surface along the algorithmic counterpart of the flow generated by Eqn.(7.55). The algorithmic construction of this flow follows a proposed procedure that was inspired by a form of Kelley's convex cutting plane method for non-linear optimization, with its basic structure inherited from Newton's method. Two fundamental advantages of this procedure are (a) the quadratic rate of convergence towards the yield surface and (b) the need for computing the gradient of the flow rule and hardening law are entirely by passed.

Step 11: Update the effective plastic stress using return mapping algorithm.

Step 12: Update the homogenized plastic stress σ_{n+1}.

$$\sigma_{n+1} = [\boldsymbol{I} - \boldsymbol{D}_{\boldsymbol{n+1}}]\bar{\sigma}_{n+1} \tag{7.66}$$

7.5 Numerical Example and Results

Chapter 7.3 presents two algorithms that involve calculating the stress-strain relationship while considering elastic-damage and plastic-damage. In this chapter, a one dimension driver problem will be performed by using MATLAB code. Both elastic-damage and plastic-damage will be compared. In addition, the stress-strain relationship for concrete and concrete with PCM under subjected to freeze-thaw action will also be compared.

7.5.1 Stress-Strain Relationship of Concrete without PCM

First we will demonstrate a loading-unloading process as case 1. A strain will be applied on the concrete until it reaches its ultimate strain and then unloaded to initial state to study the stress-strain relationship.

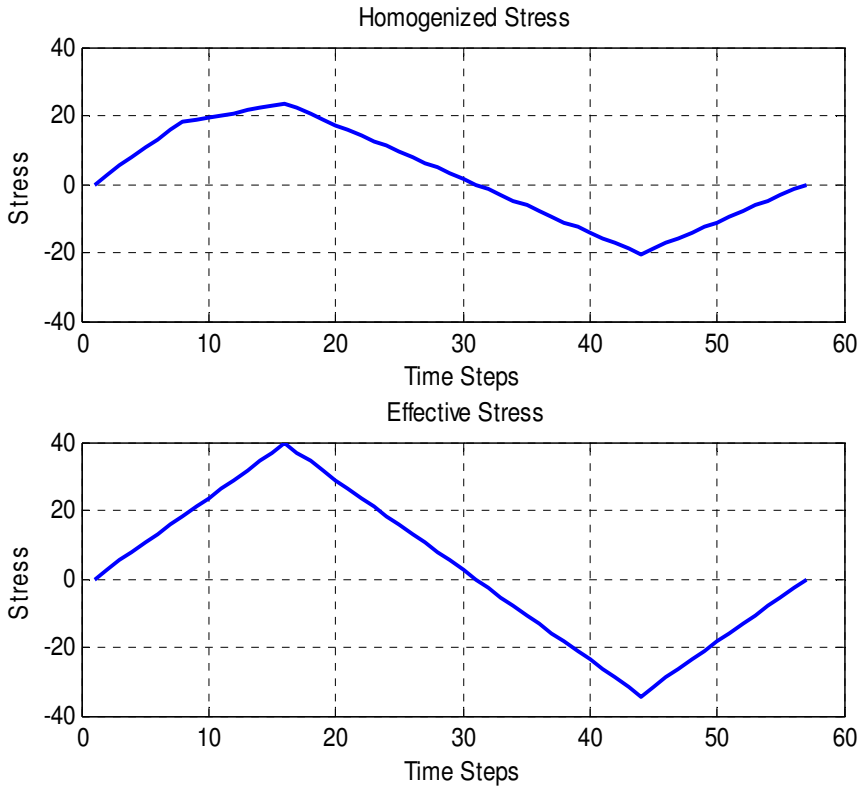

Figure 7.4 Effective stress and homogenized stress under loading and unloading condition

Figure 7.4 shows homogenized stress and effective stress when only considering elastic damage under loading and unloading conditions. We can observe that effective stress performs in linear response since there is no damage during the loading and unloading condition. However, we will be able to observe damage during the loading condition when calculating homogenized stress.

Figure 7.5 depicts the comparison between effective stress and homogenized stress. Because a concrete damage mechanism is involved, the maximum compressive stress has been reduced to about 40%.

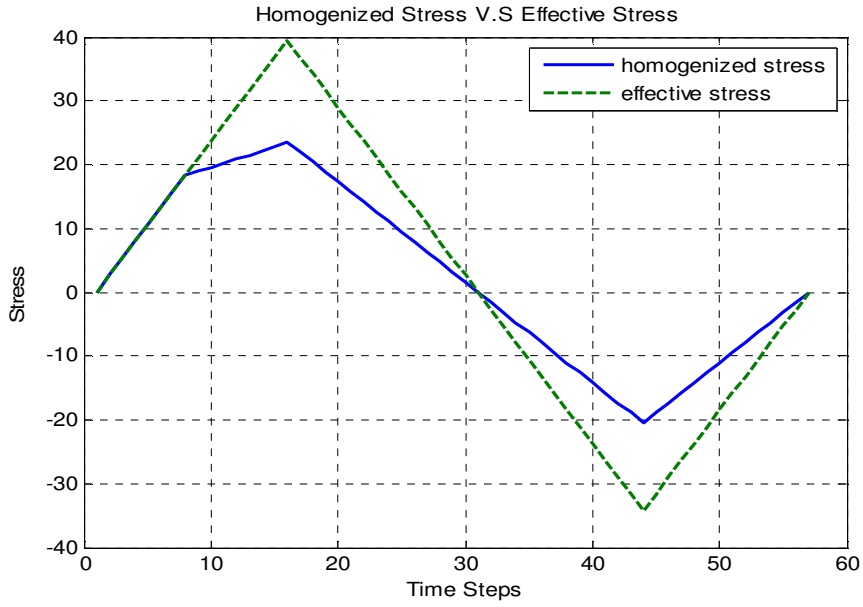

Figure 7.5 Comparison of effective stress and homogenized stress

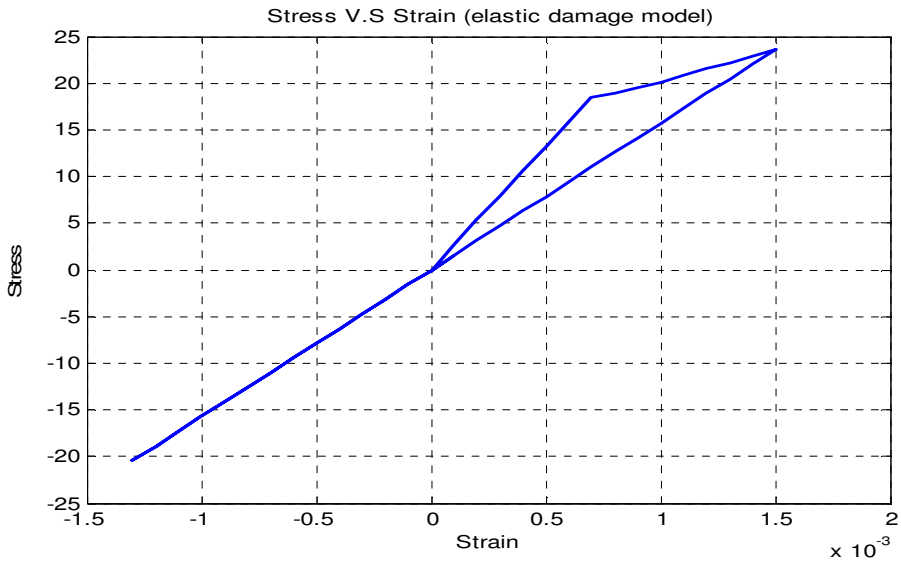

Figure 7.6 Stress-strain relationship under loading and unlading condition

Figure 7.6 shows the stress-strain relationship. We can observe that the curve is not linear during the loading condition because of damage. During the unloading process, the stress-strain curve is linear and there is no ductility.

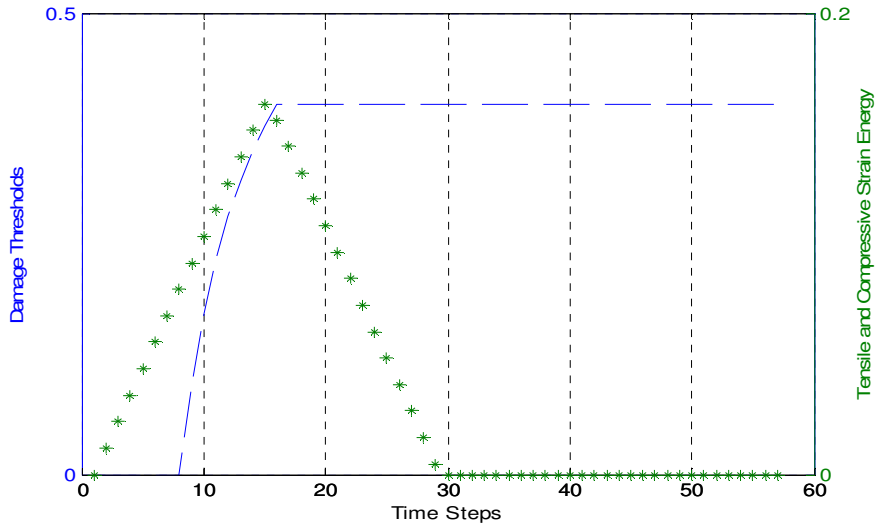

Figure 7.7 Material damage threshold v.s. strain energy

Figure 7.7 demonstrates the evolution of compressive strain energy and compare with the damage threshold. When strain energy surpasses the materiel damage threshold, damage will then occur. The result of Figure 7.7 is consistent with a stress-strain relationship.

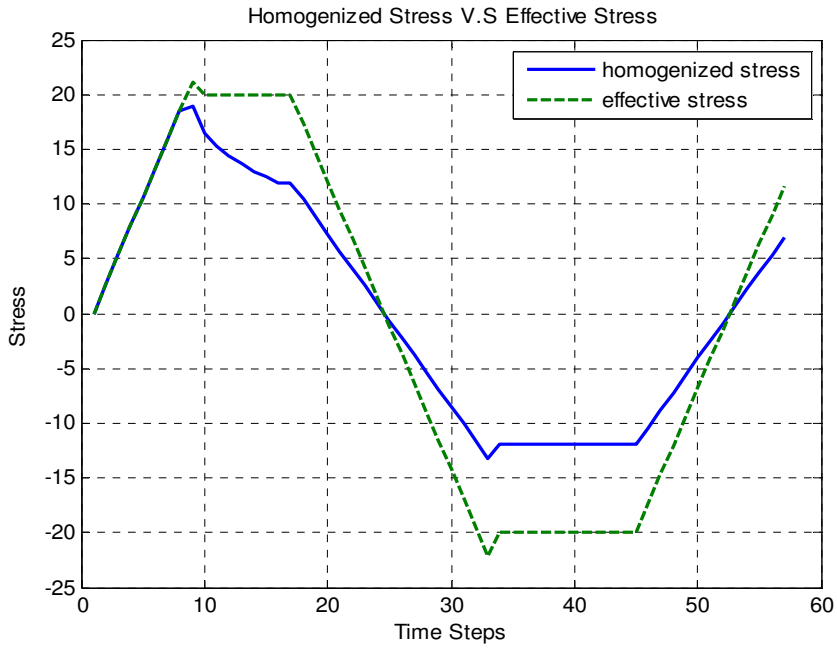

Figure 7.8 Comparison of effective stress and homogenized stress considering plasticity

Figure 7.8 shows a comparison between effective stress and homogenized stress when considering plasticity. We can observe that homogenized stress decreases more and that implies that the concrete would be damaged more because of plasticity.

Figure 7.9 demonstrates the stress-strain relationship when considering plasticity. Compared with Figure 7.6, we can observe that the stress-strain curve is more ductile during a loading-unloading condition. Unlike elastic damage, the stress-strain curve will not follow the original path during the unloading condition.

Figure 7.9 Stress-strain relationship under loading and unlading condition considering plasticity

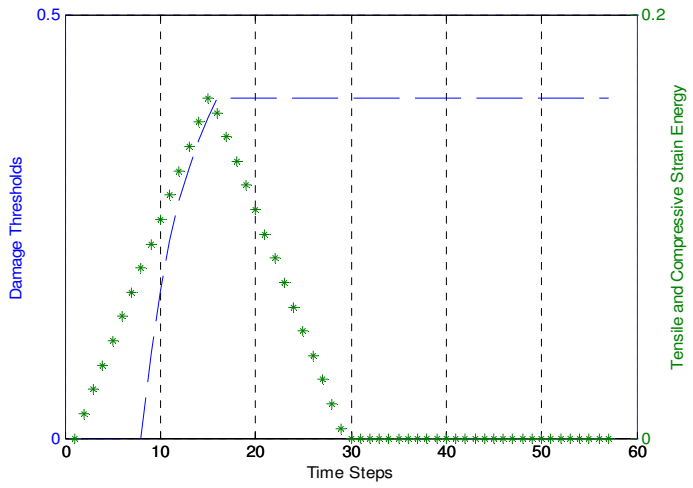

Figure 7.10 Material damage threshold v.s. strain energy considering plasticity

In case 2, strain will be applied to a certain amount after it passes its ultimate strain. The stress-strain relationship will be studied under different cycles of freeze-thaw. In addition to our damage evolution model, there are two additional stress-strain relationship models proposed by two other researchers that will also be compared.[17]

The mathematical algorithm regarding calculating damage function and corresponding effective and homogenized stress are described as the following.

$$\frac{\sigma}{\sigma_c}=\begin{bmatrix} b\frac{\varepsilon}{\varepsilon_c}+(3-2b)\left(\frac{\varepsilon}{\varepsilon_c}\right)^2+(b-2)\left(\frac{\varepsilon}{\varepsilon_c}\right)^3 & \frac{\varepsilon}{\varepsilon_c}\le 1 \\ \frac{\frac{\varepsilon}{\varepsilon_c}}{c\left(\frac{\varepsilon}{\varepsilon_c}-1\right)^2+\frac{\varepsilon}{\varepsilon_c}} & \frac{\varepsilon}{\varepsilon_c}>1 \end{bmatrix} \tag{7.67}$$

where both b and c are control parameters in the ascending and descending branch of stress-strain relationship curve, respectively. Both b and c can be defined by two different models from two researchers.

Zou Model

$$b = \text{-}0.0143\Delta P_n + 1.744 \tag{7.68}$$

$$\text{c}=0.0796\Delta \text{P}_n + 1.582 \tag{7.69}$$

where ΔP_n is decrement of dynamic young's modulus

Duan Model

$$b_D = b_0\left\{\left(6.474\times10^7\times f_c^{-7.7667}\right)N^2-\left[0.5975\exp\left(-0.1039 f_c\right)\right]N+1\right\} \tag{7.70}$$

$$c_D = c_0\left\{-\left[5.8159\exp\left(-0.3087 f_c\right)\right]N^2+\left[14.097\exp(-0.1803 f_c)N+1\right]\right\} \tag{7.71}$$

where N is number of freeze-thaw cycle, f_c is concrete 28-day ultimate strength, b_0 and c_0 are both control parameters and they are 1.7 and 2.0, respectively.

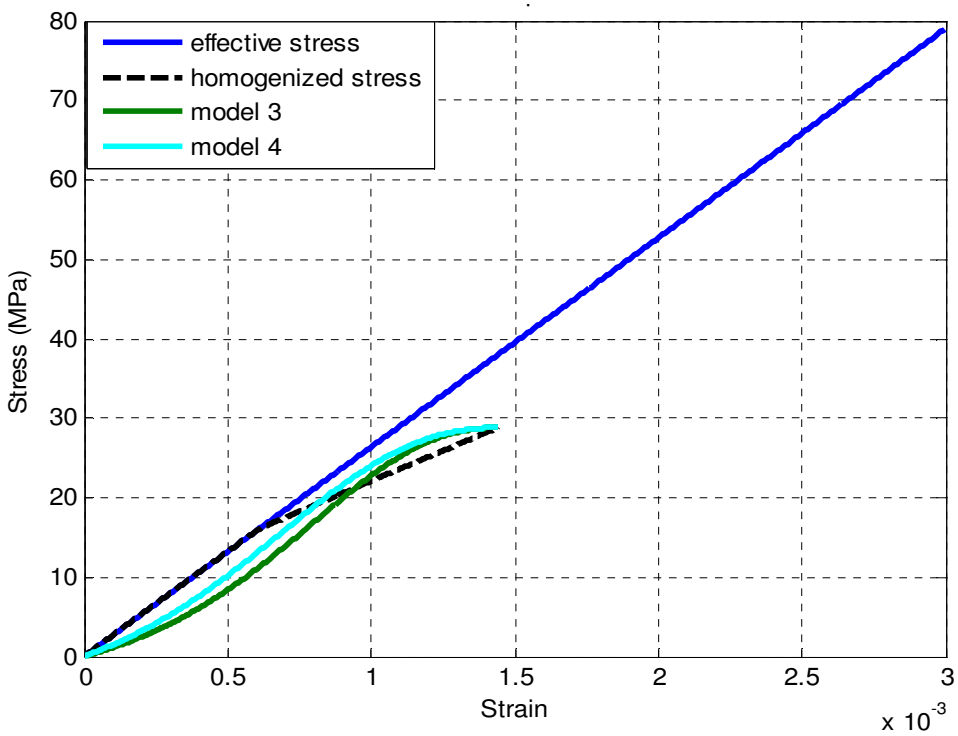

Figure 7.11 Plain concrete stress-strain relationship without freeze-thaw

Figure 7.11 shows the stress-strain relationship of plain concrete before a freeze-thaw test. Effective stress represents concrete without any damage when increasing strain. We can observe that all three models can predict experimental data well in the ascending branch. The models from Zou and Duan's are a bit overestimated in the ascending branch compared to experimental data. However, the error is in an acceptable range. There is no significant meaning in predicting the stress-strain relationship in the descending branch since the concrete would basically be crushed after it reaches its ultimate capacity.

Figure 7.12 shows the stress-strain relationship of plain concrete with different freeze-thaw cycles.

Figure 7.13 shows a stress-strain curve comparison of plain concrete after going through a freeze-thaw test. The results of stress-strain relationship under 0, 100, 200 and 300 freeze-thaw cycles have been demonstrated. We can observe that the ultimate compressive stress decreases, elastic modulus decreases, Poisson's ratio increases and ultimate strain increases with increasing freeze-thaw cycle. After concrete reaches its maximum tensile allowable stress, the stress-strain curve will drop to zero and concrete will be completely damaged. Our damage model can predict the stress-strain relationship well and matches with the other two models proposed by other researches looking at the effects of freeze-thaw cycles.

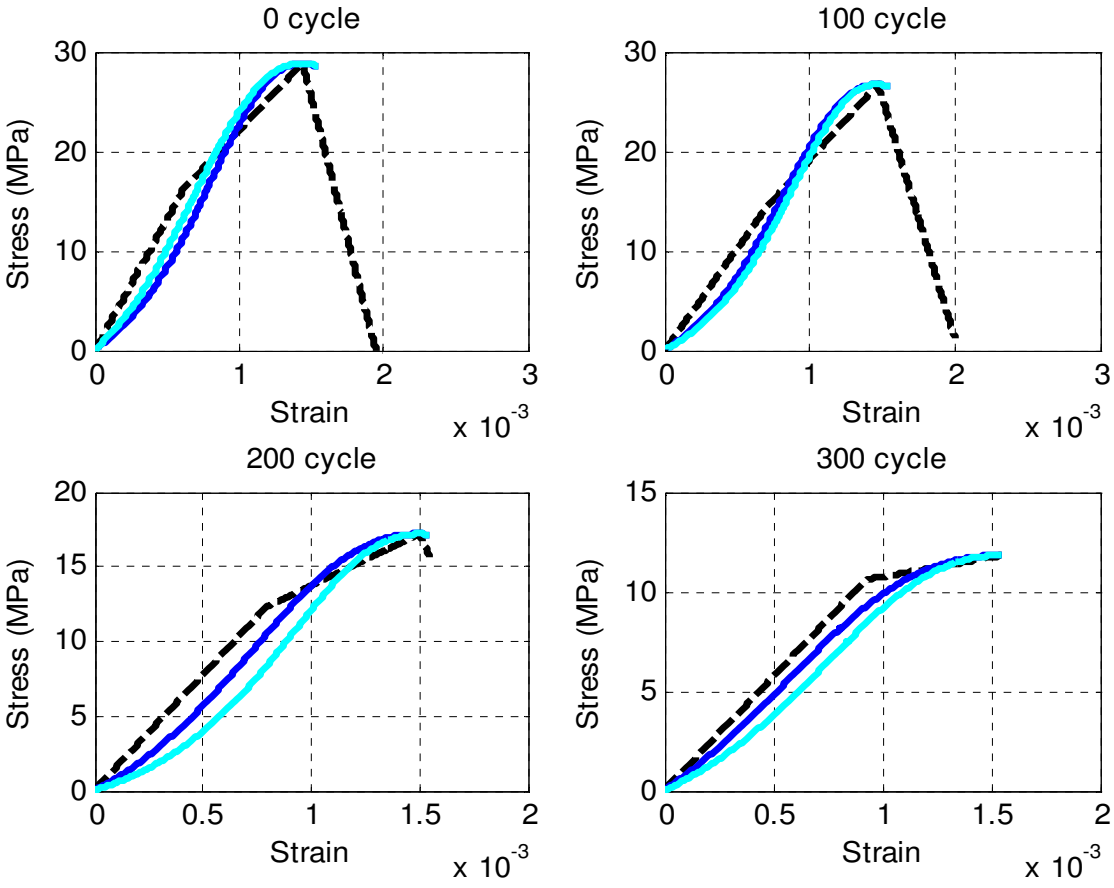

Figure 7.12 Plain concrete stress-strain relationship with different freeze-thaw cycle

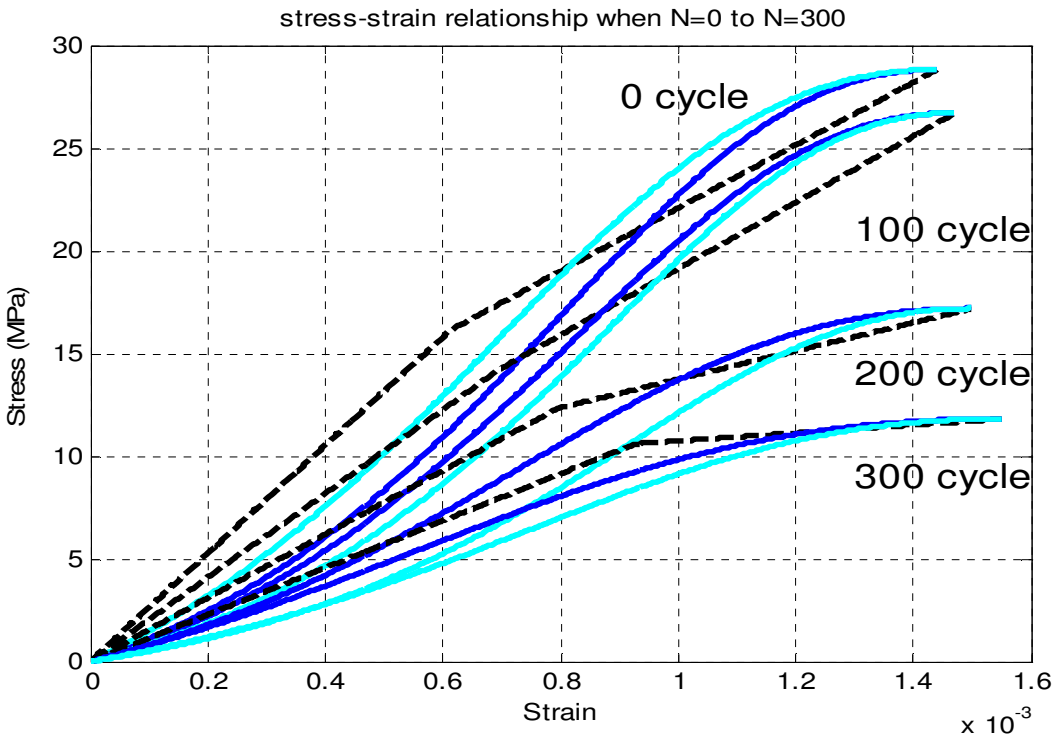

Figure 7.13 Plain concrete stress-strain relationship comparison with different freeze-thaw cycle

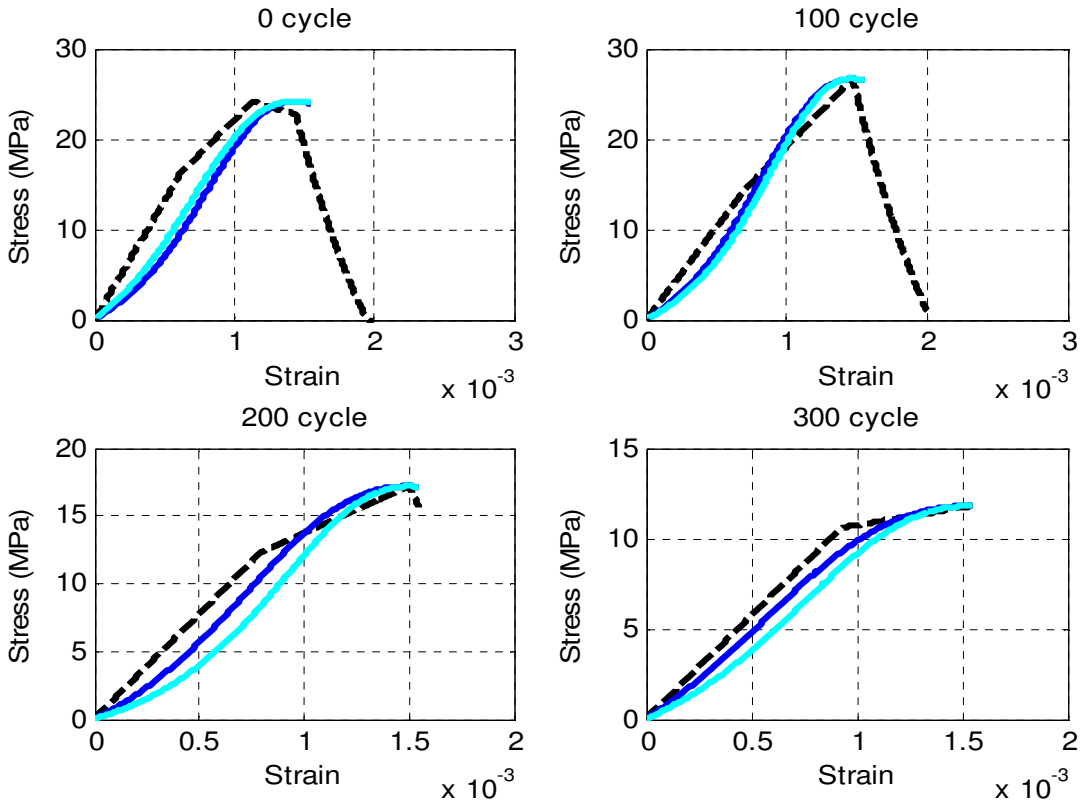

Figure 7.14 Plain concrete stress-strain relationship with different freeze-thaw cycle considering plastic damage

Figure 7.14 shows the stress-strain relationship of plain concrete with different freeze-thaw cycles when considering plastic damage. We can observe that the ultimate stress is decreased because of plastic damage. However, the stress-strain curve is smoother. When considering plastic damage, our damage model based on free energy potential can also predict well.

Next, we will compare the stress-strain relationship between plain concrete and concrete with PCM.

7.5.2 Stress Strain Relationship of Concrete with PCM

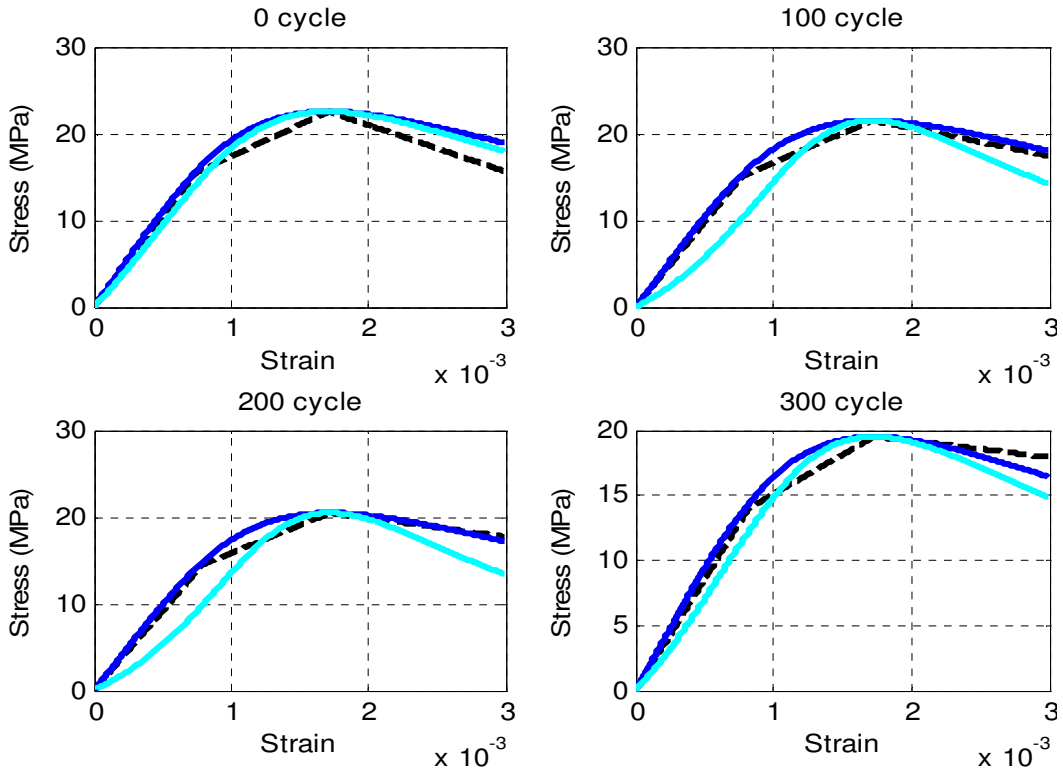

Figure 7.15 5% PCM concrete stress-strain relationship with different freeze-thaw cycle

Figure 7.15 shows the stress-strain relationship of 5% PCM concrete with different freeze-thaw cycles. We can observe that when increasing freeze-thaw cycles, our damage model can also predict the other two models well.

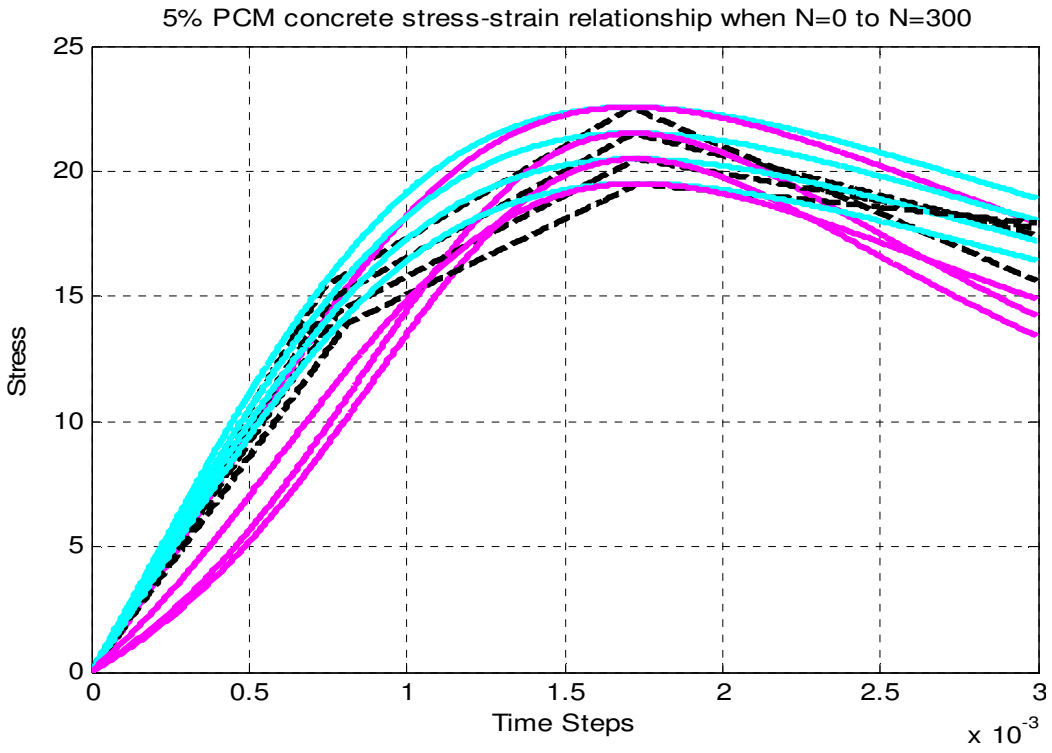

Figure 7.16 5% PCM concrete stress-strain relationship comparison with different freeze-thaw cycle

Figure 7.16 shows the stress-strain curve comparison of 5% PCM concrete after going through a freeze-thaw test. The results of a stress-strain relationship under 0, 100 ,200 and 300 freeze-thaw cycles have been demonstrated. We can observe that the ultimate stress and Young's modulus would only slightly decrease when increasing freeze-thaw cycles. This is the same observation as plain concrete, the Poisson's ratio and ultimate strain would slightly increase when increasing freeze-thaw cycles. The stress-strain curve would become slightly flatter and more ductile.

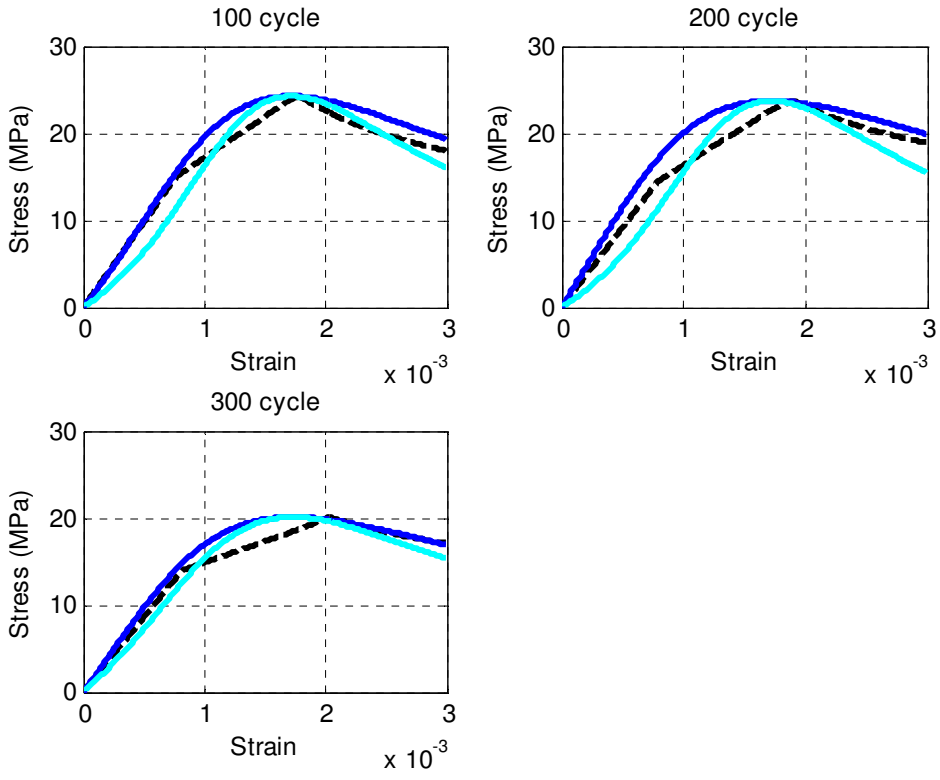

Figure 7.17 5% PCM concrete stress-strain relationship with different freeze-thaw cycle when considering plastic damage

Figure 7.17 shows the stress-strain relationship of 5% PCM concrete with different freeze-thaw cycle when considering plastic damage. This is the same as plain concrete, and our damage model can also predict well for PCM concrete when considering plastic damage.

When compared with plain concrete, all the mechanical properties would only slightly decrease instead of decreasing greatly as in plain concrete when increasing freeze-thaw cycles. This proves that PCM has a great impact on controlling concrete interior temperature and eventually maintaining concrete mechanical properties in an acceptable range after 300 freeze-thaw cycles.

We will next compare plain concrete and PCM concrete together at different freeze-thaw cycle.

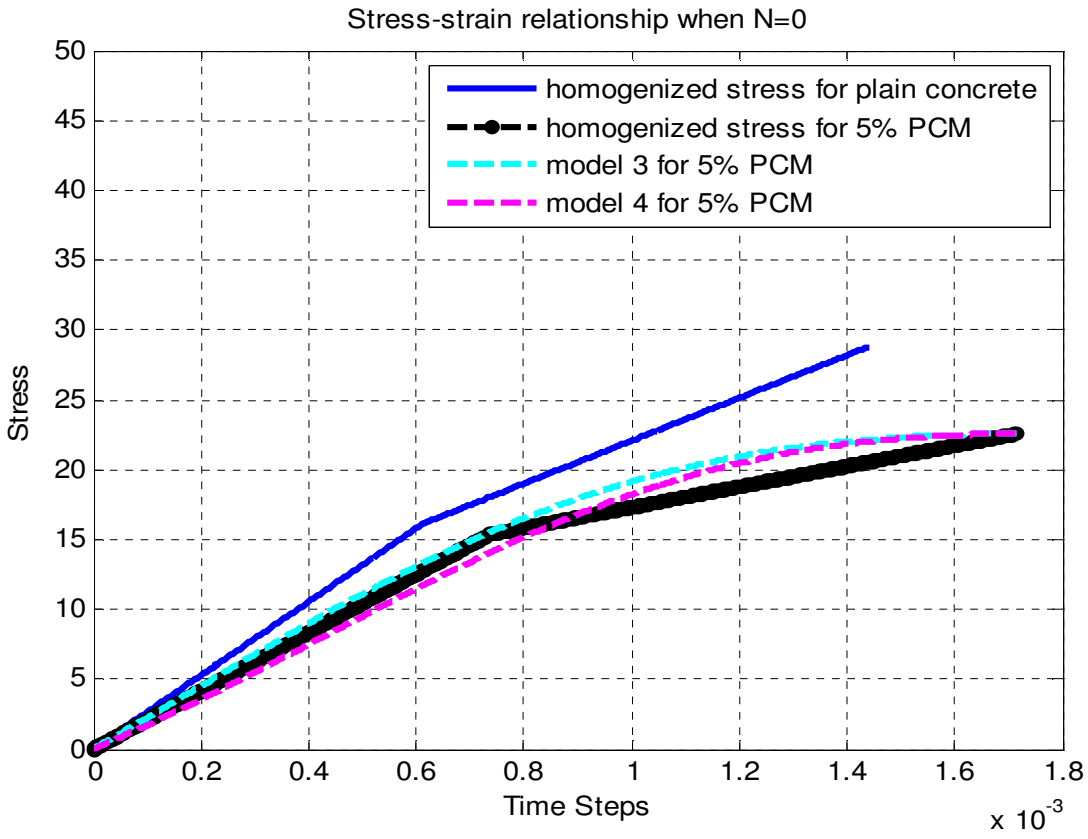

Figure 7.18 Stress-strain relationship comparison between plain and 5% PCM concrete when freeze-thaw cycle=0

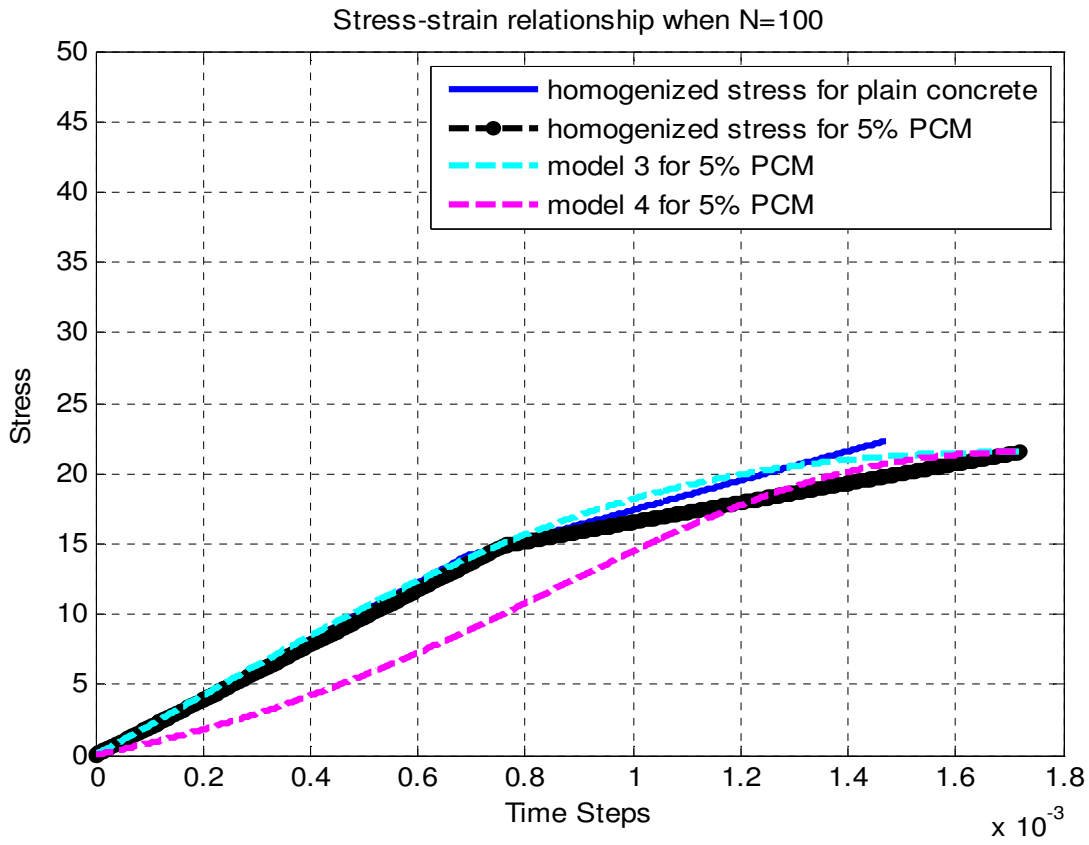

Figure 7.19 Stress-strain relationship comparison between plain and 5% PCM concrete when freeze-thaw cycle=100

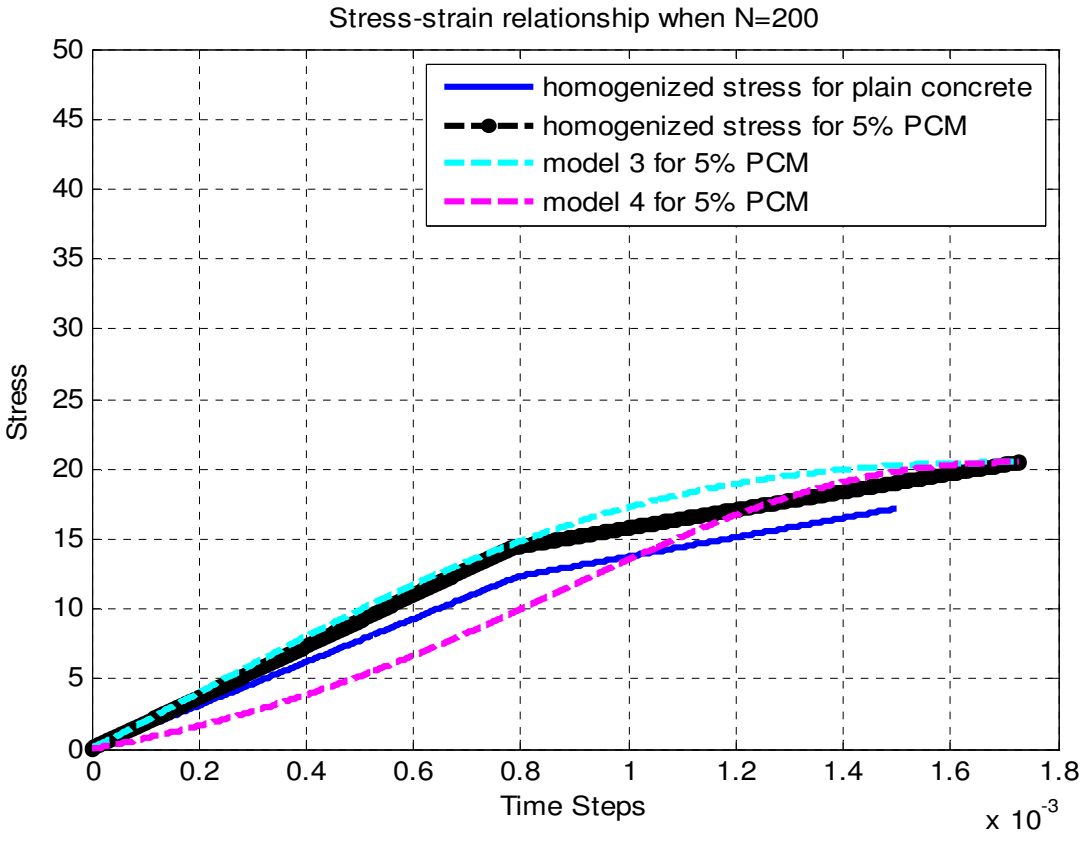

Figure 7.20 Stress-strain relationship comparison between plain and 5% PCM concrete when freeze-thaw cycle=200

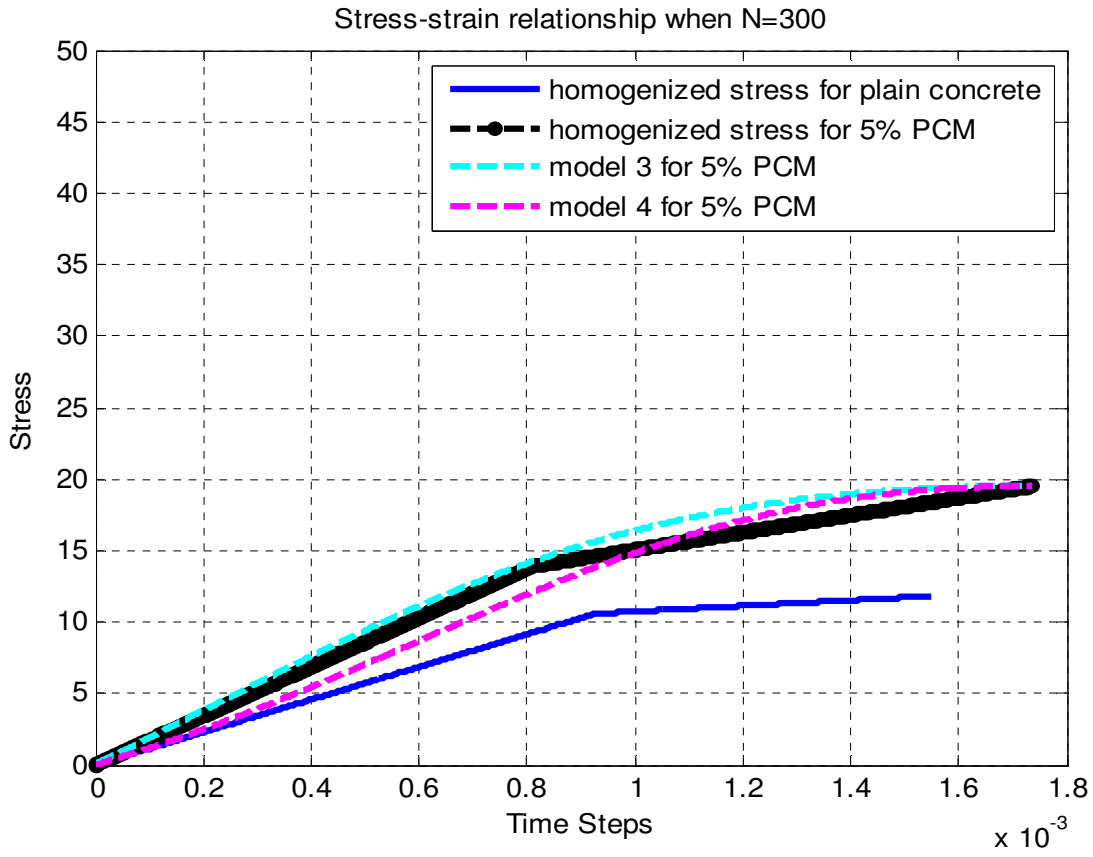

Figure 7.21 Stress-strain relationship comparison between plain and 5% PCM concrete when freeze-thaw cycle=300

Figure 7.18 to Figure 7.21 show the stress-strain comparison between plain concrete and 5% PCM concrete after different freeze-thaw cycles. We can observe that the difference between two types of concrete at each freeze-thaw cycle. Before applying any freeze-thaw test, 5% PCM concrete compressive strength was slightly lower than plain concrete because a certain amount of cement and sand need to be replaced by PCM. This observation is the same as in previous testing.

However, after going through a freeze-thaw cycle, we can observe that 5% PCM concrete compressive strength only slightly decreased and plain concrete decreased at a much higher rate. From table 7.3, 5% PCM concrete ultimate compressive strength would only drop about 10% after 300 cycle freeze-thaw cycles. In plain concrete, ultimate compressive strength would drop to about 55% after 300 freeze-thaw cycles.

From the previous chapter, we learned that concrete interior temperature can be controlled by inserting PCM into concrete. By maintaining concrete interior temperature, crack formation can be minimized and overall strength should be maintained. From the stress-strain examined relationship in this paper, we show that PCM indeed can help concrete to maintain its mechanical strength.

Freeze-thaw cycle	0	100	200	300
Plain concrete	28.82	22.46	17.12	12.71
5% PCM concrete	22.28	21.41	20.56	19.72

Table 7.3 Compressive strength comparison after freeze-thaw cycles

7.6 Conclusion

Based the analysis and numerical modeling from previous chapters, the following conclusions can be drawn.

1. The deterioration of the ultimate compressive strength and elastic modulus can be modeled by introducing damage parameter D. The damage parameter can be proposed by using a damage evolution function. This proves that adding PCM can maintain compressive strength after 300 freeze-thaw test cycles. However, plain concrete compressive strength decreases at a higher rate when increasing freeze-thaw cycle.

2. Concrete residual capacity is another interesting topic for study. From the stress-strain relationship after going through a freeze-thaw test, we learned the extent to which concrete will be able to perform at specific freeze-thaw cycles. Thermodynamics and free potential energy were introduced to derive the stress-strain relationship. Damage evolution functions were also proposed to model concrete interior damage when increasing strain. We showed that the stress-strain relationship becomes more ductile when increasing freeze-thaw cycles.

3. The results from the proposed constitutive model for a PCM concrete composite was shown to more efficient and has more residual capacity than plain concrete after a number of free-thaw cycles.

4. 7% PCM concrete was not compared with 5% PCM concrete and plain concrete in this chapter. As we learned in chapter 3 and 4, concrete ultimate stress, fracture toughness and corresponding mechanical properties would be greatly reduced because more cement and sand would be replaced by PCM. Concrete interior temperature would be maintained and

controlled. However, the difference is not significant compared to 5% PCM concrete as indicated in chapter 6. As a result, considering that concrete composite mechanical properties would be compensated and interior temperature controlled is not beneficial compared to 5% PCM concrete, we thus just compared 5% PCM concrete and plain concrete in this chapter.

The proposed constitutive model and corresponding numerical algorithms can be applied to plain concrete and PCM concrete, and also for different types of concrete composite if mechanical properties, damage degradation parameter under the action of freeze-thaw and damage evolution functions can be obtained. As a result, the model can help us to improve and enhance the concept of freeze-thaw behavior and thus better study concrete behavior when subjected to freeze-thaw cycles.

However, there are still some important issues that need to be solved in further study and to better understanding concrete structure behavior when subjected to freeze-thaw cycles.

1. More data will need to be collected to validate the accuracy of the numerical model. More accurate and effective experiment will need to be conducted.
2. After increasing freeze-thaw cycle, the behavior of concrete seems to be more ductile instead of brittle. Micromechanics can be used as a tool to study this behavior and provide us with a better understanding after going through freeze-thaw cycle.
3. More damage evolution functions can be chosen to model the stress-strain relationship and to compare with experimental data.
4. The size effect of a specimen can also be considered. It is important to correlate the freeze-thaw damage in small-sized specimens and larger concrete members. The frost depth in

larger structures is significant because the freeze-thaw damage might not reach the inside of the larger concrete members.

The relationship of freeze-thaw damage in the laboratory and in the field is also important.

7.7 References

[1] Chaoying, Z., Juan, Z., and Feng, L. (2008). "Stress-strain relationship of concrete in freeze-thaw environment." *Frontiers of Architecture and Civil Engineering in China*, 2(2), 184-188.

[2] Chen Yue-Shun, W. J., Zhao Xiao-Long (2006). "Description of Concrete Durability Damage Process." Wuhan University Journal of Natural Science, 653-656.

[3] Cho, T. (2007). "Prediction of cyclic freeze-thaw damage in concrete structures based on response surface method." *Construction and Building Materials*, 21(12), 2031-2040.

[4] Di Luzio, G., and Biolzi, L. (2013). "Assessing the residual fracture properties of thermally damaged high strength concrete." *Mechanics of Materials*, 64, 27-43.

[5] Farid, M., and Kong, W. J. (2001). "Underfloor heating with latent heat storage." *Proceedings of the Institution of Mechanical Engineers Part a-Journal of Power and Energy*, 215(A5), 601-609.

[6] Joulin, A., Younsi, Z., Zalewski, L., Lassue, S., Rousse, D. R., and Cavrot, J. P. (2011). "Experimental and numerical investigation of a phase change material: Thermal-energy storage and release." *Applied Energy*, 88(7), 2454-2462.

[7] Ju, J. W. (1989). "Energy-based coupled elastoplastic damage models at finite strains." *Journal of Engineering Mechanics-Asce*, 115(11), 2507-2525

[8] Ju, J. W. (1989). "On energy-based coupled elastoplastic damage theories – constitutive modeling and computational aspects." *International Journal of Solids and Structures*, 25(7), 803-833.

[9] Ju, J. W. (1990). "Isotropic and anisotropic damage variables in continuum damage mechanics." *Journal of Engineering Mechanics-Asce*, 116(12), 2764-2770.

[10] Ju, J. W. (1990). "On 2-dimensional micromechanical damage models for brittle solids with interacting microcracks." Micromechanics of Failure of Quasi-Brittle Materials, 105-114.

[11] Ju, J. W., and Yuan, K. Y. (2012). "New Strain-Energy-Based Coupled Elastoplastic Two-Parameter Damage and Healing Models for Earth-Moving Processes." International Journal of Damage Mechanics, 21(7), 989-1019.

[12] Ju, J. W., and Zhang, X. D. (1998). "Micromechanics and effective transverse elastic moduli of composites with randomly located aligned circular fibers." *International Journal of Solids and Structures*, 35(9-10), 941-960.

[13] Ju, J. W., and Zhang, Y. (1996). "Thermo-micromechanical damage modeling of airfield concrete pavement." *Engineering Mechanics: Proceedings of the 11th Conference, Vols 1 and 2*, 727-730.

[14] Ju, J. W., and Zhang, Y. (1998). "Axisymmetric thermomechanical constitutive and damage modeling for airfield concrete pavement under transient high temperature." *Mechanics of Materials*, 29(3-4), 307-323.

[15] Kim, J. S., and Darkwa, K. (2003). "Simulation of an integrated PCM-wallboard system." *International Journal of Energy Research*, 27(3), 215-223.

[16] Lemaitre, J. (1985). "A continuous damage mechanics model for ductile fracture." *Journal of Engineering Materials and Technology-Transactions of the Asme*, 107(1), 83-89.

[17] Liu, M. H., and Wang, Y. F. (2012). "Damage Constitutive Model of Fly Ash Concrete under Freeze-Thaw Cycles." *Journal of Materials in Civil Engineering*, 24(9), 1165-1174.

[18] Simo, J. C., and Ju, J. W. (1987). "Strain-based and stress-based continuum damage models .1. formulation." *International Journal of Solids and Structures*, 23(7), 821-840.

[19] Simo, J. C., and Ju, J. W. (1987). "Strain-based and stress-based continuum damage models .2. computational aspects." *International Journal of Solids and Structures*, 23(7), 841-869.

[20] Song YP, J. X. (2006). "Analysis on reliability of concrete under freezing thawing action and evaluation of residual life." J Hydraul Eng, 259-263.

[21] Subramaniam, K. V., Ali-Ahmad, M., and Ghosn, M. (2008). "Freeze-thaw degradation of FRP-concrete interface: Impact on cohesive fracture response." *Engineering Fracture Mechanics*, 75(13), 3924-3940.

[22] Ueda, T., Hasan, M., Nagai, K., & Sato, Y. (2004). "Stress-strain relationships of concrete damaged by freezing and thawing cycles."

[23] Voller, V., and Cross, M. (1981). "Accurate solutions of moving boundary-problems using the enthalpy method." *International Journal of Heat and Mass Transfer*, 24(3), 545-556.

[24] Voller, V. R. (1985). "Implicit finite-difference solutions of the enthalpy formulation of Stefan-problems." *Ima Journal of Numerical Analysis*, 5(2), 201-214.

[25] Voller, V. R. (1990). "Fast Implicit finite-difference method for the analysis of phase-change problems." *Numerical Heat Transfer Part B-Fundamentals*, 17(2), 155-169.

[26] Wei Jun, W. X.-h., Zhao Xiao-long (2003). "A damage model of Concrete under Freeze-Thaw Cycles." Journal of Wuhan University of Technology-Mater. SCI. Ed, 40-42.

[27] Xu, B., and Li, Z. (2013). "Paraffin/diatomite composite phase change material incorporated cement-based composite for thermal energy storage." *Applied Energy*, 105, 229-237.

[28] Yinping, Z., Xu, X., Kunping, L., Hongfa, D., and Rui, Y. (2005). "Modeling and simulation on the thermal performance of shape-stabilized phase change material floor used in passive solar buildings." *Energy and Buildings*, 37(10), 1084-1091.

[29] Zhu Jin-Peng, L. S.-C., Liu Xian-Bo, Liu Min (2009). "The Mechanical Property Deterioration Model for Concrete in the Environment with Freezing-Thawing." Journal of Architecture and Civil Engineering.

[30] Zuber, B., and Marchand, J. (2000). "Modeling the deterioration of hydrated cement systems exposed to frost action - Part 1: Description of the mathematical model." *Cement and Concrete Research*, 30(12), 1929-1939.

Chapter 8 Conclusions and Future Research

8.1 Summary and Conclusions

The present research proposed a theoretical model to investigate fiber debonding and the fiber pull-out process of PCM fiber reinforced concrete. Fracture energy was also calculated to observe concrete composite ductile capacity. Destructive tests were done and the results were compared with the theoretical model to verify model accuracy. Freeze-thaw testing was also performed to observe performance when incorporating PCM under freeze-thaw cycles. Concrete interior temperature was solved using a heat conduction equation and several algorithms and compared thru various PCM concrete composite models. Concrete mechanical property degradation was estimated by using a proposed damage model combined with experimental data. In addition, concrete composite residual capacity after freeze-thaw action was also studied by proposing a stress-strain relationship. The results and summaries are addressed in the following.

In chapter 3, we design a series of tests to observe PCM fiber reinforced concrete composite performances regarding both strength and freeze-thaw resistance. Four different types of concrete composite were mixed, including plain concrete, fiber reinforced concrete, 5% PCM fiber reinforced concrete and 7% fiber reinforced concrete. In the mixing process, there is no standard regarding mixing concrete with both fibers and PCMs. As a result, trial and error has to be performed to insure that concrete achieves a high quality. A certain amount of fine aggregates and cement have to be replaced by PCM in order to maintain the same volume fraction in the mixing formula. A compression test, splitting tension test and three point bending test were

performed as destructive tests and the results show that the strength of PCM fiber reinforced concrete will decrease because the replacement method is used in the mixing process. However, by inserting fibers to bridge crack, the amount of loss is still acceptable and overall performance is still better than plain concrete.

In order to study the freeze-thaw response when adding a phase change material, freeze-thaw testing was designed. A 340-cycles freeze-thaw test was performed for four different types of concrete. An ultrasonic test was performed in every 40 cycles to observe if there was any damage in terms of dynamic Young's modulus. In addition, mass loss measurement was also recorded after every 40 cycles. Destructive tests were also performed in 100 cycles and at the end of a freeze-thaw test. Experimental results for destructive tests and freeze-thaw test were presented.

In chapter 4, a slip-softening interfacial shear stress model was proposed to simulate fiber debonding and fiber pull-out behavior. The slip-softening interface condition between fibers and concrete matrix is assumed in this research. Since adding PCM will decrease the friction stress between concrete matrix and fibers, the usual slip-hardening or constant shear stress model would not be observed in our PCM fiber reinforced concrete. A crack bridging model was derived from a micromechanics analysis of a single fiber pull-out test. This crack bridging model is proposed for randomly distributed and randomly oriented discontinuously fibers in concrete composite. Pre-peak and post-peak bridging stress-displacement relationships were able to be derived based on the bridging mechanism associated with randomly oriented and randomly distributed discontinuous fibers in concrete composite.

In the present study, in order to take into account the slip-softening effect between fibers and a concrete matrix, parameter β was introduced into an interface constitutive relation. In addition, the snubbing coefficient f is also introduced into interface constitutive relation to account for the fiber inclination angle effect. This chapter concluded that parameter β, which depends on the slippage distance and frictional shear stress, has a greater contribution than the snubbing coefficient. The experimental results showed that when changing with parameter β and fixing with the snubbing coefficient, the error compared with experimental data will be larger than changing with the snubbing coefficient

Fracture energy was examined in light of scaling micromechanical parameters such as fiber snubbing coefficient, fiber diameter, aspect ratio, fiber volume fraction, PCM volume fraction and interface bond strength. The results show that the linear softening model accurately predicts the fracture energy in our PCM fiber reinforced concrete composite. For fiber reinforced concrete (FRC), the error can be computed as low as 2.5%. For 5% PCM+FRC, the error was only 2.01%. For 7%PCM+FRC, the error was calculated as only 0.6%. When adding more and more PCM into concrete composite, the interfacial shear stress will be decreased. As a result, the slip-softening parameter β will increase to reflect an increasing softening effect and constant interfacial shear stress τ_0 would then be decreased. The current proposed theoretical model resolves the constant interface deficiency of the shear stress model when predicting fracture energy, which is crucial for the material design of a pseudo strain hardening engineered cementitious composite. A micromechanical-based single fiber pull-out relation and bridging stress-crack mouth opening displacement are constructed theoretically and shown to be sufficient in describing the slip-softening interface behavior. It is emphasized that the fiber pull-out

mechanism has a significant influence on the total fracture energy absorption during crack propagation.

In addition to fracture energy and bridging stress-crack mouth opening displacement relationship, a theoretical model for predicting maximum applied force was also proposed. Rule of mixture and beam theory were used to derive a theoretical model. Results from the theoretical model were compared to the experimental data and showed that numerical results underestimate real performance. However, when adding more and more PCM, the maximum applied force can be predicted more accurately. All fibers are assumed to be well aligned when using rule of mixture. However, fibers are randomly located and randomly oriented in the mixing process. As a result, the real maximum applied force will be greater than what the model predicted.

We also conclude that the maximum applied force can be attributed to PVA fibers, and also steel fibers. In theory, PVA fibers bridge micro-cracks and enhance maximum applied force. However, there were only 0.1% of PVA fibers used in our PCM concrete composite. Therefore, steel fibers also help PVA fibers to bridge cracks and increase the maximum applied force.

In chapter 6, PCM incorporated into concrete was studied and the thermal performance of PCM concrete was investigated. Three different PCM concrete models were presented. At first, PCM layer and concrete layer were compared with two different numerical methods. Secondly, laminated PCM concrete was modeled to examine thermal performance. Last but not least, we also modeled uniformly distributed PCM concrete to observe its thermal performance and compare with laminated PCM concrete.

The enthalpy method and specific heat capacity method were used to model both PCM a layer and concrete layer. Details regarding both numerical methods were addressed in the

previous chapter. Results form both methods showed they could both produce reasonable results. However, enthalpy method can predict phase change process better and provide a smoother temperature gradient curve. In addition, we also proved that using a PCM layer can obtain better thermal performance than using a concrete layer based on both numerical methods.

The PCM layer added on the top of a concrete layer is more efficient because it can avoid wasting of PCM and improve thermal performance. In addition, it can utilize the strength of concrete to sustain loads. If PCMs are mixed into concrete matrix, some PCMs may not be used to absorb and release energy to improve thermal performance. Because some PCMs may locate at the bottom of concrete matrix, it will be difficult for this PCM to absorb the energy from sunlight through the concrete surface. In order to compare the efficiency of laminated PCM concrete, uniformly distributed PCM concrete was also studied in this chapter. We have showed a temperature comparison between laminated PCM concrete and uniformly distributed PCM concrete. Laminated PCM concrete had better thermal performance than uniformly distributed PCM concrete. As a result, by incorporating a PCM layer on top of concrete to absorb and release energy during phase change might be the most efficient approach.

Numerical results proved that laminated PCM concrete can improve thermal performance compared to normal concrete. The thickness of the PCM layer also plays an important role. Obviously, increasing the thickness of PCM layer can help a PCM concrete composite to improve thermal performance. However, the thickness of PCM layer cannot be continuously built up because it will compromise the strength of the concrete composite. Thermal performance is important in our application, but maintaining essential strength is also important in order to carry load.

In chapter 7, the deterioration of mechanical properties, such as ultimate compressive strength and elastic modulus can be modeled by introducing damage parameter D. This parameter proves that adding PCM can maintain compressive strength after 300 freeze-thaw test cycles. However, plain concrete compressive strength decreases at a higher rate when increasing freeze-thaw cycle.

Concrete residual capacity is another interesting topic to worthy to study. From the stress-strain relationship after going through a freeze-thaw test, we can learn the extent to which concrete will be able to perform at a specific freeze-thaw cycle. Thermodynamics and free potential energy were introduced to derive the stress-strain relationship. Damage evolution functions were also proposed to model concrete interior damage when increasing strain. We can prove that the stress-strain relationship becomes more ductile when increasing freeze-thaw cycles.

The results from the proposed constitutive model for PCM concrete composite was proved to be more efficient and has more residual capacity than plain concrete after a number of free-thaw cycles. The proposed constitutive model and corresponding numerical algorithms can be applied to plain concrete and PCM concrete, and also to different types of concrete composite if mechanical properties, damage degradation parameter under the action of freeze-thaw and damage evolution functions can be obtained. As a result, the model can help us to improve and enhance the concept of freeze-thaw behavior and thus better study concrete behavior under freeze-thaw damage conditions.

8.2 Proposed Future Studies

Experimental results were presented regarding strength and freeze-thaw resistance for PCM fiber reinforced concrete. We also derived a theoretical model for predicting fracture energy and bridging the stress-COMP relationship in current research. We also studied concrete interior temperature to determine benefits after adding PCM. Mechanical property degradation and concrete composite residual capacity after going through a freeze-thaw cycle were also proposed. However, there continues to be necessary work for the future, as described following:

1) The resources for this thesis project were limited. First, some of the materials and experimental apparatus are expensive and the research budget was limited. For example, in order to perform a freeze-thaw test in a more efficient approach, it will be necessary to utilize a rapid freeze-thaw machine. The machine can perform up to six freeze-thaw cycles per day. Because of a limited budget, a regular freezer was used in our freeze-thaw test and it can only perform one cycle per day. In addition, additional man power would be needed in order to switch out specimens every day. However, our manpower was limited and this extended our freeze-thaw testing over a long period. Third, the homogeneous distribution of the fibers and phase change materials could have been improved if the equipment was operated with more personal assistance. The mixing process was done to our best efforts, but was likely to be less than perfect.
2) For up to 340 freeze-thaw cycles, there was no significant damage in both mass loss and dynamic Young's modulus. Therefore, further freeze-thaw cycles will be required to observe damage inside of concrete specimens. However, it is not efficient to perform only one slow freeze-thaw test every day. As a result, in the near future, if research funds

are granted, a rapid freeze-thaw machine can be purchased to increase and accelerate the speed of freeze-thaw cycles. If the purchase of a rapid freeze-thaw machine is not possible, the other more efficient methods must be provided to increase the speed of the freeze-thaw testing.

3) In our slip-softening interfacial shear stress model, a simplified model was proposed to simulate the bridging stress-crack mouth opening displacement relationship. However, in order to improve the accuracy of the model prediction, only a few mechanisms of fiber-matrix interactions were considered. Other possible interactions include: fiber two-way debonding and pull-out, matrix micro-spalling, fiber pre-stretching and the Cook-Gordon effect. It is expected that an improved model will greatly benefit future material design technology in terms of steady state crack width control which is very important for structural long-term durability.

   Strong slip-hardening interfacial behavior was presented because PVA fibers can have strong bond strength. Due to strong slip-hardening behavior the pull-out load can be much higher than the load at the completion of debonding. After the completion of debonding at the short embedment side, the long embedment side may continue debonding and eventually enter a pull-out process such that a two-way fiber pull-out can then be observed. As a result, the slippage distance contribution from both sides should be included into total crack opening displacement.

   Matrix micro-spalling is also commonly observed in randomly oriented and distributed fiber reinforced concrete composite. When the pull-out force at the fiber exit is not in the same direction as fiber alignment, stress concentration at the bearing point causes local failure of the supporting matrix.

Lastly, the Cook-Gordon effect describes a premature fiber/matrix interface debonding normal to the fiber axis. As a result, additional crack opening will occur.

In addition, an interfacial shear stress model that accounts for both strain hardening behavior and strain softening behavior can also be proposed.

$$\tau = (\tau_0 + a_1 S + a_2 S^2)(1 - \beta \frac{S}{d_f}) \tag{8.1}$$

Equation (8.1) is a coupled interfacial shear stress model that includes both strain hardening and softening behavior. In chapter 4, we assume strain softening effect would dominate because interface between fiber and concrete matrix is weaken by adding PCM. However, in hybrid fiber reinforced PCM concrete composite, strain hardening effect might contribute more because PCM volume fraction is not high enough. On the contrary, strain softening effect might contribute more because higher volume fraction. As a result, equation (8.1) accounts for effects from both fiber and PCM.

4) A theoretical model for predicting performance after freeze-thaw test was constructed in chapter 6. In order to model freeze-thaw resistance, the transient problem was considered to account for time variant and combined with theories from thermal dynamics and heat transfer. The heat conduction governing equation is the key to solving a phase change problem.

$$k_m \frac{\partial^2 T_m}{\partial x^2} = \rho_m C p_m \frac{\partial T_m}{\partial t} \qquad m = 1, 2 \tag{8.2}$$

In chapter 6, we used a 1D heat conduction equation to solve for the temperature gradient. However, we only considered temperature in a vertical direction. We assume that heat energy would transfer from the surface and propagate to the bottom in one direction. In the field, the temperature gradient along the vertical direction can be also affected in the y

and z direction. As a result, we can also utilize equation (8.2) to find the temperature in both the y and z direction. Numerical analysis such as finite difference or a finite element method will need to be used. By considering the temperature effect from all three directions, we should be able to better estimate the temperature gradient inside of concrete and better understand benefits after adding PCM.

5) In chapter 6, we used rule of mixture to calculate material property and all PCM was assumed to be the same size. However, size effect would also play an important role in this model. If PCM particle is bigger with the same volume fraction, thermal performance of PCM can be more effective compared to smaller PCM particle. If PCM particle is smaller with the same volume fraction, the overall thermal performance will be affected. As a result, we can utilize **micromechanics** to account for size effect. Some researchers considered size effect to determine composite material property. Ju considered size-dependent and probability damage mechanics to discuss toughening behavior in fiber reinforced composite and metal matrix composite [13] [14] [15]. Ko and Ju also included size effect in micromechanics to study the effective moduli in three-phase hybrid fiber reinforced composite [16]. As a result, we will be able to utilize micromechanics framework to include size-effect in hybrid fiber PCM composite.

6) After solving equation (8.2), we can utilize the result and find a correlation between the strength of a concrete composite and PCM thermal performance. After performing 340 cycles of a freeze-thaw test, we observed that there was no significant change in both mass loss and dynamic Young's modulus. Because time was limited and we lacked manpower, we were not be able to keep the freeze-thaw test going until the specimen had further damage in terms of mass loss and dynamic modulus. Therefore, we will discuss

the freeze-thaw impact on concrete composite's strength. To relate PCM thermal response to linear slip-softening interfacial shear stress is another important topic to be solved. We already showed that adding PCM would cause a different interfacial shear stress behavior. However, freeze-thaw cycles might also have an effect in modifying the interfacial condition between a concrete matrix and fibers. If we can find the relationship between a freeze-thaw cycle and interfacial condition, we will be able to estimate fiber debonding and pull-out stress and calculate corresponding fracture energy after going through a freeze-thaw cycle.

7) In our PCM fiber reinforced concrete composite, it was important to understand the overall constitutive behavior of the composite, such as effective elastic modulus. From Ju and Chen [10] [11] [12], the three governing micromechanical ensemble–volume averaged field equations were derived as follow:

$$\bar{\sigma} = C_0 : (\bar{\varepsilon} - \sum_{r=1}^{n} \phi_r \bar{\varepsilon}_r^*) \tag{8.3}$$

$$\bar{\varepsilon} = \varepsilon^0 + \sum_{r=1}^{n} \phi_r S : \bar{\varepsilon}_r^* \tag{8.4}$$

$$(-A_r - s) : \bar{\varepsilon}_r^* = \varepsilon^0 + \bar{\varepsilon}_r^{'p} \tag{8.5}$$

The effective stiffness tensor for a multiphase composite medium can then be calculated by neglecting inter-particle interaction effects.

$$C_* = C_0 \cdot [I + B(I - SB)^{-1}] \tag{8.6}$$

Where

$$B \equiv \sum_{r=1}^{n} \phi_r (s + A_r)^{-1} \tag{8.7}$$

As we know, concrete composite is a multi-phases composite. In our cases, it can be characterized into four phases of composite that includes concrete matrix, steel fiber, PVA fiber and PCM. Therefore, to study and determine material properties that include Young's modulus, shear modulus and bulk modulus for multi-phases composite is important for future study. These material properties of multi-phases composite can be derived based on the micromechanical equations provided above. Eshelby's method or Mori-Tanaka' method can also be used as a micromechanics basis to calculate material properties.

8) Probabilistic analysis can also be added into the analysis. In the mixing process, PCM cannot be guaranteed to be mixed and uniformly distributed. As a result, we can also incorporate probabilistic analysis with the current model to account for random distribution of PCM.

9) In chapter 7, we proposed a damage degradation parameter and combined this with elastic damage theory and experimental results to find mechanical property degradation when subjected to freeze-thaw action. The numerical model, however, is a semi-theoretical model. Some parameters in this numerical model will need to be determined from experimental result. Therefore, it would be beneficial to develop an entirely theoretical model. We can start by solving for pore pressure inside of concrete when going through a freeze-thaw cycle. In chapter 7, the mass balance equation and other system equations can be used to find pore pressure. However, it is extremely complicated to solve those equations because of difficult numerical schemes. As a result, if we can develop an effective numerical scheme to solve those system equations, we will be able to find pore pressure and calculate the overall stress that cause concrete matrix cracking.

We can also combine this with damage mechanics to calculate a stress intensity factor and estimate crack propagation after going through a freeze-thaw cycle.

Finally, by combining the current research and the suggested future work, we can improve our understanding about the properties of PCM fiber reinforced concrete composite, and also properties of strength, fracture toughness and freeze-thaw resistance based on the proposed coupled micromechanical and computational framework.

8.3 References

[1] Benveniste, Y. (1987). "A new approach to the application of Mori-Tanaka theory in composite-materials." *Mechanics of Materials*, 6(2), 147-157.

[2] Chen, T. Y., Dvorak, G. J., and Benveniste, Y. (1992). "Mori-Tanaka estimates of the overall elastic-moduli of certain composite-materials." *Journal of Applied Mechanics-Transactions of the Asme*, 59(3), 539-546.

[3] Christen.Rm, and Waals, F. M. (1972). "Effective stiffness of randomly oriented fiber composites." *Journal of Composite Materials*, 6(OCT), 518-&.

[4] Darkwa, J. (2009). "Mathematical evaluation of a buried phase change concrete cooling system for buildings." *Applied Energy*, 86(5), 706-711.

[5] Davalos, J. F., Kodkani, S. S., Ray, I., and Lin, C. F. (2008). "Fracture evaluation of GFRP-concrete interfaces for freeze-thaw and wet-dry cycling." *Journal of Composite Materials*, 42(14), 1439-1466.

[6] Hasan, M., Mujumdar, A. S., and Weber, M. E. (1991). "Cyclic melting and freezing." *Chemical Engineering Science*, 46(7), 1573-1587.

[7] Hawes, D. W., Banu, D., and Feldman, D. (1990). "Latent-heat storage in cocnrete .2." *Solar Energy Materials*, 21(1), 61-80.

[8] Hawes, D. W., and Feldman, D. (1992). "Absorption of phase change materials in concrete." *Solar Energy Materials and Solar Cells*, 27(2), 91-101.

[9] Jariwala, V. G., Mujumdar, A. S., and Weber, M. E. (1987). "The periodic steady-state for cyclic energy-storage in paraffin wax." *Canadian Journal of Chemical Engineering*, 65(6), 899-906.

[10] Ju, J. W., and Chen, T. M. (1994). "Effective elastic-moduli of 2-phase composites containing randomly dispersed spherical inhomogeneities." *Acta Mechanica*, 103(1-4), 123-144.

[11] Ju, J. W., and Chen, T. M. (1994). "Micromechanics and effective elastoplastic behavior of 2-phase metal-matrix compoaites." *Journal of Engineering Materials and Technology-Transactions of the Asme*, 116(3), 310-318.

[12] Ju, J. W., and Chen, T. M. (1994). "Micromechanics and effective moduli of elastic composites ontaining randomly dispersed ellipsoidal inhomogeneities." *Acta Mechanica*, 103(1-4), 103-121.

[13] Ju, J.W., and Yanase, K., "Size-dependent probabilistic damage micromechanics and toughening behavior of particle/fiber reinforced composites", in *Handbook of Micromechanics and Nanomechanics*, Chapter 27, pp. 1033-1066, Ed. by Shaofan Li and Xin-Lin Gao, published by Pan Stanford Publishing, May 2013, ISBN 978-981-4411-23-3 (hardcover).

[14] Ju, J.W., and Yanase, K., "Size-dependent probabilistic micromechanical damage mechanics for particle reinforced metal matrix composites", *Int. J. of Damage Mechanics*, 20(7), 1021-1048, Sep. 2011. DOI: 10.1177/10567895-10374165, Sage Publications.

[15] Ju, J.W., and Yanase, K., "Size-dependent probabilistic damage micromechanics and toughening behavior of particle/fiber reinforced composites", **Plenary Lecture 2**, in Proceedings of the 1st International Conference on Damage Mechanics (ICDM-1), at Serbian Chamber of Engineers, pages 13 to 18, June 24 to 27, 2012, Chi L. Chow, J. Woody. Ju and Dragoslav M. Sumarac, editors, published by Serbian Chamber of Engineers, Belgrade, Serbia, 2012, ISBN 978-86-86115-09-6.

[16] Ko, Y.F., and Ju, J.W., "Effective transverse elastic moduli of three-phase hybrid fiber reinforced composites with randomly located and interacting aligned circular fibers of distinct elastic properties and sizes", *Acta Mechanica*, 224 (1), 157-182, 2013. DOI: 10.1007/s00707-012-0744-7, Springer Publications.

[17] Kurklu, A., Wheldon, A., and Hadley, P. (1996). "Mathematical modelling of the thermal performance of a phase-change material (PCM) store: Cooling cycle." *Applied Thermal Engineering*, 16(7), 613-623.

[18] Lee, T., Hawes, D. W., Banu, D., and Feldman, D. (2000). "Control aspects of latent heat storage and recovery in concrete." *Solar Energy Materials and Solar Cells*, 62(3), 217-237.

[19] Luo, J., and Stevens, R. (1996). "Micromechanics of randomly oriented ellipsoidal inclusion composites .1. Stress, strain and thermal expansion." *Journal of Applied Physics*, 79(12), 9047-9056.

[20] Mazo, J., Delgado, M., Marin, J. M., and Zalba, B. (2012). "Modeling a radiant floor system with Phase Change Material (PCM) integrated into a building simulation tool: Analysis of a case study of a floor heating system coupled to a heat pump." *Energy and Buildings*, 47, 458-466.

[21] Pasupathy, A., Athanasius, L., Velraj, R., and Seeniraj, R. V. (2008). "Experimental investigation and numerical simulation analysis on the thermal performance of a building roof incorporating phase change material (PCM) for thermal management." *Applied Thermal Engineering*, 28(5-6), 556-565.

[22] Sahmaran, M., Lachemi, M., and Li, V. C. (2009). "Assessing the durability of engineered cementitious composites under freezing and thawing cycles." *Journal of ASTM International*, 6(7), JAI102406 (102413 pp.)-JAI102406 (102413 pp.)JAI102406 (102413 pp.).

[23] Takao, Y., Chou, T. W., and Taya, M. (1982). "Effective longitudinal Young's modulus of misoriented short fiber composites." *Transactions of the ASME. Journal of Applied Mechanics*, 49(3), 536-540540.

[24] Yun, H. D., Kim, S. W., Lee, Y. O., and Rokugo, K. (2011). "Tensile behavior of synthetic fiber-reinforced strain-hardening cement-based composite (SHCC) after freezing and thawing exposure." *Cold Regions Science and Technology*, 67(1-2), 49-57.

[25] Yun, H. D., and Rokugo, K. (2012). "Freeze-thaw influence on the flexural properties of ductile fiber-reinforced cementitious composites (DFRCCs) for durable infrastructures." *Cold Regions Science and Technology*, 78, 82-88.